DEFORMATION OF BODY-CENTRED-CUBIC METALS

A Thesis submitted in supplication for the

Degree of Doctor of Philosophy



Trinity Term, 1965

Glyn Taylor,

Linacre House

CONTENTS

Abstract i

Section I - Introduction 2

Section II - Review of Literature 5

Stress - Strain Graphs 6

Glide Systems 10

Observations on Etched Surfaces 16

Geometry of Twinning 21

Effects of Impurity 29

Electron Microscopy 38

The Temperature Dependence of the Yield and Flow Stresses.... 47

Theories of Work Hardening 58

Twinning Mechanisms 76

Section III - Apparatus and Experimental Techniques.

Electron Beam Units 86

Ultra-high Vacuum Annealing Furnace 89

Devices for Cutting and Slicing Single Crystals..... 92

Grinding Jigs 95

Tensile Specimen Cutter 97

Mechanical Testing Machines 98

Compression and Tension Jigs 100

Direct Measurements of Strain 102

Goniometer Stage for the E.M. 6 104

Materials 106

Growth of Single Crystals 109

Ultra-high Vacuum Annealing 111

Preparation and Testing of Compression Specimens .. 114

Preparation and Testing of Tensile Specimens..... 117
Temperature Measurement and Control 118
X-ray Techniques 119
Preparation of Specimens for Electron Microscopy ... 120
Electron Microscopy 125

Section IV - Results and Preliminary Discussion.

Purity of Material 127
Converting Load-Time Charts into Stress-strain Curves. 128
General Observations on Mechanical Testing 133
Orientation Dependence of Slip Systems 139
Stress-Strain Curves and Optical Observations 142
Microstrain Tests 162
Electron Microscopy 168

Section V - General Discussion

Purity of Material 192
The Effect of Interstitial Impurities 193
The Effect of Substitutional Impurities 197
Ageing at Room Temperature 198
The Temperature Dependence of the Yield and Flow Stress.198
The Activation Enthalpy, Activation Volume and Theories
of the Temperature Dependence of the Flow Stress 202
Twinning 205
Slip Systems 213
Characteristics of the Work Hardening Curves 213
Electron Microscopy 216
Theories of Work Hardening 228
References 235
Acknowledgements 245

Abstract

This thesis describes work on niobium single crystals purified by annealing near to the melting point under a vacuum of $\sim 10^{-8}$ torr. The pure crystals were deformed at temperatures in the range 4.2°K to 300°K at strain rates of $\sim 10^{-4}$ sec^{-1}.

The yield and flow stresses show a similar temperature dependence to that obtained by Masters (1962) with less pure niobium; however in the present case the flow stress has a larger temperature dependence than the yield stress. It is suggested that this is due to edge dislocations having a slightly smaller temperature dependence than screws. Masters results are then explained by dislocation locking by impurity atoms.

The values of activation enthalpy and activation volume agree well with Masters' results, showing further the effect of increasing purity. It is considered that the overcoming of the Peierls-Nabarro stress with the aid of thermal fluctuations gives the best explanation of the temperature dependence of the flow stress. However there appears to be some strain, in addition to the elastic strain, from the beginning of loading.

The room temperature stress-strain curves show for suitable orientations, at least three stages of hardening as in f.c.c. crystals; however the rapid hardening rate varied from about $\frac{\mu}{250}$ for primary and conjugate glide

in compression to about $\frac{\mu}{500}$ for primary and conjugate glide in tension and primary and critical glide in compression. The slip systems operating at room temperature were of the type $\{110\}\langle 111\rangle$ and $\{211\}\langle 111\rangle$ depending on orientation and it is concluded that true glide occurred on $\{211\}$ planes since in some cases at least $\{211\}$ glide took place when $\{110\}$ was more highly stressed.

At 77°K, the specimens twinned unless previously strained at room temperature. The twin stress increased as far as 20°K but then rapidly decreased again between 20°K & 4.2°K. At 4.2°K it was not possible to obtain slip. The decrease in twin stress below 20°K cannot be explained on the basis of adiabatic softening since the temperature rise is too small. The electron microscopy confirmed that twinning was of the type $\{211\}\langle 111\rangle$ with a shear of 0.707.

At room temperature the electron microscopy of plastically deformed crystals showed similar features to f.c.c. metals:- edge dipoles and dislocations building up braids with, initially at any rate, small tilts across them. Screw dislocations were rarely observed and it is concluded that screws of opposite sign cross-slip and annihilate. At very high strains ($\gamma \sim 1.0$) high tilt boundaries ($\sim 25^{\circ}$) were observed. These are explained on the basis of edge dislocation arrays perpendicular to the slip plane or on particular $\{110\}$ planes. The arrays on $\{110\}$ planes may be stress free and it is considered that they will explain

the difference in work hardening rates described above.

Deformation at lower temperatures e.g. 158°K gave a totally different dislocation structure. Edge dislocations were absent and long screws with a high jog density were observed in parallel arrays, adjacent dislocations often being of opposite sign. Large numbers of small loops, evenly distributed, were also seen and these are believed to be due to the non-conservative movement of jogs in screws. Prior strain at room temperature gave a mixture of the two types of dislocation structure. The existing edge dislocation braids grew but no new braids were believed to have formed. These observations support the Sharp-Makin (1964) sweeping mechanism of braid formation.

The current theories of work-hardening and twinning are inadequate in explaining the present results. A few tentative suggestions and modifications are put forward to explain some parts of the results, but no new general theories have been formulated.

REFERENCES

Masters B.C. (1962) D.Phil. thesis. Oxford.

Sharp J.V. & Makin M.J. (1964) Phil.Mag. 10 1011.

SECTION I.

Section I.

General Introduction.

In 1961 B.C. Masters completed a study of the mechanical properties of body-centred cubic metals. Masters used polycrystaline niobium, tantalum and vanadium, and a few single crystals of niobium in temperature and strain-rate cycling tests; also some straight stress-strain tests were performed. Testing was in tension over the temperature range 4.2^{o}K to room temperature.

Temperature and strain-rate cycling tests give information about the thermal component of the flow stress, and since in body-centred cubic metals this part of the flow stress is largely strain independent, Masters' work was mainly concerned with the temperature dependence of the yield and flow stresses. The present study is more concerned with work hardening; the techniques used include transmission electron microscopy and lattice rotation determination using X-rays. Because of the nature of the experiments and because single crystals were used, the study has been largely confined to niobium. These single crystals of niobium were considerably purer than those of Masters and so a few specimens were subjected to temperature and strain-rate cycling for comparison. Since the ductility of b.c.c. metals tested in tension is poor, most tests were in compression. The stress-strain graphs obtained are considerably different from those of Masters and are reported in detail.

Whilst this study was in progress, two other members of the Department were also studying niobium. C.I.L. Evans examined the slip-line patterns obtained on deforming at different temperatures and D.K. Bowen studied the large scale distribution of dislocations using etch pits and the detailed orientation dependence of the work hardening graph. Bowen's work is still in progress.

The Body-Centred-Cubic Lattice, Dislocations and Deformation Systems.

The b.c.c. lattice consists of two intersecting simple cubic lattices, the corner atoms of each unit cell of one lattice being at the centre of each unit cell of the other.

The most closely packed plane is $\{110\}$ and this contains two close-packed directions, $\langle 111 \rangle$. The second most closely packed plane, $\{100\}$, does not contain a close-packed direction, but the third, a $\{211\}$ contains one $\langle 111 \rangle$ direction.

Unit glide dislocations in the b.c.c. structure are always of the type $\frac{a}{2}\langle 111 \rangle$. Two such dislocations can combine to produce a third dislocation of a different type:

$$\frac{a}{2}[111] + \frac{a}{2}[\bar{1}11] \longrightarrow a[001] .$$

Since on a simple basis the reaction is energetically favourable, such dislocations should be frequent in networks also the $a[001]$ dislocation is not normally able to move in the glide planes of either the $\langle 111 \rangle$ type dislocations.

Considering only the elastic strain energy, the $\frac{a}{2}\langle 111 \rangle$ dislocation should be able to dissociate:

$$\frac{a}{2}[111] \longrightarrow \frac{a}{6}[111] + \frac{a}{3}[111] ,$$

and $$\frac{a}{3}[111] \longrightarrow \frac{a}{6}[111] + \frac{a}{6}[111] .$$

However, since the stacking fault energy of b.c.c. metals is very high the separation of the partials should be small; the second dissociation in particular produces a very high energy fault. Other dissociations of $\frac{a}{2}\langle 111\rangle$ dislocations have been suggested, Hirsch and Segall (1961) have seen the following dissociations:

$$\frac{a}{2}[111] \longrightarrow \frac{a}{6}[11\bar{1}] + \frac{a}{6}[133] + \frac{a}{6}[1\bar{1}1] ,$$

and $$\frac{a}{2}[111] \longrightarrow \frac{a}{6}[11\bar{1}] + \frac{a}{6}[113] + \frac{a}{6}[111] .$$

Another probable dissociation is,

$$\frac{a}{2}[111] \longrightarrow \frac{a}{3}[112] + \frac{a}{6}[11\bar{1}]$$

Cohen et al. (1962) have proposed a dissociation on a (110) plane,

$$\frac{a}{2}[111] \longrightarrow \frac{a}{4}[211] + \frac{a}{8}[011] + \frac{a}{8}[011] .$$

The a $[001]$ dislocation can also dissociate,

$$a[001] \longrightarrow \frac{a}{6}[\bar{1}15] + \frac{a}{6}[1\bar{1}1] ,$$

and further $$\frac{a}{6}[\bar{1}15] \longrightarrow \frac{a}{3}[\bar{1}12] + \frac{a}{6}[1\bar{1}1] .$$

Some of these dissociations are used in twinning and will be considered further in section II.9.

In b.c.c. crystals, the glide direction is always the expected $\langle 111 \rangle$; the glide plane however, is not exclusively the $\{110\}$ type but glide on $\{211\}$ and $\{321\}$ type planes and pencil glide have been reported. The conditions under which these different glide systems operate will be reviewed later. (Section II.2)

Deformation twinning in b.c.c. metals is well known. (Barrett 1952). There are twelve twinning systems and the elements of twinning are:

twinning plane (K_1) - $\{211\}$ type,

twinning direction (η_1) - $\langle 111 \rangle$ type,

undistorted plane (K_2) - $\{211\}$ type.

The magnitude of the twinning shear S, is given by

$$S = 2 \tan \theta = 0.707$$ (see fig. I.1.).

This is in agreement with an $\frac{a}{6}\langle 111 \rangle$ partial dislocation gliding on every $\{211\}$ plane parallel to the twin plane. An interesting difference between glide and twinning deformation is that for twinning the sign of the applied stress is important; if the sign is unfavourable then twinning cannot occur. (except by a shear of twice the magnitude of the favourable case). Hence the twin system which operates in tension will be different from that operating in compression. This can readily be seen by resolving the applied stress parallel and perpendicular to the twin plane (fig. I.1). Theories of twinning will be reviewed in section II.9 .

SECTION II.

Section II.

Review of Literature

Few published reviews of literature deal exclusively with b.c.c. metals, however, most summaries of plasticity contain sections about some aspect of bc.c. deformation.

The earlier investigations have been described by Schmid and Boas (1935) and Elam (1935) ; Barrett (1952) also has several chapters dealing with glide and twinning phenomena. More recently, Maddin and Chen (1954a) have reviewed the geometrical aspects of single crystal deformation and Nabarro, Basinski and Holt (1964) in 'Plasticity of Pure Single Crystals' devote a small section to b.c.c. metals which deals with the geometry of slip, the stress-strain graph and the theory of the flow stress. Gregory, Rowe and Stroh (1962) in an A S D technical report on work hardening mechanisms in b.c.c. metals describe slip systems, dislocation interactions, point defects and impurity interactions.

Theses from this Department also contain summaries of certain aspects of b.c.c. deformation. Masters (1962) considered the grain size dependence of yield stress and cleavage strength, the temperature and strain-rate dependence of the flow stress and dislocation behaviour as observed by etch pits. Altshuler (1964) has reviewed compression testing, yielding and twinning phenomena and theories of the flow stress. Evans (1964) described the crystallography of glide and theories of work hardening.

Since the present investigation was largely confined to the compression of pure single crystals, theories of the sharp yield point, the effect of grain size and modes of fracture will not be described.

II. 1. Stress-Strain Graphs of B.C.C. Metals.

Early work showed that the work hardening of b.c.c. metals proceeded approximately parabolically and could often be described by an equation of the type,

$$\sigma = \sigma_0 + a\,\varepsilon^{\frac{1}{2}}$$ (Maddin and Chen 1954)

Where, σ_0 and a are constants,

σ, the flow stress, and

ε, the strain.

Lately, however, different shapes to the graph have been obtained and these will be described below. Often yielding was followed by a yield drop particularly in iron, niobium and tantalum though molybdenum and tungsten did not show this feature as readily. Below about 0.2 Tm, where Tm is the melting point in °K, b.c.c. metals unlike metals with close packed structures, exhibit a rapid rise in their yield and flow stresses as the test temperature falls. Theories to explain this rise will be reviewed in section II. 7.

Selected references describing the stress-strain graphs of the different metals will now be given.

Iron.

Allen, Hopkins and McLennan (1956) found a considerable yield drop followed by parabolic or linear hardening.

The rate of hardening decreased with temperature down to 77°K, at which temperature twinning was frequent. Mordike and Haasen (1962) reported only parabolic hardening but Jaoul and Gonzalez (1961) showed both linear and parabolic hardening depending on orientation; some curves showed a region of decreasing hardening rate at first followed by an increase in rate, but the differences were small. Altshuler (1964), using very pure iron crystals supplied by D.F. Stein, and testing in compression found the room temperature graph almost parabolic. At 77°K the graph was rather odd; after yielding the hardening was linear, this was followed by a higher rate of hardening which decreased parabolically. At 20°K the specimens twinned before deforming plastically. Keh (1964) reported three stage hardening analogous to that in f.c.c. crystals; however the work hardening rates in stages I and II were very similar.

Niobium.

Maddin and Chen (1953) tested niobium crystals in tension and compression. The hardening was approximately parabolic and no yield point was observed. However the room temperature axial yield stress was rather high being 15 kg. $mm.^{-2}$ Masters (1962) using purer crystals (room temperature axial yield stress 8 kg. $mm.^{-2}$) found a well pronounced yield point followed by a very low rate of hardening; even at room temperature localised flow made it impossible to compute tensile stresses after ~ 4%

elongation and at low temperatures necking immediately followed yielding. Lindtveit et al (1963) studied the orientation dependence of the stress-strain curve of niobium. Their resolved yield stresses were $2\frac{1}{2}$ - 3 kg.mm^{-2}, yielding was sometimes followed by a stress fall; in one extreme case, for a specimen oriented near ($\bar{1}11$) the drop was $\sim\frac{1}{2}$ kg. mm^{-2} over a shear strain of $\sim$ 0.13. After the yield drop, the graphs rose again usually at an ever increasing rate until just before fracture. Mitchell et al (1963) found, for suitably oriented crystals, three stages of hardening, however they still had a yield point. In stage I the hardening rate was $\sim\mu/10,000$, where μ is the shear modulus, and in stage II, $\mu/600$; this was for testing at room temperature. The hardening rate in stage II, θ_{II} , was temperature independent but the hardening rate in stage I increased with increasing temperature and decreasing strain rate. For their purest material, the room temperature yield stress was about 2 kg. mm^{-2} (resolved), at 77^{o}K the yield stress was $\sim$ 34 kg. mm^{-2} (resolved) but the crystals necked and fractured immediately after yielding.

Tantalum.

Ferriss et al. (1962) studied the temperature and orientation dependence of the stress-strain graph. Their curves usually exhibited a yield point which, for crystals inside the standard triangle, was followed by a low rate of hardening. However, crystals oriented near (001) had a

lower yield stress, no yield point and initially a higher rate of hardening. As the test temperature decreased the strain to fracture decreased, so that at 77°K the stress fell immediately after yielding. Weissmann and Hosakawa (1963) found very large yield drops with tantalum crystals; the subsequent hardening graph was firstly concave upwards and then concave downwards but in both cases the curvature was slight.

Molybdenum.

Chen and Maddin [Chen and Maddin (1951), and Maddin and Chen (1954)] found that over the temperature range, room temperature - melting point, the stress-strain curves showed no yield points and hardening was parabolic. Lawley and Gaigher (1964), found similar hardening from 4.2°K to 300°K . As the temperature decreased the initial hardening rate increased; at 4.2° K twinning sometimes occurred.

Tungsten.

The stress-strain graphs for tungsten crystals are quite remarkable. Rose, Ferriss and Wulff (1962), and Garlick and Probst (1964) both published similar curves for the orientation dependence of the stress-strain graph. The curves for orientations at the corners of the stereogram were very different; the yield stress was highest for the (011) orientation and lowest for the (001). The (011) orientation exhibited a rounded yield drop followed by a low linear hardening rate, the (001) and ($\bar{1}$11) oriented crystals both showed parabolic hardening. The actual

values of yield stress varied between 28 kg.mm^{-2} for (001) crystals to 90 kg. mm^{-2} for (011) crystals.

Rose et al. also studied the temperature and strain-rate dependence of the yield stress and work hardening graphs. For the (001) orientation the yield stress increased from ~28 to ~70 kg. mm^{-2} for test temperatures of 300°K and 77°K respectively, for different strain-rates the yield stress change was even larger; the room temperature yield stress at a strain-rate of 4×10^{-4} sec^{-1} was ~28 kg. mm^{-2}, whilst at 4×10^{-2} sec^{-1} strain-rate the yield stress was ~97 kg. mm^{-2} The rate of work hardening, on the other hand, increased as the temperature decreased but decreased as the strain-rate increased.

II. 2. The Observation of Glide Systems by Means of Slip Lines and Lattice Rotations.

Although the glide direction was always found to be a ⟨111⟩ type, there was no general agreement as to which is the glide plane; wavy slip lines were often observed (Chen and Maddin (1951), Mo; Vogel and Brick (1953), Fe; Maddin and Chen (1953), Nb; Mitchell, Foxall and Hirsch (1963), Nb; Ferriss, Rose and Wulff (1963), Ta; Evans (1964), Nb.)

In work on pure iron Taylor and Elam (1926), (1936), Sestak and Libovicky (1962), and Jaoul and Gonzalez (1961) found slip occurred on the most highly stressed plane in the ⟨111⟩ zone; Barrett, Ansel and Mehl (1937) on the other hand, reported that slip was mostly confined to {110} with

less slip on {112} and {321} . Stein and Gorsuch (1961) found considerable slip on {112} , and Calnan and Clews (1951) and Allen, Hopkins and McLennan (1956) reported that the orientation of the stress axis played a considerable role in determining the slip plane.

Silicon iron alloys containing 3-4% silicon have also been examined extensively. Opinsky and Smoluchowski (1951) found slip on {110} , {211} and {321} planes, however the resistance to slip on the different planes was not the same. Stein and Gorsuch (1961) found crystallographic glide on {211} , but Barrett, Ansel and Mehl (1937), and Hull (1963) reported that slip was mainly on {110} ; in contrast Sestak and Libovicky (1963) reported that the plane, contained in the ⟨111⟩ zone, with the highest resolved shear stress was the slip plane.

Working with niobium at temperatures > 0.5 Tm, Harris (1963) found slip occurred on {110} , {211} or {321} in some cases but not always. Mitchell et al.(1963) found slip on {110} only but Evans (1964), using crystals oriented near (011) (The unit triangle used for reference is always (001), (011) (T11).) found slip on $(\bar{2}11)$. Reid (1965) deforming at 77°K found slip on both {110} and {211} but the slip plane in tension was usually different from that in compression, the sign of the stress apparently having a similar importance as in twinning. Reid also found that in one case the elements of glide appeared to be (110) [100] .

With tantalum Mordike (1961), reported glide on {110}

and {211} planes only, but Ferriss et al. (1962) concluded that slip was on the most highly stressed plane of the ⟨111⟩ zone.

Molybdenum was found by Maddin and Chen (1954) to glide on {110} only but Tsien and Chow (1937) have reported slip on {211} as well.

Garlick and Probst (1964), working with tungsten found slip on {110} and {211} planes; however the slip lines could not be seen until ~10% strain and did not correspond to the most highly stressed {110} and {211} planes. The ratio R, of the resistance to slip on {110} to that on {211} was R = 1.88; with this value {110} should never have occurred.

Models for Non-Crystallographic Glide

Two main models have been proposed to explain glide on planes having high indices.

a) Composite glide on two {110} planes containing the same ⟨111⟩ direction. By 'composite glide' is meant cross-slip on an almost atomic scale.

b) True glide on non-crystallographic planes.

Elam (1935) suggested the composite slip model for β-brass and subsequently for iron. Since then the composite slip model has been supported by Ferriss et al. (1962) for tantalum, and Maddin and Chen (1954), for niobium and molybdenum both groups basing their support on asterism studies. However, Low (1961), believes that since b.c.c. metals have a high stacking fault energy, screw dislocations are not extended in the glide plane and therefore have no

constraint keeping them on the one plane. Sestak and Libovicky (1963), reported that work by Gremperle using an electron microscope did not reveal composite slip and therefore supported the second model. Harris (1963), working with niobium at high temperatures, found from asterism that if the crystal was oriented ideally for glide on a {110} , {211} or {321} plane then true single glide occurred; however between these orientations composite glide on two {110} planes took place.

Allen et al (1956), commenting on the conclusions of Vogel and Brick (1953) supporting true single glide, stated that wavy slip lines favoured the concept of composite glide but that the accuracy of both sets of experiments was insufficient to decide between the two models.

The Effect of Strain.

The change in slip line pattern as slip progresses has not been studied extensively and systematically. Jaoul and Gonzalez (1961) reported that little secondary glide occurred when a double glide boundary was crossed. They use as example their specimen No. 16, which was pulled in tension; its initial orientation was in the $(1\bar{1}2)$ $[\bar{1}11]$ region of the triangle, after 76% deformation the stress axis was well into the $(\bar{1}01)$ $[111]$ region but no slip lines other than those for $(1\bar{1}2)$ were observed. However for initial orientations near double glide boundaries double glide often started immediately. Calnan and Clews (1951) also working with iron, showed for both tension and compression rotations

which correspond to double glide or change of system on crossing double glide boundaries.

With silicon-iron Hull (1963) found that at 77°K , strain tended to thicken existing slip bands rather than form new ones.

Evans (1964) working with niobium could find no change in slip line spacing with strain. Mitchell et al (1963) found that as stage I proceeded, long wavy slip traces broke-up into shorter segments; in stage II these segments shortened still further and the straight slip traces, almost parallel to the slip direction, also shortened.

The Effect of Temperature and Strain Rate.

Andrade, Tsien and Chow (Andrade and Tsien (1937); Tsien and Chow (1937); Andrade and Chow (1940)) found a simple dependence of slip plane on temperature expressed as a fraction of the melting point for Na, K , Mo and α -iron:

T/TM	Plane
0.08 - 0.24	211
0.24 - 0.5	110
0.8	321 *

* Na and K only.

However, this observation has not been supported by other work at least for Mo and Fe.

With tungsten Schadler (1960) found {110} slip at 20°K and 77°K , above room temperature however the {211} plane also became active. Mordike (1961) found in tantalum

deformed at room temperature both {110} and {112} slip planes, he concluded that at low temperatures only {110} planes should operate but above room temperature slip should occur on {110}, {211} and {321} planes. Ferris et al (1962) who found non-crystallographic slip at all temperatures, reported that at 77°K the slip lines were widely spaced and thick whilst at room temperature they were thinner and more closely spaced. In contrast Evans (1964) working with niobium found at low temperatures (~158°K) that the slip lines were so fine that even after high strains they could not be seen with an optical microscope. Hull (1963) deforming silicon iron at 77°K found the slip bands were thick and straight, deforming at 242°K produced finer bands which deviated from the {110} plane by 2° or 3°. Sestak and Libovicky (1963) found in contrast that the slip bands increased in number and fineness as the temperature decreased. Opinsky and Smoluchowski (1951) also working with silicon iron found that the orientation dependence of the slip systems changed with temperature. They suggested that this was due to the temperature dependence of the resistance to slip being different for each plane.

Sestak and Libovicky (1963) deformed silicon iron in bend tests. They concludedthat dislocation velocity had the greatest influence on the crystallography of slip and temperature played an indirect rôle. Slow deformation ($\dot{\varepsilon} = 10^{-6}$ sec.$^{-1}$) at both 77°K and room temperature resulted in slip on the most highly stressed plane of the

appropriate ⟨111⟩ zone; at high strain rates, > 10 sec^{-1}., only {110} slip was observed. Sometimes at 77°K {110} slip occurred but in these cases, twins or fracture acting as stress raisers giving 'fast' dislocations were always the cause.

II. 3. Observations on Etched Surfaces.

A full review on the observation of dislocations by means of etch-pits is given by Amelinckx (1964). Since no etch pit work was carried out for the present thesis, this part of the review will be curtailed.

Etch pits are normally obtained by chemical or electrochemical attack. The orientation of the surface being etched, and the presence of impurities both in the crystal and the etchant are often important when trying to reveal dislocations by this method; ageing to segregate impurity on to the dislocations is also sometimes necessary. In some instances only dislocation nodes and not dislocations etch and therefore it is necessary to prove that each pit represents a dislocation; low angle tilt boundaries can be used for this.

Deformation Patterns.

Etch pits can show nicely the density and distribution of both primary and secondary dislocations; also such phenomena as pile-ups, polygonisation, dislocation multiplication and the growth of glide bands, and the details of débris left behind moving dislocations can be studied. Sometimes the sign of the dislocations can be determined.

Quantitative Observations

By subjecting crystals to a constant stress for a given time Johnston and Gilman (1959) were able to deduce an empirical relationship between dislocation velocity and stress, the velocity being determined from etch pit observations.

$$v = \left(\frac{\sigma}{\sigma_o}\right)^m \qquad \text{..... II. 1}$$

where v is the velocity

σ, the applied stress

σ_o, the stress for unit velocity, and

m, the velocity exponent, a constant for a given temperature.

This relationship though true for low velocities breaks down near the shear wave propogation velocity of the material concerned. By varying the stress and temperature, the temperature dependence of dislocation velocity and the stress-temperature relation (for constant velocity) can be obtained, the latter relation should approximate to that obtained for constant strain rate tests unless there is a large change in the number of mobile dislocations when the temperature is changed.

Disadvantages with the etch pit techniques are:

a) A rather low upper limit to the density of dislocations which can be observed this way;

b) for quantitative work the initial density must be very low since the internal stress field is assumed to be zero

Silicon - Iron

Low and Guard (1959) studied the slip band structure for {110} ⟨111⟩ glide produced by bending. The edge components were in straight arrays but the arrays were not co-planar over long distances. The slip bands revealed by the etch pits associated with screws were very wavy. Since the glide was produced by bending, the strain across the 'edge' face (a {211} plane) varied; this exhibited itself by a thickening of the slip bands rather than by the introduction of extra bands. In sections cut parallel to the primary slip plane, primary dislocations were usually seen as grooves. The edge component of any loop was considerably distorted by the interaction of its stress field with that of other loops; the screw component was long and straight. From these loops, it was estimated that the edge component moved 50-100 μ , and the screw component 3-5 μ . Some of the edge components ended in an etch pit and from this it was deduced that the screw component had cross-slipped.

Stein and Low (1960) measured the velocity of edge dislocations moving on {110} planes as a function of applied stress and temperature over the temperature range 77°K to 373°K . More recently, Stein and Laforce (1965) extended these experiments down to 20°K . The stress dependence of the dislocation velocity obeyed the Johnston-Gilman relation; re-written in terms of applied shear stress, τ , the following values were obtained:

T^{o}	M	$\tau_{x10^{-9}}$ DYNES/cm^{-2}
78	44	3.8
198	38	2.3
298	35	2.0
373	41	1.5
20	450	4

At low stresses there was a linear relationship between log. (velocity) and $1/T^{o}K$ for a constant stress, but this was not true for high stresses. However using this data a plot of resolved shear stress against temperature for a constant velocity, showed the same temperature dependence as the yield and flow stresses. From this Stein and Low concluded that the yield point was associated with unpinned dislocations. Erikson (1962) has found a similar result for slip on a {211} plane.

Niobium

No etch pit work on niobium single crystals has been published. However, Evans (1964a) has developed a technique for revealing dislocations in this metal and has shown examples of pile-ups, hexagonal networks and glide bands in polycrystalline material.

Tantalum

Bakish (1958) has developed a method of revealing dislocations in tantalum not by etch pits, but by pips also produced by etching. However the treatment includes an anneal at

1900°C and is therefore unlikely to be of use in deformation studies.

Molybdenum

Fong Duan and co-workers (1963; 1963; 1964) have developed etching techniques for molybdenum. Apart from etch pits revealing ends of dislocations they have observed tilt boundaries and tilt boundary junctions for ⟨111⟩ type and ⟨100⟩ type dislocations. They verify a one-to-one relationship for etch pits and dislocations by means of the Read- Shockley formula

$$\sum_i \frac{\varrho_i}{\cos\phi_i + \sin\phi_i} = 0 \qquad \text{..... II.2}$$

where, ϱ_i is the dislocation density along the boundary, and ϕ_i the angle between (in this case) [100] and the traces of the sub-boundaries.

Helical dislocations and co-axial prismatic loops were also observed; some of these had $\frac{a}{2}$ ⟨111⟩ Burgers vector but others were thought to be a ⟨100⟩ types.

Tungsten

Schadler (1961), showed that the $CuSO_4$ - Na OH etchant revealed dislocations by etch pits on {100} and {211} planes. Bend tests at 78° K followed by annealing gave good agreement with Nye's formula,

$$\varrho = 1/(R.\underline{b}.\cos\chi_o) \qquad \text{..... II.3.}$$

where ϱ is the dislocation density,

R, the radius of curvature,

$\underline{b}$, the Burgers vector,

and χ_o, the angle between the Burgers vector and the

neutral axis.

These tests also showed a tendency for glide polygonisation but no tendency for ordinary recovery polygonisation.

II. 4. Observation and Geometry of Twinning

Mechanical twinning frequently occurs in b.c.c. metals at deformation temperatures below 77°K and at very high strain rates for room temperature deformation. Some body-centred cubic alloys twin very easily at normal strain rates (10^{-4} sec.$^{-1}$) at room temperature e.g. Mo.-35% Re; Fe-25%Be; but these have too high an alloy content to be considered here.

Smith et al. (1928), Paxton (1953) and Kelly (1953) have studied twinning in α-iron. They all found that twinning was exclusively confined to the system defined in the introduction i.e. $K_1 = \{211\}$; $K_2 = \{211\}$ and $\eta_1 = \langle 111 \rangle$. Barrett (1948) and Allen et al. (1956) both described the atomic model for twinning which is useful in explaining the polarity of the twin systems. Considering only the polarity of the applied stress and not its magnitude, Frank and Thompson (1955) and Allen et al.(1956) divided up the unit triangle into areas giving for each area the permissible twin systems in tension; this division was on the basis of a few twins in a long crystal rather than a complete conversion of the crystal to twin.

In 1953, Cahn working with α-uranium published general conditions which had to be met before twins on different systems could intersect; these are:

a) the traces of the crossing and the secondary twins in the K_1, plane of the crossed twin must be parallel to each other;
b) the direction, magnitude and sign of the shear must be identical in both crossing and secondary twin.

If these conditions are not complied with then the crossing twin will come to a point before crossing. Liu (1963) considered in detail intersecting twins in the b.c.c. structure using Cahn's principles. He concluded that there is a second type of intersection in which the crossed twin is bent and the crossing twin remains straight. In these instances the secondary twin has to be the equivalent of $(55\bar{2})$, (112), $[115]$ or (172, (712) $[\bar{5}11]$.

Reed-Hill (1964) working with magnesium came to several general conclusions which can be applied to all systems.

a) Twin intersections normally involve slip and therefore continuity of the twinning shear vectors is not required for intersection; hence, Cahn's continuity conditions and Liu's corollary conditions are not required.
b) Analyses based on twin intersections should not be used as an independent method of deducing twinning elements.

Orientation Dependence of twinning systems.

There has been little detailed work on the orientation dependence of the twinning systems probably because of the difficulties due to accomodation stresses producing twins on "forbidden" systems. However Hull (1963) has determined the systems operating in silicon iron as the stress axis moves from (001) to (011). The deformation was at 20°K

in tension, at 77°K Hull obtained slip in some regions. In the following ϕ is the angle between the stress axis and (001).

$\phi < 2°$. - Large wide twins on $(1\bar{1}2)\ [\bar{1}11]$, $(\bar{1}\bar{1}2)\ [111]$, $(\bar{1}12)\ [\bar{1}\bar{1}1]$ AND $(112)\ [\bar{1}\bar{1}1]$.

$2° < \phi < 15°$.- With increasing angle, twinning became more restricted to $(1\bar{1}2)\ [\bar{1}11]$ and $(\bar{1}\bar{1}2)\ [111]$.

$15° < \phi < 40°$.- Twinning was prominent only on $(1\bar{1}2)\ [\bar{1}11]$ and $(\bar{1}\bar{1}2)\ [111]$; a few long twins on $(\bar{1}12)\ [1\bar{1}1]$ and $(112)\ [\bar{1}\bar{1}1]$. After 35° occasional twins on $(\bar{1}\bar{2}1)\ [1\bar{1}\bar{1}]$ and $(1\bar{2}1)\ [\bar{1}\bar{1}\bar{1}]$.

$\phi > 44°$. - Prominent twinning on $(1\bar{1}2)\ [\bar{1}11]$, $(\bar{1}\bar{1}2)\ [111]$, $(1\bar{2}1)\ [\bar{1}\bar{1}\bar{1}]$ and $(\bar{1}\bar{2}1)\ [1\bar{1}\bar{1}]$.

The morphology and growth of twins will now be reviewed for the individual metals.

Iron.

Recent papers, Edmondson (1961) and Jaoul and Gonzalez (1961) working with single crystals, and Sleeswyk et al. (1963) working with polycrystalline iron, report typical Neumann bands often on several systems. Jaoul and Gonzalez, and Sleeswyk et al both recorded that one side and one side only of the twins were notched, they concluded that the notches were a surface effect only; Edmondson does not comment but on examination of his photographs revealed notches on both sides of the twins. Sleeswyk and Helle (1961) working with polycrystalline iron found zig-zag twins, i.e. two par-allel,

non-colinear twins joined by a short twin at $\sim 60^{\circ}$.

Silicon Iron

Hull (1960) and (1963) found notches on one side of the twins only. Further investigation revealed that they were always on the highest side of the tilted surface and since in thin crystals the twins passed straight through the crystal, the high edge of the twin on one side corresponds to the low edge on the other. Thus Hull concluded that notches were a surface effect.

Vanadium

McHargue (1960) compressed vanadium crystals at $77^{\circ}K$. The twins obtained were very narrow and notched, however McHargue does not say whether the notches were confined to one side. All twins were on $\{211\}$ planes.

Niobium

McHargue (1962) extensively studied the morphology of twins in niobium crystals. The twins which were on $\{211\}$ planes, were produced by slow deformation at $77^{\circ}K$ or by impact tests at room temperature. At $77^{\circ}K$ profuse chevron twinning was observed, both the amount and type of which were not affected by strain-rate; at room temperature, however, the twins were far fewer in number. Perpendicular to the deformation direction the twins were notched on both sides; in some instances the notches were so large that the twins appeared as a string of diamond shapes joined at the corners. Parallel to the deformation direction the edges of the twins were straight, but inside the twins were many long markings

almost parallel to the edges. Some very fine short twins which were often connected by slip were a surface effect only since they could be removed by polishing ~400 μ off the surface. Sectioning the major twins inside the crystal indicated that the notches were not just a surface effect since they were present here also. Replicas of the twins, when examined in the electron microscope, revealed considerable detail. The long markings inside the twins were regions of untwinned crystal, so too were the notches. The sides of the notches and the ends of the twins were always parallel to $\{110\}$ planes.

Reid (1965) studied twinning at 20°K but only for low strains. After the initial batch of twins were formed further deformation was by thickening of these twins rather than by forming new ones.

Tantalum

Barrett and Bakish (1948) and Anderson and Bronisz (1959) both produced twins in coarse grained tantalum. Barrett and Bakish were only successful at 77°K using impact leading rates, whereas Anderson and Bronisz obtained them at room temperature. Both results were substantially the same, twinning occurred on $\{211\}$ $\langle 111 \rangle$ systems and like niobium both sides of the twins were heavily notched. Further twinning resulted in the thickening of pre-existing twins rather than the formation of new ones.

Molybdenum

Cahn (1955) impact loaded in compression, single crystals

of Molybdenum at 90°K. All twins were of the {211} ⟨111⟩ type and always with the correct "polarity".

Tungsten

Schadler (1960), Wolff (1962) and Koo (1963) have all examined twins in tungsten single crystals. Their results were substantially different. Schadler established that twinning occurred on {211} planes at 20°K and 77°K. These twins were long and thin. Wolff produced twins in both tension and bend tests at room temperature and confirmed that the twin plane was {211} . In these tests both plastic flow and twinning occurred and the twins were always found within a few millimetres of the fracture. The twins were quite long, but discontinuous and they occurred in small packets; they were also very narrow, the widest being ~3 μ . Some twins were notched usually on both sides.

Koo's tests did not produce twins at either room temperature or 77°K, however at 95°K and 178°K twins did form; unlike Wolff's twins these were not associated with fracture but occurred in the micro-strain region.

Notches

As we have seen from the above, the descriptions of notches conflict yet the evidence is strong for both cases. In one case the notches occur on one particular side of the twins and only near the free surface whereas in the other, the notches are on both sides of the twins and are present in internal twins as well. It is possible that they are two separate effects, anyway several explanations have been

forwarded to account for their existence.

Hull (1960) believes that they are due to the twinning partials cross-slipping out to the free surface because of the associated stress relaxation. Sleeswyk et al (1963) put forward an explanation based on the cross-slip of emissary dislocations on {110} , {211} or {321} planes of the same ⟨111⟩ zone as the twin plane. Barrett and Bakish believe that inclusions or pile-ups result in high local stress fields which inhibit local growth of the twin. The notches then grow with the twins. McHargue suggests that twins may be able to grow rapidly in the twin plane but only slowly normal to it, local slip then gives rise to the notches.

Zig-Zag Twins

Recently the only attention given to zig-zag twins has been by Sleeswyk and Helle (1961). They explain the configuration as follows: if a growing twin interupts the transverse growth of a 'newer' faster growing twin which has the same twin direction, on intersection both twins will grow together at the same rate; also transverse growth of the two twins outside the acute intersection angle will cease since the twin dislocations are the same. This gives a 60° 'joint' in the twin, a similar intersection will give the zig-zag twin.

A Critical Resolved Shear Stress for Twinning

A critical resolved shear stress for twinning (CRSST) analogous to that for glide has been suggested. Edmondson (1960) believes his own results and those of Allen et al. (1956) strongly support the existence of such a stress;

Cox et al. (1957) and Biggs and Pratt (1958) also came to this conclusion. The evidence these workers consider to be favourable is,

(i) a low scatter of results,

(ii) the most favourable oriented system produces by far the greatest number of twins.

Vogel and Brick (1953), and Steyn and Brick (1954) also working with iron disagree. Cooper (1965) obtained twins in iron crystals by deforming statically at 77°K and dynamically at 77°K, 195°K and room temperature. For the highest strain rate at room temperature and for all tests at other temperatures the CRSST was the same. However, the dynamic tests at room temperature which still produced twins gave a higher CRSST. Hull (1963) believes that despite their scatter his results support the existence of a CRSST in silicon iron. Reid (1965), on the other hand, working with niobium does not believe that a CRSST exists on a macro-scale. Wolff (1962) quotes the CRSST for tungsten to be ~45 $kg.mm.^{-2}$; this is based on room temperature twinning only.

Evidence of Slip before Twinning

Recently some work has suggested that slip has to occur before a twin can be nucleated, and some theories e.g. Priestner and Leslie (1965) require this to be so. Hamer and Hull (1964), and Worthington and Smith (1965) worked with coarse grained polycrystalline silicon iron which usually twins and fractures at the yield stress.

Hamer and Hull allowed specimens to stress relax below the yield point; sometimes twins occurred during relaxation. Worthington and Smith loaded their specimens to a stress below the yield stress and immediately unloaded; etch pit studies revealed considerable slip, nucleated at the grain boundaries, at stress levels which never caused twinning.

Altshuler (1964) worked with single crystal and polycrystalline iron, though most work was with polycrystals. At certain values of temperature and strain-rate the specimens could either twin or slip. In these instances he found the temperature and strain rate dependence determined from cycling tests, to be the same for both twinning and slip. From these results, Altshuler concluded that the movement of slip dislocations play a direct rôle in twin initiation.

II.5. The Effects of Impurity.

Impurities affect many plasticity parameters and also the mode of deformation in the transition regions. Most papers do not deal with all parameters and the parameters receiving most attention vary from metal to metal. In general removing impurities lowers the yield and flow stresses; the effect on other parameters depends on the nature of the impurity (interstitial or substitutional) though this distinction is rarely made in the literature.

Iron

It is generally accepted that the usual yield point in iron is due to carbon and nitrogen so this will not be reviewed.

Adair and Hook (1962) using polycrystalline iron showed that an additional yield point could be obtained by adding hydrogen. The ageing temperature was 200°K and the testing temperature 120°K, temperatures too low for diffusion of anything but hydrogen to occur; also iron with low hydrogen content did not show a yield point under these conditions.

The removal of interstitial impurities usually aids the formation of twins. Most reviews state that the earlier work, Tipper and Hall (1953), and Low and Feustel (1963), found that impurities promoted twinning. Such statements take no account of the nature of the solid solution formed or of the testing characteristics. In the case of Tipper and Hall, the comparison is made between iron crystals and Fe-4½% Si crystals which twinned more easily. Low and Feustel foundthat carburisation did increase the degree of twinning; however the decarburised material deformed uniformly whereas the carburised iron deformed by a Luders propagation over only 1/3 of the gauge length. Clark and Craig (1952) state that silicon, tin, phophorus and aluminium do promote twinning, however, these elements should form substitutional solid solutions rather than interstitial. Biggs and Pratt, however, using single crystals did find that carbon removal eliminated twinning, which they considered to be caused by a burst of dislocations at the upper yield stress. The following papers support the contention that removal of impurities promotes twinning: Simonsen (1960) rolling zone refined iron at room temperature; Edmondson (1961) comparing

pure iron crystals and those doped with nitrogen; Stein et al (1963) using very pure iron. Rosenfield, Averbach and Cohen (1963) followed the twinning return with room temperature ageing after pre-strain. The ageing time necessary for twinning to occur (on deforming at 77°K) increased with pre-strain.

As has already been said general purification decreases the yield and flow stresses. Papers illustrating this are by Edmondson (1961), Stein (1963), Stein et al. (1963) and Altshuler (1964). Stein also found that the velocity exponent m , when determined from mechanical tests increased with carbon content.

Using iron, decarburised iron and iron nitrogen single crystals, Edmondson (1961), studied the orientation dependence of the ductile/brittle transition line. He found that if the yield stress was raised (no matter how) the range of orientations for brittle fracture increased. The brittleness could not be associated with twinning since when the flow stress was raised by nitrogen addition cleavage occurred without the formation of twins. Biggs and Pratt (1958), on the other hand, found that if twinning was eliminated by decarburisation, brittle fracture was also eliminated.

Stein (1963), and Stein et al. (1963), found that removal of interstitial impurities lowered the temperature dependence of the yield stress; they had tested single crystals of iron containing 5×10^{-3} ppm. carbon which were also

thought to be low in nitrogen. Apart from the lower temperature dependence, this material did not exhibit a yield point nor did it strain-age. However, Stein when testing the same purity material in polycrystalline form did not find that the temperature dependence was lowered but this he concluded was due to hardening of the boundaries by the remaining impurities. Altshuler (1964), using the same purity single crystals provided by Stein, tested at as low as 20°K compared with Stein's lowest test temperature of 77°K . He found that the temperature dependence of both yield and flow stresses was the same as that for relatively impure polycrystalline iron. It now appears (Altshuler 1964a) that the differences in yield stress were largely due to interpretation. Stein considered the smallest deviation from linearity to be the yield stress; Altshuler considered such deviations, when followed by an almost infinite plastic hardening rate, to be due to stress concentrations near the grips etc., and the yield stress to be the stress just after which considerable plastic flow occurs.

Vanadium

Thompson and Carlson (1964) examined the mechanical properties of Vanadium containing various amounts of nitrogen in solid solution. From the activation energy for the yield point return, they concluded that nitrogen was responsible for the yield point. Nitrogen also resulted in maxima in the yield strength and strain

hardening exponent, and minima in the strain-rate sensitivity and elongation, at 400°C when these parameters were plotted against temperature. They also consider that oxygen or possibly carbon could give a yield point in Vanadium.

Niobium

Whilst it may be supposed that the usual yield point is due to nitrogen or oxygen no work confirming this could be found. A yield point due to hydrogen has been confirmed however by the activation energy of the yield point return. (Wilcox and Huggins (1960) and Wilcox, Brisbane and Klinger (1962).)

Leadbetter and Argent (1961) found interstitial oxygen suppressed twinning. McHargue and McCoy (1963) determined the amounts of interstitial necessary to suppress twinning at 77°K. These amounts were 1600 ppm. oxygen, 500 ppm. nitrogen or 150-200 ppm. carbon; hydrogen additions up to ~1000 ppm. however, had no effect. Stiegler, DuBose and McHargue (1964) examined niobium containing 500 ppm. carbon in the electron microscope. The grown in dislocations contained precipitate particles, subsequent deformation at 77°K gave tangles around these locked dislocations rather than the usual arrays. Stiegler et al. therefore supposed that tangle formation suppressed twinning.

Shaw and Sargent (1964) studied stress relaxation in polycrystalline niobium below the yield point. Increasing impurity concentration decreased the relaxation; the exact interaction was not determined but they suggested that

impurity clusters per se or jogs due to forced cross-slip were responsible. Mitchell et al (1963) who obtained three hardening stages in their single crystals found the following effects on purifying by successive zone passes:

a) decrease in the yield stress, the size of the yield drop and the rate of hardening in Stage I;

b) increase in the rate of hardening in stage II.

They could not correllate fracture stresses and strains with the number of zone passes. Leadbetter and Argent (1961), Wellings and Maddin and Christian and Masters found that impurities raised the yield and flow stresses at all temperatures, the temperature dependence however was not affected significantly. The effect of hydrogen on polycrystalline niobium is more complex (Wilcox and Huggins (1960), Wilcox et al. (1962)). The room temperature yield and flow stresses were raised by hydrogen addition but this was due to an increase in k_y, σ_i not being affected (see Hall-Petch eqn.). Above 120°K hydrogen addition raised both yield and flow stress, but below this temperature only the flow stress was raised. With 30 ppm. hydrogen a strain-ageing peak in the flow stress v. temperature graph occurs at 223°K; this was not detected with 10 ppm. hydrogen. At 89 ppm. hydrogen the stress-strain curve was serrated at 295°K.

Wilcox et al. (1962) also found that hydrogen raised the ductile/brittle transition temperature. The effect of strain-rate was unusual since an increase in strain rate

decreased the transition temperature.

Tantalum

Rosenfield and Owen (1963) studied the effects of ~150 ppm. oxygen on the work hardening exponent n ($\sigma = \kappa \varepsilon^n$). They found that n depended on ageing time going through a minimum at 10 min for an ageing temperature of 100°C. The minimum value of n was ~½ initial value and the subsequent rise never exceeded the initial value. Actual values of n depended strongly on test temperature.

Molybdenum

Hartley and Wilson (1963) used polycrystalline molybdenum for studying the impurity locking by the 'yield point return' technique. The activation energy corresponded to locking by oxygen or nitrogen. They concluded that locking was by the formation of micro-precipitates and that carbon, oxygen or nitrogen could be rate controlling depending on the distribution of both precipitates and dislocations.

Lawley, van den Sype and Maddin (1962-3) using multi-pass single crystals found that increased purity lowered both the yield stress and flow stress at all temperatures above ~ 4.2°K. Although ductility was also improved the stress-strain curve was relatively unaffected.

The effect of impurity on the temperature dependence of the yield and flow stresses was also studied by Lawley et al.(1962-3). They found that with increased purity the temperature dependence above ~77°K decreased, whereas below this temperature it increased with the result that at 4.2°K

impurities had no effect on the yield and flow stresses.

Tungsten

Koo (1963) studied the effect of multiple zone passes on the mechanical properties of tungsten single crystals. He found that as the purity increased the incidence of twinning increased, ductility improved and the yield stress decreased.

The residual resistivity ratio $\frac{\rho_{298}}{\rho_{4.2}}$ was $\sim$40,000, which corresponds to only a few atom ppm. in solid solution. Koo therefore assumed that all his impurity was present as precipitate; in comparing his results with those of Wolff (1962) he concluded that small differences in the type of impurity were important. Multiple zone passes eventually removed about 30 ppm. impurity and lowered the yield stress at 77°K by $\sim$28 kg.mm.$^{-2}$; theories of solid solution hardening could not account for the size of this decrease.

Solid Solution Hardening.

Several expressions have been obtained to give the theoretical increase in flow stress due to interstitial atoms.

a) Cracknell and Petch (1955) considered the bowing of dislocations between pinning points whose mean separation was $N^{-\frac{1}{3}}$, where N is the concentration of impurity atoms.

The increase in axial flow stress (assuming ideal orientation) is given by

$$2\tau = \sigma_0 = \frac{N^{\frac{11}{9}}}{(\alpha\mu)^{1/3}\, b^{5/3}} \left[\frac{16A}{\pi} \cdot \ln\left(\frac{1}{2r_0 N^{1/3}}\right)\right] \qquad \text{II. 4.}$$

where σ_0 is the increase in flow stress,

α, a constant ~0.5,

μ, the shear modulus,

$\underline{b}$, the Burgers vector of the dislocations,

A, a constant, between 1.5-3.0 x 10^{20} dynes cm^{-2}

and r_0, radius of obstacle, ~2A.

b) Fleischer (1962) used tetragonal distortion as the basis of his model. For carbon in iron he estimated the increase in flow stress at $0^{o}K$ to be

$$\tau = \frac{F\,V}{\underline{b}.l} = \frac{\mu\sqrt{c}}{10} \qquad \text{.....II.5.}$$

where F is the force/defect/atom volume,

V, the atomic volume/defect,

and l, the spacing between defects.

τ, μ and $\underline{b}$ are the same as in eqn. II.4.

c) Schoek and Seeger (1959) considered that the friction stress should increase due to a Snoek effect. The interaction of the tetragonal distortion around an impurity with a screw dislocation results in there being favoured interstitial sites within the unit cell. As the dislocation moves, the sites which are favoured change and the impurity atoms move to keep in the favoured sites. This puts a temperature independent drag on the dislocations over the temperature range in which the impurity atoms can move in this fashion. The expression obtained by Schoek and Seeger is

$$\tau = \frac{20.5\ A.\ P.}{\underline{b}.a^3} \qquad \text{.....II.6.}$$

where τ is increase in resolved stress,

A, the interaction constant, 1.84×10^{-20} dynes cm^2 for iron.

a, the lattice parameter,

and P, the concentration of interstitials.

II.6. Observations by Transmission Electron Microscopy

Most electron microscopy has been on polycrystals. The observations will be considered under three headings, (a) Miscellaneous (includes annealed and recovered structures), (b) Deformation Structures and (c) Twinned Structures.

(a) Miscellaneous

Carrington, Hale and McLean (1960), and Ohr and Beshers (1963) both working with iron polycrystals observed that inside the grains were sub-boundaries connected by a three dimensional network of random dislocations. After deformation and recovery a similar structure was again observed but with more sub-boundaries, particularly on $\{110\}$ planes. Dislocation interactions within the networks were of the type,

$$\frac{a}{2}\,[111] + \frac{a}{2}\,[\bar{1}\bar{1}1] \longrightarrow a\,[100] .$$

Votava (1963), Lawley and Meakin (1964), and Lawley and Gaigher (1963) found in molybdenum that precipitates punched out interstitial prismatic loops of the type $\frac{a}{2}\langle 111\rangle$; Lawley and Gaigher also found long dislocations stabalised by precipitate. Fourdeux and Berghezan (1962) found similar prismatic loops in niobium and impurities precipitated

onto dislocations have been reported by Stiegler et al. (1964).

Stacking faults have been observed in b.c.c. metals but only if impurity was present. Takeyama and Koepel (1963) found stacking faults and annealing twins in zone melted iron which had been annealed in a hydrogen/argon atmosphere. Lindley and Smallman (1963) observed stacking faults on {211} planes in Vanadium. There have been two reports of stacking faults in niobium; Fourdeux and Berghezan (1960-61) observed them on {211} planes and Segall (1961) observed both stacking faults and annealing twins, however both were in general, on {310} planes. Fourdeux and Berghezan also observed extended nodes in networks. Weissmann et al (1961), reported by Hirschhorn (1963) found stacking faults on {211} planes and extended nodes in tungsten after quenching from 2000°C.

Van Torne and Thomas (1964) found on re-examination of some old foils a transformation had occurred to give an f.c.c. structure of what was probably NbO. They considered that this occurred by firstly ordering of the oxygen atoms to the $(\frac{1}{2},\frac{1}{2},0)$, $(00\frac{1}{2})$ sites, then precipitation of alternating prisms of Nb and Nb O. Heating these foils gave a perfect NbO structure. The habit planes of the precipitate were the 4 {110} planes inclined at $<90^{\circ}$ to the foils; the crystallographic features are:

[001] Nb // [001] NbO and (011) Nb// (111) NbO.

In the bulk material the habit planes were {210} type; this difference is probably due to lack of constraint in the thin foils.

(b) Deformation Structures

Keh and Weissmann (1961) in a review reported that the deformation sub-structure of Fe, Nb, Ta, Mo and W were very similar; tangles which eventually ledto a cell structure being observed. Features such as jogs, super-jogs, strings of loops and elongated loops were frequently seen but pile-ups were never observed. The dislocation density for a given strain was independent of temperature below the temperature of dynamic recovery, but the distribution became more uniform as the test temperature was lowered. The dislocation density was dependent on grain size, being higher as the grain size decreased.

Iron

Carrington et al. (1960) report that tangles eventually giving a cell structure occurred. The attractive junction a $\langle 100 \rangle$ was frequent and considered important from a work hardening point of view. Ohr and Beshers (1964) cold rolled polycrystalline iron, Burgers vector analyses using the invisibility criterion and Frank's network formula confirmed Carrington et al.'s results. In addition they found loop clusters at low strains and all tangles were found to contain two sets of dislocations in the ratio 2 : 1. The primary dislocations were equally shared between the positive and negative signs. The vacancy prismatic loops were of pure edge configuration and lay on $\{111\}$ planes; they were nearly all made up from primary dislocations and were thought to be due to vacancy jogs in screws. Keh (1961)

also rolled polycrystalline iron, his results were very similar to those described in the introduction.

Yamashita and Taneda (1963) deformed flat single crystals in tension, the stress-strain curve was linear up to 0.5 shear strain. Foils were prepared by thinning parallel to the large face rather than sectioning parallel to the slip plane. They observed piled-up groups and a cell structure. At several values of flow stress they measured the number of dislocations per pile-up (a), the length of the pile-up (ℓ), the lateral spacing of the groups (L) and the spacing in the slip direction (S). These parameters together with the dislocation density ρ are tabulated below.

T. kg.mm^{-2}	a	ℓ (μ)	L (μ)	S (μ)	ρ cm^{-2}.
5.3	7	0.43	0.15	0.61	4.5×10^{9}
7.2	12	0.59	0.20	0.55	4.5×10^{9}
8.5	18	0.83	0.20	0.60	9.5×10^{9}
10	-	-	-	-	2.3×10^{10}

However, the published photographs were of poor quality and it was difficult to observe the pile-ups.

Keh (1964) also used flat crystals of iron deformed in tension; again these were thinned parallel to their largest face. Dislocation tangling was observed at the beginning of deformation, this was followed by clustering of dipoles along the primary slip plane traces. Eventually a cell

structure formed, which was not completed until stage III had been reached. If only one slip system operated the cells were elongated but for orientations on stable double glide boundaries the cells were equiaxed. The total dislocation density was a function of flow stress only but the ratio of secondary to primary dislocations depended on orientation. The work hardening rates were related to this ratio.

Low and Turkalo (1962) compressed single crystal cubes of silicon-iron 1% at room temperature. Foils were prepared from slices cut parallel and perpendicular to the slip plane. Long curly screw dislocations containing a large number of jogs were observed. Depending on their size the jogs gave cusps with edge dislocation trails, cusps with no visible trails or acted as pinning points for single ended sources. The edge dislocation trails either broke up into small loops or expanded to provide more slip dislocations.

Vanadium

Edington, Lindley and Smallman (1964) studied the effect on structure of ageing prior to re-deformation in polycrystalline material. After a light ageing, the dislocations freed themselves from their atmospheres and continued to contribute to the deformation. Longer ageing gave strong locking, the 'old' dislocations remained locked and new sources operated in narrow bands often producing dislocations with a different Burgers vector. Edington and Smallman (1964) deformed vanadium in tension. They did not observe a cell structure

and concluded that the deformation was controlled by a fine precipitate. At all temperature between 77°K and 673°K they found the increase in flow stress proportional to the square root of the dislocation density. At 20°K the root of the density was inversely proportional to the root of the grain diamter.

Niobium

Fourdeux and Berghezan (1962) prepared foils of both deformed and annealed polycrystalline niobium. The annealed foils were subsequently deformed in the microscope; pile-ups containing 3 - 6 dislocations were frequently observed in these foils but never in material deformed in bulk. It was concluded that in the bulk material cross-slip occurred preventing the formation of pile-ups. At $< 3\%$ strain the deformation was very inhomogeneous, but as the strain increased the homogeneity and dislocation density increased until at 8% cells were formed throughout the specimen. The cells were usually $\sim 0.5\,\mu$ dia. except when elongated, the length then being as much as $2\,\mu$. Often dislocation interactions producing a $\langle 100 \rangle$ dislocations were observed. Fourdeux and Wronski (1963) and (1964), and Wronski and Fourdeux(1964) used purer polycrystalline niobium. In the first paper they found that at room temperature the edge dislocations were mobile before the macroscopic yield stress. At 77°K, the foils were not reproducible owing to twinning. The tangles and cell structures were similar to those of Fourdeux and Berghezan. The latter two papers examined the effects of

purity and strain-rate. Although purity affected the stress-strain graph the distribution of dislocations was not affected; dipoles, tangles and cells were formed at all purities. The strain-rate did not affect dislocation density but markedly altered the distribution; increasing the strain-rate from $\sim 10^{-4}$ to $\sim 10^{-1}$ sec.$^{-1}$ produced more loops and also short dense walls.

Van Torne and Thomas (1963) also deformed polycrystalline niobium in tension. At the yield stress, they observed considerable cross-slip and multiplication. Throughout the deformation a relationship between flow stress, σ_f , and dislocation density, ρ , correlated well with the stress-strain graph. The grain size dependence of the yield and flow stresses could also be accounted for in terms of dislocation density. The initial dislocation structure had a marked effect on the flow stress. If precipitates stabilisedthe tangles, then a cell structure formed and the following equation described the plasticity:

$$\sigma_f \ (\text{kg.mm}^{-2}) = 8.5 \times 10^{-3} \ \mu \ \underline{b}. \ \rho^{\frac{1}{2}} + \text{constant};\ldots\ldots\text{II}$$

without precipitate the cell structure was absent and

$$\sigma_f \ (\text{kg.mm}^{-2}) = 6.5 \times 10^{-1} \ \mu \ \underline{b}. \ \rho^{1/7} + \text{constant}.$$

Stiegler, DuBose, Reed and McHargue (1963) rolled single crystals of niobium. At relatively low strains a cell structure developed inside the crystal but near the surface, where most deformation occurred, only irregular tangles were observed. At 50% reduction, the cell structure was well developed, but at 80%, the interior of the cells had

filled with dislocations obscuring the original structure.

Molybdenum

Benson, Thomas and Washburn (1963) deformed polycrystalline molybdenum, both in tension and by rolling, at room temperature. At very low strains they observed long dislocations which became jogged and left small loops behind when they moved. Local tangles developed in which the attractive junctions occurred;

$$\frac{a}{2}\ [111] + \frac{a}{2}\ [\bar{1}\bar{1}1] \longrightarrow a\ [100]\ .$$

Even at strains of $< 10\%$ a cell structure had developed with nearly all dislocations in the cell walls. Further strain causedthe cells to sub-divide so that after 50% reduction (by rolling) no clear areas remained. Lawley and Gaigher (1964), deformed in tension single crystals oriented for single slip on $(\bar{1}01)\ [111]$; the deformation temperature was in the range 4.2- 300°K, and the stress-strain curves (see II.1.) were parabolic. Slices parallel to the slip plane revealed long primary screws and secondary dislocations parallel to $[\bar{1}11]$ and $[\bar{1}11]$. The primary screws had a jog density of $10^4 - 10^5$ cm.$^{-1}$ which was considered reasonable assuming they were due to the cutting of secondary dislocations. Lawley and Gaigher expected the jogs to slow the primary screws relative to the edge dislocations and the ratio of screws to edges present should then be inversely proportional to the ratio oftheir velocities. The velocity ratio was not determined for molybdenum but by comparison with tungsten

they considered the 40 : 1, screw to edge, density ratio to be reasonable. As the deformation temperature was lowered the screws became straighter and more uniformly distributed. At 300°K there were fewer secondary dislocations a fact which could not be explained. Dislocation tangling was rare, being restricted to the vicinity of inclusions or locked dislocations.

(c) Twinning

No electron microscopy investigations have been carried out on pure b.c.c. metals deformed by twinning. However two b.c.c. alloys have been studied.

Silicon-Iron

Nishiyama, Shimizu and Kamada (1964), (1965) deformed large grained silicon iron in tension. Inside the twins they observed a mid-rib of tangled dislocations, piled-up slip dislocations in very straight rows were also observed.

Molybdenum 35 atomic % Rhenium.

This alloy which twins readily at room temperature was studied by Ogawa and Maddin (1964). Polycrystalline sheets were deformed in tension at 77°K and room temperature at a strain-rate of $\sim 10^{-4}$ sec.$^{-1}$ Many of their twins were small and were contained within the foil. Some twins were severely stepped, this was interpreted as being due to emissary dislocations; slip inside the twins was always on the $\{110\}$ plane which contained the twinning direction. Fringe contrast, observed in non-coherent boundaries, was explained on a similar basis to stacking fault fringes using the kinematical theory of diffraction contrast.

Fuzziness in the fringe pattern near the centre of the foil was considered due to electron absorption. An oscillation in the intensity of the transmitted beam was found in regions where absorption was prominent and where the twinning dislocations were closely spaced.

II.7. The Temperature Dependence of the Yield and Flow Stresses.

The well known Hall-Petch equation relates flow stress (or yield stress) to the grain size.

$$\sigma_A = \sigma_i + k\, d^{-\frac{1}{2}}$$

where σ_A is the applied stress,

σ_i the friction stress,

k, a constant and

d, the grain diameter.

The '$k\, d^{-\frac{1}{2}}$' term is assumed zero for single crystals, since it is due to the grain boundaries. Except under specialised conditions (see Cottrell 1963) the large temperature dependence of the yield and flow stresses is due to the σ_i term and is thus present in single crystals. The friction stress can be considered as made up from two parts,

$$\sigma_i = \sigma^* + \sigma_s$$

σ_s is temperature independent and is due to e.g. long range stress field of dislocations or temperature independent interactions with interstitial impurity atoms. The σ^* term, often referred to as the effective stress, is temperature dependent and is largely due to the lack of thermal energy available for overcoming short range obstacles

to dislocation glide; there is also a much smaller contribution from the change in shear modulus with temperature.

Brown and co-workers (Brown and Ekvall (1962), and Kossowsky and Brown (1963)) do not agree that the yield and flow stresses are strongly temperature dependent, at least not in iron or molybdenum. From micro-strain work, they concluded that the macroscopic yield stress was really a flow stress at the end of a high linear hardening stage. Though this point of view has been recently supported by Lawley and Gaigher (1964), it is not generally accepted.

Activation Enthalpy and Activation Volume

The thermodynamic treatment of the temperature dependence of the flow stress has been made by many workers. The initial common assumption is that for a singly activated process the strain-rate may be written

$$\dot{\gamma} = \nu \exp. \left(- \frac{G}{kT}\right) \quad \ldots\ldots\ldots\ldots \text{II.8a}$$

where, $$\nu = \nu_o \, NA\underline{b} \quad \ldots\ldots\ldots\ldots \text{II.8b}$$

and $\dot{\gamma}$ is the shear strain-rate,

G, the free energy of activation,

k, Boltzmann's constant (8.631×10^{-5} eV/ ^{o}C.)

T, the temperature ^{o}K,

N, the number of possible activation sites,

A, the area swept out per successful activation

$\underline{b}$, the dislocation Burgers vector,

ν_o, the attempt frequency.

By differentiation and using G = H - TS, where H is the enthalpy and S the entropy of activation, the following expressions may be obtained:

at constant strain-rate,

$$H_{\left(\frac{\dot{\gamma}}{\nu}\right)} = \frac{-kT^2\left(\frac{\partial \tau}{\partial T}\right)_{\left(\frac{\dot{\gamma}}{\nu}\right)}}{\left(\frac{\partial \tau}{\partial \ln\left(\frac{\dot{\gamma}}{\nu}\right)}\right)_T} \qquad \text{..... II 9.}$$

and at constant stress,

$$H_{\tau^x} = -k\left(\frac{\partial \ln\left(\frac{\dot{\gamma}}{\nu}\right)}{\partial T}\right)_{\tau^x} \qquad \text{..... II.10.}$$

where τ^x is the effective stress.

The equations can also be written in terms of the axial stress and strain since in eqn. II. 9 the stress term appears in both numerator and denominator and the strain term in both equations is inside the ' $\ln$ ' bracket.

The activation enthalpy was assumed to be H = H (τ^x, T) but the change in shear modulus was neglected and the frequency factor assumed to be independent of strain-rate, temperature and stress. The detailed second order terms vary with the functional assumption of the activation enthalpy. Basinski (1957) and (1959) assumed H = H ($\frac{\tau}{\mu}$) where μ is the shear modulus, and ν and S to be temperature independent. Conrad and Wiedersich assumed H = H (τ^x, T), where τ^x was given by $\tau^x = \tau_A - \tau_\mu$, τ_A being the applied stress and τ_μ, the long range internal stress which is temperature dependent only in so far as the shear modulus is temperature dependent. Further discussion of the assumptions made and the validity of the thermodynamic approach can be obtained from the following papers:

Baskinski and Christian (1960), Conrad (1961) and (1963), Mordike and Hassen (1962), Conrad and Hayes (1963), Osbourne (1963), Gregory, Stroh and Rowe (1963), Christian and Masters (1964), Li (1965) and Schoek (1965).

The activation volume v can be defined as the negative stress derivative of the activation free energy at constant temperature i.e.

$$v = -\left(\frac{\partial G}{\partial \tau^*}\right)_T \qquad \text{..... II.11.}$$

On differentiating eqn. II.8. we get

$$v = \frac{kT}{\left(\frac{\partial \tau^*}{\partial \ln\left(\frac{\dot{\gamma}}{\nu}\right)}\right)_T} \simeq \frac{2kT}{\left(\frac{\partial \sigma^*}{\partial \ln\left(\frac{\dot{\gamma}}{\nu}\right)}\right)_T} \qquad \text{..... II.12}$$

Often v is not defined this way but from the work done by the stress in a successful activation ($\tau^* \underline{b}$ A). This gives $v = \underline{b}.A$ where $\underline{b}$ and A are as defined above. A full discussion and interpretation of theactivation volume has been given by Conrad (1961) and Christian and Masters (1964).

Mechanisms Controlling the Yield and Flow Stresses.

Conrad (1961) and (1963), has considered most of the mechanisms suggested to explain the temperature dependence of the yield and flow stresses.

(1) Breaking away from Cottrell atmospheres. (Cottrell 1957)

(2) Intersection of glide and forest dislocations (Conrad (1961) suggested as a possibility)

(3) Cross-slip. (Brown and Ekvall (1962))

(4) Non-conservative movement of jogs in screw or mixed dislocations producing vacancies or interstitials (Schoek 1961)

(5) Overcoming interstitial precipitates. (Mordike and Haasen (1962))

(6) Overcoming the Peierls-Nabarro stress. (Basinski and Christian (1960) Conrad and Hayes (1963), and others)

(7) Overcoming the interaction of dislocations with impurity atoms. (Stein et al. (1963))

Apart from the last mechanism, which was critically appraised by Christian and Masters (1964), Conrad discussed and listed major objections to most of the above models.

(1) Since at low temperatures, the processes of yielding and flow have the same values of frequency factor, activation enthalpy and activation volume, they are likely to be controlled by the same mechanism which must be concerned with 'free' dislocations. Hence Cottrell locking cannot be rate controlling.

(2) (i) The experimental activation volume is too small;

(ii) the activation volume should decrease with strain.

(3) Activation enthalpy and volume for yielding and flow are the same as for the mobility of edge dislocations, which cannot cross-slip. The value σ_E which Brown and Ekvall consider to be the true yield stress is not accepted by Conrad (or by Christian and Masters) to be the stress necessary to move dislocations at the applied strain-rate. Conrad gave two possible explanations for σ_E which may also explain the spectrum of activation energies found by Chambers (1962) for creep of tantalum at strain-rates in the 10^{6} - 10^{11} sec^{-1} range;

(a) the motion of specific dislocations located in favourable stress fields,

(b) lateral motion of single kinks or jogs in screws.

Both of these mechanisms would soon be exhausted and then the stress would rise in order for (true) flow to begin.

(4) (i) Activation enthalpy and volume are independent of structure,

(ii) Activation enthalpy and volume for yielding and flow are the same as that for the mobility of edge dislocations which do not move non-conservatively.

(iii) Another objection, not raised by Conrad, is that at the temperatures concerned diffusion is at an almost negligible rate. The process is not thermally activated since the point defects remain in the crystal.

(5). (i) Activation enthalpy and volume are independent of impurity content and the quantity of precipitate,

(ii) the effective stress decreases with increase in quantity of precipitate.

(6) The Peierls-Nabarro force theory has been put forward in several forms. Firstly Heslop and Petch (1956) suggested that the friction stress was temperature dependent because the dislocation width varied with temperature. However this does not explain the strain-rate dependence of the friction stress. This objection has also been levelled against the theories of Dietze (1952) and Kuhlmann-Wilsdorf (1960) which

proposed an intrinsic temperature dependence of the Peierls-Nabarro force (Christian and Masters (1964)).

The current Peierls-Nabarro force theories consider that the force is overcome with the aid of thermal energy. (7). The evidence for this theory was not available at the timeof Conrad's review and consequently was not considered by him. The evidence and Altshuler's contradiction has already been given in section II.5. under iron. However accepting the results of Stein et al. as correct, Christian and Masters who considered quantitatively the resistance due to impurity interaction, cannot accept that impurities give rise to the high flow stress at $0^{\circ}K$. C.+ M. consider a realistic interaction energy to be 0.5 eV and at $0^{\circ}K$ this must be equal to the work done by the stress which is $\tau^{x}\,\underline{b}\,\ell\,d$, where τ^{x} is the local shear stress, ℓ, the separation of the pinning points and d, the distance over which the force is effective.

For $\tau^{x} = 50 kg.mm^{-2}$, $\underline{b} = 2.5\,\text{Å}$, $\ell d = 65\,\text{Å}^2$ so if $d = \underline{b}$ then ℓ is only 26 Å (~10 atomic distances) which since the dislocation cannot bend between such closely spaced obstacles requires ~10 atomic % impurity. The impurity content requirement would be greatly reduced if d was much smaller; if 100 ppm. impurity were sufficient to give the observed yield stress of ~50 $kg.mm^{-2}$, then assuming the dislocations could bend in the glide plane, $\frac{b}{\ell} = C^{\frac{1}{2}}$, where C is the atomic

concentration of impurity, this give ℓ = 100b and d = 0.26 Å. However for 0.01 ppm. impurity this gives a contribution to the flow stress at 0°K of only 0.5 kg.mm^{-2}. and even at 77°K Stein et al. observed an increase of ~6kg.mm^{-2} over the room temperature yield stress. Christian and Masters therefore concluded that at 0°K the high flow and yield stresses were due to the Peierls-Nabarro force but impurity atoms could modify the activation process at intermediate temperatures.

Models for Overcoming the Peierls-Nabarro Force

Three models for overcoming the Peierls stress have been suggested and two of these have been modified since they were first introduced.

(1) Seeger-Donth Oscillator Model (Seeger (1956), Donth (1957))

(2) Lothe-Hirth Quasi-equilibrium Model. (Lothe and Hirth (1959)

(3) Dorn-Rajnak Model. (Dorn and Rajnak (1964)).

All these models are basicly (A1) similar in that they deal with sideways motion of kinks. If a dislocation is lying along a close-packed direction in a crystal, its energy per unit length is a periodic function of its position, y, with respect to the crystal, where y is normal to the dislocation line. (Peierls 1940). The energy per unit length can be expressed as a Fourier series:

$$E_{(y)} = E_0 + E_1 \cos.\frac{2\pi y}{a} - E_2 \cos.\frac{4\pi y}{a} + \ldots \text{II.1}$$

It is often assumed that $E_{n+1} \ll E_n$ and so the higher terms are then neglected; this gives maximum and minimum energies of $E_0 + E_1$ and $E_0 - E_1$ respectively. The Peierls

stress, the minimum stress necessary to lift the dislocation from one energy valley to the next without any thermal or quantum mechanical aid, is then given by

$$T_p = \frac{2\pi E}{a.\underline{b}} \qquad \text{..... II.14.}$$

where T_p is the Peierls stress,

$\underline{b}$ the Burgers vector

and a the period. (often equal or simply related to $\underline{b}$)

Dislocations lying approximately parallel to a close packed direction contain kinks which lie across the Peierls barriers. Under the action of a positive applied stress the kinks will glide so that the dislocation moves in the positive sense. The formation of kink pairs by thermal vibrations will also be influenced in thesame sense by the applied stress; kinks, in a pair, attract each other and with no applied stress glide together and annihilate. However, a positive applied stress will tend to separate "positive" kink pairs and since the attraction between kinks falls off with (the square of the) distance for a given stress, there is a critical separation of the kinks.

As has been said, the models are similar in that they all consider the motion of kinks, they differ in their methods of calculating the rate parameters i.e. the activation energy and the pre-exponential factor. These models will now be described qualitatively.

(1) Seeger (1956) discussed the oscillation of a dislocation line lying in the Peierls valley, with an energy approaching

$2H_k$ which is the energy necessary to form a double kink. Donth (1957) considered how an oscillator with initially low energy could accept energy from thermal vibrations so that eventually it would have energy $\sim 2H_k$. At low stresses, the activation energy $H \simeq 2H_k$ and the frequency of kink formation ν is given by

$$\nu = \nu_0 \exp\left(-\frac{H}{kT}\right) \quad \ldots\ldots\ldots\ldots \text{II.15.}$$

where ν_0 is a temperature independent frequency.

(2) Lothe and Hirth (1959) assumed a quasi-equilibrium concentration of double kinks in the critically activated state. The number of such kinks was computed from the ratio of the partition functions for the critically activated and the normal states. The double kinks were assumed to diffuse out of the critical configuration rather than pass the saddle-point with the average thermal velocity. Seeger and Schiller (1962) modified this theory to take account of long range kink-kink interactions.

Jøssang, Skylstad and Lothe (1963) reconsidered both the above models. The Lothe-Hirth model gives an absolute rate of activation but is limited in application to steady-state conditions. The oscillator model suffered in that there was no precise determination of the number of unactivated oscillators and that therefore the pre-exponential in the rate equation was uncertain. From a revised Donth diffusion treatment they were able to calculate a pre-exponential in the rate equation which agreed with statistical mechanical

calculations; they also concluded that quasi-equilibrium theories for overcoming the Peierls stress were still applicable.

(3) The Dorn-Rajnak model was designed to overcome the limitations they considered to be present in theother two theories. The Seeger-Donth model was unsatisfactory since it was only applicable when small effective stresses were operating (i.e. $\tau^* \ll \tau_p$); this was because the kink width is considered constant, which is clearly untrue for small separations. They consider that quasi-equilibrium models are again only applicable at low stresses and so neither theory is useful at low temperatures.

Dorn and Rajnak based their approach on the line energy concept of a dislocation and on a suggestion by Friedel (1963) that the interaction between kinks can be expressed in terms of the change in line energy as the kinks approach each other. They calculated the saddle-point free energy required to nucleate a pair of kinks, as a function of the effective stress. The frequency of nucleation of kink pairs and the annihilation of kinks was formulated to give the yield stress as a function of temperature and shear strain-rate.

Seeger's final equations for the variables and parameters discussed are:

<u>Activation energy,</u>

$$H = H_K \left[1 + \frac{1}{4} \ln\left(\frac{16\,\tau_p}{\pi\,\tau^*}\right)\right] \qquad \text{.....II.16.}$$

single kink energy, neglecting En for $n \geqslant 2$,

$$H_K = \frac{2a}{\pi} (E_0 E_1)^{\frac{1}{2}} \qquad \text{.....II.17}$$

the pre-exponential term,

$$V_0 = \frac{V_t}{a}\left[\frac{E_1+4E_2}{E_0}\right]^{\frac{1}{2}} \qquad \text{..... II.18}$$

Where V_t is the shear wave velocity in the material concerned, all other symbols are given in the text.

II.8 Theories of Work Hardening.

Nearly all theories of work hardening have been for metals with close-packed structures. The early theories predicted parabolic hardening which then was the observed shape of the stress-strain graph. Later, when hardening in f.c.c. crystals was observed to be in 3 stages, two of which were linear, linear hardening theories were developed. It is only recently that similar three stage hardening has been observed in b.c.c. metals and as yet no attempt has been made to make these theories compatible with the peculiarities of this structure.

The volume of literature on work hardening is very large and no attempt will be made to detail it here. Two comprehensive reviews have been published recently (Clarebrough and Hargreaves (1959), and Nabarro, Basinski and Holt (1964)) from which some of the information in this sub-section is taken.

Parabolic Hardening Theories.

(i) Taylor's Theory

This was the first dislocation theory of work hardening. (Taylor (1934)). Slip was considered to occur almost

homogeneously throughout the crystal by the separation of positive and negative dislocations. Due to the interaction of their stress fields the dislocations stopped within the crystal so that a 'superlattice' array of positive and negative dislocations was built up. The back stress from these arrays prevented the new dislocations from moving at the old value of applied stress and so the crystal work hardened. Taylor further assumed that the dislocation spacing in the slip plane was equal to the spacing between these planes, and obtained the following expression

$$\tau = k \mu \left(\frac{b \gamma}{L}\right)^{\frac{1}{2}}$$

where τ is the shear stress,

μ, the shear modulus,

$\underline{b}$, the Burgers vector,

γ, the shear strain,

L, twice the slip distance, and

k, a constant.

The major arguments against this theory have been listed by Cottrell (1953) as,

(a) a uniform superlattice of dislocations is not compatible with the experimentally observed heterogeneities such as slip bands and secondary slip;

(b) a pair of arrested dislocations is not a barrier to slip since although the attraction between them is strong other dislocations can force them to move as a pair;

(c) three stages of hardening have now been observed and therefore parabolic hardening theories are inadequate.

(ii) Mott's Parabolic Theory.

Mott (1952) proposed a parabolic hardening theory which would account for slip lines. It was assumed that each Frank-Read source emitted dislocations which formed a pile-up against a sessile dislocation. Each piled-up group consisted of either all positive or all negative dislocations and to prevent them running back to their sources on removal of the applied stress, sessile interactions between the edge components of the primary dislocations with the secondary dislocations was supposed. These secondary dislocations were formed in order to relieve the stress near the head of the pile-up. If the pile up separation in the glide plane is $2L$, and the distance between glide planes x, then the density of groups is $\frac{1}{xL}$, and the mean distance between them $(xL)^{\frac{1}{2}}$.

The mean stress at the head of the pile-up is given by

$$\tau_i = \frac{\mu n b}{2\pi (xL)^{1/2}} \qquad \text{.....II.20}$$

The plastic strain γ is the product of the density of pile-ups times the slip distance times the effective slip vector i.e. $n\,b$,

$$\gamma = \frac{n b}{x} \qquad \text{.....II.21}$$

and combining eqns. II.21 and II.20.

$$\tau_i = \frac{\mu}{2\pi}\left(\frac{n b \gamma}{L}\right)^{\frac{1}{2}} \qquad \text{.....II.22}$$

thus the hardening is parabolic.

Mott further assumed that a source might operate dynamically once the first loop had been emitted until the back stress

stopped the source operating, this gave

$$\tau_i = \mu \left(\frac{b\gamma}{2\pi\ell}\right)^{\frac{1}{2}} \qquad \text{.....II.23}$$

where ℓ is the source length.

Again this gives a parabolic relationship between stress and strain so long as ℓ is constant. However Mott pointed out that this was unlikely since the longer sources should operate first.

Stage I (Easy Glide) Hardening

Theories of easy glide hardening have been rather tentative. Mott suggested that most dislocations slipped out of the crystal during this stage. Koehler (1952) considered easy glide to be an exhaustion process, the longest sources operating first and when these were stopped by the back stress, shorter sources requiring a higher applied stress operated. Kuhlmann - Wilsdorf (1962) suggested that easy glide was a process in which the crystal became filled with slip dislocations.

The observation of micro-slip at low strains led Mott to propose that each source could only give a limited amount of slip before the back stress stopped it operating. This required many more sources than was supposed for his parabolic hardening theory. Mott obtained a linear relationship between stress and strain, the rate of hardening being inversely proportional to the slip distance; if the slip distance was about the same as the crystal diameter then the correct rate of hardening was obtained.

From slip line observations, Seeger, Mader and Kronmuller (1963) proposed a theory to explain the hardening rate in easy glide of f.c.c. crystals and for low temperature hardening in h.c.p. crystals. They assume the density of sources N, is constant and given by,

$$N = \frac{1}{L_1 L_2 X} \qquad \text{.....II.24}$$

where L_1, is the edge slip length of the loop,

L_2, the screw slip length,

and X, the slip plane spacing.

As the external stress rises, the sources emit more dislocations, each dislocation moves a certain distance before it is held up by, say, the stress field of another dislocation on a parallel plane. In order to pass this obstacle the dislocation will have to wait until the rest of the crystal hardens sufficiently for its own source to emit more dislocations. The resulting stress multiplication will then be sufficient for further glide to occur. Seeger et al. obtained the following expressions.

$$\tau = \tau_0 + \frac{\mu b n}{2\pi \sqrt{R_0 L_2}} \qquad \text{.....II.25}$$

$$\theta = \frac{8\mu}{9\pi}\left(\frac{x}{L_2}\right)^{3/4} \qquad \text{.....II.26}$$

where τ, is the flow stress,

τ_0, the critical resolved shear stress,

n, the number of dislocations emitted per source,

R_0, the average distance between dislocation sources,

and θ_1, the rate of work hardening.

This theory has been criticised by Nabarro et al. (1964); they state that although they are unable to follow the details of the model, any model in which the slip distance is determined by interaction with dislocations from other sources, randomly arranged throughout the crystal, must have an inverse relationship between the slip distance and the density of sources. In the model of Seeger et al the slip distance is proportional to the square root of the source density.

The end of easy glide

There is no general agreement as to how easy glide ends. Koehler believes it ends when all the easy to operate sources are exhausted; often secondary slip is suggested as the cause, if so it must be produced by stress concentration since the macroscopic resolved shear stress is rarely sufficient.

Seeger et al. (1957) consider that in f.c.c. crystals secondary and primary dislocations interact to produce Lomer-Cottrell locks; they further suggest that these locks will explain the effects of temperature and orientation on the extent of and hardening rate in easy glide.

The extent of easy glide is often found to be inversely proportional to the diameter; adherent surface films also shorten this stage, it may be therefore, that the end of easy glide is strongly connected with dislocation interactions near the surface.

Stage II, Rapid Linear Hardening.

The theories of Stage II hardening in f.c.c. crystals are very numerous. There are some important differences between

b.c.c. and f.c.c. crystals which clearly prevent the application of many of these theories.

(i) Wavy slip lines, which are observed at all but the lowest strains, indicate that cross-slip of screw dislocations is fairly easy. In f.c.c. metals cross-slip is not usually observed until stage III is reached.

(ii) At room temperature, at least, the incremental stress change for a given step change in strain-rate is independent of strain except perhaps at very low strains (see Basinski and Christian, Christian and Masters). This means that the thermal component of the flow stress is independent of strain and that the work hardening is due to a long range stress field. In f.c.c. metals there is dispute over the results of strain-rate change work. Cottrell and Stokes observed that the ratio of the stress increment to the flow stress i.e. $\frac{\Delta\sigma}{\sigma}$ was constant and they have since been supported by Basinski, and Hirsch and co-workers; however, Seeger and co-workers claim that the 'Cottrell-Stokes Law' is, in general, not true except towards the end of linear hardening.

(iii) B.c.c. metal crystals have a high stacking fault energy, and the glide dislocations are therefore not extended. Dislocations in f.c.c. crystals are often seen in the electron microscope to be extended.

Pile-up theories of hardening require that the dislocations should not cross-slip and this usually means that they are extended in the glide plane, hence observations

(i) and (iii) will exclude these theories . However if the pile-ups interact with secondary dislocations to form tangles, the stress field of the tangles may be equivalent to that of the pile-ups so that the hardening is the same.

The jog theory of Hirsch and Mott required the jogs in the glide dislocations to be extended. In order to move conservatively, thermal activation was required, this theory is therefore not in keeping with observations (ii) and (iii).

Intersection with forest dislocations can produce jogs in either or both of the crossing dislocations. Since a jog of length b is a piece of dislocation line with the same length, the energy of a jog u_j is often given as $\sim \mu b^3$, Saoda (1963), however quotes Friedel as having calculated the jog energy as $\sim \frac{\mu b^3}{30}$. The jog is created in $\sim$ one jump of the dislocation and since this is small it is often assumed to be thermally activated, the activation energy u being given by

$$u = u_j - \tau b^2 \ell \qquad \text{.....II.27}$$

where ℓ is the spacing of the forest dislocations along the glide dislocation, and u_j is the energy to form a jog which has been given above. However since the jog is a permanent feature and exists after the 'activation' all the work for its crea-tion must be done by the applied stress and hence if the creation of jogs is a thermally activated process the 'u_j' term in eqn. II.27 must be larger than the jog energy. In view of this dispute forest theories of hardening will not be described neither will the attractive junction theory

of Saada (1963) since part of the hardening is based on jog creation.

Theories which will be described are listed below.

(1) The Kuhlmann-Wilsdorf (1962) theory.

(2) The modified long range stress theory of Seeger. (Seeger et al. 1963)

(3) The tangle theory of Hirsch. (Hirsch 1963, 1964).

(1) The Kuhlmann-Wilsdorf Theory.

Kuhlmann-Wilsdorf (1962) summarised her theory of stage II hardening as follows.

(i) Throughout the stage a quasi-uniform dislocation distribution exists which changes in scale but not in character.

(ii) The average dislocation density, ρ is connected to $\bar{\ell}$, the average length of dislocation which can move coherently, by

$$\rho = m \bar{\ell}^{-2} \qquad \text{.....II.28.}$$

(iii) Work hardening is mainly due to an increase in dislocation density and therefore a decrease in $\bar{\ell}$. This gives the temperature independent part of the flow stress as

$$\tau_\ell = \frac{\mu b}{\pi \bar{\ell}} \qquad \text{.....II.29}$$

(iv) Dislocation loops spread until stopped by other dislocations; only a fraction, $\frac{1}{\alpha}$, of all dislocations can block the progress of any given loop.

(v) Because of mutual annihilation of loops, only a fraction, β, of any new loop is added to the total dislocation content.

From the above assumptions and arguments, Kuhlmann-Wilsdorf calculates the work hardening rate to be

$$\theta_{II} = \frac{\mu}{K} = \frac{\beta \mu}{8\pi\alpha} \qquad \text{.....II.30}$$

Since only dislocations nearly parallel to each other can stop each others movements, α is estimated to be $3 \leq \alpha \leq 15$. β is thought to vary between $\frac{1}{4}$ and 1; however the variations in α and β are such that $\alpha/\beta \simeq 12$, this gives a value of $K \sim 300$. The hardening is principally due to a shortening of the source length (eqn. II.29), which is not a thermally activated process, the Cottrell-Stokes Law is explained separately on the basis of tangle formation and dislocation intersection. Since both $\bar{\ell}$ and the distance between intersections depend on the dislocation density, the ratio of the short range to the long range contribution to the flow stress is constant.

(2) Seeger's Long Range Stress Theory.

Originally this theory was based on pile-ups, in its most recent form, reviewed by Seeger, Mader and Kronmuller (1963), the pile-up is incorporated in a dislocation tangle.

It is assumed that obstacles are formed throughout stage II, their formation is dependent on secondary glide but this is the only important role of secondary dislocations.

The relation between slip distance and strain, γ , was experimentally determined by Mader (1963),

$$L_1 \simeq 2 L_2 = \frac{2 \Lambda_2}{\gamma_s} \qquad \text{.....II.31.}$$

where L_1 is the slip distance of an edge dislocation,

L_2 the slip distance of a screw dislocation,

γ_s the shear strain in stage II

and Λ_2 is a length parameter defined by the equation.

The number of dislocations n, emitted from one source is assumed to be constant and independent of strain, and since the slip distance decreases with strain, further strain must be due to an increase in the number of sources, N,

$$d\gamma = L_1 L_2 n \, .\underline{b}. \, dN$$

Substituting from eqn. II.31 for L_1 and L_2, and integrating,

$$N = \frac{\gamma_s^3}{6 n \underline{b} \Lambda_2^2} \qquad \text{.....II.32.}$$

To calculate the passing stress for the first dislocation from a new source the following are assumed;

(i) the dislocations in a neighbouring, parallel, non-coplanar slip zone act as one dislocation with a Burgers vector n $\underline{b}$, where n is the number of excess dislocations of one sign;

(ii) the extension of each group is of the order of the group separation;

(iii) the distance between these groups is approximately equal to the source separation Ro; Ro is given by

$$Ro = \frac{1}{\sqrt{NL_1}} \qquad \text{.....II.33}$$

(iv) the first dislocation loop, which experiences a higher opposing stress than the subsequent loops, is assumed to glide a distance $\sim$ Ro before being held up.

Using these assumptions, the stress necessary to overcome the opposing stress field is given by

$$\tau_G = \frac{\alpha \mu n b}{2\pi R_o} \qquad \text{.....II.34.}$$

where α is a constant between 0.8 and 0.9 whose value depends on the detailed dislocation arrangement.

With a stress τ_G , the source can emit (n - 1) more loops which then glide distances L_1 and L_2 until they reach an insurmountable obstacle.

From eqns. II.31, II.32, and II.34, the rate of hardening $\theta_{II}\left(= \frac{\tau_G}{\gamma_s}\right)$ is obtained,

$$\theta_{II} = \frac{\alpha}{2\pi}\mu\sqrt{\frac{n\,b}{3\,\Lambda_2}} \qquad \text{.....II.35.}$$

Seeger et al. (1963) believe that for any metal or alloy, the ratio $\frac{n\,b}{\Lambda_2}$ is substantially constant, since θ_{II} is usually $\sim \frac{\mu}{300}$. They further extend their arguments to show that theoretically $\frac{n\,b}{\Lambda_2}$ should be constant.

If the stress on a source is τ_Q and

$$\tau_Q = \tau_A - |\tau_i|$$

where τ_A is the applied shear stress and τ_i the long range internal stress, then the source stops operating when the back stress τ_B equals the forward stress i.e.

$$\tau_B = \tau_Q = \tau_A - |\tau_i| \qquad \text{.....II.36.}$$

when the applied stress is removed, the loops will return to their source unless $\tau_i \gg \tau_B$ therefore

$$\tau_i = \beta\,\tau_A \qquad \text{.....II.37.}$$

where $\beta = \frac{1}{2}$.

But since $\tau_B\left(= \beta\,\tau_A\right) = \frac{\Pi}{2}\frac{\mu\,n\,b}{L} \qquad \text{.....II.38.}$

where L is the slip distance $\left(= \frac{\Lambda}{\gamma_s}\right)$ and therefore

$$\tau_A = \frac{\pi}{2\beta} \frac{\mu n b \gamma_s}{\Lambda}$$

and,

$$\theta_{II} = \frac{\alpha^2 \beta}{6\pi^3} \frac{\pi n b \mu}{2\beta \Lambda} \qquad \text{.....II.39.}$$

From eqns. II.35 and II.39, eliminating Λ, n and b,

$$\theta_{II} = \frac{\alpha^2 \beta}{6\pi^3} \mu \qquad \text{.....II.40.}$$

(3) The Tangle Theory of Hirsch

This theory has been described by Hirsch (1963),(1964). Hirsch first outlined the physical principles on which his theory is based.

At the end of Stage I long obstacles at the end of the slip lines block the dislocations almost all the way around the source. As the dislocations agglomerate against these obstacles the resolved stress on the secondary systems builds up to a critical value at which profuse secondary slip occurs. During the transition stage, secondary slip spreads throughout the crystal raising the flow stress. At the start of stage II there exists a uniform distribution of obstacles which are able to block the slip lines all the way around.

During stage II, an increment in stress produces a complete new slip line; the dislocations glide until stopped by an obstacle, around which, the stress builds up on the secondary systems until relieved by glide. The secondary dislocation slip distance is small, so that although the secondary density is high, the secondary strain is small; also by remaining near the obstacles the dislocation

distribution stays non-uniform. This secondary glide terminates the life of the source. The total flow stress is controlled by (i) the elastic interactions with forest dislocations (ii) jogs (iii) the effective source length; however the relative contributions from these hardening mechanisms is not determined by the theory. The long range stress is not considered to harden the crystal since slip is considered to occur where this stress aids the applied stress.

For simplicity Hirsch assumed square loops of side 2L, M obstacles $cm.^{-2}$ of radius R and that new sources were near to old obstacles. The blocking condition is,

$$2\,MRL = 1 \qquad \text{.....II.41.}$$

Old slip lines are able to block if their length $2L^1$ is greater than the new slip line length 2L. However for a new obstacle to form, the pile-up must have the same sign as the old obstacle since if they are of opposite sign, the two regions of secondary slip overlap. (secondary slip only occurs on one side of the pile-up.) In a small stress interval dN sources operate, the obstacle density is given by,

$$M = 2 \int_{L_o}^{L} (L' - L).\, dN \qquad \text{.....II.42.}$$

where L_o is the slip line length at the start of stage II which for practical purposes is assumed infinite.

The obstacle size is difficult to define since it is stress dependent. Secondary slip has occurred throughout the crystal during the transition stage so that sources for

more slip are readily available. At the start of stage II the secondary slip extends over radius a_s which is equal to the obstacle spacing D_o. However a_s is not the size of the obstacle, this size is estimated from the amount of secondary slip which occurs and Hirsch considers the radius of the obstacle R, to be given by

$$R \sim \tfrac{1}{4} D \qquad \text{.....II.43.}$$

where D is the obstacle spacing throughout stage II.

Flow Stress - Since the obstacles are at a distance D, the maximum source length is $\sim D$; the flow stress τ, is then

$$\tau = \frac{\mu b}{D} + \tau_f + \tau_i + \tau_o \qquad \text{.....II.44.}$$

where τ_f is the forest contribution, including jogs;

τ_i the long range internal stress (which may be negative),

τ_o the friction stress.

The forest density is controlled by the stress on the secondary systems and is therefore proportional to $(\tau - \tau_o)$, hence the forest contribution to the flow stress will be proportional to $(\tau - \tau_o)$. The internal stress at a distance D from a pile up varies as $\frac{1}{D}$, hence from II.44.

$$(\tau - \tau_o) = \frac{k_3}{D} \qquad \text{.....II.45.}$$

where k_3 is a constant to be determined.

At the start of stage II, the primary pile-up length, a, is given by

$$a = \frac{\mu n b}{\pi(\tau - \tau_0)} \qquad \text{.....II.46}$$

The distance over which secondary slip occurs, a_s (=Do) will be proportional to 'a', say

$$a_s = 4 k_1 a = D \qquad \text{.....II.47}$$

Hence, assuming the number of dislocations n, in a pile-up does not change with strain from eqns. II.45, II.46, II.47.

$$k_3 = \frac{4 k_1 \mu n b}{\pi} \qquad \text{.....II.48.}$$

The maximum internal stress at a distance a_s normal to the pile-up is given by

$$\tau_i = \frac{\beta a}{a_s}(\tau - \tau_0)$$

where β is a constant.

If the stress necessary to operate the secondary sources is $P\tau$ where P is an overshoot factor, then

$$P\tau = S\tau + \left(\frac{\beta a}{a_s}\right)(\tau - \tau_0)$$

where s is the Schmid factor.

Re-arranging we get,

$$\frac{a_s}{a} = \frac{\beta(\tau - \tau_0)}{(P - S)\tau} \qquad \text{.....II.49.}$$

Neglecting the friction stress and using eqn. II.47, we get,

$$\frac{a_s}{a} = \frac{\beta}{(P - S)} = 4 k_1 \qquad \text{.....II.50}$$

From eqns. II.45 and II.48

$$(\tau - \tau_0) = \frac{4 k_1 \mu n b}{\pi D} \qquad \text{.....II.51}$$

If D is the pile-up spacing, since the pile-up is a line defect their density M will be inversely proportional to D^2; each pile-up contains n dislocations so that the primary dislocation density is $\sim n/D^2$. If the forest density is approximately equal to the primary density the total dislocation density ρ_t is given by

$$\rho_t = \frac{2n}{D^2} \qquad \text{.....II.52.}$$

Substituting for D in eqn. II.51 gives

$$(\tau - \tau_0) = \frac{2\sqrt{2}\, k_1 \mu \sqrt{n}\, b}{\pi} \sqrt{\rho_t} \qquad \text{.....II.53.}$$

For screw pile-ups Hirsch has estimated β (eqn.II.50) to be $\sim$0.1 for the conjugate and critical systems and $\sim$ 0.4 for the cross-slip system. If $P = 1$, and s = 0.5 for the conjugate and critical systems and s = 0 for the cross-slip system, then k, is $\sim \frac{1}{12}$. This gives for n = 20

$$(\tau - \tau_0) = 0.24\, \mu\, \underline{b}\, \sqrt{\rho_t} \qquad \text{.....II.53.}$$

<u>The Work Hardening Rate</u> - In a strain increment $d\gamma$, d N sources operate,

$$d\gamma = 4L^2\, n\, \underline{b}.\, dN. \qquad \text{.....II.54.}$$

The increase in density of edge (or screw) pile-ups is

$$d\rho' = 4L^1\, dN \qquad \text{.....II.55.}$$

From eqns. II.41, II.42, II.55 and putting $\rho = 1/D^2$, Hirsch obtained,

$$L = 12\, D \qquad \text{.....II.56}$$

For $\varrho' = \varrho$ and $L^1 = L$, we get from II.54 and II.55

$$d\gamma = L \, n \, \underline{b} \, d\varrho \qquad \text{.....II.57}$$

From eqn. II.45 and $\varrho = 1/D^2$

$$d\varrho = \frac{2 \, d\tau}{k_3 \, D} \qquad \text{.....II.58}$$

Combining eqns. II.57 and II.58 and substituting for L (eqn. II.56) and k_3 (eqn. II.48) gives

$$d\gamma = \frac{6\pi \, d\tau}{k_1 \mu}$$

From which

$$\theta_{II} = \frac{d\tau}{d\gamma} = \frac{k_1 \mu}{6\pi} \qquad \text{.....II.59}$$

Using the previously estimated value for k_1 gives

$$\theta_{II} \simeq \frac{\mu}{250}$$

which in view of the approximations made, Hirsch considers to be in good agreement with the experimentally observed values of $\mu/300$ for Cu, Ni and Al, and $\mu/250$ for Au.

Stage III Hardening.

In f.c.c. metals where the dislocations are extended in the glide plane, stage $\overset{\text{III}}{\wedge}$ starts when thermally activated cross-slip of screw dislocations from out of the pile-ups occurs. Hardening still occurs, but at a reduced rate. Since in b.c.c. crystals the dislocations are not extended then this model is unlikely to be of use in its present form.

II. 9 Twinning Mechanisms.

It is usually considered that the resistance to twinning is due to the difficulty in creating a twin nucleus; once the nucleus is formed, the twin is thought to grow easily and rapidly.

There are 4 twinning models for b,c.c. crystals, these will be summarised chronologically.

(1) Pole mechanism of Cottrell and Bilby.

(2) Sleeswyk's model.

(3) Ogawa's model.

(4) Priestner and Leslie's model.

(1) Pole Mechanism of Cottrell and Bilby.

This twinning model was proposed by Cottrell and Bilby in 1951; it has been applied to several structures but will only be described for b.c.c. crystals here.

The twinning shear in a b.c.c. crystal can be accounted for by the movement of an $\frac{a}{6}\langle 111\rangle$ dislocation on successive planes of a $\{211\}$ type. Considering a particular glide type dislocation which is not in its slip plane, it can dissociate,

$$\frac{a}{2}[111] \longrightarrow \frac{a}{6}[11\bar{1}] + \frac{a}{3}[112].$$

The $\frac{a}{6}[111]$ partial is mobile and capable of producing twins in (112) $(2\bar{1}1)$ and $(\bar{1}21)$ planes. The $\frac{a}{3}[112]$ partial is an edge dislocation lying in the (112) plane; it is however sessile, since its Burgers vector is perpendicular to this

plane, and will be called the pole dislocation. This pole dislocation has a component $\frac{a}{6}$ $[\bar{1}21]$ perpendicular to the $(\bar{1}21)$ plane which corresponds to the planar spacing. The $\frac{a}{6}$ $[11\bar{1}]$ partial, the sweeping dislocation, can rotate around the pole dislocation and as it rotates it leaves a layer of stacking fault on the $(\bar{1}21)$ plane; for each revolution, the sweeping dislocation climbs one plane, the stacking faults 'combine' to build up a thick twin.

Cottrell and Bilby described in general terms the conditions necessary for the pole mechanism to operate.

(i) The sweeping dislocation must produce the correct shear displacement.

(ii) The Burgers vector of the pole dislocation must have a component perpendicular to the sweeping plane which is equal to the plane spacing.

(iii) The pole dislocation must be anchored firmly enough to prevent movement under stress.

(iv) The dislocations must form a node in which the sweeping dislocation is free to move in the sweeping plane; the sweeping plane must be intersected by the pole dislocation.

(2) Sleeswyk's Theory.

Sleeswyk considered the dissociation of $\frac{a}{2}$ $\langle 111 \rangle$ screw dislocations. His calculations showed that whereas dissociation on to $\{110\}$ planes is unfavourable, the screw could dissociate on to $\{211\}$ planes. Under zero applied stress, the stable configuration was one where two $\frac{a}{6}$ $\langle 111 \rangle$

partials moved on to two {211} type planes whilst the third remained at the origin i.e. the line of intersection of the {211} planes.

Under the action of an applied stress, the stable configuration changed to one in which two of the partials move out from the origin onto the same type of {211} plane but on adjacent actual planes. The stress necessary to produce this configuration is given by the following equation which can only be solved graphically,

$$\frac{2\pi F}{\mu b^2} \cdot r_1 = 3\left[1 - \frac{3b\tau'}{F} + \left\{3\left(\frac{b\tau'}{F}\right)^2 - 3\frac{b\tau'}{F} + 1\right\}^{\frac{1}{2}}\right]^{-1} \quad \text{.....II.60}$$

where $F = \frac{\mu b^2}{2\pi}\left(\frac{1}{r_1} + \frac{1}{r_2}\right)$ AND $\tau' = \frac{\sigma}{2} \cdot \sin 2\lambda$

F is the back force per unit length acting on the dislocation due to the stacking fault,

r_1 and r_2 are the distances from the origin of partials 1 and 2; partial 3 is still at the origin,

σ is the axial applied stress,

λ, the angle between the slip direction and the stress axis. The other symbols have their usual meaning.

If the applied stress is raised to a sufficiently high value, the third partial can also glide along the same {211} type plane on the next adjacent actual plane. When the stress is this high, all three partials can glide producing a three layer twin. The stress required τ'' is given by

$$\tau'' = \frac{F}{3b} \cdot \sec(\alpha + 120). \quad \text{.....II.61(a).}$$

where cos $\alpha = \frac{\cos\phi}{\sin\lambda}$, and

ϕ is the angle between the pole of the twin plane and the stress axis.

τ'' is a minimum when $\alpha = 60$, since then

$$\tau'' = \frac{F}{3b} \qquad \text{.....II.61(b)}$$

The three layer twin can thicken by a pole mechanism, a suitable pole dislocation being a unit $\frac{a}{2}\langle 111\rangle$ screw with a Burgers vector component of $\frac{2a}{\sqrt{6}}$ normal to the twin plane (e.g. for a $(\bar{1}12)$ twin plane, an $\frac{a}{2}[\bar{1}11]$ dislocation). The three partials rotate around the pole dislocation; after the first revolution one of the partials is annihilated but the other two continue.

(3) Ogawa's Model.

Again this is a model for producing a three layer twin which once formed is assumed to thicken by a pole mechanism.

In a b.c.c. crystal the bonds normal to and crossing the coherent twin boundary are compressed ~5.8%. The correcting force F for a small change in bond length can be expressed as

$$F = K\left[\left(\frac{r_e}{r_x}\right)^m - \left(\frac{r_e}{r_x}\right)^n\right] \qquad \text{.....II.62}$$

where m,n and K are constants and $m > n$

r_x is the bond length, and
r_e the equilibrium bond length

If m is large as it is in b.c.c. metals, F is large and the twin boundary energy is high.

A monolayer twin (i.e. a stacking fault) has two boundaries formed immediately by the one partial dislocation and therefore ~ twice as much work has to be done by this dislocation than by the boundary dislocations of thicker twins.

A normal $\frac{a}{2}\langle 111\rangle$ glide dislocation can on the basis of strain energy dissociate into three $\frac{a}{6}\langle 111\rangle$ partials. If this occurs on a $\{211\}$ plane then two of the partials remain very close together since a high energy fault is formed if they separate. However an edge dislocation can dissociate into partials on the three parallel $\{211\}$ planes which pass through its core. If the last partial is fixed by the distortion (tension and compression) associated with the core of the edge dislocation, then the two twinning partials, say D_1 and D_2, can glide away if

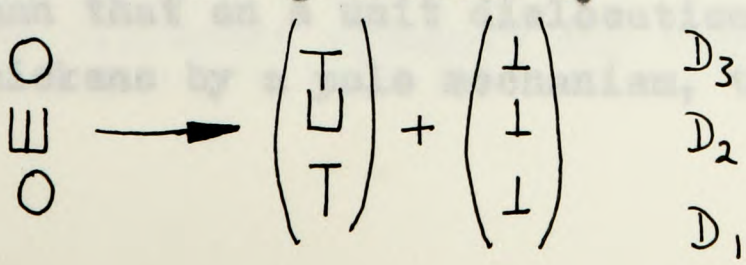
$$\tau \cdot 2\left(\frac{b}{3}\right) \geqslant \gamma'' + \sigma_i 2\left(\frac{b}{3}\right) \qquad \text{.....II.63.}$$

where τ is the applied shear stress,

γ'', the interfacial energy of a two layer twin,

σ_i, the friction stress on a twinning dislocation with Burgers vector $\left(\frac{b}{3}\right)$.

If the third partial, D_3, can break away from the core distortion then a three layer twin is formed. This dissociation is represented by



.....II.64.

In the distorted region the total Burgers vector is zero (1st term .R.H.S eqn. II.64), but the region between the planes containing D_2 and D_3 is in compression and the region between the planes containing D_1 and D_2 is in tension. This latter region is equivalent to a vacancy and can only move by diffusion but if the distorted region can follow the partial dislocations no twinning can take place. The compressed region has a strong attractive interaction with the partial D_3. The associated stress

$$\tau' = \frac{\mu}{2\pi(1-\nu)} \cdot \left[\frac{1}{r} - \frac{r(r^2-4)}{(r^2+2)^2}\right] \qquad \text{.....II.65.}$$

where r is the separation divided by the Burgers vector of the twinning dislocation.

The maximum interaction will be at the core radius which is $\sim 5. \left(\frac{b}{3}\right)$, (the core radius is taken to be the distance from the centre of the dislocation at which the stress becomes equal to the theoretical strength of a perfect crystal $\sim \frac{\mu}{30}$) ; hence the shear stress necessary to nucleate three twinning dislocations, τ_i is given by

$$\tau_i = \frac{5.4 \times 10^{-2}}{2\pi(1-\nu)} \cdot \mu \qquad \text{.....II.66.}$$

Once free from the core distortion the three twinning dislocations glide easily since the interfacial energy per partial is relatively low (cp monolayer twin), the attraction for the core distortion decreases and the friction stress is less than that on a unit dislocation. If this three layer twin thickens by a pole mechanism, the stress at the head

of the twin is magnified and propagation catastrophic.

Ogawa also considered, on the basis of this model, how the testing variables affected the propensity to twin. From consideration of the kink jump frequency of kinks in edge dislocations, and the ease of glide of a dissociated edge dislocation, the critical strain rate $\dot{\gamma}_c$, can be expressed as,

$$\dot{\gamma}_c = 1{\cdot}63\ \nu\ \varrho\ k\ \underline{b}^3 \exp\left(-\frac{E_m - 1{\cdot}63\tau_i b^3}{kT}\right) \qquad \text{.....II.67.}$$

where, ν is the jump frequency of a kink,

ϱ, dislocation density,

k, kinks / unit length of dislocation,

E_m, migration activation energy of core distortion,

and τ_i, the critical resolved shear stress for twinning.

If $\dot{\gamma} > \dot{\gamma}_c$ then twinning will occur.

The effects of temperature, strain-rate and pre-strain can immediately be seen from the equation; ageing a pre-strained specimen simply locks the free dislocations and lowers the effective value of ϱ in eqn. II.67. and hence $\dot{\gamma}_c$ is lowered.

Substitutional alloying elements, and interstitial atoms can have two opposing effects.-

(a) Interstital impurities increase the difficulties associated with forming the compression bonds across the coherent boundary.

(b) All impurities raise the yield stress and so increase the likelihood of twinning.

(c) Two different elements may react chemically with each

other e.g. rhenium and oxygen in molybdenum and silicon and oxygen in iron, to remove the interstitial from solid solution. This then tends to aid twinning and may explain the ease of twinning in these alloys.

(4) The Model of Priestner and Leslie.

This model (Priestner and Leslie 1965) requires prior slip on intersecting slip lanes and local stress concentrations of up to 50 times the applied stress.

When two glide dislocations of the type $\frac{a}{2}\langle 111\rangle$ intersect, provided their Burgers vectors are suitable, they can form an attractive junction,

$$\frac{a}{2}[111] + \frac{a}{2}[\bar{1}11] \longrightarrow a[001]$$

Under suitable conditions, this dislocation can dissociate

(a) back to its original components;

(b) into two other $\frac{a}{2}\langle 111\rangle$ dislocations;

(c) into partials.

Priestner and Leslie considered the dissocation of attractive junctions situated at the intersection of (i) a $\{110\}$ and $\{211\}$ plane, (ii) two $\{211\}$ planes.

(i) Barrier at Intersection of $\{110\}$ and $\{211\}$ Planes.

This dissocation yields an $\frac{a}{6}\langle 111\rangle$ glissile on a $\{112\}$ plane, the sessile $\frac{a}{6}\langle 115\rangle$ staying in the line of intersection,

$$a[001] \longrightarrow \frac{a}{6}[\bar{1}15] + \frac{a}{6}[1\bar{1}1] .$$

when the $\frac{a}{6}$ $[1\bar{1}1]$ partial glides away the sessile dislocation further dissociates,

$$\frac{a}{6}\ [\bar{1}15] \longrightarrow \frac{a}{6}\ [1\bar{1}1] + \frac{a}{3}\ [\bar{1}12]$$

The $\frac{a}{6}$ $[1\bar{1}1]$ partial is again glissile in the $\{112\}$ plane and follows the first partial to produce a two layer twin. In gliding away from the barrier line, each partial strips an $\frac{a}{6}$ $[1\bar{1}1]$ partial off one of the intersecting dislocations $\left(\frac{a}{2}\ [1\bar{1}1]\right)$. This leaves an $\frac{a}{6}$ $[\bar{1}\bar{1}1]$ at the node which then also glides in the $\{211\}$ plane. The node now moves along the line which once contained the a $[001]$ dislocation eliminating the $\frac{a}{3}$ $[\bar{1}12]$ and $\frac{a}{6}$ $[\bar{1}15]$ dislocations until it eventually reaches the second node. Along the lines once occuppied by the a $[001]$ and $\frac{a}{2}$ $[1\bar{1}1]$ dislocations remains a 'dipole', which is equivalent to the distorted region left behind the D_3 twinning dislocation in Ogawa's theory.

From consideration of the dissociation energies it was calculated that a stress concentration of 45 times the applied stress is required for dissociation.

(ii) Barrier at Intersection of Two $\{211\}$ Planes

In this case the dissociation is much simpler, it can be represented overall by,

$$a\ [001] \longrightarrow 3.\frac{a}{6}\ [\bar{1}11] + 3.\frac{a}{6}\ [1\bar{1}1]\ .$$

In detail the dissociation occurs in three stages, at each

stage one of each type of dislocation is produced, and three layer twins are built up on both {211} planes. The stress concentration necessary to nucleate these two twins is only 15 times the applied stress.

If one of the {211} planes cannot accept twins because of the sign of the applied stress, then an $\frac{a}{2}$ ⟨111⟩ dislocation is formed in this plane and a twin in the other. This condition is almost similar to the first type of intersection and requires the same stress concentration i.e. 45 times.

Other conditions discussed by Priestner and Leslie did not produce twins. If both intersecting plane are of the {110} type, then two unit dislocations are produced and the stress concentration required is 135 times. If both {211} planes are unable to accept twins then again glide dislocations are produced though in this case an intermediate barrier may give rise to cleavage fracture.

Yet again this model requires a pole mechanism to produce thick twins from the three layer nucleus.

SECTION III

Apparatus and Experimental Arrangements

A. Introduction.

As this work followed that of Masters (1962), it was decided that electron microscopy, a technique with which Masters, would be the most useful. However, to enable us to study small, homogeneous strains, the material had to be purified and this pure material gave quite a different response to the stress-strain curve. Therefore, some work was necessary to check that the values of activation energy and volume agreed with Master's values for copper single crystals. Some of the testing equipment was already available but most apparatus had to be made or bought.

If the apparatus has already been described in departmental theses reference will be made to these theses and description curtailed. Apparatus built or designed by the author will be described in detail.

B. Electron Beam Heating Units.

Three electron beam units (E.B.U.) were used to grow crystals used in this work.

The Mark I Electron Beam Unit

This machine was built by J. Halliwell and P.B. Masters and was similar to the Halliwell design (Halliwell, Davis and Lever (1957). A full description has been given by Masters (1962).

Electrons emitted by the tungsten filament (Fig.III.1)

SECTION III.

Apparatus and Experimental Techniques.

A. Introduction.

As this work followed that of Masters (1964), it was decided that electron microscopy, a technique not used by Masters, would be the most useful. However, in order to study small, homogeneous strains, the material had to be purified and this pure material gave quite a different shape to the stress-strain curve. Therefore, some work was necessary to check that the values of activation energy and volume agreed with Master's values for impure niobium. Some of the testing equipment was already available but other apparatus had to be made or bought.

If the apparatus has already been described in Departmental theses reference will be made to those theses and description curtailed. Apparatus built or designed by the author will be described in detail.

B. Electron Beam Heating Units.

Three electron beam units (E.B.U.) were used to grow crystals used in this work.

The Mark I Electron Beam Unit

This machine was built by A. Hellawell and B.C. Masters and was similar to the Calverly design (Calverly, Davis and Lever (1957). A full description has been given by Masters (1962).

Electrons emitted by the tungsten filament (fig.III.1)

were focussed onto a short length of the specimen by two tantalum plates. Central holes in these focussing plates allowed the specimen to pass straight through this cathode assembly. The cathode assembly was fixed and the specimen moved parallel to its long axis. Thus a hot or molten zone was passed along the specimen. The maximum power available was 3 KV at 500 mA. The available zone speeds were 3 , 60 and 180 mm/hour and the useful traverse 12 cms. This apparatus had three main drawbacks, two of which only applied when large specimens were used.

(a) The sliding specimen carriage overheated and then tended to stick. This gave vibration which resulted in striations parallel to the liquid/solid interface.

(b) The pumping system was too small; the pressure fluctuated between 5×10^{-5} and 3×10^{-4} torr instead of being $\sim 1 \times 10^{-5}$ torr. These fluctuations affected the efficiency of power transfer giving an uneven specimen diameter.

(c) The cathode design did not shield the specimen from the filament. Tungsten, evaporating from the filament, contaminated the specimen. The low accelerating voltage available did not permit the use of a shielded filament design.

The Mark II Electron Beam Unit.

Because of the limitations of the Mark I it was decided to make a second .E.B.U.; D.K. Bowen did the detailed design and building, and the apparatus will be described by him

elsewhere.

The main advantages of this design were as follows.

(a) A stable vacuum - a 6 inch diffusion pump capable of pumping 600 litres sec^{-1} kept the pressure below 3×10^{-6} torr during zone melting.

(b) Improved cathode assembly - the cathode was of the cage type described by Cole, Fisher and Bucklow (1961) With this design (Fig.III.2) there was less contamination from the filament and the volatile impurities were allowed to escape from the cathode assembly (unlike some other focussing cages) . The beam focus was controlled by adjusting filament height; raising the filament gave a finer focus.

(c) Increased power - the maximum rating of this unit was 10 KV at 1 amp. Hence thicker samples could be melted and a focussing cage cathode used.

(d) Longer crystals - the useful cathode traverse was 36 cms. (cf. 12 cms of Mark I)

<u>The Miles Hivolt Electron Beam Unit.</u>

For a period of about 3 months, when the Mark I was being replaced by the Mark II, Dr. K. Mendelssohn allowed the author to grow crystals with the Miles Hivolt E.B.U. owned by the Clarendon Laboratory. This was a commercial model based on the Calverley et al (1957) design. About 10 , 10cm. niobium single crystals were grown with this machine.

C. The Ultra-High Vacuum, High Temperature Annealing Furnace.

The pumping system of the ultra-high vacuum unit (U.H.V.U.) was very simple. (Fig. III 3, a block diagram). An 80 litre sec^{-1} oil diffusion pump was backed by a 50 litre $min.^{-1}$ rotary pump. The accessories were standard components supplied by Edward's High Vacuum Ltd., If the power supply failed, the isolation valve first sealed off the diffusion pump etc., and then let air into the rotary pump. Air was let into the vacuum chamber by a manually operated valve. Above the diffusion pump, the apparatus was baked in a demountable oven made of 3cm thick marine asbestos and wound with 1mm thick nichrome wire. Baking was done at $\sim 200^{o}C$ The maximum baking temperature was limited by the viton 'O' rings which were used on the high vacuum side of the diffusion pump. Attempts to seal the system with only gold 'O' rings failed as the glass bell jar was not strong enough.

The pressure was measured with a Mullard IOG -13 immersion gauge head and a WPS-3 ionisation gauge control unit. This gauge could measure pressures within the full scale ranges of 10×10^{-3} to 10×10^{-11} torr.

The Furnace Power Circuit

The high temperature was obtained by directly heating the specimen with a large current. The electrical circuit is shown in fig. III 4. Fuse F_1 was in the mains plug and rated at 13 amps. S_1 was a 20 amp. switch made from a 10 amp 2 pole single throw switch. The variable transformer was a "Variac" type 50B giving 20 amps. at 0 - 270 volts. The

ammeter A, which was in series with the primary of the transformer had a full scale reading of 30 amps. Switch S_2 was made from a 3- pin power point plug and socket and contained fuse f_2 rated at 25 amps. The 10 KVA step-down transformer gave a maximum current of 500 amps. at 20V. The leads connecting the transformer to the vacuum lead-throughs (see fig. III 6) were made of copper braid and were capable of carrying 500 amps.

The Oven Power Circuit

Since baking and annealing were not simultaneous operations, the same equipment as far as S_2 (fig.III 5) was used for both. The oven, which had a resistance of 32 Ω , was in series with a 12 Ω resistor, R_1. R_1 could be short circuited by the solenoid switch S_3 . S_3 was controlled by an Ether "capacitrol" controller using a chromel/alumel thermocouple as the sensing device. The thermocouple was placed near the top of the oven, the temperature variation throughout which was within the limits $\pm^{0}_{10}{}^{o}C$

The Vacuum Chamber.

The vacuum chamber (Fig.III 6, partly diagramatic) consisted of a stainless steel (EN58) base plate and a 12 inch dia., 15 litre pyrex bell jar sealed with a viton 'O' ring. Four ports were cut into the base plate. The central port connected with the pumps, two ports were for the water-cooled copper vacuum lead-through and the last port was for the ionisation gauge head. The gauge head was sealed with a gold 'O' ring, all other seals were with viton 'A'. The gauge

head and cold baffle were bolted to the base plate; the lead-throughs, however, had a flange sealed to the inside of the base plate and a tightening nut outside. One of these lead-throughs was insulated with mica (Fig. III.7)

Two cross-arms made of RF31 stainless steel were able to slide on the lead-throughs. Their positions were controlled with copper collars. The free end of each cross-arm contained a molybdenum plug, drilled out to take a sliding chuck which was also made of molybdenum. The specimen was held in these chucks usually with a little sheet as packing.

The gauge head was shielded with a tantalum sheet. Without this shield, the gauge gave a negative pressure reading when the specimen was hot enough for evaporation to occur. The reason for this is not known.

The vacuum chamber was water cooled. A jet of water, which spread out to form a continuous film, cooled the bell jar. This water collected in a pool on the base plate and was removed by a water pump. The pool of water helped to cool the base plate which was also cooled by conduction to the cold baffle on to which extra water cooling coils were soldered.

Temperature Measurement.

The annealing temperature was measured with a disappearing filament pyrometer using light with wavelength $\lambda = 0.665\ \mu$. The radiation losses through the bell jar were corrected by using a standard lamp in place of the specimen.

In the temperature range 1300 - 2300°C these losses were equivalent to a temperature drop of 47 $\pm$ 5°K at all temperatures. The emissivity correction was made using the following equation

$$\frac{1}{T} = \frac{1}{Ts} + \frac{\lambda \ln \varepsilon_\lambda}{C_2}$$

where, T = true temperature °K,

Ts = pyrometer reading + 47° in °K,

λ = 0.665 μ - working wavelength of the pyrometer,

ε_λ = 0.38 - spectral emissivity of niobium for λ = 0.665 μ,

C_2 = 1.438 cm. deg. - a constant.

A graph of true temperature v. pyrometer reading was drawn (fig. III 8) and this was referred to for temperatures below 2300°C. Once above 2300°C, evaporation from the specimen made temperature readings with a pyrometer inaccurate. The final annealing temperature was nearly always the melting point and /as

(a) the equilibrium concentration of nitrogen in solution varied inversely as the temperature;

(b) a rapid cool, without cooling stresses, was obtained;

(c) the annealing temperature was reproducible.

D. Devices for Cutting and Slicing Single Crystals.

1) Jeweller's Saw and Block.

The single crystals were glued to an accurately milled aluminium block which fitted into a channel in a much larger

block of mild steel. (Fig. III 9). The end face of the mild steel block was hardened by carburising. By keeping the saw blade against this face the crystals could be cut perpendicular to their length. A locking screw held the inner block steady whilst sawing and subsequent cuts were made by moving the inner block and relocking.

A similar arrangement was used for cutting slices from a deformed crystal. The inner block was equipped with a rotatable table onto which the specimen was glued (fig.III 10). The table, which could be turned with a screwdriver, was calibrated with 5° marks. The specimen was tilted by putting wedges under the aluminium block. Sawing against the end face was not very satisfactory if large tilts were used, as the saw tended to slide off the crystal. Therefore, a 200 μ wide slit in the mild steel block was used instead. The saw blade was 150 μ thick.

2. Spark Cutting Unit.

A Servomet spark cutter, model SMC, was available from Feb. 1963. It was equipped with all the accessories available at the time of purchase, but was deficient in the following -

a) an extending tool-holder arm,

b) a collet tool-holder,

c) a means of measuring depth of cut,

d) a moving wire cutter for slicing.

A) The Extending Tool-holder arm.

This type of arm was necessary if the tool had to be moved

relative to the work without altering their relative orientation. e.g. cutting thin slices.

The arm could be rotated about the actuator shaft and extended by an internal rack and pinion movement. (fig III.11.). The brass gibs which were screwed onto the upper section of the arm, engaged slots in the lower section. A rack was bolted to the top of the lower section; it was engaged by a pinion which could be turned with a knob located on the side of the arm. The useful traverse was about 10 cms. The connections to the actuator and the tool holder were standard.

b) The Collet Tool-holder.

The Collet tool-holder was necessary for holding round tools perpendicular to the work. This tool-holder (fig.III 12) used the same type of tightening mechanism as a collet chuck. By turning the brass disc, the tapered collet was pulled further into the fixed, insulated tube. This action closed the collet around the tool. Six collets were made to take tools ½", ⅜", ¼", ⅛", 3mm, and 1/16" diameter.

c) Measuring the Depth of Cut

The depth of cut was measured with a dial gauge which could measure 1" x 0.0005". The dial gauge was attached to the actuator and so measured both the depth of cut and the tool wear. The rate of tool wear depended on a) the materials concerned b) the dimensions of the tool, and had to be determined for each job.

d) The Moving Wire Cutter.

The moving wire cutter had the following advantages -

1) the mass of tool in the cut was small, reducing the tendency for a thin slice to bend over,

2) for a given range the cutting speed was greater,

3) the effective tool wear was zero.

This wire cutter was designed by D.K. Bowen, and was similar in operation to commercial models now available. Unfortunately the time needed to cut niobium was prohibitively long - about 20 hrs to cut through 3 mm. dia. rod. Attempts to increase the cutting speed by using different wires and cutting ranges were not successful.

3. The Acid Saw.

Attempts to cut thin slices with an acid saw were not very successful. The cuts were wide and not very sharp so that with small specimens (i.e. 3mm dia.) it was not possible to section parallel to a particular plane. The saw (fig.III 13) consisted of a thread which moved through an acid bath and over the specimen. The acid chemically polished the specimen in the region of the thread and eventually cut right through. Tension in the thread was maintained by a small running weight and the thread speed was about 10 mm.sec^{-1}. For niobium the acid used was 1 : 1 HF : HNO_3.

E. Grinding Jigs for Compression Specimens.

These jigs were used for grinding the compression specimens to gauge length so that their ends were perpendicular to the cylindrical axis.

The jigs for 8 mm. and 6mm. long specimens (Fig III 14)

were identical except for thickness. In both cases, the thickness was about 0.25 mm. less than the gauge length; [use of jigs is given under sub-section III.N.] . The body of the jig, a 1½" diameter brass disc, was held in a stepped collet chuck whilst the faces were being turned. This ensured that these faces were parallel to ~ 0.0003 radians. The slot was milled radially with its sides perpendicular to the faces of the disc (to 0.001 radians). The specimen was held against one corner of the jig by a polythene push rod moved with a 4 B.A. Allen headed grub screw. Between the push rod and this screw was a steel ball which removed any tendency for the push rod to rotate when tightening the screw. The diameter of the slot, its depth and the angle made with the push rod were chosen so that equal reaction forces were exerted by the sides of the jig.

The jig for the 0.100" long specimens was similar to the jigs described above except for the push rod arrangement. A polythene push rod 0.050" dia. did not have sufficient rigidity and a metal push rod with a polythene end marked the specimen. Therefore a brass push rod with a piece of a "Blue Gillette" razor blade between it and the specimen was used. The razor blade was hard but very smooth and because of the relatively large area of contact did not damage the specimen.

An earlier model grinding jig had, instead of a milled slot, a square broached hole. However, the sides

of the hole were not perpendicular to the faces of the jig to within the required tolerance so this jig was not used.

F. The Tensile Specimen Cutter.

This jig consisted of a rotating P.T.F.E. wheel partly immersed in acid. The specimen blank was a rod 30mm x 3mm. dia. which rested on top of the wheel (Fig.III 15). As the wheel rotated acid was brought into contact with the specimen and chemical polishing occurred over the gauge length. The rotation of the wheel caused the specimen to spin around its own axis. It was essential to keep the specimen spinning otherwise a "flat" occurred. Acid spume put a film of corrosion product on the ends of the specimen and if these ends were allowed to touch the sides of the acid bath the specimen stopped spinning. A piece of P.T.F.E., in contact with the specimen only over the gauge length, stopped it touching the walls of the acid bath and allowed it to spin freely.

The acid used was a 70 : 30 mixture of HNO_3 and HF. To get a continuous film of acid on the wheel, it was necessary to reduce the surface tension by adding a few drops of 'teepol' to the bath. To make a tensile specimen 1½ mm. dia. by 10 mm gauge length took about 15 mins.

G. The Mechanical Testing Machines

Three mechanical testing machines were used. Two were built in the laboratory and the third was a commercial model.

The Mark I Testing Machine

This machine has been described in many theses from this laboratory (Mitchell 1962, Masters 1962, Sharp 1964) and will not be described in detail here. The machine was modified to increase both the maximum load and the cross-head speed.

The new driving unit was a $\frac{1}{6}$ H.P. A.C. motor. This was connected to a worm via a step down gear box and a roller chain. The worm and wheel gave a further reduction of 60 : 1 and drove a 20 T.P.I. lead-screw connected to the moving cross-head . The cross-head speed was measured with a dial gauge and stop watch; several runs lasting ~30 minutes each gave a cross-head speed of 284 μ/min.

The mechanics of this testing machine resulted in the load on the lead-screw threads shifting from one side to the other at the carriage weight. An antibacklash device prevented this change-over altering the cross-head speed. The machine was originally designed for a maximum load of 100 kgs. and when used up to its new maximum of 1000 kgs. excessive wear of the antibacklash device occurred. With 3mm. diameter specimens the change-over occurred at about the room temperature yield load and manifested itself as a kink on the load-time chart. A new antibacklash device was designed which kept the load on one side of the threads only

and which was not susceptible to thread wear. The device (fig III 16) consisted of two threaded plates (referred to as "top cap" and "main body") kept apart by a powerful spring (a valve spring off a Ford 8 engine). The slots and 4 B.A. screws allowed axial but not rotational movement of the top cap relative to the body. Compressed, the spring exerted a force about 20 kgs. greater than that due to the carriage weight. The lead-screw threads were now pressed against the bottom of the main body threads instead of resting on top as before. Any wear of the threads was taken-up by the spring. The device was attached to the wheel with a pipe screw and pinned to prevent slip.

The load was measured with a J.L. Thomson BT2 1000 kg. load cell and a Sunvic potentiometric recorder. The circuit (fig.III 17) was similar to that of Sharp (1964).

The load cell specification was as follows -

a) Sensitivity = 2.992 mV/Volt applied,

b) Accuracy $> 0.5\%$ F.R.O.,

c) "Softness" = 250 μ at full load.

The recorder range was 2.5 mV f.s. and corresponded to 50 kgs. load. The load was suppressed in steps of 40 kgs. The chart speed was either 1 inch $min.^{-1}$ or 3 in. $min.^{-1}$

A gear box, which could give a step change of 10x was constructed. It was satisfactory up to 40 kgs. load but above this value the magnetic clutches started to slip. As the Mark II machine was used for all strain rate change work, this gear box will not be described in detail.

The Mark II Testing Machine.

This machine and its cryostat has been fully described by Altshuler (1964), therefore only its specification will be given -

Maximum Load - 240 kgs.

Load Magnification - 2 inches per kilogram.

Cross-head Speeds - 5×10^{-4} - 1×10^{-7} inches sec^{-1}.

Testing Temperature Range - 2^{o} - $300^{o}K$.

The Instron Testing Machine.

This machine, supplied by the Instron Engineering Corp. of High Wycombe, was a table model TM-M-L. It had a maximum load of 100 kgs. and the cross-head speed range was from 5 μ/ minute to 10^{5} μ /minute. The recorder pen had a response time of $\frac{1}{4}$ sec f.s. and the load could be suppressed with a 10 step zero suppression unit.

H. Compression and Tension Jigs.

Compression Jig for Mark I Machine.

This jig (fig. III 18) was made entirely of EN 57. The upper anvil was connected to the moving cross-head via the top plate and compression tube. The lower anvil, which was fixed during the test, was connected to the load cell through a framework and tension rod. This framework moved through two guide holes and a slot, in the upper anvil. The faces of the anvils were mechanically ground and polished to remove machining marks. The minimum + maximum anvil separations

were 0 and 15 mm. respectively. With no load, friction at all temperatures was below the limits of measurement. Friction under load was not measured because the carriage of the testing machine precluded the attachment of weights.

Tension Jig for the Mark I Machine.

The tension jigs used previously in this laboratory were not suitable for high loads; the specimen grips were difficult to make and gave alignment and setting - up problems. Therefore a new design was used (fig.III 19). The jig itself was made out of EN 57 stainless steel and consisted of an outer compression tube attached to the moving cross-head and a tension rod connected to the load cell. The bottom end of the compression tube had a 45^{o} bevel on its inner face and a hole drilled opposite the specimen to allow the coolant to circulate. The top specimen grip was accurately aligned by screwing it up against a shoulder on the tension rod. The bottom grip was made from a stainless steel (EN58) ball. Under load this grip was self aligning due to its contact with the bevel on the compression tube. Both grips were drilled slightly larger than the specimen diameter, the hole in the bottom grip being radial. The specimen was cemented into the grips with araldite which had to be cured at 100^{o}C for 4 hours. After testing the gauge length of the specimen was cut out with a saw, and the stumps and araldite removed from the grips with a 70 : 30 mixture of nitric and hydrofluoric acids.

At room temperature the araldite joint held firm up

to 150 kgs. load. It was also suitable for tests at 158°K but at 77°K it was brittle. The main disadvantage with this type of grip was the long preparation time; the cure at 100°C did not affect the yield stress.

Compression Tests with the Mark II Machine.

These tests were done with the semi-automatic compression jig designed by T.L. Altshuler. It has already been fully described by the designer (Altshuler (1964)) and will not be described here.

Tension Jig for the Instron Machine.

This jig was made by D.K. Bowen. Its design was similar to the jig on the Mark I Machine, but with the araldite grips replaced by "Eclipse" pin-chucks. The collets of the pin-chucks were drilled and tapped 6 B.A. With these grips the preparation and setting-up time was short (cp. araldite grips) .

I Attachment for Measuring Strain Directly.

The strain was measured with a Sanborn 7DC DT - 500 displacement transducer, the output of which was fed into a Rikadenki 3-pen recorder. The transducer was a differential transformer whose output voltage depended on core position. It had a stroke of ± 0.500 inches and a scale factor of 6.6 V. /inch for 6v. excitation. Both input and output were D.C., the chopper and demodulator and filter being built into the transducer. The Rikadenki recorder

had 3 separate channels each connected to a pen. Each pen had a f.s. response of $< \frac{1}{2}$ sec and was displaced 1 mm. with respect to the other pens. Each channel had -

a) an attenuator giving f.s. ranges of 2.5, 25,250 mV.

b) a zero adjustment control,

c) a ten step suppression unit.

The suppression unit was placed between the attenuator and the potentiometer slide wire so that all ranges could be fully suppressed ten times. The available chart speeds were 120, 240 and 480 mm. per minute and per hour. and the chart width was 250 mm.

The transducer was fixed to the compression jig on the Mark I Machine (fig. III 20). The extension rod and supporting tube were attached directly to the compression anvils.

Due to their massive size, the elastic bending of these anvils was negligible so that only specimen strain was measured. The relative position of the core to the windings was adjusted with the micrometer screw thread. This thread was made such a tight fit that the holder had to be turned with a tommy bar. This ensured that it did not turn accidently during a test. Small zero errors on the recorder were corrected with the electronic zero adjustment.

J. Goniometer Stage for the E.M.6. Microscope.

The A.E.I. E.M.6 electron microscope was not equipped with a high tilt, high resolution goniometer; it was therefore decided to make one. It was based on Valdre's tubular lever goniometer which was designed for the Siemen's Elmiskop I (Valdre 1962).

The goniometer (fig.III 22) was made of phosphor bronze. The main body contained four pistons, two were moved by screws in the stage carrier and two were spring loaded. They were arranged so that a spring loaded piston horizontally opposed one controlled by a screw. The two pairs were mutually perpendicular. The tubular lever was fixed in a ball joint at the top of the main body and the position of its free (lower) end was controlled by the pistons. Also attached to the main body were lugs for carrying the goniometer through the air lock into the microscope. The ends of these lugs were bent over to fit into locating holes in the stage carrier. The tilting head was set in the lower body. It was held tightly in a ball joint which for convenience was split by 6 fine cuts. The other half of the tilting head also had a spherical outer surface and this fitted closely into the tubular lever. Thus any movement of the lever tilted the head. The specimen was held in the tilting head with a split ring. The head was recessed 0.25 mm. beyond the centre of the ball because the specimen usually had a 0.25 mm. thick rim. The maximum tilt and movement available were $\pm$ 20^{o} and $\pm$ 0.5 mm. respectively.

The stage carrier (fig.III 21) was also made of phosphor bronze. It was designed to accept the standard A.E.I. fittings for translational movement. The goniometer fitted into the tapered, central hole; the lugs ensured correct location i.e. the screws and pistons matched up. The phosphor bronze screws, which were lubricated with 'apeizon B' fluid, had 40 T.P.I. and 1½ turns gave the full tilt of 40°. The pre-existing stereo-tilt knob controlled one of the tilts, the other tilt control was put through the front window frame. A minor modification was made to the carrying cradle and 0.5mm. was removed from the top of the objective aperture rod.

K. Materials.

Niobium, tantalum, molybdenum and tungsten were readily available in sheet form. Small quantities of each of these metals were bought from Murex Ltd., in the form of rolled and annealed strips 12mm. wide x 0.1mm. thick.

The makers analysis was -

METAL ELEMENT	NIOBIUM P.P.M.	TANTALUM P.P.M.	MOLYBDENUM P.P.M.	TUNGSTEN P.P.M.
Carbon	100	100	-	-
Aluminium	300	-	-	-
Silicon	200	-	-	-
Iron	300	-	100	200-500
Chromium	<100	-	-	-
Magnesium	<100	-	-	-
Chlorine	<100	-	-	-
Lead	<100	-	-	-
Niobium	-	<1000	-	-
Others	-	trace	trace	trace

Niobium, tantalum and molybdenum rods 3,4 and 5 mm. dia. were bought in several batches.

a) Powder metallurgical niobium and molybdenum from Murex Ltd. had the following makers analysis -

Element	Niobium P.P.M.	Molybdenum P.P.M.
Carbon	100	40
Aluminium	300	-
Silicon	200	-
Iron	300	80
Chromium	<100	-
Magnesium	<100	-
Chlorine	<100	-
Lead	<100	-
Oxygen	-	20
hydrogen	-	1
Nitrogen	-	10

b) Electron beam melted niobium and tantalum was supplied by S.G.M. de Hoboken S.A. of Belgium. The makers analysis was -

Element	Niobium P.P.M.	Tantalum P.P.M.
Oxygen	50	10-100
Nitrogen	65	15-200
Hydrogen	2	0.5-10
Carbon	300	15-20
Silicon	170	<20 n.d.
Tantalum	500	-
Niobium	-	500
Titanium	<20 n.d.	<20 n.d.
Nickel	<10 "	<10 "

continued over leaf.

Element	Niobium P.P.M.	Tantalum P.P.M.
Copper	<50 n.d.	<10 n.d.
Zirconium	<60 "	-
Tin	<10 "	<10 "
Aluminium	<10 "	<30 "
Magnesium	<10 "	<30 "
Lead	<10 "	<10 "
Cadmium	< 5 "	<10 "
Zinc	<10 "	<10 "
Chromium	<20 "	<10 "
Phosphorus	<10 "	-
Vanadium	<20 "	<10 "
Boron	<1 "	-
Beryllium	<70 "	-
Iron	<15 "	<15 "
Tungsten	<20 "	<40 "
Molybdenum	<10 "	-

n.d. = not detected.

c) Electron beam melted niobium from Murex Ltd. The makers analysis was

Element	P.P.M.
Oxygen	57
Hydrogen	<1
Nitrogen	<50
Carbon	10
Iron	10

continued overleaf

Element	P.P.M.
Silicon	150
Tungsten	250
Tantalum	1000
Titanium	<100

L. Growing Crystals.

Flat Strip Crystals.

Attempts were made to grow flat crystals of niobium, tantalum and tungsten by pre-straining and annealing. The specimens were cut in a template to give a gauge length of 20 mm. and a gauge cross-section of 8mm x 0.1mm. They were chemically polished to remove the damaged edges strained between 2 and 6% and set-up in the Mark I E.B.U. The filament and focussing plates were U-shaped and slotted respectively so that the specimen was heated evenly across its width. A hot zone, whose temperature was a few hundred degrees below the melting point of the specimen, was passed along its length at 1mm. min^{-1}. No single crystals were obtained; the method was abandoned when it was decided to use round crystals.

Round Crystals Grown by the Floating Zone Technique.

Niobium and tantalum single crystals could be grown with all three electron beam units, but due to excessive outgassing molybdenum could not be grown with the Mark I unit. By the time the other E.B.U.'s became available

(June 1964) the foil preparation difficulties with niobium had been overcome and work had advanced advanced with this metal so no molybdenum single crystals were tested.

No special growing techniques were used. Initial joints were either lap (Mark I) or, if adjustable chucks were available (Mark II & Miles Hivolt), butt. Nearly all crystals were grown at $\sim$ 10mm. $min.^{-1}$ by one zone pass. A few multiple pass crystals were grown, the zones being passed both up and down the rod. The zone speed was too fast for zone refining to occur, so purification was by evaporation only. Refractory metal impurities were not removed this way. Some of the thicker (5mm) rods were swaged between passes to reduce their diameter; after swaging they were chemically polished to remove surface impurities (e.g. carbon, oil). Multiple pass details will be given for individual rods in the results section.

The first few crystals were grown with random orientation, subsequent rods were seeded with pieces of old crystals. The accuracy of seeding was $\sim 3^{\circ}$. Niobium crystal rods Nos. 1 - 20 were grown with the Mark I E.B.U., Nos. 21 - 29 with the Miles Hivolt and Nos. 30 - 50 with the Mark II.

Crystals grown in the Mark I E.B.U. were usually of uneven cross-section. These rods were set inside thick-walled brass tubes with araldite. The tubes were turned between centres to 'true-up' the outer faces and then held in a collet chuck with about $\frac{1}{4}$" protruding. This end

was turned down to a pre-decided final diameter before more of the rod was fed from the collet. This was repeated until the whole rod ~12 cm was machined. The size of cut was ~100μ to start but was reduced to 25μ as the final diameter was approached. The rod was chemically polished to remove ~200μ before annealing in the U.H.V. unit.

Round Crystals Produced by Secondary Growth.

When polycrystalline rods were annealed in the U.H.V. unit at ~2300°C, the grain grew right across the rod giving a bamboo structure. Individual crystals were as long as 14 mm. but most were only 6 - 7 mm. Some of the long crystals were used for mechanical tests. Preliminary attempts to grow long crystals (say 30 - 50 mm.) by pre-straining and annealing were not successful and were discontinued when the Miles Hivolt E.B.U. became available.

M. The Ultra-high Vacuum Anneal.

This treatment both purified and annealed niobium. A typical proce-dure was as follows : -

a) The specimen was mounted in the sliding chucks and positioned so that the stop on the bottom chuck was ~3mm from the bottom cross-arm. This allowed for expansion. The chucks fitted loosely into the cross-arms so that the thermal conductivity of the joint was low.

b) The glass bell jar was fitted and the system pumped

for 1 - 2 hours. This was to check for leaks, if leak tight the pressure was $\sim 10^{-6}$ torr.

c) All water cooling connections, the safety screen and the leads to the vacuum gauge were removed. The oven was assembled and the system baked at 200°C for 48 hours. (The vacuum gauge could not be operated if the skirt temperature was above 100°C)

d) After baking, the system was allowed to cool slowly to 150°C (to prevent excessive cooling stresses in the glass) and then quickly to room temperature.

e) Liquid nitrogen was added to the trap and the water cooling system turned on. The pressure fell to about 10^{-8} torr.

f) The power supply was connected to the specimen and the temperature raised to about 2300°C. The pressure rose to about 10^{-6} torr. A niobium specimen 12cm x 3mm dia. would require about 4½ v. and 220 amps. (these values were not measured directly but estimated from the "Variac" dial reading and the current in the transformer primary). At 2300°C, the niobium evaporated on to the glass bell jar and the base plate. This process had a rapid pumping action and pumped the system from 10^{-6} torr to 10^{-8} torr in about 4 hours. When the pressure fell below 10^{-8} torr, the temperature was raised slowly until the rod melted over a short length. The specimen cooled quickly to $\sim$ 1000°C by radiation.

g) After cooling and letting air into the system, the

apparatus was left for a few hours to allow the viton 'O' rings to unstick. The bell jar was then removed with the aid of a wedge and the specimen recovered. The parts of the rod which were in the chucks plus 1 cm. off each end were rejected, as during the anneal a temperature drop of about 50°C was detected over this region.

Some variations of the above technique were tried.

a) The specimens were annealed at 1800°C before baking and annealing proper were carried out. At this temperature carbon and water vapour should have reacted to produce carbon monoxide and hydrogen. An excess of water vapour was present due to desorption from the glass bell jar. This treatment did not measurably affect the yield stress so it was concluded that either the carbon was removed in the E.B.U. or carbon does not strongly interact with dislocations in niobium. Therefore the practice was discontinued.

b) The chucks tended to stick in the cross-arms during the anneal at 2300°C. If the specimen wasrather long (> 10 cms. for 3 mm. dia.) it sometimes bent when the temperature was raised. With the long (30 cm.) specimens from the Mark II E.B.U., both cross arms were positioned at the top of the lead-throughs; the specimen was bent to a U- shape and suspended from the chucks. With this method there was no danger of spoiling crystals by thermal expansion and the losses due to initial bending were small.

c) With long specimens the heat dissipated was rather large and the base plate temperature rose to ~50°C in certain

parts. The outgassing from these hot regions made it difficult to get the pressure below 1 x 10^{-8} torr. To reduce the power required for these long specimens and to shield the base plate a radiation shield was used. The shield was not a success however because although the base plate remained cool, the evaporation of niobium onto the glass was largely suppressed and without its pumping action the pressure remained at $\sim 10^{-7}$ torr.

d) Baking the apparatus above 200°C to speed up outgassing was not successful. At 250°C the viton 'O' rings decomposed and the fluorine emitted attacked both the glass and the stainless steel base plate. Even at 200°C a little fluorine was evolved and to stop this the baking temperature was eventually lowered to 180°C.

N. The Preparation and Testing of Compression Specimens.

The single crystal rods were cut into lengths, $\sim$ 1mm. longer than the gauge length, either with a saw (see section D.) or with the spark cutter. The specimen was washed with acetone to remove all traces of glue and mounted in the grinding jig with an equal length projecting on either side. Sometimes the specimen was wrapped in cellophane to prevent the jig scratching the surface. However, the cellophane was quite slippery and more pressure from the locking screw was required to hold the specimen. The ends of each specimen were ground on 400C and 600 C silicon-carbide papers until

the gauge length was reached. During grinding the jig was protected by shims of suitable thickness. When the specimen was ground to gauge, it was removed from the jig; the ends were deburred with 600C silicon-carbide paper and the specimen washed with acetone. The specimen was then weighed. The initial cross-sectional area, Ao, was calculated from the weight using

$$Ao = \frac{W.\ 10^3}{8.58.lo} \quad mm.^2$$

where W = weight in grams.

lo = gauge length in mm.

The density of niobium is 8.58 gms. cm^{-3}.

The majority of specimens were 3mm. diameter and 8mm. gauge length. Some 10 mm. gauge length specimens were tried but these buckled during the compression. Sometimes, 6 mm. gauge (and 3mm dia.) were used for temperature change experiments.

Some crystals were only 2.3 - 2.5 mm. diameter after machining; the gauge length for these specimens was 6 mm.

These relatively large diameter specimens were tested with the Mark I Machine in the compression jig described in section H. Each specimen was centred to within 0.1 mm. with a depth gauge. For low temperature tests, the specimens were centred at room temperature and held with a small load ($\sim$ 1 kg) whilst cooling. Once at temperature the load was removed and the test proceeded in the usual way. A similar proceedure was followed if the temperature was

changed in the middle of a test.

Specimens tested with the Mark II machine were always of a size which could be used in the semi-automatic compression jig, i.e. gauge length 0.097" - 0.103" and diameter 0.050" - 0.066". The technique used with this apparatus has been described in detail by Altshuler (1964) and will not be given here. This apparatus was used for strain rate and temperature change tests and also for low temperature constant strain rate tests.

Some compression tests were done measuring strain directly with the attachment described in section I. Before introducing the specimen, the displacement transducer was calibrated so that full scale on the 2.5 mV range (of the recorder) corresponded to 10 μ movement of the anvils. This was done with the recorder on the 25 mV range; a 1,000 μ block was used to displace the core, and the excitation voltage was adjusted until the recorder pen balanced at 10 suppressions, zero. The load cell was calibrated in the usual way but its output was put into the Rikadenki recorder. The specimen was put in position and the displacement transducer re-zeroed when there was just no load on the specimen. The test then proceeded in the usual way. Initially the recorder was operated with the channels reading 50 kgs. and 10 μ f.s. range, but after the yield stress the strain channel was changed to 100 μ f.s.; on the most sensitive range a strain of 10^{-5} corresponded to a pen displacement of 2 mm. The advantages of measuring

strain directly in this way were a) strain rate was also measured, b) the pre-yield strain was greatly magnified.

O. Preparation and Testing of Tensile Specimens.

The tensile test specimens were produced by acid machining as described in section F. The gauge length was always 10 mm. but the gauge diameter varied from specimen to specimen in the range 1¼ - 1½ mm. The diameter was very even over the gauge length providing that a continuous film of acid was kept on the wheel. The gauge diameter was usually measured with a micrometer; this was occassionally checked by weighing a known length cut from the specimen after deformation, and calculating the original cross-sectional area assuming homogeneous deformation.

The first tests were done with the araldite grips and the Mark I machine. However, it was soon established that the collet grips did not affect the stress-strain curve and so most work was done using the Instron machine as this was more convenient and had a more sensitive stress scale.

All tests were done at constant strain rate, since their main purpose was to compare tension stress-strain curves with those obtained in compression.

P. Temperature Measurement and Control During Mechanical Testing.

Tests with the Mark I and Instron Machines.

Tests were done with these machines at the following temperatures -

77°K - Boiling point of liquid nitrogen.
90°K - Boiling point of liquid oxygen.
158°K - Melting point of ethyl alcohol.
273°K - Melting point of ice.
295°K - Room temperature.

Room temperature was measured with a mercury thermometer. The melting point of ethyl alcohol was measured with a thermocouple and always found to be 158 $\pm$ 0.5°K. The other temperatures were assumed. The thermocouple was made from - gold 2.11% cobalt and silver 0.37% gold (atomic %) wires supplied by Johnson Matthey and Co. Ltd., who also supplied a calibration curve (fig. III 23). This was checked with boiling nitrogen and melting ice giving the reference temperatures.

The tensile or compression jig was immersed in a dewar of the constant temperature bath and left for 30 mins. At the end of this time the specimen was assumed to be at temperature and was tested.

Tests with the Mark II Machine.

The temperatures were measured with platinum and carbon resistance thermometers and checked where possible by the vapour pressure of the cryogenic fluid. Full details of

the positioning and calibration of these thermometers have been given by Altshuler (1964).

Q. X-Ray Techniques.

All Laue photographs were taken with a Hilger Micro-focus X-ray Unit. The detachable film holder was fixed to the collimator stand. The specimen table was perpendicular to the film and could be moved in a horizontal plane by two micrometer screws. Specimen film distance was 3 cms.

Single crystal rods were held parallel to both film and specimen table. Because of their great length (10 - 30 cms.) these rods could be lined up by 'eye' to within about $\frac{1}{2}^{o}$. Using the 200 μ collimator the exposure time was 10-15 mins.

Compression specimens were easily and accurately aligned. The ground ends were perpendicular ($\pm$ 0.05^{o}) to the cylindrical axis so it was only necessary to place the specimen on the table and X-ray. The important axis in compression was the perpendicular to the compression anvils, as this rotated towards the pole of the slip plane. The degree of rotation was determined by X-raying before and after deformation. After deformation the 80 μ collimator was always used in order to keep the Laue spot size reasonably small. Exposure times varied with the amount and type of defomation e.g. after a shear-strain of $\sim$ 0.80 on one system the exposure time was $\sim$ 24 hours; the same

strain due to heterogeneous glide on two systems gave a streak rather than a Laue spot and required an exposure time of ~ 120 hours.

Laue photographs of tensile specimens were taken after deformation. The specimen was mounted horizontally like the crystal rods. The initial orientation was determined by X-raying the undeformed portion between the gauge and the part held in the grip. The specimen was then moved parallel to the film with the micrometer screws and the deformed region was X-rayed. After determining the initial orientation, it was possible to index particular low indiced spots on both films. This was desirable when, due to overshoot, the pole of the crystal rotated into an adjacent triangle.

R. Preparation of Specimens for Electron Microscopy.

Cutting Slices from Deformed Crystals.

The slip lines were neither prominent nor straight, so an X-ray method was used to reference the crystal accurately. Only compression specimens were used, the slip plane was determined from the pole rotation and the slip direction assumed to be the appropriate $\langle 111 \rangle$ direction. For clearness reference will be made to the $(\bar{2}11)$ $[111]$ slip system. The slicing technique varied a little with type of slice.

Four types of slice were taken, viz.

a) parallel to the slip plane,

b) perpendicular to the slip plane but containing the slip direction,

c) perpendicular to both slip plane and slip direction,

d) at 45° to the slip plane but containing the slip direction.

a) The specimen was glued to the table of the goniometer block (fig.III 10) and examined at low magnification with an optical microscope. Using cross-wires for reference, the deformation marks were aligned parallel to the short edge of the block. The specimen was X-rayed; matching the ascribing lines of the block with reference lines on the X-ray table gave reference directions. By rotating the specimen according to the X-ray information the [$\bar{2}$11] was put in a plane parallel to the X-ray table. The angle between the [$\bar{2}$11] direction and the plane of the film was calculated and a wedge of that angle cut. The goniometer block and wedge were then inserted into the cutting block and slices 1 - 1½ mm. thick cut out with a saw (see III.D).

b) Bearing in mind the shape of the specimen it was glued to a brass block (4 x 2½ x 1 cms.) and X-rayed. The orientation of the specimen was altered (by unsticking and reglueing) until the [0$\bar{1}$1] direction was perpendicular to the film. The specimen was then ground on silicon-carbide papers, protecting the block with shims about 2 mm. thick. The specimen was reversed on the block and the other side ground using shims, ¾ mm. thick, to protect the block and determine the specimens' thickness. This

process gave a flat sheet 8 x 3 x ¾ mm.

c) These slices were cut similarly to (a) except that the slip lines were set perpendicular to the short edge of the goniometer and the [$\bar{1}$11] direction was used for reference.

d) The X-raying procedure was the same as that for (a). However the wedge angle was increased by 45° (taking sign into account) when mounting in the cutting block. This gave a slice 15° off ($\bar{1}$01) in the (0$\bar{1}$1) direction (see stereogram).

Some slices were cut using the spark cutter and the goniometer supplied. This should have been a very convenient method but, unfortunately, due to the small specimen size and the poor conductivity of the "conducting" glues available many crystals were spoilt and the method abandoned.

All slices except type (b) were then ground flat on one side (say side (a) for reference), glued to a brass block, and ground with shims to produce a par-allel sided disc ~ 0.75 mm. thick.

Trepanning and Dishing.

The slices were glued to the spark cutter's goniometer with a conducting mixture of durofix and graphite and with side 'a' up. The goniometer was set perpendicular to the tool. Discs ~ 3½ mm. dia. were trepanned but left glued to the goniometer. A tool, consisting of a 1½ mm. ball soldered on to the end of a brass rod, was used to dish the centre of each disc; for this work the spark cutter was operated

on its finest range, range 7. The dishing was followed with a dial gauge attached to the actuator. The tool was also eroded away and if a brass ball was used an actuator movement of 1 mm. gave a dish 0.25 mm. deep. In this case tool erosion was useful as it increased the radius of curvature of the dish.

Chemical and Electrochemical Thinning.

The depth of each dish was measured with a dial gauge. The disc was then chemically polished in 70 : 30 nitric/ hydrofluoric acid mixture until the disc thickness was ~25μ greater than the depth of the dish. Disc thickness was measured with a micrometer, the flat side being protected with a filter paper.

The disc was finally electropolished in an almost transparent polypropylene beaker, the electrolyte being freshly made sulphuric 10% hydrofluoric acid at 45°C. The polishing conditions were ~ 10V and 0.02 amps; the cathode was a platinum sheet. The specimen was held around its rim in a stainless steel holder. One side of the specimen was illuminated by a strong beam of light, the other side was viewed with a microscope at 50X magnification. Polishing was stopped as soon as a hole appeared. The specimen was washed first with water and then with methanol; it was dried between filter papers.

Other Methods of Thinning 0.5mm. Discs.

These methods usually required a pump which could handle very corrosive liquids over a wide range of temperatures.

Therefore, a centrifugal pump was made entirely of polythene. The polythene parts were moulded from polythene powder by heating in an oven at ~120°C and cooling under pressure. Polythene obtained this way was very hard; it could be machined, drilled and tapped with ease.

a) Dishing with an Electrolytic Jet.

This method has been fully described by Blankenbergs and Wheeler (1964). A jet of electrolyte was squirted on to a disc and about ~ 80 volts applied. A dish was produced by electrolytic polishing. Specimens dished on both sides by this method were finally polished to perforation using the light technique. This method was not very successful with niobium. Only Cortes solution, 5% H_2SO_4, 1.5% HF in methanol would produce a dish and this was usually pitted and anodised. Other electrolytes did not have any effect. The technique was successful with molybdenum, but as no single crystals were deformed the technique will not be detailed here.

b) The P.T.F.E. Holder.

With this technique (described in detail by Briers, Dawe, Dewey and Brammer (1964)) the specimen was polished in a P.T.F.E. holder immersed in a bath of electrolyte. This straight forward method did not work very well with niobium. The only electrolyte which would give a polish was sulphuric 20% hydrofluoric acid; the polishing rate with this solution was so slow that it took ~60 hours to thin a disc 0.5 mm. thick. Attempts to speed up polishing by

increasing the voltage and stirring were not successful as gas bubbles and pitting occurred. Towards the end of the work another attempt was made to produce thin foils quickly with this holder. The sulphuric 20% hydrofluoric acid was again used as electrolyte. Instead of immersing the holder in a bath, two jets were positioned so that a thin film of electrolyte flowed continuously over both sides of the disc. Polishing was done at 10-20V. and ~0.06 amps; perforation occurred after ~ ½ hour.

S. Electron Microscopy.

Nearly all the microscopy was done with an A.E.I. E.M.6 microscope operating at 100 KV. A few foils were also examined with a J.E.M. 6A. microscope at A.E.R.E., Harwell; this was to compare the two microscopes for penetration and brightness. The apertures used in the E.M.6 were, -

a) Condenser - 250 or 400 μ dia.,

b) Objective - 25 or 50 μ dia.,

c) Diffraction - 25 or 50 μ dia.

Though the smaller objective and condenser apertures gave better resolution, the large apertures were preferred because they gave a brighter image. The diffraction apertures were placed in the back focal plane of the objective lens. The diameter of the selected area could therefore be calculated knowing the aperture dia. and the magnification of the objective lens. This diameter could

also be measured on the photographic plate. The stated objective lens magnification was ~38.5 X, the magnification necessary to explain the diameter of the selected area was 50 X. The manufacturers, when told of this, could not give a satisfactory explanation but suggested that objective lens magnification, which depended on specimen position, may have changed with the new tilting stage. However this would alter the overall magnification by 50/38.5. The magnification was checked with a replica of a light diffraction grating and found to be correct within 2%.

The camera constant, λL, (wavelength X a fictitious distance in the microscope) was checked from time to time with an evaporated film of thallous chloride. The variations were quite large (1.682 - 1.692 A cm.) but as only spot indexing was necessary they were not troublesome.

The rotation of the micrograph with respect to the diffraction pattern was determined using the cube edge of molybdenum oxide as a reference. (Figs. III 24 and III 25).

SECTION IV

SECTION IV - Experimental Results & Preliminary Discussion

IV.1 Purity of Material.

The purified material was not chemically analysed. However, J. Lowell of the Clarendon Laboratory measured the resistivity ratios $\rho_{300} / \rho_{4.2}$ before and after the ultra high vacuum anneal. The measurements at 4.2°K were made in a magnetic field which was increased until the resistivity value saturated (4 - 5 k. gauss) since at this temperature niobium is normally super-conducting.

The impure specimen, a single crystal 40 mm x 3 mm. dia., had a resistivity ratio $\rho_{300} / \rho_{4.2} \simeq 200 : 1$.

The vacuum annealed specimen, after swaging and annealing at $>2400^{\circ}C$ and $<5 \times 10^{-9}$ torr, consisted of several grains in a bamboo structure. Its dimensions were 40 mm. x 1.17 mm. dia. and the values of excitation current (I) and associated voltage drop ($\bar{V}$) are detailed below.

Temp.	300°K	4.2°K.
I	0.05 amps	0.5 amps
$\bar{V}$	$(1.21 \pm 0.01) \times 220\ \mu V$	$(0.003 \pm 0.001^{*}) \times 220\ \mu V$

* More likely to be "minus" than "plus".

These values give a resistivity ratio $\rho_{300} / \rho_{4.2} \simeq 4000:1$.

At 20°K the resistivity was again measured and the ratio $\rho_{300} / \rho_{20} \simeq 2000 : 1$.

IV.2. Converting Load-Time Charts into Axial Stress v. Strain and Shear Stress v. Glide Strain Graphs.

During a mechanical test the load was recorded on a strip chart moving at constant speed. The load at a particular time was measured directly off the chart; the change in specimen length at that same time could not be measured directly (except when using the differential transformer) because allowance had to be made for machine "softness". With the Mark I and Instron testing machines the machine "hardness" line was superimposed onto the specimen chart; the distance between the "hardness" line and the specimen line, divided by the magnification factor (Chart Speed/ Cross-head Speed) gave the change in length of the specimen.

IV.2. 1. Axial Stress v. Nominal Strain Graphs.

The nominal strain, ε , is always considered positive and calculated assuming uniform deformation; it is defined to be

$$\varepsilon = \frac{\Delta \ell}{\ell_o} \qquad \text{.....IV(1)}$$

where $\Delta \ell =$ change in specimen length.

$\ell_o =$ gauge length.

When using the Mark II testing machine the nominal strain was computed using a slide rule, made by T.L. Altshuler, which though based on the above equation also allowed for machine hardness.

In compression tests, the axial stress, σ , is given by

$$\sigma = \frac{P}{A} = \frac{P}{A_o}(1-\varepsilon) \text{ kg. mm}^{-2} \qquad \text{.....IV.(2)}$$

where P = load in kilograms.

Ao = initial cross-sectional area, mm^2.

A = the instantaneous cross-sectional area at strain .

Ao was computed from

$$A_o = \frac{W.\ 10^3}{\rho\ l_o} \quad \text{or} \quad \frac{\pi\ d^2}{4}$$

where W = weight of the specimen, gms.

ρ = density, 8.58 gms./c.c. for niobium

d = diameter of the specimen.

In tension tests the stress is given by

$$\sigma = \frac{P}{A_o}(1+\varepsilon) \quad kg.\ mm^{-2} \qquad \text{.....IV (3)}$$

IV.2.2. Shear Stress v. Glide Strain Graphs.

The equations for calculating the shear stress (τ) and glide strain (γ) of a crystal deforming on one glide plane in either tension or compression are well known (Schmid and Boas).

Single glide in tension

$$\tau = \frac{P}{A_o}\cos\theta_o\sqrt{1-\left(\frac{l_o}{l}\right)^2\sin^2\lambda_o} \qquad \text{.....IV.4.a}$$

$$\gamma = \frac{1}{\cos\theta_o}\left[\sqrt{\left(\frac{l}{l_o}\right)^2 - \sin^2\lambda_o}\right) - \cos\lambda_o\Big] \qquad \text{.....IV.4.b.}$$

where θ_o = initial angle between the tension axis and the pole of the glide plane.

λ_o = initial angle between the tension axis and glide direction

l = specimen length at a particular time.

Other symbols have already been given.

Single glide in compression.

$$\tau = \frac{P}{A_0}\cdot\left(\frac{\ell}{\ell_0}\right)^2\sqrt{1-\left(\frac{\ell}{\ell_0}\right)^2\sin^2\theta_0}\,\Big)\cdot\cos\lambda_0 \qquad \text{.....IV.5.a}$$

$$\gamma = \frac{1}{\cos\lambda_0}\left[\sqrt{\left(\frac{\ell_0}{\ell}\right)^2-\sin^2\theta_0}\Big) - \cos\theta_0\right] \qquad \text{.....IV.5. b}$$

Recently, Mitchell (reported by Mitchell, Foxall and Hirsch (1964)) has derived the equations for shear stress and glide strain assuming double glide on $(\bar{1}01)\ [111]$ and $(101)\ [\bar{1}11]$ systems in tension. The value for glide strain was taken as the arithmetical sum of the glide strains on each system.

Double glide in tension on $(\bar{1}01)\ [111]$ and $(101)\ [\bar{1}11]$ (Primary and Conjugate systems)

$$\tau = \frac{P}{A_0}\cdot\frac{\ell}{\ell_0}\cdot\frac{1}{\sqrt{3}}\cdot\cos(45-\beta)\cos\beta \qquad \text{.....IV.6.a.}$$

$$\gamma = \sqrt{6}\cdot\ln\left[\frac{1+\cot\beta}{1+\cot\beta_0}\right] \qquad \text{.....IV.6.b.}$$

where β = angle between stress axis and $[011]$

β_0 = initial angle of β at the onset of double glide.

β is given by

$$\sin\beta = \frac{\ell_d}{\ell}\sin\beta_0 \qquad \text{.....IV.6.c.}$$

where ℓ_d is the value of ℓ at the onset of double glide.

D.K. Bowen of this Laboratory has derived the following equations:

Double glide in tension on $(\bar{2}11)\ [111]$ and $(211)\ [\bar{1}11]$. (Primary and Conjugate)

$$\tau = \frac{\sqrt{2}}{3} \cdot \frac{P}{A_0} \frac{l}{l_0} \cos^2 \beta \qquad \text{.....IV.7.a.}$$

$$\gamma = \frac{3}{\sqrt{2}} \ln \left[\frac{\cot \beta}{\cot \beta_0} \right] \qquad \text{.....IV.7.b.}$$

where β and β_0 are the same as in eqns. IV.6.

Double glide in compression on $(\bar{1}01)\ [111]$ and $(011)\ [\bar{1}\bar{1}1]$. (Primary and conjugate systems)

$$\tau = \frac{1}{2} \cdot \frac{P}{A_0} \cdot \frac{l}{l_0} \cdot \cos \beta \cos (35°16' - \beta) \qquad \text{.....IV.8.a.}$$

$$\gamma = \sqrt{6} \ln \left[\frac{1 + \sqrt{2} \cot \beta}{1 + \sqrt{2} \cot \beta_0} \right] \qquad \text{.....IV.8.b.}$$

where β = angle between the stress axis and $[\bar{1}12]$ and β_0 is the value of β at the start of double glide,

and where $\sin \beta = \frac{l}{l_d} \sin \beta_0$ IV.8.c

Double glide in compression on $(\bar{2}11)\ [111]$ and $(\bar{1}21)\ [\bar{1}\bar{1}1]$. (Primary and conjugate systems).

$$\tau = \frac{\sqrt{11}}{6} \cdot \frac{P}{A_0} \cdot \frac{l}{l_0} \cos \beta \cos (64°47' - \beta) \qquad \text{.....IV.9.a.}$$

$$\gamma = 3\sqrt{2} \ln \left[\frac{3 + \sqrt{2} \cot \beta}{3 + \sqrt{2} \cot \beta_0} \right] \qquad \text{.....IV.9.b.}$$

where β is the angle between the stress axis and $[\bar{3}32]$ and β_0 is the value of β at the start of double glide,

and where $\sin \beta = \frac{l}{l_d} \sin \beta_0$ .....IV.9.c.

Double glide in compression on $(\bar{1}01)\ [111]$ and $(101)\ [\bar{1}11]$. (Primary and critical systems)

$$\tau = \frac{1}{\sqrt{3}} \cdot \frac{P}{A_0} \cdot \frac{\ell}{\ell_0} \cdot \cos\beta \cos(45-\beta) \qquad \text{.....IV.10.a.}$$

$$\gamma = \sqrt{6} \cdot \ln\left[\frac{1+\cot\beta}{1+\cot\beta_0}\right] \qquad \text{.....IV.10.b.}$$

where β is the angle between the stress axis and $[001]$ and β_0 is the value of β at the start of double glide,

and where $\sin\beta = \frac{\ell}{\ell_d} \sin\beta_0$ .....IV.10.c.

Double glide in compression on $(\bar{2}11)\ [111]$ and $(211)\ [\bar{1}11]$. (Primary and critical systems).

$$\tau = \frac{\sqrt{2}}{3} \cdot \frac{P}{A_0} \cdot \frac{\ell}{\ell_0} \cdot \cos^2\beta \qquad \text{.....IV.11.a.}$$

$$\gamma = \frac{3}{\sqrt{2}} \cdot \ln\left[\frac{\cot\beta}{\cot\beta_0}\right] \qquad \text{.....IV.11.b.}$$

where β is the angle between the stress axis and $[011]$, and β_0 is the value of β at the start of double glide,

and where $\sin\beta = \frac{\ell}{\ell_d} \sin\beta_0$ .....IV.11.c.

In addition Bowen has written 'KDF 9 Algol' programmes of all the above equations. These equations and programmes were used for computing the shear stress v. glide strain graphs given in this thesis. The graphs were computed using an English Electric Leo KDF 9 computer available in the University.

IV. 3. General Observations on Mechanical Testing.

The equations given in section IV.2. assume perfect homogeneous deformation and take no account of barrelling, end friction or zonal glide which occur in practice. For a compression specimen to barrel secondary glide is necessary to maintain continuity between regions with different strains. It is noticable that less barrelling occurred in specimens oriented well away from a double glide boundary.(fig.IV.1 a&b.)

IV.3.1. The Effect of End Friction. (Compression Tests)

End friction affects the yield and flow stresses in two opposing ways:-

a) end friction giving rise to barrelling.

b) end friction per se.

a) This effect has been considered by Read, Markus and McCaughey (1948). They assumed the specimen was plastically isotropic and made up from a large number of axial elements. The outer elements, being bent to the shape of the barrelled surface, exerted a tensile stress (laterally) on the material inside and so reduced the applied stress. The stress of a uniformly deformed specimen σ_o, is then given by

$$\sigma_o = \frac{A_o\ \sigma_m}{A^*(1-\varepsilon)\left(1-\frac{a}{4R}\right)} \qquad \text{.....IV.12.}$$

where σ_m = measured stress on specimen at strain ε .

Ao = original cross-sectional area.

A* = maximum cross-sectional area.

a = "radius" of the largest cross-section after deformation.

R = radius of curvature of the barrelled section

$$R = \frac{\left(\frac{\ell}{6}\right)^2 + \Delta a^2}{2\,\Delta a}$$

where ℓ = length of the specimen

Δa = difference between "radii" at the centre of the specimen and at $\frac{\ell}{6}$ from the centre.

As already said this treatment assumes a plastically isotropic material; this would have a circular cross-section at all strains, a single crystal, however, usually deforms in one direction so that the cross-section is elliptical. Thus the "radius" 'a' is in this case the major axis of the ellipse.

If this correction is applied to Nb.19.G. (Fig.IV.1 b.) we get $\sigma_o = 1.05\ \sigma_m$.

b) This treatment only considers the back pressure due to end friction opposing the motion of the specimen over the compression anvils. An isotropic material deforming in plane strain is assumed. The flow stress σ_o, for no end friction is given by

$$\sigma_o = \frac{\sigma_m \cdot X \cdot \mu}{\ell\left[\exp\left(\frac{\mu X}{\ell}\right) - 1\right]} \qquad \text{.....IV.13.}$$

where σ_m and ℓ are the same as in eqn. IV.12.

X = width of the specimen (major axis of ellipse)

μ = coefficient of friction.

There is some evidence (section IV.3.4.) that the coefficient of friction is 0.14 , this gives a yield stress

$$\sigma_y = 0.973\,\sigma_m$$

(where X = 3 mm. AND ℓ = 8mm.)

Altshuler (1964) made several attempts to reduce end friction using a number of lubricants including graphite, molybdenum disulphide and P.T.F.E. In view of his work little attempt was made to find a suitable lubricant. A spray-on layer of P.T.F.E. was tried however, but no advantage was detectable and all tests reported here were conducted with the ends "dry".

IV.3.2. The Effect of Machine "Softness".

Due to machine softness the strain rate $\dot{\varepsilon}$, is much lower in the initial elastic region than in the plastic part of the stress-strain graph. At the yield stress there is a continually varying strain rate. In the elastic region the test approximates to a constant loading rate test which, since there is a negligible increase (or decrease) in cross-sectional area results in a constant stress rate test.

With the Mark I testing machine the loading rate was $\sim 2 kg.\ sec^{-1}$ for a cross-head speed of 284 μ/min; with a specimen 8mm. x 3mm. dia. this gives a nominal strain rate $\sim 6 \times 10^{-4}\ sec^{-1}$ and a stress rate $\sim \frac{2}{7}$ $kg.mm^{-2}.\ sec^{-1}$

In the elastic region of the crystal

$$\dot{\varepsilon}_E = \frac{\dot{\sigma}}{E} \qquad \text{.....IV.14.}$$

where $\dot{\varepsilon}_E$ = the total strain rate on the crystal before yield,

E = Young's modulus of elasticity = $10,500 kg.mm^{-2}$ for niobium. (approx.)

$\dot{\varepsilon}$ = 2.72 x 10^{-5} sec^{-1} (cp. nominal strain rate 6 x 10^{-4} sec^{-1}.)

This difference in strain rate makes it difficult to determine the yield stress particularly at low temperatures since the time available for plastic flow at stresses between 0.9 σ_Y and σ_Y itself is greater.

IV. 3.3. Low Temperature Tests.

When testing in tension, in order to continue uniform deformation, the work hardening rate (W.H.R.) must be sufficient to compensate for the reduction in cross-sectional area. This manifests itself as a continuous rise in load; once the load falls non-uniform deformation starts and the specimen necks either to fracture or to a Luders band. (This may not be true for single crystals deforming in single glide, see below.)

Mathematically, for uniform deformation we have,

$$\theta \geqslant \frac{\sigma}{1+\varepsilon} \qquad \text{.....IV.15.}$$

where θ = rate of work hardening.

At low temperatures b.c.c. metals have high yield and flow stresses and low rates of work hardening (Masters (1962)) and so fracture occurs at low values of strain.

Testing in compression should not be subject to this limitation, however many specimens strained at 77°K deformed in a narrow zone(s). (fig.IV.2.). This was not observed at 158° K nor at higher test temperatures, nor in Nb.28

which had a higher W.H.R. at low temperatures than the usual testing material and a smaller length to diameter ratio.

The possible exception to the uniform deformation criterion mentioned above is for crystals oriented for $(\bar{1}01)$ [111] glide. The load fell soon after yielding giving an "easy glide" stage of strain $\varepsilon \simeq 0.25$ (see fig. IV 21). If deformation had proceeded non-uniformly then secondary glide would have been necessary in order to maintain continuity between the slipped and unslipped parts of the crystal. This would have been observed by

a) X-ray determination of lattice rotation,

b) visual observation of a propagating Luders band.

That neither of these was observed suggests that uniform glide on one system occurred.

IV. 3.4. Termination of Compression Tests.

Tension tests end naturally by fracture. In compression such an obvious end is not obtained so tests were terminated when one of three conditions arose.

a) The maximum capacity of the testing machine was reached.

b) Zonal deformation occurred.

c) The ends of the specimen moved well away from their initial positions and the load decreased.

a) This condition is really trivial but was a serious drawback when using the Mark II testing machine.

b) Once zonal glide occurs the stress, strain and strain rate are all unknown and subsequent deformation is of limited use. Zonal glide was usually accompanied by a fall in load.

c) This condition, which is a result of lattice rotation, was the usual end to single glide tests. (Fig.IV.1.a.) The effect can be considered by reference to fig. IV.3. When the ends of the specimen move away from their initial positions, the deforming load is no longer axial and exerts a tipping moment on the specimen. This tipping moment is opposed by a correcting moment due to friction between the ends of the specimen and the compression anvils. We have (see fig. IV. 3.)

$$\text{Tipping Couple} = P.\ell.\tan\alpha$$

$$\text{Correcting Couple} = P.\mu.\ell$$

If $P\ell\tan\alpha > P.\mu\ell$

i.e. $\tan\alpha > \mu$ IV.16

then an additional couple is needed to oppose the tipping couple. This is obtained by a redistribution of the load on the ends of the specimen. (see. fig. IV.3.b). Immediately before $\tan\alpha > \mu$ the deformation should proceed uniformly; as soon as the stress is redistributed the parts of the ends of the specimen "connected" by the short diagonal will deform rapidly under a higher stress, whilst the other parts of the ends will hardly deform at all since the stress has decreased. In practice the load should stop rising at this point.

Measurement of α will give a value to μ , the coefficient of friction. In fig.IV.1.a. $\alpha = 8^{o}$,therefore

$$\mu = \tan \alpha = 0.14.$$

IV.4. The Orientation Dependence of the Glide Systems.

The orientations of all the Nb crystals used in this work are given in fig. IV. 4. The glide systems operating for orientations in the different parts of the triangle have been mainly determined by X-rays. Assuming glide on $\{110\}$ and $\{211\}$ planes, and in $\langle 111 \rangle$ directions only, the standard triangle can be divided up into three regions on the basis of resolved shear stress. In fig. IV.5. in the regions A, B and C the systems $(\bar{2}11)$ $[\bar{1}11]$, $(\bar{1}01)$ $[\bar{1}11]$ and $(1\bar{1}2)$ $[\bar{1}11]$ respectively have the highest resolved shear stress.

Along line X - X' $(\bar{2}11)$ $[\bar{1}11]$ and $(\bar{1}01)$ $[\bar{1}11]$ are equally stressed; it is part of the great circle joining the (111) pole to the bisector of the $(\bar{2}11)$ and $(\bar{1}01)$ poles. Along Y - Y' $(\bar{1}01)$ $[\bar{1}11]$ and $(1\bar{1}2)$ $[\bar{1}11]$ are equally stressed. This line is only approximate; the points Y and Y' were calculated using stereographic triangles but the line between was approximated to a straight line joining the two.

Along the symmetry boundaries (001) (011) and (001) $(\bar{1}11)$ we have the following systems equally stressed

a) (001) - Y' , $(1\bar{1}2)$ $[\bar{1}11]$ and $(\bar{1}\bar{1}2)$ $[\bar{1}11]$.

b) Y' - X' , $(\bar{1}01)$ $[\bar{1}11]$ and (101) $[\bar{1}11]$.

c) X′ - (011), $(\bar{2}11)$ $[\bar{1}11]$ and (211) $[\bar{1}11]$.

d) (001) - Y , $(1\bar{1}2)$ $[\bar{1}11]$ only (not a double glide boundary).

e) Y - X , $(\bar{1}01)$ $[\bar{1}11]$ and (011) $[\bar{1}\bar{1}1]$.

f) X - $(\bar{1}11)$, $(\bar{2}11)$ $[\bar{1}11]$ and $(\bar{1}21)$ $[\bar{1}\bar{1}1]$.

The boundary (011) $(\bar{1}11)$ is not a double glide boundary.

In compression tests the stress axis (perpendicular to the compression anvils) rotates towards the pole of the glide plane. The glide direction is then assumed to be the appropriate $\langle 111 \rangle$. In tension tests the stress axis rotates towards the glide direction, the glide plane is then assumed. The primary glide system is the most highly stressed system in the crystal. Secondary systems are defined by the change in Schmid Factor ($\cos\theta \cdot \cos\lambda$) as the lattice rotates due to glide on the primary system; if the Schmid Factor increases the system is described as conjugate and if it decreases as critical. Since the rotation in compression is approximately opposite to that in tension, the conjugate system in one becomes the critical system in the other and vice versa.

Region A. - in this region well away from the double glide boundary (001) (011) glide occurred on the $(\bar{2}11)$ $[\bar{1}11]$ system at both room temperature and 158°K. However for crystals oriented within about 4° of this double glide boundary glide occurred on the primary and critical (for compression) systems $(\bar{2}11)$ $[\bar{1}11]$ and (211) $[\bar{1}11]$. In this case the stress axis did not move at least to within the accuracy of the Laue photograph. Double glide was not always homogeneous,

compare figs. IV. 6 and 7., which are Laue photographs taken after deformation of Nb.19F. (ε = .34) and Nb. 25A (ε =0.30) respectively. In fig.IV.7. one end of the streaks corresponds to glide on $(\bar{2}11)$ $[\bar{1}11]$ the other end to glide on (211) $[\bar{1}11]$; the centres of the streaks correspond to double glide. In both photographs the spot which shows very little asterism is $(0\bar{1}1)$ which is perpendicular to both glide directions.

Nb. 4b behaved differently from all the other crystals from the centre of this region in that glide occurred on $(\bar{3}12)$; since this result was surprising it was checked on 4 specimens (all cut from Nb.4b). However Nb 4b was different from the usual material in that it was grown from Nb.35 which had been given 10 molten zone passes. Compression specimens which deformed in single glide never reached the double glide boundary (001) $(\bar{1}11)$ since the tests were stopped due to end movements. (IV.3.4.c.). Tension tests with orientations like that of Nb.32 II. fractured before the double glide boundary (001) (011) was reached, whereas orientations much nearer that boundary gave parabolic hardening curves and were assumed to have slipped on two systems from the start.

Region B - in compression this region behaved much like A except that the glide plane was $(\bar{1}01)$. The stress axis rotation of Nb.28 could not be determined though several attempts were made. However from the room temperature stress-strain curve and the optical observations (two sets of slip lines) it appears likely that double glide on primary and critical systems occurred from the start of deformation.

In tension Nb.23.c deformed almost entirely on the primary system (fig.IV.8.) even to the extent of overshooting the symmetry boundary by $\sim 9^{o}$.

Region C. Only one specimen Nb.17a. was tested. Unfortunately it was strained to such an extent that no reliable Laue photograph could be obtained.

Border Regions - As can be seen from fig. IV.4. crystals Nb.(F.P.)6. and Nb.29 are just in region B; they are however close enough to the lines X - X' and Y - Y' to be considered borderline cases.

Nb.(F.P.)6 slipped on the $(\bar{2}11)$ $[111]$ system. Its orientation was such that it was very easy to distinguish between the possible glide planes ($(\bar{1}01)$, $(\bar{3}12)$ and $(\bar{2}11)$) fig. IV.9 shows the stress axis rotation of Nb.(F.P.)6 and the possible rotation paths.

Nb.29. was tested in tension. Its Laue photograph is reproduced in fig. IV.10. One end of the streaks corresponds to a $[\bar{1}11]$ glide direction and the other end to a $[111]$. (fig. IV.11.). From this it is inferred that glide occurred heterogeneously on $(1\bar{1}2)$ $[\bar{1}11]$ and $(\bar{1}01)$ $[111]$.

IV.5. Stress v. Strain Graphs and Optical Observations.

The following stress v. strain graphs are given as shear stress v. glide strain wherever possible. If the glide system was not determined then the most appropriate system

based on fig. IV 5 has been used. Where twinning has intervened or comparison is made with a twinned specimen then the axial stress v. nominal strain graph is given.

To facilitate description the f.c.c. stress-strain terminology has been adopted i.e. work-hardening stages O. I, II and III.

Unless stated otherwise the nominal strain rate is, $\dot{\varepsilon} = 6 \times 10^{-4}$ sec^{-1} for compression and $\dot{\varepsilon} = 5 \times 10^{-4}$ sec^{-1} for tension tests.

IV. 5. 1. Room Temperature Deformation.

a) Single glide in compression on $(\bar{2}11)$ [111]

Fig. IV.12. shows the stress (τ) v. strain (γ) graph and initial orientation of Nb.32 II.B. Immediately after yielding there is a small stage O which is parabolic; this is followed by two linear stages wherethe W.H.R. θ_I and θ_{II} are 3.28 and 16.9 kg. mm.$^{-2}$ respectively. On a very fine scale stage I exhibits small oscillations; these are shown on the load-time graph fig.IV.13. The load-time graph in stage II shows no such oscillations. The test was stopped when the load ceased to rise. This is illustrated by a photo-copy of the chart, fig. IV.14.

As can also be seen from fig. IV 12, the stress axis did not reach the double glide boundary and optical examination of the specimen revealed only one set of slip lines. The rotation of the stress axis usually agreed with the calculated rotation to within about 5%.

b) Double glide in compression on $(\bar{2}11)\ [111]$ and $(211)\ [\bar{1}11]$

In compression, $(211)\ [\bar{1}11]$ is the critical system for crystals whose stress axes lie in region A (fig. IV.5). The initial orientation and stress (τ) v. strain (γ) of Nb. 19.A. curve is shown in fig. IV.15. The graph is generally slightly convex upwards with a dip at a strain ~ 0.75. The average W.H.R., $\theta = 8.33$ kg.mm.$^{-2}$

Heterogeneous glide which sometimes occurred on these systems does not affect the stress-strain graph very much e.g. Nb.25A had an average W.H.R. only 7% lower than Nb.19.A.

Nb.19.D was examined optically after a strain $\gamma = 0.42$. On the 'screw' face $\sim(100)$ the slip lines were very wavy (fig. IV.16); mid-way between the 'edge' and 'screw' faces two sets of slip lines were seen fig.IV.17.

NOTE. By 'screw'face is meant the face of the crystal through which the screw dislocations emerge. For $[\bar{1}11]$ and $[111]$ dislocations and a stress axis near (011) this face is (100). Similarly 'edge' face.

c) Single glide in tension on $(\bar{2}11)\ [111]$

Fig. IV.18. shows the stress (τ) v. strain (γ) graph of Nb.32 II.A. The graph shows three stages of hardening, stages I and II are linear with W.H.R. $\theta_I = 3.57$ and $\theta_{II} = 9.74$ kg. mm^{-2} respectively. Stage III is parabolic and starts at stress $\tau_{III} = 3.8$ kg. mm^{-2}. Fracture occurred before the double glide boundary was reached.

d) Double glide in tension on $(\bar{2}11)\ [111]$ and $(211)\ [\bar{1}11]$.

The stress (τ) v. strain (γ) graph of Nb. 25 C is shown

in fig. IV.19. together with the initial orientation. The graph is parabolic and although some glide on the $(\bar{2}11)$ [111] system only should have occurred, it is probable that double glide was present from the start.

e) Single glide in compression on $(\bar{1}01)$ [111] .

Fig. IV.20 showes the stress (τ) v. strain (γ) graph of Nb.32 I.C. It shows several stages of hardening. Stage 0; immediately after yielding, is very large compared with the same stage in $(\bar{2}11)$ [111] glide; as before it is parabolic but now extends to a strain of 0.03 with a stress increment of 1.2 kg. mm^{-2}. Stage I and Stage II are again linear with W.H.R. θ_I = 3.00 and θ_{II} = 17.8 kg. mm^{-2}. Again, like specimens which slipped on the $(\bar{2}11)$ [111] system, stage I showed small undulations on the load-time chart but in this instance they were even smaller. Stage II, and the test, was terminated when zonal glide occurred at a stress $\tau_{III} \simeq$ 5.5kg. mm^{-2}. Nb. 23.A was deformed after zonal glide had started and continued to harden parabolically.

Optical observations confirmed that glide on one system only had occurred but the calculated rotation (assuming uniform deformation) was usually ~10 - 15% lower than that measured with Laue photographs.

f) Single glide in tension on $(\bar{1}01)$ [111]

This specimen, Nb.23,C, as shown in fig. IV.8., overshot the symmetry boundary by ~9°. This means that double glide did not occur at the symmetry boundary and if single glide is assumed (to obtain a value for maximum strain)

then of the total strain of γ = 1.04, glide on the conjugate system accounts for only $\sim$0.11 strain.

Fig. IV 21 is the stress v. strain graph assuming glide on the primary system only; fig. IV 22 assumes double glide started at the symmetry boundary. The strain at which the stress axis reaches the symmetry boundary is marked ↑.

Until the symmetry boundary is reached both graphs are of course exactly the same. As with the $(\bar{1}01)$ $[\bar{1}11]$ compression test stage 0 is parabolic and large, extending to a strain of 0.05 and giving a stress increment of 1.0 kg. mm^{-2}. Stage I, the "easy glide" stage is, however, no longer linear. After stage 0, there is a linear work softening region with W.H.R, θ = - 1.32 kg.mm^{-2}, which extends to a strain $\gamma \simeq 0.20$; the slope then becomes less steep until at the strain at which the stress axis reaches the symmetry boundary, the W.H.R. becomes positive again.

If single glide only is assumed, stage II extends from γ = 0.47 to γ = 0.80 and has a linear W.H.R., θ_{IIS} = 5.47 kg. mm^{-2}. Stage III starts at a stress τ_{III} = 4.6 kg.mm^{-2} and extends over a strain of 0.24.

Assuming that double glide starts at the symmetry boundary alters these parameters. Stage II extends from γ = 0.54 to γ = 0.86 with a W.H.R. θ_{IID} = 7.64 kg. mm^{-2}. Stage III starts at a stress, τ_{III} = 5.70 kg.mm^{-2}. and extends for only 0.12 γ. The total strain γ_F is also less being 0.98 (cp. 1.04).

Optical examination showed only one set of slip lines

except near the fracture where there were two sets. Thus it is probable that the stress-strain graph assuming single glide only is more correct.

g. Double glide in compression on $(\bar{1}01)\ [111]$ and $(101)\ [\bar{1}11]$.

Nb.28.A. was deformed in the Mark II testing machine at a strain rate $\dot{\varepsilon} = 7 \times 10^{-4} sec^{-1}$. Its length to diameter ratio was considerably less than that of the other compression specimens which were tested in the Mark I machine. Its dimensions were 0.100" x 0.064" dia. Its stress (τ) v. strain (γ) graph and initial orientation are given in fig.IV 23. The linear part of the graph has a W.H.R., θ , = 19.5 kg. mm^{-2} and extends from γ = 0.10 to 0.30.

h. Single glide in compression on $(1\bar{1}2)\ [\bar{1}11]$.

Apart from a slight increase in the W.H.R. immediately after yielding, Nb.17a (fig.IV.24) deformed parabolically. After about 0.30 strain the W.H.R. changes more slowly, some sample values are $\theta_{0.1\gamma}$ = 21.4 kg.mm^{-2}. and $\theta_{0.5\gamma}$ = 3.3 kg.mm^{-2}.

(i) Double glide in tension on $(1\bar{1}2)\ [\bar{1}11]$ and $(\bar{1}01)\ [111]$.

It was not possible to derive general equations which would give the resolved shear stress and glide strain for glide on these two systems, hence fig. IV.25. is the axial stress (σ) v. nominal strain (ε) graph of Nb.29. This stress-strain graph is parabolic, the test was stopped, after a strain ε = 0.15, for Laue photographs to be taken (see IV.4.). Optical examination of the specimen confirmed that double glide had occurred.

IV.5. 2. Deformation at 158°K

a) Single glide in compression on $(\bar{2}11)$ $[111]$.

The resolved stress (τ) v. strain (γ) graph of Nb.26.C. is given in fig. IV.26.

Stage 0 is parabolic and extends to a strain $\gamma = 0.07$. Stages I and II are both linear and have W.H.R. $\theta_I = 11.25$ kg. mm^{-2} and $\theta_{II} = 25.5$ kg. mm^{-2} respectively. Stage I extends from $\gamma = 0.070$ to 0.324 and stage II from $\gamma = 0.400$ to 0.560. Stage III started at stress $\tau_{III} = 22.5$ kg.mm^{-2}.

Visual examination of the specimen after the test showed that zonal glide had just started; this was probably responsible for the specimen going into stage III.

Optical examination of several specimens deformed at 158°K (e.g. 26D and 26E), showed the expected single set of slip lines on faces intermediate between the edge and screw faces, but on the screw face itself no slip lines were seen. However, scratches on this face which were within $\pm 30^\circ$ of the stress axis were crossed by short parallel lines approximately perpendicular to the stress axis. These are possibly signs of the slip lines.

b). Double glide in compression on $(\bar{2}11)$ $[111]$ and (211) $[\bar{1}11]$

Fig. IV.27. shows the stress (τ) v. strain (γ) graph and initial orientation of Nb.6B. After a parabolic region of $\gamma \simeq 0.20$ there is a region of almost linear hardening which extends out to $\gamma \simeq 0.78$ at which strain the test was stopped. The W.H.R., $\theta = 3.09$ kg. mm^{-2}.

Optical examination of the specimen after deformation showed two sets of slip lines.

c). Tension tests at 158°K.

Only three specimens were tested in tension at 158°K. Despite differences in orientation, the stress-strain graphs were very similar, all being parabolic. The shear stress (τ) v. glide strain (γ) for Nb.32I and the orientations of all three crystals tested are given in fig. IV.28.

IV. 5.3. Deformation at 77°K.

a). Deformed at 77°K only.

All specimens were tested in compression and since twinning intervened the graphs are given as axial stress (σ) v. nominal strain (ε).

Fig. IV 29 shows the stress v. strain graph and initial orientation of Nb.3A. There is no detectable glide before the first 'twin drop' (abrupt fall in load), which occurs at σ_T = 41 kg. mm^{-2} ; resolving on to the $(\bar{2}11)$ $[111]$ system gives a twinning shear stress τ_T = 19.5 kg.mm^{-2}. After two such twin drops, each ~ 0.02 strain, plastic flow starts; the W.H.R. is rapid and linear, θ = 144 kg.mm^{-2}. (dividing these W.H.R.s by 5 gives a rough value for comparison with the shear stress v. glide strain rates). Extrapolating this plastic flow line back to zero strain shows that the W.H.R. during the twin drops was about the same. At a stress σ ~75 kg. mm^{-2} and a strain ε = 0.27 there is a

rapid fall off in the W.H.R. to $\theta = 8$ kg.mm^{-2}.

The stress (σ) v. strain (ε) graph of Nb.6A shows some features common to the graph of Nb.3A and to all tests of this type. (about 12 tests in all); these are:

(i) no detectable plastic flow before twinning,

(ii) a high rate of work hardening after twinning.

The significant differences between the two graphs are:

(i) the strain increment during a twin drop varies considerably,

(ii) plastic flow after twinning occurs at stresses well below the initial twin stress,

(iii) the extrapolated plastic flow line does not coincide with the 'twin stress line'.

Often in the elastic region following a twin drop, the load rose faster than during a "hardness" determination so that when allowance for the machine's extension was made the strain in the specimen decreased.

The reproducibility of the initial twin stress is not very good for specimens taken from different crystal rods. The average of 9 tests gave an initial resolved twin stress of 20.9 kg. mm^{-2} and a scatter of results of $\pm$ 4 kg. mm^{-2}. However, sometimes specimens from the same rod have good reproducibility e.g. Nb. 9A & 9 B.

	FIRST TWIN DROP		SECOND TWIN DROP	
	STRESS (σ)	STRAIN (ε)	STRESS (σ)	STRAIN (ε)
9A	44.8	0.030	38.0	0.026
9B	44.8	0.027	38.2	0.018

Optical examination of Nb. 9B after two twin drops (ε = 0.053) revealed that deformation had occurred over only half the crystal and consisted of two sets of chevron twins. To see if each set of twins was associated with a twin drop, deformation of Nb 9D was stopped after only one such 'drop'. Unfortunately the strain in this twin drop was very large ($\sim$0.05), fig. IV.31 is a photomicrograph of the unpolished surface approximately parallel to the strain direction. Two sets of twins can be seen at about 80° to each other; the larger members of each set are near the edge of the micrograph. Although not obvious on the micrograph the total amount of twinning on one system was 2 - 3 times that on the other. The small twins in the centre of the micrograph do not intersect each other very easily i.e. the end of a twin comes to a point when against the side of another twin before crossing.

After deformation, Nb.14.A. was given a light chemical polish. Fig. IV 32 shows the surface parallel to the deformation direction; the end of the specimen was included for reference. The two sets of twins make an acute angle of $\sim 70^{\circ}$ with each other and equal angles of $\sim 35^{\circ}$ with the stress axis (perpendicular to compression anvils). On the surface perpendicular to the deformation direction the twin markings were parallel with each other and with the compression anvil. It can be seen in fig. IV 32. that the twins cross each other without first coming to a point; this is in accordance with the twinning systems being $(\bar{2}11)$ $[111]$ and (211) $[\bar{1}11]$.

b) Pre-straining at room temperature before deformation at $77^{\circ}K$

These graphs are given as axial stress (σ) v. nominal strain (ε) to allow comparison with the graphs in section IV.5.3.a. above.

Generally a pre-strain $\geqslant$ 0.02 suppressed twinning, a typical graph is Nb.2C shown in fig. IV.33. At $77^{\circ}K$ a linear hardening region with W.H.R., θ = 38.7 kg.mm^{-2} follows the rounded re-yield. At a strain of ε = 0.22 the work hardening rate increases. Examination of the specimen after deformation revealed zonal glide; the side of the crystal sliding down the zone had hit the compression anvil. This sudden increase in cross-sectional area probably accounts for the rise in W.H.R. (fig. IV 33) since the stress v. strain curve was computed assuming uniform deformation.

Often on re-straining at the lower temperature there was a yield drop (fig. IV 34(a)) and sometimes a double yield drop. Once, a similar fall in stress occurred after quite a large strain though in this instance the W.H.R. was high. (fig. IV.34(b).). These stress drops are probably associated with zonal glide since such a zone was always present after a drop.

The average flow stress change $(\Delta\sigma)_{\dot{\varepsilon}} = (\sigma_{77^{\circ}K} - \sigma_{295^{\circ}K})_{\dot{\varepsilon}}$ was 62 kg. mm^{-2} and the scatter $\pm$ 2 kg. mm^{-2}.

IV. 5.4. The Effect of Temperature on the Yield Stress and Work Hardening Graph.

In this series of tests only specimens cut from rod Nb.28 were used. This rod was given a different 'purification' treatment from the usual material, in that several zone passes were given. Molten zones were passed in the Miles Hivolt E.B.U., the detailed treatment being as follows:

(i) 4 mm. dia. rod given 4 zone passes at 10 $mm.min^{-1}$, - swaged to 3 mm. dia. and chemically polished to remove 0.25 mm.;

(ii) central portion removed and given 2 zone passes at 3mm. min^{-1}. - swaged in two steps to 0.071" and chemically polished to 0.064";

(iii) central portion removed and given one pass at 15 mm. min^{-1}.

(iv) annealed for 7 hrs. at $> 2400^{\circ}C$ until pressure $< 1 \times 10^{-8}$ torr.

All specimens were tested in compression at a strain rate $\dot{\varepsilon} = 7 \times 10^{-4} sec^{-1}$ with the Mark II testing machine. The initial orientation has already been given in fig. IV 23. The axial stress v. nominal strain (σ v. ε) graphs for a number of temperatures viz. 294, 167, 77, 20.4, 14 and $4.2^{\circ}K$ are given in figs. IV 35 and IV 36.

The room temperature stress-strain graph is nearly linear for the first 0.14 strain (ε) with a W.H.R., $\theta = 88$ kg. mm^{-2}. After this strain the W.H.R. decreases parabolically. The test was stopped after 0.30 strain.

At 167°K the stress v. strain graph is parabolic up to $\sim$ 0.22 strain. At a strain $\varepsilon = 0.30$ a linear hardening stage starts, with a W.H.R., $\theta = 48.4$ kg. mm^{-2}.

The stress v. strain graph at 77°K is very like that at 167°K again the curve is parabolic followed by a linear hardening stage; at this temperature however the W.H.R. is much greater being $\theta = 112.5$ kg. mm^{-2}. Several specimens were tested at this temperature, some of which twinned; the twinning however did not affect the subsequent hardening.

Three specimens were tested at 20.4°K; in two tests there was measurable plastic flow followed by a large twin drop ($\varepsilon = 0.08$), in the third test the specimen twinned at a considerably lower stress without any detectable prior plastic strain. The deformation after the initial twin was by plastic flow, the hardening was linear with a W.H.R., $\theta = 290$ kg. mm^{-2}.

At 14°K yielding started with a twin drop, there being no suggestion of prior plastic flow. Twin drops also occurred frequently throughout the subsequent deformation which was linear with a W.H.R., $\theta = 400$ kg. mm^{-2}. The work hardening rate over the twin drop strain was the same as that for plastic flow.

At 4.2°K only twinning occurred; using the tops of each twin drop for reference gives a W.H.R., $\theta = 375$ kg. mm^{-2}. 12% pre-strain at 20.4°K did not suppress twinning.

The yield stress v. temperature graph is shown in fig. IV 37. The values of yield stress at 4.2°K and 167°K are for

one result only; the values of yield stress at other temperatures are average values. The actual yield stresses are also shown and where yielding was by twinning the symbol is marked with a 'T'. The yield stress rises rapidly as the temperature decreases until 20.4°K is reached; below this temperature the yield falls again. However at about 20.4°K the mode of deformation changes from being mainly plastic flow (above) to deformation by twinning.

IV. 5. 5. The Temperature and Strain Rate Dependence of the Flow Stress - Activation Enthalpy and Activation Volume.

For this work all the specimens were cut from crystal rod Nb. 28. Its purification treatment has been given in section IV.5.4. and its initial orientation in fig. IV 23. The temperature change tests were all done at a strain rate $\dot{\varepsilon} = 7 \times 10^{-4} sec^{-1}$. The flow stress difference between two temperatures was always measured for a decrease in temperature (increase in stress), since work softening makes the reverse change difficult to measure. Further, for the computation of the flow stress v. temperature graph it is assumed that

$$\Delta\sigma_{13} = \Delta\sigma_{12} + \Delta\sigma_{23} \qquad \text{.....IV.17.}$$

where $\Delta\sigma_{ij}$ is the reversible flow stress between the two temperatures i and j.

Below are tabulated the values of $\Delta\sigma$ for the given

temperature changes.

Temperatures ^{o}K	Stress Change $\Delta\sigma$, $kg.mm^{-2}$	Average $\Delta\sigma$
294 - 77	47.0; 43.0; 49.3; 50.0	47.3
294 - 20.4	66.5	66.5
20.4 - 14	7.0	7.0
20.4 - 4.2	2.0 (Twinned)	2.0

Fig. IV.38. shows the reversible axial flow stress v. temperature graph; the reversible flow stress is plotted as (σ_T - $\sigma_{294^{o}K}$) where $\sigma_{294^{o}K}$ is the total flow stress at $294^{o}K$ and σ_T is the total flow stress at temperature $T^{o}K$. There is an increasingly rapid rise in stress as the temperature falls until $14^{o}K$, between $14^{o}K$ and $4.2^{o}K$ there is a slight fall in stress. However, both points were obtained by a temperature change from $20.4^{o}K$; when changing to $14^{o}K$ the subsequent deformation was by plastic flow but at $4.2^{o}K$ the specimen twinned.

The change in flow stress for a change in strain rate was always measured for an increase in strain rate. Due to machine softness excessive plastic flow at intermediate strain rates made measurements of the flow stress change on decreasing the strain rate inaccurate.

The strain rate change was achieved by altering the motor speed, nominally by a factor of 10 . It was rare for this change to be exactly 10x and so the value of $(\Delta\sigma)_T$ (the flow stress change, temperature constant) was corrected

using

$$\Delta\sigma_{10} = \Delta\sigma_x \cdot \frac{\ln 10}{\ln x} \qquad \text{.....IV.18.}$$

where $\Delta\sigma_{10}$ is the stress change for a strain rate change of exactly 10 times,

and $\Delta\sigma_x$ is the stress change for a strain rate change of x times.

This equation can be derived as follows:

The Johnston-Gilman experimental velocity - stress relationship is

$$\bar{v} \propto \sigma^{x^m} \qquad \text{.....IV.19}$$

where $\bar{v}$ = average dislocation velocity,

σ^x = effective stress on the dislocations,

and m = constant.

Since, $$\dot{\varepsilon} \propto \varrho \bar{v} \qquad \text{.....IV.20}$$

where $\dot{\varepsilon}$ = strain rate

and ϱ = density of moving dislocations.

then $$\dot{\varepsilon} \propto \varrho \sigma^{x^m} \qquad \text{.....IV.21}$$

Assuming that during an "instantaneous" strain rate change the density of moving dislocations does not change, then for a strain rate change $\dot{\varepsilon}_1$ to $\dot{\varepsilon}_2$ we can write

$$\frac{\dot{\varepsilon}_2}{\dot{\varepsilon}_1} = \left(\frac{\sigma_2^x}{\sigma_1^x}\right)^m$$

Taking logarithms and writing for σ_2^x, $(\sigma_1^x + \Delta\sigma_a^x)$ we get, $$\ln\left(\frac{\dot{\varepsilon}_2}{\dot{\varepsilon}_1}\right) = m \ln\left(1 + \frac{\Delta\sigma_a^x}{\sigma_1^x}\right)$$

Expanding $\ln\left(\frac{\Delta\sigma^x}{\sigma_1^x} + 1\right)$ and neglecting powers of $\frac{\Delta\sigma_a^x}{\sigma_1^x}$ greater than unity

we get, $$\ln\left(\frac{\dot{\varepsilon}_2}{\dot{\varepsilon}_1}\right) = m\,\frac{\Delta\sigma_a{}^{x}}{\sigma_1{}^{x}} \qquad \text{.....IV.22}$$

For a different strain rate ratio but with the same basic strain rate we have,

$$\ln\left(\frac{\dot{\varepsilon}_3}{\dot{\varepsilon}_1}\right) = m.\,\frac{\Delta\sigma_b{}^{x}}{\sigma_1{}^{x}}$$

and eliminating m by combination with eq. IV. 22 we get

$$\Delta\sigma_b{}^{x} = \Delta\sigma_a{}^{x}\,\frac{\ln\left(\frac{\dot{\varepsilon}}{\dot{\varepsilon}_1}\right)}{\ln\left(\frac{\dot{\varepsilon}_2}{\dot{\varepsilon}_1}\right)} \qquad \text{.....IV.23}$$

Now, $$\sigma^{x} = \sigma - \sigma_i \qquad \text{.....IV.24.}$$

where σ is the applied stress and σ_i the long range internal stress.

σ_i is independent of strain rate, and so for a strain rate change $\Delta\sigma_i = 0$

$$\therefore\ \Delta\sigma = \Delta\sigma^{x}$$

Substituting in eq. IV.24 we get,

$$\Delta\sigma_b = \Delta\sigma_a\,\frac{\ln\left(\frac{\dot{\varepsilon}_3}{\dot{\varepsilon}_1}\right)}{\ln\left(\frac{\dot{\varepsilon}_2}{\dot{\varepsilon}_1}\right)} \qquad \text{.....IV.25.}$$

which giving values to the strain rate ratios, gives eq. IV.18.

The values of $(\Delta\sigma)_T$ for a strain rate change, corrected to a ratio of 10, are tabulated below. The strain rates used were $\sim 7 \times 10^{-5}\ sec^{-1}$ and $7 \times 10^{-4}\ sec^{-1}$.

Temperature ^{o}K	Stress change, $\Delta\sigma$, $kg.mm^{-2}$	Average $\Delta\sigma$.
14	2.35; 2.33.	2.34
20.4	1.36; 1.51.	1.44
77	2.37; 2.24; 2.39.	2.33

The activation enthalpy and activation volume were calculated using the equations of Conrad and Wiedersich (1960).

$$(H)_{\frac{\dot{\varepsilon}}{\nu}} = \frac{-kT^2 \left(\frac{\partial\sigma}{\partial T}\right)_{\frac{\dot{\varepsilon}}{\nu}}}{\left(\frac{\partial\sigma}{\partial \ln\left(\frac{\dot{\varepsilon}}{\nu}\right)}\right)_T} \qquad \text{.....(eq.II.9)}$$

$$v^x = \frac{2kT}{\left(\frac{\partial\sigma}{\partial \ln\left(\frac{\dot{\varepsilon}}{\nu}\right)}\right)_T} \qquad \text{.....(eq.II.12)}$$

where H = activation enthalpy

V^* = activation volume

ν = Frequency factor

$\left(\frac{\partial\sigma}{\partial T}\right)_{\frac{\dot{\varepsilon}}{\nu}} \simeq \left(\frac{\partial\sigma}{\partial T}\right)_{\dot{\varepsilon}}$ and is obtained from the slope of the flow stress v. temperature graph. (Fig. IV.38.)

$$\left(\frac{\partial\sigma}{\partial \ln\left(\frac{\dot{\varepsilon}}{\nu}\right)}\right)_T \simeq \left(\frac{\partial\sigma}{\partial \ln\dot{\varepsilon}}\right)_T = \frac{(\Delta\sigma)_T}{2.3}$$

where $(\Delta\sigma)_T$ is the stress change for a strain rate change of 10 times.

The values of activation enthalpy and activation volume, are tabulated below.

Temperature ^{o}K	H, e V	V*, $\AA^3$
14	2.60×10^{-2}	38.7
20.4	3.64×10^{-2}	55.3
77	13.38×10^{-2}	225

IV. 5.6. The Effect of Purification on Yield Stress and Work Hardening.

Niobium crystals grown by one zone pass in an electron beam unit had a room temperature yield stress (σ) of ~8 kg. mm^{-2}. After annealing at $> 2400^{o}C$ under a pressure of 1×10^{-8} torr. the yield stress (σ) fell to ~2 kg. mm^{-2}. There was also a marked difference in the shape of the stress v. strain graphs. For example, fig. IV.39 shows the graphs of Nb.19 before and after annealing. Nb.19 was oriented for double glide on the primary and critical systems $(\bar{2}11)\ [111]$ and $(211)\ [\bar{1}11]$. (compression). The impure material has a yield point and several stages of hardening; whereas the pure material has only one stage of hardening.

At $77^{o}K$, the mode of deformation changed with purity. The purified niobium twinned at ~ 40kg.mm^{-2}; the impure material yielded plastically at ~ 72kg.mm^{-2}. However the temperature dependence of the flow stress between room temperature and $77^{o}K$ was similar.

Crystals subjected to several zone passes behaved rather differently. Nb.35 was given 10 zone passes using

the shielded filament cathode in the Mark II E.B.U. The yield stress after this treatment was 4.06 kg.mm. (cp.~8kg. mm^{-2}. for 1 zone pass). After swaging, re-growing the crystal by one zone pass, and high vacuum annealing the yield stress only fell to 3.0 kg. mm^{-2}. (cp.~2kg. mm^{-2}, 1 pass + anneal). In addition, this particular crystal (now known as Nb.46) glided on a $(\bar{3}12)$ plane instead of the expected $(\bar{2}11)$, see section IV.4. Nb.28 (6 passes, unshielded cathode filament) also had a high room temperature yield stress, (σ), of 4.3 kg. mm^{-2}.

At 77°K, however, the results of Nb.28 disagree with Nb. 46; the former yielding plastically at ~38 kg.mm^{-2}, the latter twinning at ~ 50 kg.mm^{-2}.

IV. 5.7. Room Temperature 'Ageing'.

An effect, first noticed by D.K. Bowen, was that if the high vacuum annealed niobium was left for about 3 months in the laboratory atmosphere the yield stress rose appreciably. An example is Nb.23 which had a yield stress, τ , of 1.0 and 1.3 kg. mm^{-2}. before and after 'ageing' respectively.

IV. 5. 8. The Effect of High Vacuum Annealing on the Yield Stress of Tantalum.

A few mechanical tests were carried out on tantalum to find

the effects of a high vacuum, high temperature anneal on the yield stress. These results together with some results of Ferriss, Rose and Wulff (1962) are tabulated below.

Test Temp. ^{o}K	Yield Stress (σ)kg. mm^{-2}.		
	Ta.2.	Ta.3.	Ferriss et al.
295	10.5	24.8	10 (91L)
77	57.3	101.4	75 (41)

The initial orientations of Ta.2, Ta 3 and of the chosen results of Ferriss et al. are given in fig. IV 40. Ta2 was annealed at 2500^{o}C and Ta3 very near to the m. pt. (2996^{o}C), both in a vacuum of $<1 \times 10^{-8}$ torr. Both crystals cooled quickly, by radiation loss, to $\sim$1000^{o}C, and then more slowly to room temperature. The material of Ferris et al, was not annealed in this way but was given 3 molten zone passes at 4 $mm.min^{-1}$. Consequently, the material must have cooled relatively slowly from high temperature.

IV. 6. Microstrain Tests.

Specimens for these tests were all cut from one crystal, Nb.56, which had been grown by only one zone pass and then annealed in the U.H.V. apparatus. This crystal rod was seeded with a piece of Nb.32 II which had the best orientation for single slip on the $(\bar{2}11)$ plane, but seeding was not

entirely successful as can be seen in the standard triangle inset of fig. IV.41. However, X-ray determination of the lattice rotation showed that the slip plane was $(\bar{2}11)$, and the room temperature shear stress-glide strain curve (Fig. IV 41.) is typical for $(\bar{2}11)$ $[111]$ slip, θ_I being 3.25 kg.mm^{-2}. and θ_{II}, 18.70 kg. mm^{-2}.

The compression specimens were deformed at three temperatures viz. 295°K, 158°K and 77°K. Since the first 0.01375 nominal strain (110 μ) could be measured at a magnification of ~25,000 x (i.e. 10^{-5} ε = 2mm.) it is of interest to compare the initial part of the stress-strain curve with a line calculated from Young's modulus. Young's modulus, E, varies both with temperature and with crystallographic direction; the latter is particularly important in niobium which has an anisotropy coefficient A of only ~0.527. A is given by:

$$A = \frac{2\,C_{44}}{C_{11} - C_{12}} \qquad \text{.....eqn.IV.26}$$

where C_{ij} is an elastic stiffness constant. The only published values of the elastic stiffness constants are those given by Bolef (1961) for 300°K. However, C.N.Reid of Birmingham University kindly made available to the author some unpublished work by K.J. Carroll of Rice University which gives these constants over the temperature range 4.2°K to 300°K. (Table IV.1). Unfortunately the niobium used by Carroll contained voids so the values may be in error.

TABLE IV 1

ELASTIC CONSTANTS OF NIOBIUM

(K.J. Carrol)

Units are those of 10^3 kgms. mm^{-2}.

T(^oK)	C_{11}	C_{12}	C_{44}
300	25.04	14.14	2.987
290	25.05	14.05	2.988
280	25.07	13.96	2.988
270	25.09	13.86	2.989
260	25.10	13.77	2.991
250	25.13	13.70	2.994
240	25.15	13.63	2.995
230	25.17	13.58	2.998
220	25.20	13.53	3.001
210	25.22	13.51	3.005
200	25.25	13.51	3.009
190	25.27	13.53	3.015
180	25.29	13.56	3.022
170	25.32	13.61	3.028
160	25.35	13.64	3.034
150	25.37	13.69	3.040
140	25.40	13.72	3.047
130	25.43	13.75	3.055
120	25.45	13.79	3.066
110	25.49	13.83	3.079
100	25.52	13.85	3.092
90	25.55	13.84	3.104
80	25.59	13.78	3.114
70	25.64	13.72	3.125
60	25.70	13.70	3.135
50	25.75	13.70	3.142
40	25.78	13.71	3.149
30	25.79	13.70	3.154
20	25.78	13.68	3.156
10	25.76	13.63	3.157
4.2	25.76	13.58	3.157

Young's modulus was calculated using, (Nye 1957)

$$\frac{1}{E} = S_{11} - 2\left[S_{11} - S_{12} - \frac{S_{44}}{2}\right]\left[l_1^2 l_2^2 + l_2^2 l_3^2 + l_1^2 l_3^2\right] \qquad \text{....eqn.IV.27}$$

where

$$S_{11} = \frac{C_{11} + C_{12}}{(C_{11} - C_{12})(C_{11} + 2C_{12})} \qquad \text{.....eqn.IV 28a}$$

$$S_{12} = \frac{-C_{12}}{(C_{11} - C_{12})(C_{11} + 2C_{12})} \qquad \text{.....IV.28 b.}$$

$$S_{44} = \frac{1}{C_{44}} \qquad \text{.....eqn.IV.28 c.}$$

and l_i = cos α_i , the direction cosine for the particular direction concerned.

For crystal Nb56, $\alpha_1 = 37.3^\circ$; $\alpha_2 = 54.5^\circ$; and $\alpha_3 = 74.5^\circ$ the values of Young's modulus at the three temperatures nearest the testing temperatures are

$$E_{300^\circ K} = 9{,}568 \text{ kg.mm}^{-2} ,$$

$$E_{160^\circ K} = 9{,}786 \text{ kg.mm}^{-2} ,$$

and $$E_{80^\circ K} = 10{,}006 \text{ kg. mm}^{-2}$$

The full shear stress-glide strain curve at a nominal axial strain rate, $\dot{\varepsilon}$, of 5.92×10^{-4} sec^{-1}, for the compression test at 295°K is given in fig. IV 41. Fig.IV 42 shows the initial part of this curve on a greatly expanded scale; the line marked E was calculated from Youngs modulus (to give values of ε for given stresses σ) and eqns. IV 5a and IV 5b. The numbers on the curves in Fig. IV 41 and

IV 42 refer to the table below; this table gives the axial strain rate $\dot{\varepsilon}$, measured on the extension - time part of the recorder chart, and the corresponding resolved shear stress(τ).

Point	$\dot{\varepsilon}$ sec^{-1}	τ $kg.mm^{-2}$.
1	4.47×10^{-5}	0.20
2	8.40×10^{-5}	0.54
3	1.48×10^{-4}	0.79
4	2.00×10^{-4}	0.95
5	4.50×10^{-4}	1.00
6	5.90×10^{-4}	1.13
7	5.90×10^{-4}	1.30
8	5.00×10^{-4}	4.50

It can be seen from fig. IV 42 that the curve does not pass through the origin but crosses the strain axis at $\sim 0.0003\ \gamma$. This corresponds to a movement of $\sim 0.12\ \mu$ and is due to errors in setting the differential transformer output at zero; this has to be set mechanically since the electronic zero adjustment attached to the recorder is positioned between the recorder slide wire and the attenuator and consequently gives an equal pen displacement on all ranges. Hence using this to set the zero would give considerable inaccuracies on the attenuated ranges. It can be seen from fig. IV 42 that the initial linear portion of the curve differs considerably from the calculated elastic line consequently there is some unexpected strain from the start of loading. The strain rate in this linear region is approximately an order of magnitude

lower than the nominal strain rate; the first deviation from linearity i.e. the micro-yield stress occurs at ~ 0.54 kg.mm^{-2} and at a strain rate of 8.40×10^{-5} sec^{-1} compared with $\sim$ double this value for the macro-yield stress. The strain rate and flow stress increase with strain, the decrease in 'hardening rate' being responsible for the strain rate increase. Even in the high strain regions e.g. points 7 and 8, machine softness still gives a noticable difference in strain rate.

Figs. IV 43 and IV 44 are the shear stress-glide strain curves for the test at 158^{o}K and correspond to figs. IV 41 and IV.42. for the room temperature test. Since the features are so similar their description will not be repeated except to point out the much greater rounding of the stress-strain curve near the yield point because of an apparent increase in machine softness due to the higher yield stress. (see section IV. 3.2.). Below are tabulated the strain rate ($\dot{\varepsilon}$) and shear stress (τ) values corresponding to particular points on the curves in fig. IV 43 and 44.

Point	$\dot{\varepsilon}$ (sec^{-1})	τ (kg. mm^{-2})
1	4.60×10^{-5}	5.0
2	5.10×10^{-5}	7.6
3 *	5.92×10^{-5}	8.3
4	8.20×10^{-5}	11.0
5	1.29×10^{-4}	12.4
6	3.08×10^{-4}	13.4
7	4.71×10^{-4}	14.1
8	5.00×10^{-4}	17.5

* First deviation from linearity.

One further type of test was carried out at 158°K. The specimen was loaded to a stress of ~14 kg.mm^{-2} (about 6.7 kg. mm^{-2} resolved) and immediately unloaded. No permament strain was observed, the difference between the calculated and the experimental lines corresponds to a change in specimen length of ~3μ which would give a recorder pen displacement of ~3 inches were this all plastic strain. However, with the two pen recorder hysteresis loops, as observed by Brown and Ekvall, cannot be seen.

At 77°K the specimens twinned. Fig. IV 45 shows the axial stress - nominal strain curve up to the first load drop. The strain rate in this 'elastic' region is 4.76 x 10^{-5} sec^{-1}. The line marked 'E' has a slope equal to Young's Modulus and again, as in the other tests, the experimental slope is much less than that calculated; in this case the slope, $E_{exptl.}$ = 7,140 kg. mm^{-2} (cp. 10,006 kg. mm^{-2}). The experimental line is shown straight in fig. IV 45 but when drawn on a much larger scale it was seen to be concave upwards initially and then concave downwards; however the curvature was very slight, no points being more than a strain of 10^{-4} off the straight line. Before the large load drop due to twinning, three small twins occurred but in none of these instances was there any observable slip before twinning. Fig.IV 46 shows the stress-strain curve immediately after the large load drop due to twinning. (~ 0.05 strain (ε).) It can be seen that after twinning there is a negative strain even though the stress is continually increasing. The same effect occurred even

after small twins though in these cases the negative strain was so small that although seen on the chart it cannot be seen in fig. IV 45.

IV. 7. Electron Microscopy

Introduction

This part of the thesis was originally intended to be the major part; however the marked change in the form and orientation dependence of the stress-strain curve with increasing purity complicated the situation and made necessary work on slip plane determination etc. In addition, due to modifications and mishaps the electron microscope has been largely inoperative since September 1964. The condition of foils examined in the microscope can be classed as :

(a) undeformed;

(b) single glide on $(\bar{1}01)$ $[111]$ at room temperature;

(c) single glide on $(\bar{2}11)$ $[111]$ at room temperature;

(d) double glide on $(\bar{2}11)$ $[111]$ and (211) $[\bar{1}11]$ at room temperature;

(e) single glide on $(\bar{2}11)$ $[111]$ at $158^{\circ}K$;

(f) deformation at $77^{\circ}K$.

Class (d) has been examined most thoroughly since, initially, only crystals with long axes near to the $[011]$ direction could be grown as seeds for other orientations were not

available; when crystals oriented for single glide were grown, the microscope was not in full working order.

The kinematical and dynamical theories of electron diffraction, which explain image contrast, have been mainly developed by Hirsch, Whelan, Howie and co-workers; papers on this subject are very numerous but the results have been summarised in two recent books - Amelinckx (1964); Hirsch, Howie, Pashley, Whelan and Nicholson (1965). Though some phenomena require the details of the dynamical theory of diffraction, the most important criterion for the present work is a qualitative one - that of dislocation invisibility. When the reciprocal lattice vector $\underline{g}$, which represents the normal to the reflecting planes, is perpendicular to the Burgers vector, $\underline{b}$, of the dislocation i.e. when $\underline{g} \cdot \underline{b} = 0$, the dislocation is invisible. This is strictly true only for screw dislocations; for edge or mixed dislocations, there is a transverse displacement perpendicular to both the line of the edge (or edge component) dislocation and the Burgers vector which is usually expressed mathematically as $\underline{b} \times \underline{u}$, where $\underline{u}$ is a vector along the line of the edge dislocation. Contrast from this displacement is normally masked by the Burgers vector contrast, also this contrast is weak except when $S \longrightarrow 0$, since the kinematical theory predicts only weak contrast (Amelinckx 1964). Hence images due to transverse displacement contrast are normally only important when examining a section perpendicular to a glide direction though edge and mixed dislocations are not completely invisible

unless both $\underline{g} \cdot \underline{b}$ and $\underline{g} \cdot \underline{b} \times \underline{u}$ are zero.

One of the difficulties of Burgers vector determination, was that the area viewed tended to move when the specimen was tilted. (since the tilting stage does not tilt around the electron beam). In order to ensure that the same area was being examined under different reflections, it was necessary to tilt small amounts at a time and change from diffraction pattern to image between each small tilt. This method worked quite well but was slow; it could not be used in the most recent experiments because the contamination rate was too high. To determine the Burgers vectors in these experiments items of contrast insensitive material, such as the dry residues from washing alcohol, were left on the foil; these were then used as reference marks, all tilting being done with the microscope in the 'diffraction' condition. Since the stress axis is always considered to be located in the stereographic triangle (001) (011) ($\bar{1}11$), the primary glide planes are ($\bar{1}01$) and ($\bar{2}11$); the dislocations present are considered to be of the type $\langle 111 \rangle$ or $\langle 100 \rangle$ and for convenience the $\{111\}$ planes and the ($\bar{1}01$) and ($\bar{2}11$) zone axes are shown on the standard (001) cubic projection, figs. IV 47 and 48 respectively; the $\{100\}$ type planes are easy to see. For sections cut parallel to the ($\bar{1}01$) plane, the most useful zone axis within tilting range ($\pm 20^{o}$) is $[\bar{1}01]$. The most useful reflections and the Burgers vectors of the dislocations which are invisible ($\underline{g} \cdot \underline{b} = o$) when only those reflections are operating are tabulated below.

$\underline{g}$		$\underline{b}$			
101	:	$\bar{1}11$	, $1\bar{1}1$	, 010	.
010	:	100	, 001	.	
121	:	$1\bar{1}1$	.		
$1\bar{2}1$	:	111	.		

Other available zone axes can give further information but they are difficult to work with e.g. the $[\bar{3}13]$ zone axis contains the $(0\bar{3}1)$ and (130) planes and these differentiate between the $[100]$ and $[001]$ dislocations. Unfortunately due to the symmetry of the $[\bar{1}01]$ zone axis, it is not possible to definitely distinguish between the primary dislocations and those secondary dislocations on the same slip plane, using only the invisibility criterion. The only way to do this, is to put a permanent reference mark on the slice cut from the crystal and mount the subsequent foil into the holder with the mark in a known direction, first having calibrated the microscope for rotation between the diffraction pattern and the specimen. This method because of its obvious practical difficulties, was not used instead the primary dislocations were distinguished by their density which should be considerably higher than the $[1\bar{1}1]$ dislocations at the strains used.

The $(\bar{2}11)$ slip plane did not present the same difficulties as the $(\bar{1}01)$ since this plane contains only one slip direction. However the $\underline{g}$ vector $[0\bar{1}1]$ which removes the primary dislocations, $[\bar{1}11]$, also removes $[\bar{1}11]$ and $[100]$

dislocations as can be seen in the table below:

$\underline{g}$	$\underline{b}$
$0\bar{1}1$	: 111 , $\bar{1}11$, 100 .
$21\bar{3}$	: $\bar{1}\bar{1}1$.
$2\bar{3}1$	: $1\bar{1}1$.

If the $[100]$ dislocations are ignored then by tilting to the $[\bar{1}11]$ zone axis (only just within tilting range and not always available) the $[111]$ and $[\bar{1}\bar{1}1]$ dislocations can be distinguished from each other. The following table gives the useful reflections available with this zone axis and also the dislocations invisible on the $\underline{g}$. $\underline{b}$ = o criterion.

$\underline{g}$	$\underline{b}$
$0\bar{1}1$	: $\bar{1}11$, 111 , 100 .
101	: $\bar{1}11$, $\bar{1}\bar{1}1$, 010 .
110	: $\bar{1}11$, $1\bar{1}1$, 001 .

Having identified the $[0\bar{1}1]$ reflection by using the $[\bar{2}11]$ zone axis, the $[\bar{1}11]$ zone axis was always used if possible since better transmission was obtained using the $\langle 110 \rangle$ type reflections rather than any other type. The other zone axis within tilting range which has some extra usefullness is $[\bar{3}11]$; here the $[103]$ and $[130]$ $\underline{g}$ vectors distinguish between $[010]$ and $[001]$ dislocations. When tilting particularly over large angles, Kikuchi lines were used as guides, since one reflection must be common to both zone axes, e.g. when tilting from the $[\bar{2}11]$ to $[\bar{1}11]$ zone axis the $[0\bar{1}1]$ Kikuchi line was kept on the $[0\bar{1}1]$ spot.

At the higher strains, tilts and rotations across boundaries were measured using selected area diffraction patterns taken from either side of the boundary. The accuracy of selected area diffraction (S.A.D.) is important since some of the areas from which diffraction patterns were obtained were small. The possible errors have been summarised by Hirsch et al. (1965) :-

a) Spherical aberration.

b) Incorrect focussing of objective lens.

c) Incorrect focussing of first projector lens.

d) Transverse deflection of first projector lens.

d) Magnetic coupling between the objective and first projector lens.

Only the first three errors can be corrected for to some extent during operation. The spherical aberration constant is fixed but the selected area error is proportional to the cube of the Bragg angle, hence reflections with low Miller indices are best. The S.A.D. aperture is situated in the back focal plane of the objective lens and it is necessary for the objective image plane to be exactly in the same plane as the aperture. To do this the aperture is first focussed with the first projector lens and then the image is brought into focus using the objective lens. Until the recent modifications it was not possible to carry out the first part of this procedure with the A.E.I. E.M.6 microscope. After turning to 'diffraction', the spots are made as small as possible by adjusting the current through the first

projector lens.

Small tilts across or rotations about an axis perpendicular to particular boundaries were measured with Kikuchi lines. Selected area diffraction patterns were taken from either side of the boundary; two crossing Kikuchi lines present in both patterns were chosen and the magnitude and direction of movement of the cross-over point measured. Since the Bragg angles are small, the tilt α is given by -

$$\tan \alpha = \frac{\Delta R}{L} \qquad \text{.....IV.29.}$$

where ΔR is the movement

and L, the camera length.

Resolving ΔR parallel and perpendicular to the boundary gave the required rotation and tilt respectively. Rotations across a boundary could only be measured if they were large, in these cases the whole diffraction pattern rotated about an axis perpendicular to its own plane.

Foil Thickness

The foil thickness is important on two accounts; firstly the foil has to be thick enough to hold the bulk dislocation structure against the image forces, and secondly, knowledge of the foil thickness is necessary for density calculations; satisfying the first criterion is the more important. The foil thickness could not be measured, this was because-

a) the thin areas of the foil tended to buckle so that it was not possible to count thickness contours for one reflection;

b) no suitable pair of bend contours were observed (necessary for the Amelinckx 'S' method);

c) since the slip plane can be one of a number, slip traces cannot be used to determine foil thickness.

The foils were considered thick enough for three reasons:-

1) In the parts of the foils examined, the nature of the structure did not change with further increase in thickness.

2) One specimen etched in the final stages of thinning so that in some parts of the foil there was a thickness variation but no hole. In such areas thickness fringes were observed, fig. IV 49; with a $\langle 110 \rangle$ reflection operating about 12 contours could be counted before the thickness became too great for them to be still visible, dislocations however, were still visible in this thicker region. The extinction distance for a $\langle 110 \rangle$ reflection from niobium is ξ_{110} = 261 A (see Hirsch et al. 1965 for a table of extinction distances). Therefore, the foil must have been at least 3000 A thick. However changes in the Bragg deviation vector $\underline{s}$ and in ξ_g for multiple reflections have not been taken into account.

3) In a section cut at 45° to the slip plane, $(\bar{2}11)$, a large number of parallel dislocations were seen, fig. IV 50. If these are assumed to be on the slip plane then a foil thickness of 2500 Å taking AA or 7200 Å taking BB (fig.IV 50) is indicated. Which value to take is rather difficult to decide; BB may appear longer because it could be made up of overlapping groups, on the other hand AA dislocations

are possibly on ($\bar{1}01$) or they may not run through the foil; however either value should be sufficient.

In view of the high yield stress at room temperature (cp. Al) it is thought that a foil thickness of ~1000 Å should be sufficient to hold the dislocation structures (other than such configurations as pile-ups of course).

Measurement of Dislocation Density.

The dislocation density was measured using the method of Ham (1961) and the modification of Steeds (1963). Six circles with random centres were drawn on transparent paper; this was placed over the micrograph and the number of dislocation - circle intersections counted. The density, ρ, is then given by -

$$\rho = \frac{2N}{Lt} \qquad \text{.....eqn.IV.30}$$

where N is the number of dislocation - circle intersections,

L the total circumferential length of the circles

and t, the foil thickness.

Ham obtained this equation by combining two other equations available in the literature. Bailey and Hirsch (1960) showed that for an isotropic distribution the dislocation density is given by -

$$\rho = \frac{4}{\pi}\frac{R_p}{At} \qquad \text{.....eqn. IV.31}$$

where R_p is the projected line length;

and Smith and Guttman (1953) showed that

$$R_p = \frac{\pi NA}{2L} \qquad \text{.....eqn. IV.32}$$

where A, is the area of the foil being examined.

Ham used random straight lines, which due to local rotations of the dislocations in the foil, can give errors of up to 20% (aluminium). Steeds overcame this drawback by using circles.

For convenience two sets of circles were drawn, one with 100 cm. total circumferential length, the other with 50 cm.; this latter set were used for measuring densities in narrow regions such as cell walls. Measurements were taken on several micrographs (usually 3) and the densities averaged; this was to take account of the inhomogeneous nature of deformation. The foil thickness was usually assumed to be 2000 Å.

Damage and Loss of Dislocations During Foil Preparation.

A further source of error is that dislocations may be introduced during slicing and subsequent handling of the thin foil. Foils prepared from undeformed crystals had a density of $\sim 10^7$ dislocations cm^{-2} except for a few areas in which the density was $\sim 10^8$ dislocations cm^{-2} The dislocations in these areas could be seen to have come from a source operating at the edge of the foil (fig. IV 51) and in these cases the dislocation distribution was quite different from that in a deformed specimen. It is therefore concluded that neither sawing nor spark cutting introduced any appreciable damage.

The loss of dislocations during thinning of the foils was not accounted for. Valdrè and Hirsch (1963) working with stainless steel masked off one side towards the end of polishing. Examination of the slip traces indicated that $\sim$20% of the dislocations had escaped from the foil or had

moved. However polycrystalline stainless steel work hardens at a high rate and it may be that the internal stress fields are very high so it is possible that the loss from niobium single crystals is less.

Slip on $(\bar{1}01)$ $[111]$ at Room Temperature.

Three crystals oriented for $(\bar{1}01)$ $[111]$ slip, were deformed for microscopy. Specimen Nb 32 I F was deformed to a strain about half way into stage I and both Nb 23B and Nb 32 I D to the beginning of stage II. All foils were prepared from slices cut parallel to the slip plane.

Fig. IV 52 shows at low magnification a section through a foil from 32 IF (about 200 μ x 15 μ). Looked at as a whole, it is possible to envisage that it represents the early stages in the building of a hexagonal cell structure. The longest groupings are $\sim 8\mu$ long and $\sim 1.5\mu$ wide; their lateral separation is $\sim 5\mu$ and adjacent groups do not lie side by side but tend to be displaced so that there is the minimum of overlap. The plane of the foil was not exactly $(\bar{1}01)$ but was tilted $\sim 1\frac{1}{2}$ degrees either towards the (011) plane or the $(0\bar{1}1)$ plane. (X-rays). If the tilt was towards the former the length of the groupings (or braids) is in agreement with their having negligible thickness perpendicular to the slip plane and a foil thickness of ~ 2000 Å, in which case their true length, though greater than 8 μ, is unknown. An alternative explanation is that the true length is $\sim 8\mu$ but that the braids are really walls, however it is clear that they cannot be both very long and high.

If the tilt is towards $(0\bar{1}1)$ then 8μ is the true length of the braid and the height or thickness is unknown.

The densest braids are those approximately perpendicular to the slip direction, $[111]$; the dislocations in all braids have a much greater component perpendicular to the slip direction than parallel with it. Fig. IV 53 a and b show a typical area with two different reflections operating, $[1\bar{2}1]$ (fig. IV 53a) and $[101]$ (fig. IV 53b). The dislocations invisible in the first micrograph can only be the primary dislocations $[111]$. Detailed examination of these groupings (fig. IV 54) shows that they are largely composed of primary edge dipoles and loops. Their lengths vary considerably but most seem to be between 0.1 and 0.2μ. These dipoles may be formed by jogs in screw dislocations; fig. IV 53b shows at point 'A' a loop attached to a screw dislocation. (The poor contrast in this photograph is due to contamination within the microscope).

Foils from Nb 23B show a much more uniform structure. The groupings are much wider (fig. IV 55) and in some cases (fig. IV 56) the dislocations are no longer mainly perpendicular to the slip direction. Sometimes the loops end in a line approximatelyparallel to the slip direction, e.g. at 'A' in fig. IV 55; not all the loops end at exactly the same line and it is probable that they end on a plane which is steeply inclined to the foil and which contains the $[111]$ direction. Such a plane is $(\bar{1}10)$, it is at 60° to the foil and if the foil is 2000 Å thick, then the

projected width of $(\bar{1}10)$ is $\sim 0.1\,\mu$. The loops referred to in fig. IV 55 all end within about half of this distance. If the loops do end on a secondary glide plane then they may have been cut off by secondary glide.

Foils cut from Nb 32 ID showed some considerably different features from Nb 23B. Fig. IV 57 shows a cell structure; the cells are slightly elongated varying between 3 and 5 μ in length and 2 to 4 μ in width. The cell walls are continuous and often much narrower than in 23B, though this is not always so (fig. IV 58 a and b); the proportion of loops and the preferential alignment of dislocations has also decreased.

The deformation data and dislocation densities are summarised in table IV 2 below. ($\underline{g}$ = [101])

Specimen	Shear Strain	Flow (τ) Stress	Yield (τ_0) Stress	($\tau - \tau_0$) $kg.mm^{-2}$	Wall density	Overall density
32 IF	0.098	2.68	1.50	1.18	7.59×10^{9}	1.25×10^{9}
23 B	0.159	2.61	1.05	1.56	1.00×10^{10}	3.45×10^{9}
32 ID	0.203	3.36	1.50	1.86	1.61×10^{10}	6.27×10^{9}

Slip on $(\bar{2}11)$ [111] at Room Temperature.

Only two crystals, deformed on this system, were examined in the electron microscope. The first, Nb32II G, was deformed to a glide strain of 0.196, which is a little way into stage II; the second, Nb32II B, to 0.32 which is just in stage III; however since stage III in compression is probably a geometrical effect it is perhaps better to

consider this crystal as being deformed well into Stage II.

Foils from 32 II G were taken parallel with the glide plane; the dislocation arrangements (fig. IV 59) are in general similar to those obtained by deformation to the same strain on the $(\bar{1}01)$ $[111]$ i.e. a cell structure, loops and a tendency for the dislocations to be lined up perpendicular to the slip direction; the cell walls, however, are not so continuous and are wider. Fig. IV 60a shows part of IV 59 enlarged with $\underline{g} = [112]$, fig. IV 60 b shows the same area with the $[0\bar{1}1]$ reflection operating (A, B & C are reference points); the secondary density is seen to be considerable. To determine more satisfactorily the secondary density, several areas were taken using the three $\langle 110 \rangle$ reflections of the $[\bar{1}11]$ zone axis; of these reflections, $[0\bar{1}1]$ is definite but $[101]$ and $[\bar{1}10]$ may be reversed. These micrographs are shown in fig. IV 61 a, b and c and fig. IV 62 a, b and c. The densities and other relevant information are given in the table below.

Fig.	Shear Stress	Yield Stress	$(\tau-\tau_0)_2$ kg.mm^{-2}	Density ρ for $\underline{g} = [h\ k\ l]$ $[110]$	$[101]$	$[0\bar{1}1]$
IV 61	2.49	1.38	1.11	6.20×10^9	4.68×10^9	4.36×10^9
IV 62				4.44×10^9	3.66×10^9	3.34×10^9
	Average densities disloc./cm			5.32×10^9	4.17×10^9	3.85×10^9

If, the $\langle 100 \rangle$ dislocations are ignored, the $[\bar{1}11]$ dislocations considered absent from all micrographs since $S \neq 0$ and the dislocations present are isotropically

distributed then we have

$$(111) + (\bar{1}\bar{1}1) = 5.32 \times 10^9 \quad \ldots\ldots\ldots \text{a}$$
$$(111) + (1\bar{1}1) = 4.17 \times 10^9 \quad \ldots\ldots\ldots \text{b} \qquad \text{eq.IV33}$$
$$(\bar{1}\bar{1}1) + (1\bar{1}1) = 3.85 \times 10^9 \quad \ldots\ldots\ldots \text{c}$$

where $(h\ k\ l)$ is the density of $[h\ k\ l]$ dislocations.

This gives $(111) = 2.82 \times 10^9$ disloc. cm^{-2}

$(\bar{1}\bar{1}1) = 2.50 \times 10^9$ disloc. cm^{-2}

$(1\bar{1}\bar{1}) = 1.35 \times 10^9$ disloc. cm^{-2}

The last requirement in particular (i.e. isotropic distribution) is not true however it can be seen that the secondary density exceeds that of the primary.

Sections from Nb 32 II B were taken perpendicular to the glide direction. A prominent feature in these foils (fig. IV 67) is a series of long tangles running in a $\langle 110 \rangle$ direction i.e. parallel to the trace of a $\{211\}$ plane. If this plane is assumed to be the slip plane, $(\bar{2}11)$ then the $\langle 110 \rangle$ direction is $[0\bar{1}1]$; the other $\langle 110 \rangle$ directions cannot be labelled unambiguously but are $[1\bar{1}0]$ and $[\bar{1}01]$. The tangles are not perfectly straight, and sometimes short segments develop on other $\{211\}$ planes as can be seen in fig. IV 67. The primary dislocations have their Burgers vector coming out of the foil; screw dislocations should only be seen by the 'end on' contrast described by Tunstall, Hirsch and Steeds (1964) whilst edge dislocations may be seen by transverse displacement contrast (fig. IV 63). However, it is difficult to decide whether images due to this contrast are present

because of the secondary dislocations. When the $[0\bar{1}1]$ reflection is used the micrograph (fig. IV 64) shows alternating black and white bands, the contrast changing on crossing a tangle. The tilts across several boundaries were measured with Kikuchi lines. Their values varied up to $\sim 45'$, however on crossing two consecutive boundaries the tilts were in the opposite sense. The tilts were not wholly across the boundary but could be resolved into a tilt across, and a twist about an axis perpendicular to the boundary e.g. fig. IV 65 and IV 66.

Fig.	Boundary	Tilt	Twist	Total
IV 65	22-21	$25.3'$	$37.6'$	$45.4'$
IV 65	21-23	$-8.4'$	$-12.5'$	$-15.1'$
IV.66	25-26	$20.7'$	$32'$	$38'$

Fig. IV 67 a, b and c, show the same area using different $\langle 110 \rangle$ reflections (A B and C are reference points on each micrograph). Since S was always large and positive the primary edge dislocations should be invisible in all micrographs, and this appears to be so; primary screws are difficult to see because of the presence of the other dislocations and the contamination left on the specimen for reference. The dislocation densities for each reflection and the deformation data are tabulated below.

Shear Strain	Flow Stress	Yield Stress	$(\tau-\tau_0)^2$ kg.mm^2	Density for g = [h k l] $[1\bar{1}0]$	$[0\bar{1}1]$	$[\bar{1}01]$
0.323	4.42	1.31	3.11	5.66×10^9	4.48×10^9	5.08×10^9

Using the same assumptions as above we get

$(\bar{1}11)$ = 3.13 disl. cm^{-2}.

$(\bar{1}\bar{1}1)$ = 1.95 disl. cm^{-2}.

$(1\bar{1}1)$ = 1.35 disl. cm^{-2}.

Double glide on $(\bar{2}11)$ $[111]$ and (211) $[\bar{1}11]$ at Room Temperature

This deformation gives the hardening curve shown in fig. IV 15 which is of Nb 19A. Other specimens cut from crystal Nb 19 and also from Nb 25 were deformed given amounts and used for microscopy. Their deformation treatment is summarised below:

Specimen	Shear Strain	Shear Stress (τ)	Yield Stress (τ_0)	$(\tau-\tau_0)$ kg.mm^{-2}
19B	0.083	2.40	0.901	1.50
19H	0.129	2.97	0.872	2.10
19C	0.251	4.42	0.926	3.49
19D	0.419	6.36	0.896	5.46
19E	0.592	7.67	0.879	6.79
19F	0.880	10.09	0.879	9.21
25B	0.242	3.70	1.000	2.70

Sections parallel to the glide plane $(\bar{2}11)$.

Foils from 19B showed long, narrow groupings of dislocations (braids) as can be seen in fig. IV 68. In some cases the braids themselves were part of a larger grouping which extended at an angle of $\sim 60^\circ$ to the length of the braids. Each braid, which was about 6 μ long, was made up of dislocations and dipoles lying along the $[0\bar{1}1]$ direction (fig. IV 69); at this stage in the deformation, they were

rather loosely knit and it was easy to distinguish individual dislocations. Burgers vector analysis, revealed that the braids contained few $[\bar{1}1\bar{1}]$ and/or $[1\bar{1}1]$ dislocations lying in the general direction of $[0\bar{1}1]$. Fig. IV 69 was taken with g = $[110]$ and s = o; no dislocations definitely giving transverse displacement contrast can be identified and so it is considered that only $[\bar{1}11]$ dislocations, mainly of edge character, are present in this braid. It is possible that the $[\bar{1}11]$ dislocations have slipped out of the foil, since the degree of tangling is low. The dislocation density in and around this braid was 5.64×10^9 disloc. cm^{-2}; the overall density could not be measured since there were insufficient suitable micrographs.

As the deformation increased (19H) the braids became narrower and more densely packed and often it was not possible to see the individual dislocations inside them.(fig. IV 70). The arrangement of the braids with respect to each other was like a series of parallel broken lines, adjacent lines being 'out of phase'; fig. IV 71 shows two examples of this; at present the author is unable to tell whether the inside of one of the long braids is dark because $s \rightarrow o$ and dislocations of the second system are giving transverse displacement contrast or whether strong absorption is occurring anyway. Sometimes two narrow braids joined to form one. The tilt across the double braid shown in fig. IV 72 was $10'$; it was not possible to measure the tilt across each separate braid since at that time, the selected area aperture size was too large and the

accuracy of the selected area low. However the tilt across other single braids was ~30′ . At this strain the Burgers vectors of the dislocations were still mostly [111] (and probably [$\bar{1}$11]) as can be seen by comparing figs. IV 73 and 74 with figs. IV 70 and 72 respectively.

At 25% glide strain a well developed 'corridor' structure in black and white contrast is seen (fig. IV 75). The walls of the corridors are very narrow and almost continuous. The [$\bar{1}\bar{1}$1] and [1$\bar{1}$1] dislocation content of the walls is still low. (fig. IV 76). One unexpected item observed in this foil (19C) is illustrated in fig. IV 77 a and b. With g = [110] both braids are visible, however when the [0$\bar{1}$1] reflection is used only one disappears. Foils from specimens 19D and 19E exhibit similar features to those from 19C. However barriers across the corridors became more prominent and eventually a chess-board like pattern of elongated black and white areas was built up. (fig. IV 78). Kikuchi line shifts in changing from area '14' to '15' (fig. IV 78) are consistant with an 11′ twist and a 27′ tilt across the boundary; however the boundary is wide, and possibly this is the net angular change across two boundaries of opposite sign. Fig. IV 79 a and b shows a large increase in dislocations with [$\bar{1}\bar{1}$1] and [1$\bar{1}$1] Burgers vectors compared with foils from 19C.

Other Sections.

25B was sectioned at 45° to the ($\bar{2}$11) glide plane but still contained the [111] glide direction. Figs. IV 80 and 81 show, at different magnifications, arrays of parallel

dislocations. The arrays are in the [111] direction generally, but are not confined to one plane and hence give a wavy appearance. Using a [1$\bar{1}$0] reflection, the dislocations did not disappear completely but gave a weak zig-zag image. This means that they are probably [111] edge dislocations on the ($\bar{2}$11) planes; other possibilities are [111] edge dislocations on ($\bar{1}$01) planes or less likely, [$\bar{1}$11] screws on (0$\bar{1}$1) planes. However any of the above configurations is inconsistant with the observations on foils parallel with the glide plane.

Crystal 19F was sectioned perpendicular to both glide planes, ($\bar{2}$11) and (211), but contained the glide directions, [111] and [$\bar{1}$11] i.e. the foil plane was (0$\bar{1}$1). Fig.IV 82, taken at low magnification, shows an elongated cell structure with very dense walls and relatively few dislocations between. The walls are wavy and appear to be on three planes, the ($\bar{2}$11), ($\bar{1}$11) and (011), but not on the second glide plane (211) nor the (111) plane. When crossing a boundary, the lattice rotates about an axis perpendicular to the foil. The rotations are large but consecutive boundaries have rotations in opposite directions e.g. in fig. IV 83 rotations A-B = 26°, A-C = 20° and B-C = 6°. Again the observations are not consistant with those on sections parallel to the glide plane unless these sections only passed through walls on (011) planes

Occassionally net-works were seen in these foils e.g. fig. IV.84. These were not fully analysed but the net work shown is consistant with <111> screws combining to give the

⟨100⟩ attractive junction,

$$\frac{a}{2}\left[111\right] + \frac{a}{2}\left[1\bar{1}\bar{1}\right] \longrightarrow a\left[100\right]$$

where a $[100]$ dislocations are invisible. At 'A' in fig. IV 85 is a Moiré pattern; assuming this to be a twist Moiré due to a cross-grid of screws, the rotation θ, is given by,

$$\theta = \frac{d}{D} \qquad \text{.....eq.IV 34.}$$

(= 0.0466 rad. or $2^{o}40$ in the instance cited.)

where d = lattice spacing of the reflecting planes, (d_{011}=2.33Å)

and D = Moiré spacing, (50 Å)

The dislocation spacing in the cross-grid, S, is given by

$$S = \frac{b}{\theta} \qquad \text{.....eq.IV 35.}$$

where b is the Burgers vector, which gives S = 61 Å.

Single Glide on $(\bar{2}11)$ $[111]$ at $158^{o}K$.

The deformation data of Nb 9H is given below.

Shear Strain γ	Shear Stress τ	Yield Stress τ_o	$(\tau-\tau_o)$ kg.mm^{-2}	Dislocation Density ρ disl.cm^{-2}
0.118	15.83	12.42	3.41	4.92×10^{9}

The micrographs are quite different from those obtained after room temperature deformation. Fig. IV 86 shows a typical area. The dislocation distribution is fairly uniform and consists of long dislocations lying in general along the $[111]$ direction. Burgers vector analysis, fig. IV 87 a and b, shows that these are primary screw dislocations. Adjacent screw dislocations

are generally of opposite sign; fig. IV 88 illustrates this showing dark and light areas bounded by the screws. The screws are frequently 'pinned', probably by jogs, the distance between pinning points being 1000 Å - 3000 Å. Small loops can also be seen which in general lie perpendicular to the screws, i.e. in the $[0\bar{1}1]$ direction, and since they also disappear with a $[0\bar{1}1]$ reflection they are primary edge loops probably produced by the dragging of jogs in screw dislocations. Fig. IV 89 is possibly an example of this happening; however here, the loop is not lined up parallel to $[0\bar{1}1]$ and is therefore not a primary edge loop.

Deformation at 77°K

Pre-straining at room temperature allowed deformation by slip only to occur at 77°K. Nb.7C was pre-strained 0.02 axial strain then deformed to $\varepsilon = 0.16$ at the lower temperature. The resolved shear stress was highest on $(\bar{1}01)$ $[111]$ but only just so being almost as large on $(\bar{2}11)$ $[111]$. The slip plane was not determined; foils were prepared from sections taken parallel to the slip markings (a method now considered inaccurate for small crystals) and were found to be $\sim 10^{\circ}$ off the $(\bar{2}11)$ plane but contained the $[111]$ direction. The structures seen (fig. IV 90a) are a mixture of the types seen by deforming at room temperature and at 158°K alone. Fig IV 90b confirms that nearly all the dislocations present are primary $[111]$ dislocations. The braids are much larger and denser than would be expected for 2% deformation; it is probable, therefore, that they have been added to during the

TABLE IV 3

If twinning occurs on the $(\bar{2}11)$ $[11\bar{1}]$ system, the twin reflections are given by,

$$h^t = {}^1/_3\,(h - 2k - 2\ell)$$
$$k^t = {}^1/_3\,(-2h - 2k + \ell)$$
$$\ell^t = {}^1/_3\,(-2h + k - 2\ell)$$

$(h\ k\ \ell)$	$(h^t\ k^t\ \ell^t)$	$(h\ k\ \ell)$	$(h^t\ k^t\ \ell^t)$
(200)	$1/3\ (2\bar{4}\bar{4})$	(211)	$1/3\ (\bar{2}\bar{5}\bar{5})$
(020)	$1/3\ (\bar{4}\bar{4}2)$	$(\bar{2}11)$	$(\bar{2}11)$
(002)	$1/3\ (\bar{4}2\bar{4})$	$(\bar{2}\bar{1}1)$	$1/3\ (\bar{2}71)$
(110)	$1/3\ (\bar{1}\bar{4}\bar{1})$	$(2\bar{1}1)$	$1/3\ (2\bar{1}\bar{7})$
(101)	$1/3\ (\bar{1}\bar{1}\bar{4})$	(112)	$1/3\ (\bar{5}\bar{2}\bar{5})$
(011)	$1/3\ (\bar{4}\bar{1}\bar{1})$	$(\bar{1}12)$	$1/3\ (\bar{7}2\bar{1})$
$(\bar{1}10)$	$(\bar{1}01)$	$(\bar{1}\bar{1}2)$	$(\bar{1}2\bar{1})$
$(\bar{1}01)$	$(\bar{1}10)$	$(1\bar{1}2)$	$1/3\ (\bar{1}2\bar{7})$
$(0\bar{1}1)$	$(01\bar{1})$	(121)	$1/3\ (\bar{5}\bar{5}2)$
(222)	$(\bar{2}\bar{2}\bar{2})$	$(\bar{1}21)$	$1/3\ (\bar{7}\bar{1}2)$
$(\bar{2}22)$	$1/3\ (\bar{1}022)$	$(\bar{1}\bar{2}1)$	$1/3\ (17\bar{2})$
$(\bar{2}\bar{2}2)$	$1/3\ (\bar{2}10\bar{2})$	$(1\bar{2}1)$	$(11\bar{2})$
$(2\bar{2}2)$	$1/3\ (22\bar{1}0)$		

deformation at the lower temperature.

Specimens which twinned before yielding were usually sectioned after one load drop. Nb9D (ε = 0.0545) was sectioned perpendicular to the two twin planes and parallel to the twin directions. Diffraction patterns (fig. IV92) taken either side of the twin boundary (fig. IV 91) were consistant with twinning on $(\bar{2}11)$ and the shear corresponded to the movement of $\frac{a}{6}$ $[111]$ partials on every $(\bar{2}11)$ plane i.e. the expected twin system in b.c.c. metals. The positions of the twin spots in terms of the matrix axes were calculated for a twin on the $(\bar{2}11)$ plane by the method of Meieran and Richman (1963) and are given in table IV 3. Even though all deformation occurred in the load drop, which is usually considered to be due to the twinning, the dislocation density throughout the foil was very high, making it difficult to observe anything apart from a dense dislocation tangle. Sections parallel to the twin plane showed similar features, the twin boundaries in these cases being due either to the second system, (211) $[\bar{1}11]$, or to secondary accomodation twins. Sometimes, between two boundaries were seen narrow dislocation structures on (101) planes; these are illustrated in fig. IV 93a and at higher magnification in IV 93b. Unfortunately the Burgers vectors of these dislocations were not determined, but since they appear on (101) planes they are probably $[\bar{1}11]$ or $[\bar{1}\bar{1}1]$ the former being more likely. The deformation during a twin drop was very inhomogeneous on a larger scale; some foils from the twinned region showed

no deformation at all e.g. fig. IV 94 taken from a specimen which had been deformed 0.0462 axial strain.

Miscellaneous Observations.

Two foils showed structures which are illustrated in fig. IV 95. The diffraction pattern, fig. IV 96, was streaked in the $[0\bar{1}1]$ direction, i.e. perpendicular to the interfaces seen in fig. IV 95, and each spot has 4 major satellite spots with other weaker spots between. This diffraction pattern was very persistant despite large angles of tilt so it is difficult to tell whether the zone axis perpendicular to the foil is $[\bar{1}11]$ or the expected $[\bar{2}11]$. The phenomenon is probably the same or similar to that reported by Van Torne and Thomas (1964) i.e. niobium - oxygen solid solution transforming to niobium oxide. The oxygen was probably introduced during electro-polishing, since then the specimen is anodic.

SECTION V.

SECTION V

General Discussion

1. Purity of Material.

The purity of the niobium crystals is not known but the large resistivity ratio and low yield stress indicate 'good' purity.

The high vacuum anneal should remove oxygen, nitrogen and hydrogen rapidly on the basis of Sievert's law, and low boiling point metals should be removed by evaporation. The other likely interstitial impurity, carbon, should be removed by reaction with water vapour in the furnace atmosphere.
The zone speed used in the E.B.U. was too high for true zone refining to occur; however the high temperature and relatively poor vacuum should remove the low boiling point metals and carbon respectively. Unfortunately since the filament is of tungsten zone passes may introduce small amounts of this element.

Cost and Wert (1963) have published curves showing the amount of nitrogen in niobium at different pressures and temperatures; fig. V 1 is an extrapolation of their data. At a partial pressure of nitrogen of $\sim 10^{-8}$ torr, the nitrogen concentration at 2450°C is < 3 atom ppm. However cooling re-introduces nitrogen since the heat of solution is negative. Hydrogen is similar; extrapolating Komjathy's (1960) results at 1500°C gives a hydrogen content at 10^{-8} torr of ~ 0.05 atom ppm. There are no similar curves for oxygen however Cost and Wert estimate that the oxygen content is ~ 0.1 the nitrogen content.

Impurities in tantalum, for the most part, would be expected to behave in a similar manner to those in niobium. However it is clear from the critical resolved shear stress values (CRSS) at room temperature (section IV 5.8) that a gaseous interstitial element which gives considerable hardening has a positive heat of solution.

2. The Effect of Interstitial Impurities.

The amounts of impurity present are still difficult to estimate since neither the partial pressures of the individual gases nor the final equilibrium temperature are known. However if we assume 1 atom ppm. nitrogen then we should still get a yield point if this is segregated to the dislocations; 1 c.c. contains 6.6×10^{22} niobium atoms and hence 6.6×10^{16} nitrogen atoms, for a dislocation density of 10^7 dislocation cms./cms.^{3} there are 6.6×10^9 atoms cm^{-1} which should be sufficient to lock the dislocation. There are three possible explanations of the yield point absence:

1) the nitrogen content is much lower;
2) fresh dislocations have been introduced below the temperature at which diffusion can occur;
3) the interstitial atmosphere is dispersed.

The last possibility appears the most likely.

Most theories of hardening by interstitial impurities rely on tetragonal distortion to increase the resistance to slip by screw dislocations. Schönberg (1954) could not

detect any tetragonality by nitrogen addition, however Miller (1959) shows by graphs that nitrogen hardens niobium at a very rapid rate compared with oxygen and hydrogen. Comparing the CRSS at room temperature for crystals Nb35 and Nb46 we get

Nb 35 (10 zone passes in E.B.U at 10^{-6}torr.) τ_y = 2kg.mm^{-2}

Nb 46 (11 zone passes plus U.H.V. anneal at 10^{-8}torr) τ_y=1.5 kg. mm^{-2}.

If it be assumed that 1) no extra tungsten added nor any substitutional element decreased by the additional zone pass and U.H.V. anneal, 2) the change in oxygen and hydrogen contents due to the U.H.V. anneal had no effect on the yield stress, then the 0.5 kg.mm^{-2} difference in yield stress is probably due to the difference in nitrogen content. The cooling after the U.H.V. anneal was virtually a quench, it may therefore be assumed that the nitrogen content is the equilibrium concentration at the melting point i.e. $<$ 3 atom ppm. The cooling after zone passing was relatively slow so that the nitrogen content will be equal to the equilibrium content at a lower temperature say 2000^{o}C which, from fig.V 1, gives a nitrogen content of about 120 atom ppm. This gives a hardening rate of about 42 kg.mm^{-2} per atom % (compare 15 kg.mm^{-2} per atom % for oxygen - Leadbetter and Argent, 1961). Since the material twins at 77^{o}K we cannot get a comparison of yield stresses, however the flow stress change between room temperature and 77^{o}K was independent of interstitial impurity and therefore the hardening due to nitrogen cannot

be reduced by thermal activation.

Using the experimental hardening rate in Schoeck and Seeger's equation (II 6.) we get

$$A = \frac{\underline{b}\, a^3 \times 42}{0.205}$$

For niobium $a = 3.30$ Å, $\underline{b} = 2.86$ Å which gives

$$A = 2.11 \times 10^{-24} \text{ kg. mm}^2.$$

From Cochardt, Schoeck and Wiedersich (1955), the interaction energy E, is given by

$$E = A \frac{\cos \phi}{r} \qquad \text{V.1.}$$

where for the lowest energy positions $\phi = 60^\circ$ and if the nearest atoms are considered, $r \simeq b$, therefore

$$E = 0.226 \text{ eV}$$

The non-dilational strain $\Delta\varepsilon$ is calculated from A,

$$\Delta\varepsilon = \frac{3 \pi A}{\sqrt{2}\, b\, a^3 \mu} \qquad \text{V2.}$$

If the rigidity modulus μ, is assumed to be 4,600 kg.mm^{-2} and b, a and A are as above then,

$$\Delta\varepsilon = 0.297 \text{ per atom \%.}$$

Fleischer's model for hardening is derived for 0°K and the rôle of temperature is uncertain. However since to a first approximation, the hardening is temperature independent it is of interest to calculate the stress increase for 100 ppm. impurity. Equation II.5 gives,

$$\tau = \frac{\mu \sqrt{c}}{10} = 4.6 \text{ kg. mm}^{-2}$$

where c is the atomic concentration of impurity.

This hardening is much greater than the experimental increase (0.5kg. mm^{-2}) and this is mainly because the spacing of interstitials along the dislocation line is proportional to $\sqrt{c}$; in the present case this is not true since in order to make nearest neighbour contact the dislocation would have to bend between pinning points. The maximum radius of curvature r , is given by (Nabarro reported by Cottrell 1953)

$$r = \frac{\mu b}{2\tau} \qquad \text{V 3.}$$

which for $\tau = 0.5$ kg. mm^{-2} gives $r = 4{,}600$ b. For 100 ppm., in order to make nearest neighbour contact the radius of curvature would need to be as small as 100 b.

The equation of Cracknell and Petch (eqn. II 4.) assumes that the dislocation can bend to make nearest neighbour contact in space; this in itself is unlikely even assuming the stress necessary was available. 100 ppm. atom ratio gives N, the concentration in their equation, of 6.6×10^{15} atoms mm^{-3} . This gives a hardening (in terms of shear stress) of 0.055 kg. mm^{-2}.

Clearly the best agreement is with the Schoeck-Seeger theory; most estimates of interaction energies are less than 0.5 eV so E = 0.226 eV is very reasonable. It is however surprising that a tetragonal distortion of 0.297 should not be detected by X-ray lattice parameter measurements

since the solubility limit at $\sim 300^{\circ}C$ is ~ 500 ppm. which would give $\Delta\varepsilon = 0.015$.

The impure material has in addition to a yield point a low initial hardening rate even when oriented for double glide (fig. IV 39). This is considered to be due to a Lüders type deformation.

3. The Effect of Substitutional Impurities

The substitutional elements which evaporate during the U.H.V. anneal affect only the temperature independent part of the flow stress. However, crystals given several zone passes in the E.B.U. had a higher yield stress at room temperature and a lower yield stress at $77^{\circ}K$. The temperature dependence of the flow stress between $77^{\circ}K$ and room temperature was also lower than that for the single pass material. Below $77^{\circ}K$ we have no results for single pass material but comparison with the results of Christian and Masters (1964) shows that at $20^{\circ}K$ the trend is maintained. The only likely difference between the multipass material and the one-pass is that the former probably has a higher tungsten content. Why this should affect the temperature dependence of the flow stress is not known.

Multiple zone passes also affected the slip system at room temperature giving slip on $(\bar{3}12)$ rather than $(\bar{2}11)$. This is also attributed to tungsten; it is possible, but perhaps unlikely, that $(\bar{3}12)$ slip has a lower temperature

dependence than ($\bar{2}11$) though as yet it is not known whether slip occurs on ($\bar{3}12$) at low temperatures. If substitutional impurities can affect the slip systems then this will explain the difference in slip systems recorded in the literature.

4. Ageing at Room Temperature.

The increase in yield stress, which occurs on leaving crystals for a period of time before testing, can only be explained by assuming that some gaseous element, either oxygen, nitrogen or hydrogen, is diffusing in.

The diffusion rate equation is

$$D = Do \exp\left(-\frac{H}{RT}\right) \qquad V4.$$

where D is the rate of diffusion in $cm.^2$ $sec.^{-1}$,

Do, a constant,

H, the activation enthalpy for diffusion (cals $mole^{-1}$),

and R, the gas constant (2 cals $mole^{-1}$ $^oK^{-1}$).

For oxygen and nitrogen Ang (1953) gives:

Oxygen - $Do = 1.5 \times 10^{-2}$ $cm.^2$ $sec.^{-1}$ and $H = 27{,}600$ cals $mole^{-1}$.

Nitrogen - $Do = 9.8 \times 10^{-2}$ $cm.^2$ $sec.^{-1}$ and $H = 38{,}600$ cals $mole^{-1}$.

For hydrogen Albrecht et al. (1959) give

$Do = 1.5 \times 10^{-2}$ $cm.^2 sec.^{-1}$ and $H = 9370$ cals.$mole^{-1}$.

The rate of penetration S is given by

$$S = \sqrt{D\ t} \quad cm \qquad V5.$$

where t is the time in secs.

At 300^{o}K in 100 days the penetrations are

$S_{oxygen} = 3.60 \times 10^{-8}$ cms.

$S_{nitrogen} = 3.26 \times 10^{-12}$ cms.

$S_{hydrogen} = 1.80 \times 10^{-1}$ cms.

Hence although no allowance is being made for the dissociation and initial absorption only hydrogen can penetrate a 3mm dia. crystal sufficiently to affect the yield stress. A possible source of hydrogen was leakage from the cryostat.

D.K. Bowen is investigating this phenomenon further and is having specimens analysed.

5. The Temperature Dependence of the Yield and Flow Stresses.

Except where twinning has intervened, the temperature dependence of the yield and flow stresses is generally as expected i.e. the stress increases exponentially as the test temperature is lowered. Even before the intervention of twinning it is clear that the flow stress has a greater temperature dependence than the yield stress. This is exactly opposite to the results of Christian and Masters who found that the yield stress had the greater temperature dependence. This difference may be due to:

a) a temperature dependent contribution to the yield stress from dislocation locking by impurity atoms;

b) inhomogeneous yielding raising the yield stress by increasing the dislocation velocity. Though this in itself is not temperature dependent the velocity

may change with temperature due to different "Lüders" band widths.

Both of the above processes will increase the apparent temperature dependence of the yield stress in the less pure material.

At 77°K some attempt was made to determine over which range of strain the temperature dependent part of the flow stress was strain dependent. Since between 1.5 and 10% axial strain the flow stress change was constant the strain dependent part is in the first 1.5% but the exact range is not known. Before using the electron microscopy results in this part of the discussion there is one qualification; the electron microscopy was with crystals of different purity. These crystals had a lower room temperature yield stress and twinned at 77°K; pre-straining at room temperature to suppress twinning resulted in a much larger temperature dependence of the flow stress between room temperature and 77°K than in either the yield or flow stresses shown and is about equivalent to the yield stress variation found by Christian and Masters. Further, the temperature dependence of the yield stress of this material is not known (twinning).

At 158°K, the deformation structures produced consist of long screws and small loops; there is a marked absence of edge dislocations, of braids or tangles. Pre-straining at room temperature produced a small braid which grew considerably on subsequent deformation at 77°K. The braid consisted mostly of primary edge dislocations. This suggests that

without the braids, the edge dislocations glide out of the crystal and that therefore the slip distance is about half the width of the crystal (1500 μ). The presence of braids will reduce the slip distance to about 10-30 μ . If the stress necessary to move edge dislocations has a smaller temperature dependence than that for screws then this will explain the difference in temperature dependence between yield and flow stresses since the former depends on edge dislocation movement whereas the latter requires either the movement of screws or the break down of the braid. Since without the movement of screws there can be no dislocation multiplication, the yielding at low temperatures should be rounded much more than the re-yield after room temperature pre-strain and this is observed to be so,

The amount of strain possible without dislocation multiplication can be roughly estimated from

$$\gamma = k \rho \ell \underline{b} \qquad V6$$

where ℓ is the slip distance, k a constant and the other symbols have their usual meaning. Only about a $\frac{1}{4}$ of the dislocations will have a suitable Burgers vector and about $\frac{1}{2}$ of these will be edge, thus k = $\frac{1}{8}$.

For a dislocation density of 10^7 cm^{-2} and a slip distance of 2000 μ, the shear strain is

$$\gamma = .00715$$

6. The Activation Enthalpy, Activation Volume and Theories of the Temperature Dependence of the Flow Stress.

The values of activation enthalpy and volume have been calculated in the results section. If the enthalpy is plotted on the same graph as Christian and Masters results (fig. V 2), it can be seen that good agreement is obtained showing further the effect of increasing purity. Plotting activation volume against flow stress change (fig. V3) again gives good agreement with the results of Christian and Masters but in this case the range of volumes is small.

That the two sets of results support each other suggests that the same mechanism is rate controlling in both cases i.e. the Peierls-Nabarro force. Since the interstitial impurity content (nitrogen) was about 3 ppm. in the purest material and about 100 ppm. in the less pure, if interstitials were responsible for the rise in yield and flow stresses about 90% of the temperature dependent flow stress would be absent from the purer material. Since this was not so unless the interaction per atom increases markedly when fewer impurity atoms are present, interstitial impurities cannot give rise to the large temperature dependence of the yield and flow stresses.

Brown and Ekvall (1962) consider that the high macroscopic yield stress is due to the reluctance of screw dislocations to cross-slip at the lower temperatures. The true yield stress, is that stress necessary to move dislocations through the lattice, from their micro-strain

results they suggest that this stress is not very temperature dependent. The dislocations form pile-ups, and macroscopic flow is not observed until the stress is large enough for the screw dislocations to cross-slip out of the slip plane, relieving the stress and forming new sources. It is suggested that the activation enthalpy and volume for this process is the same as that for the Peierls-Nabarro force theory, so that no differentiation can be made on that basis. Some of the arguments against this theory have already been given in section II, further arguments are given below.

a) The resistance to cross-slip is said to increase as the temperature is lowered because of two observations.

(i) the slip lines are straighter;

(ii) microscopy of specimens deformed at low temperatures show screws arranged in long, parallel arrays.

However, Sestak and Libovicky (1963) have shown that cross-slip is velocity dependent and that temperature has an indirect rôle. Further, there is no reason for screws to pile-up since there are no barriers and the present results show that adjacent screws in these arrays often have opposite sign.

b) It is not clear that it is necessary for screws to cross-slip in order to produce new sources. F.c.c. metals and alloys with low stacking fault energy appear to have sufficient sources for macroscopic flow without cross-slip.

c) The micro-strain work of Brown and Ekvall showed several stages of hardening. The present micro-strain work of

about the same sensitivity showed only one 'hardening' stage. However this 'elastic' line does not agree with Young's modulus; for a given stress the strain is too large. It was stated in section III that the compression jig was so massive that no bending occurred on loading but in view of the unexplained strain it is worth examining this again. The bending stresses on the bottom plate are too complex to work out a precise solution. However a maximum value can be obtained by considering the plate to be a slab in simple bending. The deflection δ is then given by

$$\delta = \frac{M \ell^2 (1-\nu^2)}{2 EI} \qquad V7$$

where M is the bending moment,

ℓ the separation of the pulling bars, (20 mm.)

ν, Poisson's ratio,

E, Young's modulus for EN 57 steel,

I, second moment of area ($\frac{b d^3}{12}$)

For a load of 400 kgs. (the load at the twin stress for 77°K deformation) the deflection δ is $\sim 1 \mu$ whereas the strain to be accounted for is equivalent to about 15 μ. Further this is a maximum value; in practice the siting of the transducer connections were such that most of this deflection was not measured.

Ignoring the unexplained strain, the present results do show a linear relation between stress and strain whereas Brown and Ekvall's do not. However they were using

polycrystalline iron which had been swaged or pre-strained to produce unpinned dislocations ; either process would produce internal stresses across grain boundaries which might give rise to dislocation movements at low stresses.

In conclusion, it appears that the Peierls-Nabarro force theory offers the best explanation of the temperature dependence of the yield and flow stresses but there are some features which have yet to be explained.

7. Twinning.

The electron microscopy confirmed that twinning was in agreement with $\{211\}\langle 111\rangle$ twins with a shear of 0.707. The optical observations of twins and twin intersections were generally as expected i.e. the most highly stressed system usually operated and Cahn's intersection rules were obeyed (see figs. IV 31 and 32). Sometimes, in electron micrographs, dislocation structures were seen along the trace of the (101) slip plane (the foil was $\sim$ perpendicular to $[\bar{1}11]$). Ogawa and Maddin (1964) found that slip occurred inside their twins in Mo - 35atom % Rh; the slip plane was always the $\{110\}$ plane containing the twin direction. The structures seen in the present work are probably the same since twins observed in sections parallel to $(\bar{2}11)$ can be of the type $(211)\ [\bar{1}11]$. Since the slip plane is always $\{110\}$ type it is probable that slip occurred during the load drop when the deformation rate is high.

A critical resolved shear stress for twinning.

Most of the present twinning results are for deformation at 77°K; at this temperature the resolved shear stress is reasonably reproducible especially in specimens cut from the same crystal. It is therefore concluded that at this temperature there is a CRSS for twinning but that it is sensitive to impurity. Below 77°K the twin stress is not so reproducible. However the results are few and all specimens were taken from one "multipass" crystal which resulted in the twin/slip boundary moving into the test region i.e. 14-20°K. Below 20°K the initial twin stress decreased with temperature so that at 4.2°K it had a lower value than at 77°K. This feature is rather surprising; there are several possible explanations.

a) Stress concentrations.

b) Thermal unstability - adiabatic softening.

c) The 'true' twin stress is lower at 4.2°K than at 20°K.

a) Since slip is more difficult at the lower temperatures any stress concentration is unlikely to be relieved by slip. This is equivalent to increasing the 'sharpness' of the concentration as the temperature is decreased. However, Bolling and Richman (1965) have shown that local stress concentrations only produce local twins; the first 'twin' drop at 4.2°K resulted in $\sim$0.05 axial strain thus local concentrations would be necessary at many points throughout the crystal. The only way in which this could arise is by micro-slip which would require a low Peierls-Nabarro force

(see sub-section V.6).

b) Basinski (1960) has examined adiabatic softening extensively. Adiabatic softening can occur if the specific heat and thermal conductivity are low and the flow stress has a strong temperature dependence. In practice, these conditions are only found at low temperatures. Where only plastic flow occurs the low thermal conductivity and specific heat are required in order to 'trigger' the load drop which occurs; if the specimen twins then this can act as a 'trigger' for further deformation. This second mechanism is of little use since we still have to explain the twin drop. Twinning does occur as this had been confirmed by optical microscopy though it is not known if every load drop, the first load drop or all of each load drop is explained by twin formation.

Basinski has given the equation for calculating the temperature rise as

$$P.\,\delta\ell = W H_T \qquad \ldots\ldots\ldots\ldots V\,8$$

where P is the load

$\delta\ell$, the change in specimen length,

W, the mass of specimen which is heated.

H_T the total enthalpy is given by

$$H_T = \int_{4.2}^{T} Cp.\, dT \qquad V9$$

where Cp is the specific heat and T the final temperature in degrees K.

For the first load drop at 4.2°K. P = 50 kg. and $\delta\ell$ = 0.125

w can be calculated by assuming that all deformation is equivalent to twinning; 5% axial strain is ~ equivalent to 12% in shear, the twinning shear is 0.707 hence the portion of the crystal sheared = 0.17. Since the crystal weighed 0.0412 gm w = 0.0070 gms. Thus from equation V 8,

$$H_T = 1.6 \text{ joules/gm}$$

From the enthalpy - temperature graph (fig. V 4) this corresponds to a temperature rise of ~50°K. The thermal conductivity at 4.2°K is only 0.027 watts cm^{-1} $^oK^{-1}$ hence there is a good chance that the heating is almost adiabatic. The initial specific heat is also low, 0.27 x 10^{-3} joules gm^{-1} $^oK^{-1}$. at 4.2°K but the temperature rise is insufficient to give slip at 22kg. mm^{-2} (about 180° required). However the volume associated with the deformation was calculated assuming the twinning shear for each part of the deformation, if the deformation was confined to a much smaller volume then an adiabatic load drop may have occurred. One further point against the first drop being due to adiabatic softening is that no detectable plastic flow occurred prior to the load drop.

c) Bolling and Richman (1965) in a set of very recent papers proposed that the twin stress was not governed by twin nucleation but by propogation. They consider that around every advancing twin is a work hardened zone. The size of this zone increases with temperature and so raises the twin stress. From this they predict a positive temperature dependence and a negative strain-rate dependence for the

twinning stress. This will qualitatively explain the results below 20°K but not the results at 77°K. However their theory is based on observations of twinning in Fe 25 atom % Be alloys which twin readily with very little tendency to slip; at 77°K niobium can deform plastically relatively easily also the strain per load drop is very large. There is likely to be a limit to the amount of plastic work possible since eventually the plastic zones around two parallel twins overlap and the resistance to twinning will then depend on the resistance to slip within a fixed volume. If this be so then for niobium the temperature for the maximum twin stress will lie between 20°K and 77°K and between this temperature and 77°K the twin stress will show the same sign as the yield stress with respect to temperature and strain rate changes. Altshuler's results on iron may be explained on the same basis; he found that over approximately the same temperature range slip and twinning had the same temperature and strain rate dependence.

Work hardening during twinning.

Bolling and Richman (1965) consider work hardening is due to the stress fields around the twins. In the present work chevron twinning where the twins pass through the crystal were most common so that such stress fields are likely to be small. The rate of hardening was also much higher than that obtained by Bolling and Richman (~ 400kg. mm^{-2} compared with 40 kg. mm^{-2}). The electron microscopy showed a very high

dislocation density around the twins and if subsequent twins have to move these dislocations the hardening rate is likely to be very high until the plastic flow stress is reached. In support of this is that pre-straining at a higher temperature either eliminated twinning or raised the twin stress

The negative strain which occurred after each twin drop cannot be explained easily. Both untwinning and secondary twinning on unfavourable systems will require high back stresses. However since the amount of negative strain is small the stress may arise from small twins which do not traverse the specimen.

Theories of twin nucleation

Some theories of twin nucleation require slip before twinning can occur (e.g. Priestner and Leslie 1965) and most require some form of stress concentration. The micro-strain results for 77°K did not show any obvious slip immediately before twinning but there remains the doubt about the extra strain in the 'elastic' line. The extra strain is by no means small being 17 x 10^{-4} axial strain, which gives ~0.35 x 10^{-4} shear strain and if this is translated into slip distance for a mobile density of 10^{7} disloc./cm^{2} (using $\gamma = e\,\underline{b}\,l$) we get a slip distance of 1.2 μ . If dislocations can move such distances before the apparent yield stress then yielding is not controlled by the Peierls stress and slip before twinning always occurs. However nearly all other evidence favours the existance of a high Peierls stress so it is quite probable that there is another explanation of the extra strain in the 'elastic' line.

Priestner and Leslie (1965) require a stress concentration of 15 x in the most favourable circumstances; in less favourable dissociations a stress of 45 x is required before twinning can occur. This theory therefore requires considerable slip before twinning.

Sleeswyk does not give a minimum value of stress necessary to form a twin but it can be calculated from (eq. II 60 & 61 b)

$$\tau_i = \frac{\mu b}{6\pi}\left(\frac{1}{r_1} + \frac{1}{r_2}\right) \qquad \text{.....V 10}$$

Using the equations of Teutonico (1965) the partials' separation is given by

$$r_1 = r_2 = \frac{0.118\ (C_{11} - C_{12} + C_{44})\ a^2}{6\pi\ E_f} \qquad \text{V 11}$$

where E_f is the stacking fault energy, (the other symbols have been given before).

For E_f = 100 ergs.cm^{-2} we get

$$r_1 = r_2 = 9.6\ \text{Å}.$$

Since niobium is anisotropic the rigidity modulus has to be calculated for each particular pair of orthogonal directions. Love (1927) gives the rigidity modulus as

$$\mu = \frac{\Pi}{(D_{11}, D_{22}, \ldots\ldots D_{12} \ldots\ldots).(2l_1l_2, 2m_1m_2, 2n_1n_2, m_1n_2+n_1m_2, n_1l_2+l_1n_2, l_1m_2+m_1l_2)^2}$$

where Π is the determinant of the stiffness constants

D_{rr} denotes the minor determinant corresponding with C_{rr}

and $(l_1 m_1 n_1)$ and $(l_2 m_2 n_2)$ are the two orthogonal directions

which have been normalised.

For cubic crystals Rousseau (1965) has reduced this to

$$\mu = \frac{C_{44}\,(C_{11} - C_{12})}{4K^2 C_{44} + (1-2K^2)\,(C_{11}-C_{12})} \qquad \text{V 12}$$

where $K^2 = (l_1^2 l_2^2 + M_1^2 M_2^2 + N_1^2 N_2^2)$; for $(\bar{2}11)$ $[\bar{1}11]$ this gives,

$$\mu = 4{,}280 \text{ kg. mm}^{-2}$$

Using these values in eqn. V 10 . gives

$$\tau_i = 45.6 \text{ kg. mm}^{-2}$$

This appears to be a reasonable value since it is only about twice the value of the twin stress at 77°K. However if the stacking fault energy is much higher say 1000 ergs.cm^{-2} then the twin stress increases to 456 kg. mm^{-2}.

Ogawa's equation for the twinning stress is

$$\tau_i = \frac{5.4 \times 10^{-2}}{2\pi} \frac{\mu}{(1-\nu)}$$

where ν is Poisson's ratio $\left(= \frac{C_{12}}{C_{11}+C_{12}} = 0.351\right)$

This gives $\tau_i = 56.6$ kg. mm.

Thus all three theories require stress concentration to explain the low measured twinning stresses. Ogawa's theory is the most fully developed but some of his conclusions (e.g. the rôle of interstitials) could be applied equally well to Sleeswyk's theory.

8. Slip Systems

In dividing up the standard triangle into regions for which different slip systems operated no account was taken of the difference in resistance to slip on the two slip plane types $\{110\}$ and $\{211\}$. In compression tests crystals cut from Nb56 and Nb (F.P.) 6 which are just in the $(\bar{1}01)$ region slipped on $(\bar{2}11)$ and in tension Nb 29 showed much more slip on $(1\bar{1}2)$ than would be expected. However Nb17a which was in the $(1\bar{1}2)$ region gave a parabolic stress-strain curve in compression which suggests double glide (the slip plane could not be determined). Reid (1965) found that for the same orientation $\{211\}$ was the slip plane if twinning could occur and $(\bar{1}01)$ if it could not; consequently the slip system changed in changing from tension to compression. This would explain the present results but it appears difficult to imagine that the resistance to slip dislocations changes with the sign of the stress. However since in some instances at any rate slip occurs on $(\bar{2}11)$ whilst $(\bar{1}01)$ is more highly stressed true glide and not composite glide is considered to occur on $(\bar{2}11)$.

9. Characteristics of the Work-hardening Curves.

At room temperature single slip on $(\bar{1}01)$ $[111]$ in either tension or compression is characterised by a large stress rise in stage 0. This feature does not occur for slip on

any other system (s) but always occurs for single glide on ($\bar{1}01$). W.H.R. θ_I for ($\bar{1}01$) slip is often much lower than θ_I for ($\bar{2}11$) slip particularly in tension where $\theta_{I\,(110)}$ is sometimes negative. This may well be connected with the large stage 0. In compression the length of stage I for slip on the two systems is about equal but in tension this is not so stage I for ($\bar{1}01$) being very long indeed.

The rate of hardening in stage II in compression is about double the rate in tension; however double glide in compression on primary and critical systems has the same hardening rate as stage II in tension. It appears significant that the lower hardening rate involves, in each case, [$\bar{1}11$] dislocations as the second or likely second system; the very low hardening rate for ($\bar{1}01$) tension coupled with a 9^{o} overshoot of the symmetry boundary may however be due to a separate effect.

The stress at which stage III starts, τ_{III}, varies considerably; τ_{III} is 4.3, 5.5 and 3.8 kg. mm^{-2} for ($\bar{2}11$) and ($\bar{1}01$) glide in compression and ($\bar{2}11$) glide in tension respectively. The τ_{III} value for ($\bar{1}01$) glide in tension is 4.6 or 5.7 kg. mm^{-2} depending on whether single or double glide is assumed at the double glide boundary. The compression values may have no significance since, as has been discussed, theyare associated either with specimen tilting or with zonal glide. This latter process may represent the limit of hardening in the crystal but the process has not been studied in sufficient detail to warrant

further discussion. The τ_{III} value for single glide in tension is rather low compared with the others and these crystals fractured at comparatively low strains; however again the number of results are few.

At 158°K the only single glide compressionresults are for $(\bar{2}11)$ slip. The rounded yield has already been discussed and will not be considered further. The rates of hardening in both stage I and stage II increase, θ_I by about 400% to 11.25 kg. mm. and θ_{II} by about 40%. τ_{III} has a very large value but this is mostly due to change in the lattice friction stress; however the total hardening to stage III still amounts to ~10 kg.mm^{-2}. Unlike the room temperature double glide, glide on $(\bar{2}11)$ $[\bar{1}11]$ and (211) $[\bar{1}11]$ in compression gave parabolic hardening. Tension curves were also all parabolic despite differences in initial orientation; this, however, may be a geometrical instability.

Twinning at 77°K has already been discussed. Room temperature pre-strain often resulted in 'yield points' at 77°K sometimes after considerable deformation. Since they were relatively slow events (cp. twin drops) they cannot be due to adiabatic softening. The work hardening rate at this temperature is rather low and since the load drops appear to be connected with zonal glide they are probably a consequence of this.

10. Electron Microscopy.

The most striking feature of the electron microscopy results is the lack of screw dislocations after room temperature deformation and the lack of edge dislocations after deformation at lower temperatures, (e.g. 158°K). This result may be explained by the change in frictional force with change in temperature. The attraction between two parallel screws of opposite sign a distance , r, apart is almost temperature independent. The force per unit length F_r, is given by

$$F_r = \frac{\mu b^2}{2\pi r} \qquad V\,13$$

For a given orientation the ratio α , of the resolved stress on the cross-slip plane to the resolved stress on the primary plane is fixed. Neglecting the change in resistance to slip on different planes and the internal stress field cross-slip can occur when

$$\frac{\mu b}{2\pi r} \geq (1-\alpha)\tau \qquad V\,14$$

where τ is the friction stress.

In b.c.c. crystals there are a number of possible cross-slip planes e.g. if the primary plane is $(\bar{1}01)$ then $(\bar{2}11)$ and $(\bar{1}10)$ are possible cross-slip planes. The resolved stress on the $(\bar{2}11)$ is always greater than on $(\bar{1}10)$ but since the angle between $(\bar{2}11)$ and $(\bar{1}01)$ is 30° whereas $(\bar{1}10)\,\hat{}\,(\bar{1}01)$ is 60° the separation of the screws, r, at the cross-slip point is larger for $(\bar{2}11)$ cross-slip. Hence the chosen cross-slip

plane will depend on orientation and applied stress.

Let us consider the separationof slip planes ¦a¦ between which the screws can cross-slip and annihilate on the above basis. Nb 32II was oriented for $(\bar{2}11)$ $[\bar{1}11]$ slip, suppose the cross-slip plane is $(\bar{1}01)$. Initially,

$$\alpha = \frac{\cos \theta_{\bar{1}01}}{\cos \theta_{\bar{2}11}} = 0.865$$

The maximum separation of the $(\bar{2}11)$ planes is then given by

$$a = r \sin 30 = \frac{\mu b \sin 30}{2\pi (1-\alpha)\tau}$$

At room temperature, μ = 4,630 kg. mm^{-2} (for $(\bar{1}01)$ $[\bar{1}11]$), τ = 1.0 kg.mm^{-2} and $\underline{b}$ = 2.86 Å. This gives a = 10,500 Å. At 158°K, μ = 4,910 kg. mm^{-2} (for $(\bar{1}01)$ $[\bar{1}11]$), τ = ~12.5 kg. mm^{-2} This gives a = 893 Å. However on warming up to room temperature screws may still annihilate if

$$F_r = \frac{\mu b^2}{2\pi r} \gg \tau b. \qquad \text{V15}$$

Since there is no applied stress the screws will cross slip when closest together ie. a = r ,(cross-slip plane $(0\bar{1}1)$) and this gives, a = 1360 Å.

Thus when the crystal returns to room temperature there will be further considerable annihilation unless the dislocation is held by jogs (which although themselves can be annihilated by the cross glide may pin the dislocation on the glide plane by skewing it off the perfect screw orientation). The jogged screws of opposite sign seen

in fig. IV88 are $\sim 3500^{\circ}$A apart in the slip plane projection; however the separation of the planes is not known.

The argument in favour of edge dislocations remaining in the crystal during room temperature deformation but slipping out at low temperatures has already been given. (i.e. much easier to move edge dislocations than screws which therefore control the applied stress). The effect of pre-strain is to produce a dipole grouping; since there is little tangling it might be supposed that the stress necessary to move the whole group is small. However the force per unit length on the group is $n\tau\underline{b}$ where n is the number of 'excess sign' dislocations. At the lower re-yield the resistance to movement of the group is $\sim(n + 2d)\ \tau_f\ \underline{b}$ where τ_f is the friction stress, and d is the number of dipoles in a cross section of the braid. Since $d \simeq n$ (may be much greater) τ must be greater than $\sim 3\tau_f$ which is unlikely for large values of τ_f unless $\tau_{f\ screw} \gg \tau_{f\ edge}$ or stress multiplication can occur in which case for a pile-up,

$$N\ (\tau - \tau_{fedge})\ \underline{b} + n\ \tau\ \underline{b} \gg (n + 2d)\ \tau_{fedge}.\underline{b}.$$

where N is the number of dislocations in the pile-up and τ is probably $\sim\tau_{f\ screw}$.

Dipole Formation.

Theories of dipole formation are numerous; many have been criticised because they require conditions not always available, however different mechanisms may operate under

different conditions and more than one mechanism at any one time. A comprehensive review has been given by Tetelman (1962) (and Sharp (1963)); we shall only consider mechanisms which can operate in b.c.c. metals AT room temperature or below.

Seeger and Mader (1961) suggested that dipoles were formed by theoperation of cone sources. If one end of a dislocation source (Frank-Read) is a dislocation with a Burgers vector component $\underline{b}'$ perpendicular to the glide PLANE then the rotating dislocation is given a jog of height $\underline{b}'$ for every revolution. Eventually the jog grows to such a size that the loops emitted trail an edge dipole.

Tetelman (1962) proposed that mixed dislocations of opposite sign but with the same Burgers vector gliding on parallel slip planes should re-align themselves so that long lengths of edge component are parallel. The screw components then cross-slip to produce a dipole. Hirsch has criticised this mechanism since it does not explain the short lengths of most dipoles.

Kuhlmann-Wilsdorf (1962) claimed that jog production due to 'dislocation uncertainty' was the prime method of dipole formation. According to her theory the uncertainty of a screw dislocation perpendicular to the slip plane, δ, is given by

$$\delta \simeq 2\,\bar{u}\,\left(\frac{\mu}{\pi\tau}\right)^{\frac{1}{2}} \qquad \text{V 16}$$

where $\bar{u}$ is the mean displacement due to thermal motion, and τ the maximum shear stress the plane can support in the absence of dislocations.

It is also claimed that at low temperatures δ is only large for glide dislocations in c.p.h. or f.c.c. metals and that at liquid air temperatures b.c.c. metals should not contained jogged dislocations or loops. This is contrary to the present observations. Hirsch has criticised this theory on the grounds that it does not explain the grouping of dipoles; however this criticism may not be valid since Sharp and Makin (1964) have shown that edge dislocations can 'sweep-up' edge dipoles into braids.

Hirsch (1963) proposed that successive intersection of a forest dislocation by glide dislocations gave rise to dipoles. Each unit jog produced by the intersection left a trail of vacancies which condensed into an edge dipole. Further dipoles can be produced by cross slip (induced by the dipole) of subsequent glide dislocations (Fourie and Murphy 1962). This mechanism has been criticised by Sharp (1963) since the dipoles produced lie 'side-by-side' instead of 'end-to-end'.

Basinski (1963) suggested that dipoles were produced in the following manner. Edge dislocations of opposite sign align themselves into long narrow groups by mutual attraction. This braid is then chopped up into smaller pieces by secondary glide. He believes that this explains the decrease in dipole length as deformation proceeds. Basinski criticised dipole formation by the dragging of jogs formed by cross-slip, since (1) it is unlikely that long lengths of dislocation would cross slip and (2) closely spaced jogs should glide conservatively and annihilate.

Bullough and Sharp (1964) calculated the force perpendicular to the glide plane on a glide dislocation in the region of a forest dislocation. They concluded that the force was sufficient to cause cross-slip and that one of the jogs produced was attracted to the forest dislocation whereas the other repelled. If the second jog glides away conservatively subsequent motion of the screw can leave an edge dipole. They also believe that edge dipoles produced randomly in this manner are swept into braids by the subsequent glide of edge dislocations.

The termination of dipoles has been considered by Li and Swann (1964). The most likely method was considered to be as follows. Since the jogs dragging behind a dislocation are unlikely to be evenly spaced the screw components on either side of any one dipole move forward different amounts; the most advanced segment bows out beyond the semi-circle configuration and part of this cross slips to terminate the dipole and form a new jog a little way further along the dislocation. The termination by interaction with a cross-gliding dislocation of the same Burgers vector was possible but not very likely since an interaction which did not terminate was possible. The successive jogging by secondary dislocations was also considered unlikely to lead to termination since the amount of secondary glide necessary is large. The kinking within a dipole method of Tetelman (1962) was not considered to occur. What appears (to the author) to be the simplest

method of termination, the conservative movement of a jog of opposite sign was not considered.

The present results show dipoles in two forms. Individual dipoles are quite short, 0.1 - 0.2 μ long; however the tilts across braids, in which individual dipoles are only rarely seen, are of the order of 30′ . For a foil 2000 Å thick, 30′ of tilt corresponds to an excess of edge dislocations of one sign of ~6; since usually there are many more dislocations in a braid or corridor wall most must be paired with dislocations of opposite sign. These dipoles, if they may be referred to as such, are much longer than the first type; their length is determined by the distance the screws move before cross-slipping and perhaps by the amount of secondary glide. A possible example of the termination (or production) of dipoles by secondary glide is shown in fig. IV.55. The shorter dipoles and loops may have been formed by the Hirsch (1963) method but since screw dislocations, when present, appear to contain jogs a dragging jog method also seems possible. The problem of removing the second jog appears to have been overcome by the Bullough - Sharp mechanism of cross-slip near a forest dislocation. The conservatively moving jog will still annihilate another jog of opposite sign (unless it reaches a node first) but in general the annihilated jog will already have produced a dipole.

At low temperatures the dipoles have broken up into small loops and the dislocations appear to be more heavily

jogged. Since on the Bullough-Sharp mechanism the cross-slipping force is approximately constant whereas the friction stress has increased considerably it is expected that the jog height should decrease. The repulsed jog will also, in general, not move far from the forest dislocation so that the chance of annihilation is less. In this case both jogs produce dipoles, one 'vacancy' the other 'interstitial'. Since the temperature is low it is not expected that the dipoles will be able to diffuse towards each other however if the dipole is narrow sufficient diffusion may occur for it to break-up into little loops especially when the crystal warms up to room temperature again. Although the above will explain qualitatively the high density of jogs and loops obtained after low temperature deformation, we have no quantative evidence of loop density with strain or forest density, nor do we know whether the loops formed are both 'vacancy' and interstitial or of one type only.

Tilts and Twists across boundaries.

The tilts across boundaries have already been attributed to the presence of edge dislocations of one sign. In sections perpendicular to the glide direction (fig.IV 65 & 66) the tilts across boundaries were rather small compared with the twists. This is not altogether surprising since primary edge dislocations having their Burgers vector perpendicular to thefoil do not contribute to the tilt. The $(\bar{2}11)$ plane is unlikely to contain a twist boundary, however (011) which is at an angle of $\sim 35^{\circ}$ to the foil and has the same

projected line as $(\bar{2}11)$ can contain a twist boundary made up of $[11\bar{1}]$ and $[1\bar{1}1]$ dislocations. A twist of about $1^{o}6'$ corresponds to a screw spacing of ~150 Å and in view of the high secondary density this spacing seems quite probable. Such a twist would give a twist of $38'$ around the $[\bar{2}11]$ axis but only $\sim 1/3'$ around the $[0\bar{1}1]$ axis; hence the tilt across the boundary (fig. IV 65) is due to edge dislocations of the $[\bar{1}11]$ type.

Dislocation densities.

In calculating the dislocation densities from the same area using different reflections it was assumed that the dislocations were isotropically distributed. This is, of course, incorrect; a true density could only be obtained by knowing the distribution of each type of dislocation amongst its possible slip planes (6 planes for each $\langle 111 \rangle$) and also the ratio of edge to screw components. Since most dislocations are likely to be on their most highly stressed planes i.e. $(\bar{2}11)$ for $[\bar{1}11]$, $(\bar{1}21)$ for $[\bar{1}\bar{1}1]$, $(\bar{1}12)$ for $[1\bar{1}1]$ and (211) for $[\bar{1}11]$ and since for foils perpendicular to the primary glide direction (Nb 32 IIB) the first three planes make a large angle with the foil the calculated densities for $[\bar{1}\bar{1}1]$ and $[1\bar{1}1]$ dislocations are likely to be low whilst $[\bar{1}11]$ may be high. However estimating the distributions is likely to be inaccurate and no attempt will be made to do so here.

Many theories of work hardening predict a proportionality between the stress increase and the dislocation density.

Fig.V 5 shows this relationship ($(\tau - \tau_0)$ v. $\sqrt{\rho}$) for $[\bar{1}01]$ slip over the range studied. Since there are only three points on this graph its usefulness is suspect despite good agreement; however if the slope is assumed to be $\frac{\mu b}{w}$ (see Nabarro et al. (1964)) then w = 7.9 which is larger than most theories predict (3-5).

Compatibility of sections taken from crystals deformed at room temperature in double glide.

As has already been stated the three types of section do not appear to be compatible with each other. Considering again the 90° section (perpendicular to both slip planes) it is clear that the two $\{211\}$ type planes are not equivalent since boundaries are approximately parallel to one but not the other. Since our labelling of the two (slip) systems was arbitary we may exchange their identities. The $(\bar{2}11)$ sections are now compatible with 90° section and it is seen that the corridor walls are parts of large sheets of dislocations on (011) or (111) planes. The '45° section' could not have been at 45° to the 'first system's'slip plane $(\bar{2}11)$, but must have been cut at 45° to the 'second system's ' slip plane, (211) i.e. a $(2\bar{1}3)$ foil rather than a $(\bar{2}\bar{1}3)$ foil; the rows of edge dislocations seen are probably of the first system i.e. $[\bar{1}11]$ which have polygonised by climbing onto the (111) plane.

Structures of the high tilt boundaries.

In sections parallel to the $(0\bar{1}1)$ plane, boundaries were

seen on (011), (111) and (211) planes with rotations of up to 25° about the $[0\bar{1}1]$ direction.

a) The (111) boundaries.

These are the simplest to explain; primary edge dislocations $[111]$ of the same sign undergo glide polygonisation to form low energy boundaries perpendicular to the glide plane, $(\bar{2}11)$. In order to attain a tilt of 25° the vertical spacing of the dislocations is required to be 6.5 Å i.e. ~ 2.3 b.

b) The (211) boundaries.

Since arrays of $[\bar{1}11]$ dislocations on (211) planes are equivalent to a pile-up they are unlikely to occur. The tilts across these boundaries are so large that the (111) planes in adjacent crystallites cannot be parallel; thus what appear to be (211) planes are probably (111) and the boundaries are the same as (a).

c) The (011) boundaries.

The (011) plane does not contain either of the Burgers vectors $[111]$ and $[\bar{1}11]$. However $[111]$ edge dislocations on $(\bar{2}11)$ planes and $[\bar{1}11]$ on (211) may meet and provided they are of the correct sign ($[\bar{1}\bar{1}1]$ and $[\bar{1}11]$ say) combine to form $[100]$ dislocations. If this happens on successive planes then a sheet of $[100]$ dislocations one above the other builds up on a (011) plane. If two $\{111\}$ type boundaries of suitable sign cross then again a reduction in energy may be obtained by their 'zipping' up to form one boundary.

Li (1963) has calculated the stress free stable

net-works possible in b.c.c. crystals. Using $[111]$ and $[1\bar{1}\bar{1}]$ edge dislocations on $(\bar{2}11)$ and (211) planes with a spacing ratio of 3 : 1 he obtains a stress free wall on (011). This wall has an angle of tilt of $\frac{\sqrt{6}.a}{3\ h_2}$ where 'a' is the lattice parameter and h_2 the smaller spacing; (arbitary selection, but convenient to choose h_2 as the spacing of the $[1\bar{1}\bar{1}]$ dislocations). For a 25^{o} tilt $h_2 = 6.18$ Å. Apart from being stress free, Li's type of boundary has the advantage that it will account for the absence of boundaries on $(\bar{1}11)$ planes and yet allow equal densities (and therefore glide) of $[111]$ and $[\bar{1}11]$ dislocations. It should be possible to add up the product (length x angle of rotation) for the boundaries and roughly equate them as

$$2\sqrt{2}\ [111] = 4.5\ [011]$$

where $[hkl]$ is the above product for the (hkl) plane.

One of the assumptions in calculating boundaries of minimum energy is that only the elastic strain energy need be considered. However in the above boundaries the dislocations are so close together (~ 2.3 b apart) that their cores (radius ~ 5 b) must overlap and the core energies taken into account. However the simplified dislocation model given above does explain the results and therefore to a first approximation, is probably true.

11. Theories of Work-Hardening

Stage 0

Since, at room temperature, a substantial stage 0 does not occur for $(\bar{2}11)$ slip but only for $(\bar{1}01)$, stage 0 should be explainable by some difference in the condition of dislocations on the two planes. The edge dislocations remain on the slip plane except at the higher strains when glide polygonisation occurs; the screw dislocations are believed to have cross-slipped in stage I since electron micrographs show a lack of screws. If the screw dislocations are extended on the $(\bar{1}01)$ plane then cross slip will be inhibited and hardening by mutual attraction between screws of opposite sign will occur. However in order to obtain a hardening of ~ 1 kg.mm^{-2} the separation of the planes containing the screws would need to be (assuming no stress multiplication)

$$a = \frac{\mu b}{4\pi\tau} \simeq 1000\text{Å}. \qquad \text{V 17}$$

At present there are no calculations of the extension of screw dislocations on $\{110\}$ planes. Teutonico has calculated their extension on $\{211\}$ in terms of the stacking fault energy which is unknown anyway. Unless there is a large difference between the stacking fault energies on the two planes, it is not expected that the extension on $\{110\}$ will be very different since the rigidity moduli on the two planes in the $[111]$ direction are identical.

The present electron microscopy was done on specimens

strained well beyond stage 0 so it is not possible to check if screws remain in the crystal after low strain. Low and Turkalo (1962) deformed silicon iron $<1\%$ on $(\bar{1}01)$ $[111]$; their micrographs show a high proportion of screw dislocations. However silicon iron at room temperature may be 'equivalent' to pure metals at much lower temperatures.

Stage I

The lower rate of hardening usually found on $(\bar{1}01)$ slip (compared with $(\bar{2}11)$) is probably due to a reduction in the stage 0 hardening masking the true hardening rate in stage I. i.e. the screws cross-slip during stage I. If this is so then the hardening rate to be explained is ~ 3.5 kg.mm^{-2} or $\sim \mu/1200$.

Apart from the hardening rate, any theory should explain the extensive easy glide obtained for $(\bar{1}01)$ slip in tension and the very large overshoot factor P. For Nb 23C with a 9^{o} overshoot, the overshoot factor P is

$$P = \frac{\cos\ \theta_s \cos\ \lambda_s}{\cos\ \theta_p \cos\ \lambda_p} = 1.12 \qquad \text{V 18}$$

where θ and λ have their usual meaning and the subscript indicates secondary or primary. This large overshoot factor probably excludes any theory which involves a large loss of dislocations through the slip distance being greater than the crystal diameter.

The theory of Seeger, Mader and Kronmuller, (1963).

This theory predicts a hardening given by (eq. II 26)

$$\theta_I = \frac{8\mu}{9\pi} \cdot \left(\frac{x}{L_2}\right)$$

where x and L_2 are the slip plane spacing and the slip distance of the screws respectively. These have to be measured or estimated. Since we have no optical microscopy results on niobium it is difficult to check the theory; however if the slip distance is estimated to be about the length of the edge braids then L_2 is $\sim 8\mu$ (Nb32IF) and x calculated from eq.II 26 is ~ 340 Å . This latter value is unlikely to agree with other estimates since the slip line spacing, often measured with an optical microscope, is of the order of 1μ .

The stress rise in stage I is given by eq. II 25.

$$(\tau - \tau_0) = \frac{\mu \underline{b} \quad n}{2\pi \sqrt{R_0 L_2}}$$

If the separation of the sources R_0, is approximately equal to the slip distance then

$$(\tau - \tau_0) = \frac{\mu \underline{b}}{2\pi} \quad n^3 \sqrt{N} \quad \ldots\ldots\ldots \text{V 19}$$

where N, is the source density, and n, the number of dislocations per source, changes with strain.

Up to the end of stage I, the stress rise is proportional to the square root of the dislocation density, a relation which cannot bepredicted by eqn. V 19 .

Stage II

In terms of the shear modulus the hardening rates to be

explained are $\sim\frac{\mu}{250}$ for room temperature single glide in compression; $\frac{\mu}{500} - \frac{\mu}{600}$ for room temperature single glide in tension and double glide on primary and critical {211} in compression; and $\frac{\mu}{175}$ for compression single glide at 158° K.

Unfortunately, we do not have the dislocation densities throughout stage II, so the relation $(\tau - \tau_0) = \frac{\mu b}{w}\sqrt{\epsilon}$ cannot be checked. However, since all theories of hardening in stage II are designed to predict this relation with approximately the same value for w, this is not a basis for distinguishing between them.

With the limited information available it is not possible to make a quantitative distinction between the various theories; however some unsatisfactory aspects of the theories can be shown on qualitative arguments. Recalling again the basis of each theory:

a) Kuhlmann-Wilsdorf - the temperature independent hardening is due to a decrease in source length.

b) Seeger et al. - hardening is chiefly due to the back stress from a pile-up preventing the source operating. The back stress may or may not be confined to a narrow zone around the slip plane.

c) Hirsch - no one dominant hardening mechanism decided upon but contributions from several mechanisms shown to be

proportional to the reciprocal of the obstacle spacing. However in general the long range stress from pile-ups is not considered to harden the crystal since slip occurs where the long range stress aids the applied stress.

Since screw dislocations in b.c.c. crystals can cross-slip relatively easily it is not expected that pile-ups alone should prevent the movement of screws. However the stress field from a tangle which has some thickness perpendicular to the slip plane may be wide enough to prevent cross-slip. The source may also be prevented from operating if the stress field from an edge pile-up is sufficient to stop the loop forming. The conjugate systems for compression single glide are (011) $[\bar{1}\bar{1}1]$ and ($\bar{1}$21) $[\bar{1}\bar{1}1]$ for ($\bar{1}$01) and ($\bar{2}$11) glide respectively. The interaction of edge dislocations of the primary and conjugate systems do not form low stress field boundaries such as those formed by $[\bar{1}11]$ and $[\bar{1}\bar{1}1]$ dislocations on ($\bar{2}$11) and (211) planes. Hence, the difference in W.H.R.s is probably due to the difference in long range stress field.. If this is so at least 60% of the hardening is due to long range stress fields and the basis of Kuhlmann-Wilsdorf's theory is insufficient. The conclusion of Hirsch, that the internal stress field does not contribute to the hardening is also wrong; however his theory is not mechanistic enough to be rejected on these grounds.

The Kuhlmann-Wilsdorf theory and the Seeger theory do not account for the effect of temperature (except by the change in rigidity modulus) on the rate of hardening;

however the Hirsch theory contains the friction stress in the constant k_1 and the W.H.R. is given by (eqn.II 59)

$$\theta_{II} = \frac{k_1 \mu}{6\pi}$$

From equations II 47 and II 49 we get

$$k_1 = \frac{1}{4} \cdot \frac{\beta}{\tau} \cdot \frac{(\tau - \tau_0)}{(P-S)}$$

writing $(\tau - \tau_0) = \Delta\tau$ gives

$$k_1 = \frac{\beta}{4\,(P-S)} \cdot \frac{\Delta\tau}{(\tau_0 + \Delta\tau)} \qquad \text{V 20}$$

Hence reducing the test temperature which increases τ_0, should decrease the hardening rate. Further, since k_1 is stress dependent θ_{II} is not linear but increases with strain. For single glide in compression on $(\bar{2}11)$ $[111]$ at 158°K the W.H.R. is higher than at room temperature in contradiction of the theory; however the stage I hardening rate has also increased, and since the electron microscopy results do not show long obstacles of any description, it would be surprising if the theory did predict the experimental W.H.R.

Stage III

Since cross-slip theories of stage III hardening require the dislocations to be extended in the slip plane, they are not likely to be applicable to b.c.c. metals.

Stage III in niobium may be connected with break down of the barriers or long range cross-slip to circumvent large obstacles. Two other possibilities are (1) groupings of opposite sign merge and annihilate each other (see double

slip at room temperature micrographs); (2) primary and secondary edge dislocations may form low stress boundaries by a mechanism, which at present, is not known. The only evidence for this latter suggestion, is that some crystals oriented for $(\bar{1}01)$ $[\bar{1}11]$ single slip in compression, when deformed after the end of stage II, continued to harden at the same rate (approximately) as the double glide in compression on primary and critical crystals.

REFERENCES

Adair A.M. & Hook R.E. (1962) Acta Met. 10 741.

Allen N.P., Hopkins B.E. & McLennan J.E. (1956) Proc.Roy.Soc. A 234 221.

Altshuler T.L. (1964) D. Phil. thesis. Oxford.

" (1964a) Private communication.

Amelinckx S. (1964) 'Direct Observation of Dislocations' A.P.

Anderson R.N. & Bronisz S.E. (1959) Acta Met. 7 645.

Andrade E.N. & Chow Y.S. (1940) Proc. Roy.Soc. A175 220.

Andrade E.N. & Tsien L.C. (1937) Proc.Roy.Soc. A163 1.

Ang C.Y. (1953) Acta Met. 1 123.

Bailey J.E. & Hirsch P.B. (1960) Phil. Mag. 5 485.

Bakish R. (1958) Acta Met. 6 120.

Barrett C.S. (1948) 'Cold Working of Metals' ASM P.65.

" (1952) 'Structure of Metals' McGraw Hill.

Barrett C.S. & Bakish R. (1958) TAIME. 212 122.

Barrett C.S., Ansel G & Mehl R.F. (1937) TASM 25 702.

Basinski Z.S. (1957) Acta Met. 5 686.

" (1959) Phil. Mag. 3 393.

" (1960) Aust J. Phys. 13 354.

" (1963) Communication to Sharp 1963.

Basinski Z.S. & Christian J.W. (1960) Aust.J.Phys. 13 299.

Benson R., Thomas G. & Washburn J. (1963) 'Electron Microscopy and the strength of Crystals' Interscience.

Biggs W.D. & Pratt P.L. (1958) Acta Met. 6 694.

Blankenbergs G. & Wheeler M.J. (1964) J.Inst.Met. 92 337.

Bolef D.I. (1961) J. App. Phys. 32 100.

Bolling G.F. & Richman R.H. (1965) Acta Met. 13 605.

Bowen D.K. (1965) Private Communication.

Briers G.W., Dawe D.W., Dewey M.A.P. & Brammer I.S. (1964) J. Inst. Met. 93 77.

Brown N. & Ekvall R.A. (1962) Acta Met. 10 1101.

Bullough R. & Sharp J.V. (1964) AERE Report R-4739. Harwell.

Cahn R.W. (1953) Acta Met. 1 49.

" (1955) J. Inst. Met. 83 493.

Calnan E.A. & Clews C.J.B. (1951) Phil. Mag. 42 616.

Calverley A., Davis M. & Lever R.F. (1957) J. Sci Inst. 34 142.

Carrington W., Hale K.F. & McLean D. (1960) Proc.Roy.Soc. A259 203.

Chambers R. (1962) AIME Meeting New York. (Reported by Conrad 1963)

Chen N.K. & Maddin R. (1951) T.AIME 191 937.

Christian J.W. & Masters B.C. (1964) Proc.Roy.Soc. A281 223.

Clarebrough L.M. & Hargreaves M.E. (1959) Prog.Met.Phys. 8 1.

Clark R. & Craig G.B. (1952) Prog.Met.Phys. 3 128.

Cochardt A.W., Schoeck G. & Wiedersich H. (1955) Acta Met. 3 533.

Cohen J.B., Hinton R., Lay K. & Sass S. (1962) Acta Met. 10 894.

Cole M., Fisher C. & Bucklow I.A. (1961) Brit J. App.Phys. 12 577.

Conrad H. (1961) JISI 198 364.

" (1963) Conference at NPL London. P.476.

Conrad H. & Hayes W. (1963) T.ASM 56 249.

Conrad H. & Wiedersich H. (1960) Acta Met. 8 128.

Cooper R.H. (1964) Ph.D. thesis. Auckland, N.Z.

Cost J.R. & Wert C.A. (1963) Acta Met. 11 231.

Cottrell A.H. (1953) 'Dislocations and Plastic Flow in Crystals' Oxford.

" (1957) London Conference Inst.Mech.Eng. P.448.

" (1963) Conference at NPL London. P.456.

Cottrell A.H. & Bilby B.A. (1951) Phil. Mag. 42 573.

Cox J.J., Horne G.T. & Mehl R.F. (1957) T.ASM 49 118.

Cracknell A. & Petch N.J. (1955) Acta Met. 3 186.

Dietze H.D. (1952) Z.Phys. 132 107.

Donth H. (1957) Z.Phys. 149 111.

Dorn J.E. & Rajnack S. (1964) T.AIME 230 1052.

Edington J.W., Lindley T.C. & Smallman R.E. (1964) Acta Met. 12 1025.

Edington J.W. & Smallman R.E. (1964) Acta Met. 12 1313.

Edmondson B. (1961) Proc.Roy.Soc. A264 176.

Elam C.F. (1935) 'The Distortion of Metal Crystals' Oxford.

Evans C.I.L. (1964) Part II thesis. Oxford.

Evans P.V.R. (1964a) J. L-C. Metals 6 253.

Erikson J.S. (1962) General Electric (U.S.A.) Research Report.

Ferriss D.P., Rose R.M. & Wulff J. (1962) T.AIME 224 975.

Fleischer R.L. (1962) Acta Met. 10 835.

Fong Duan et al. (1963a) Sci.Sin. 12 909.

" " Sci.Sin. 12 976.

" " Sci.Sin. 13 339.

Fourdeux A. & Berghazan A. (1960-61) J. Inst. Met. 89 31.

" " (1962) 6th Colloque de Metal. Saclay,

Fourdeux A. & Wronski A. (1963) Acta Met. 11 1270.

" " (1964) J. L-C. Metals 6 11.

Fourie J.T, & Murphy R.J. (1962) Phil. Mag. 7 1617.

Frank F.C. & Thompson N. (1955) Acta Met. 3 30.

Friedel J. (1963) 'Electron Microscopy and Strength of Crystals' Interscience. P.605.

Jaoul B. & Gonzalez D. (1961) J. Mech. Phys. Sol. 9 16.

Johnston W.G. & Gilman J.J. (1959) J. App. Phys. 30 129.

Jøssang T. Skylstad K. & Lothe J. (1963) Conference at NPL, London P.528.

Garlick R.G. & Probst H.B. (1964) T.AIME 230 1120.

Gregory D.P., Rowe G.H. & Stroh A.N. (1962) 'Work Hardening Mechanisms in b.c.c. metals' ASD Report.

Gregory D.P., Stroh A.N. & Rowe G.H. (1963) T.AIME 227 678.

Ham R.K. (1961) Phil.Mag. 6 1183.

Hamer F.M. & Hull D. (1964) Acta Met. 12 682.

Harris B. (1963) J.Inst. Met. 92 89.

Hartley C.S. & Wilson R.J. (1963) Acta Met. 11 835.

Heslop J. & Petch N.J. (1956) Phil. Mag. 1 866.

Hirsch P.B. (1962) Phil. Mag. 7 67.

" (1963) Conference at NPL. London P.39.

" (1964) Disc. Farad. Soc. 38 111.

Hirsch P.B., Howie A., Pashley D., Whelan M.J. & Nicholson R.B. (1965) 'Electron Microscopy of Thin Crystals' Butterworths.

Hirsch P.B. & Segall R.L. (1961) WADD TR-61-181.

Hirschhorn J.S. (1963) J. L-C. Metals 5 493.

Hull D. (1960) Acta Met. 8 11.

" (1963) Proc.Roy.Soc. A274 5.

Keh A.S. (1961) AIME Symposium California (Pub.1963 Interscience)

" (1964) U.S. Steel Report PR-263.

Keh A.S. & Weissmann S. (1961) AIME Symposium California.

Kelly A. (1953) Proc. Phys. Soc. A66 403.

Kocks U.F. (1964) T.AIME 230 1160.

Koehler J.S. (1952) Phys.Rev. 86 52.

Komjathy S. (1960) J. L-C Metals 2 466.

Koo R.C. (1963) Acta Met. 11 1083.

Kossowsky R. & Brown N. (1963) AIME Meeting, Ohio (Reported by Lawley & Gaigher 1964)

Kuhlmann-Wilsdorf D. (1960) Phys. Rev. 120 773.

Kuhlmann-Wilsdorf D. (1962) T.AIME 224 1047.

Kuhlmann-Wilsdorf D. (1963) Acta Met. 10 584.

Lawley A. & Gaigher H.L. (1964) Phil. Mag. 10 15.

Lawley A. & Meakin J.D. (1964) Phil. Mag. 10 737.

Lawley A., Van den Sype J. & Maddin R. (1962-63) J.Inst.Met. 91 23.

Leadbetter M.J. & Argent B.B. (1961) J. L-C Metals 3 19.

Li J.C.M. (1963) J. Aust. Inst. Met. 8 206.

" (1965) T.AIME 233 219.

Li J.C.M. & Swann P.R. (1964) Phil. Mag. 10 617.

Lindley T.C. & Smallman R.E. (1963) Acta Met. 11 361.

Lindtveit T., Kvernes I. & Storvik P. (1963) Mutual Weapons Development Programme AD -418326.

Liu Y.S. (1963) T.AIME 227 775.

Lothe J. & Hirth J.P. (1959) Phys. Rev. 115 543.

Love A.E.H. (1927) 'Theory of Elasticity' C.U.P.

Low J.R. (1961) 'Iron and Its Solid Solutions' P.217, AIME.

Low J.R. & Guard R.W. (1959) Acta Met. 7 171.

Low J.R. & Feustel R.G. (1953) Acta Met. 1 185.

Low J.R. & Turkalo A.M. (1962) Acta Met. 10 215.

McHargue C.J. (1960) Acta Met. 8 900.

" (1962) T.AIME 224 335.

McHargue C.J. & McCoy H.E. (1963) T.AIME 227 1170.

Maddin R. & Chen N.K. (1953) T.AIME 197 1131.

" " (1954a) Prog.Met.Phys. 5 53.

" " (1954b) T.AIME 200 280.

Masters B.C. (1962) D. Phil. thesis, Oxford.

Meieran E.S. & Richman M.H. (1963) T.AIME 227 1044.

Miller G.L. (1959) 'Tantalum and Niobium' Butterworths.

Mitchell A. (1962) D.Phil thesis, Oxford.

Mitchell T.E., Foxall R.A. & Hirsch P.B. (1963) Phil.Mag. 8 1895.

Mordike B.L. (1961) Z.Metall. 52 587.

Mordike B.L. & Haasen P. (1962) Phil. Mag. 7 459.

Mott N.F. (1952) Phil. Mag. 43 1151.

Nabarro F.R.N., Basinski Z.S. & Holt D.B. (1964) Adv. Phys. 13 193.

Nishiyama Z., Shimizu K. & Kamada A., (1964) Acta Met. 12 446
" " " (1965) T.Jap.Inst.Met. 6 40

Nye J.F. (1957) 'Physical Properties of Crystals' Clarendon Press.

Ogawa K. (1965) Phil. Mag. 11 217.

Ogawa K. & Maddin R. (1964) Acta Met. 12 713.

Ohr S.M. & Beshers D.N. (1963) Phil. Mag. 8 1343.
" " (1964) Phil. Mag. 10 219.

Opinsky A. & Smoluchowski R. (1951) J.App.Phys. 22 1488.

Osbourne P.W. (1963) Acta Met. 11 999.

Paxton H.W. (1953) Acta Met. 1 141.

Peierls R. (1940) Proc. Phys. Soc. 52 34.

Petch N.J. (1953) J ISI 174 25.

Priestner R. & Leslie W.C. (1965) Phil. Mag. 11 895.

Read T.A., Markus H. & McCaughey J.M. (1948) 'Fracturing of Metals', ASM P.228.

Reed-Hill R.E. (1964) T.AIME 230 809.

Reid C.N. (1965) Colloquium, University of Birmingham.

Rose R.M., Ferriss D.P. & Wulff J. (1962) T.AIME 224 981.

Rosenfield A.R., Averbach B.L. & Cohen M. (1963) Acta Met. 11 1100.

Rosenfield A.R. & Owen W.S. (1963) T.AIME 227 603.

Rousseau J.S. (1965) Private Communication.

Saada G. (1963) 'Electron Microscopy and Strength of Crystals', P.651, Interscience.

Schadler H.W. (1960) T.AIME 218 649.

Schadler H.W. (1961) 'Direct Observation of Lattice Defects', P.593, AIME.

Schmid E. & Boas W. (1935) 'Kristalloplastizität', Springer, Berlin.

Schoeck G. (1961) Acta Met. 9 382.

" (1965) Phys. Stat. Sol. 8 499.

Schoeck G. & Seeger (1959) Acta Met. 7 469.

Schönberg N. (1954) Acta Chem. Scand. 8 208.

Seeger A. (1956) Phil. Mag. 1 651.

Seeger A., Diehl J., Mader S. & Rebstock H. (1957) Phil.Mag. 2 323.

Seeger A. & Mader S. (1961) Phys. Stat. Sol. 1 K78.

Seeger A, Mader S. & Kronmüller H. (1963) 'Electron Microscopy and Strength of Crystals' P.665.Interscience.

Seeger A. & Schiller P. (1962) Acta Met. 10 348.

Segall R.L. (1961) Acta Met. 9 977.

Šesták B. & Libovický S. (1962) Czech. J. Phys. B12 131

" " (1963) Conference at NPL, London P158.

Sharp J.V. (1963) (1964) D. Phil thesis. Oxford.

Sharp J.V. & Makin M.J. (1964) Phil. Mag. 10 1011.

Shaw B.J. & Sargent G.A. (1964) Acta Met. 12 1225.

Simonsen E.B. (1960) Acta Met. 8 809.

Sleeswyk A.W. (1963) Phil. Mag. 8 1467.

Sleeswyk A.W., de Geus A. & Helle J.N. (1963) Acta Met. 11 337.

Sleeswyk A.W. & Helle J.N. (1961) Acta Met. 9 344.

Smith C.S. & Guttman L. (1953) T.AIME 197 81.

Smith S.W. J., Dee A.A. & Young J. (1928) Proc.Roy.Soc. A 121 477.

Steeds J.W. (1963) Conference on Electron Microscopy Cambridge.

Stein D.F. (1963) Ph.D. thesis. Rensselaer Institute.

Stein D.F. & Gorsuch P.D. (1961) Acta Met. 9 904.

Stein D.F. & Laforce R.P. (1965) J. App. Phys. 36 661.

Stein D.F. & Low J.R. (1960) J.App. Phys. 31 362.

Stein D.F., Low J.R. & Seybolt A.u. (1963) Acta Met. 11 1253.

Steijn R.P. & Brick R.M. (1954) T.ASM 46 1406.

Stiegler J.O., Du Bose C.K., Reed R.E. & McHargue C.J. (1963) Acta Met. 11 851.

Takayama T. & Koepel E.J. (1963) Phil. Mag. 8 1713.

Taylor G.I. (1934) Proc. Roy. Soc. A145 P.P. 362 & 368.

Taylor G.I. & Elam C.F. (1926) Proc. Roy.Soc. A112 337.

Tetelman A.S. (1962) Acta Met. 10 1813.

Thompson R.W. & Carlson O.N. (1964) J.L-C. Metals 7 321.

Tipper C.F. & Hall E.O. (1953) JISI 175 9.

Tsien L.C. & Chow Y.S. (1937) Proc.Roy.Soc. A169 912.

Tunstall W.J., Hirsch P.B. & Steeds J.W. (1964) Phil.Mag. 9 99.

Valdrè U. (1962) J. Sci.Inst.39 278.

Valdrè U. & Hirsch P.B. (1963) Phil. Mag. 8 237.

Van Torne L.I. & Thomas G. (1963) Acta Met 11 881.

" " " (1964) Acta Met. 12 601.

Vogel F.L. & Brick R.M. (1953) T.AIME 197 700.

Votava E. (1963) Acta Met. 11 1105.

Weissmann S., Nakayama Y. & Imura T. (1961) WADD TR-61-181

Wellings J.F. & Maddin R. 'Low Temperature Tensile Properties of Zone Refined Niobium' Univ.of Pennsylvania.

Wilcox B.A., Brisbane A.W. & Klinger R.F. (1962) T.ASM 55 179.

Wilcox B.A. & Huggins R.A. (1960) J. L-C. Metals 2 292.

Wolff U.E. (1962) T.AIME 224 327.

Worthington P.J. & Smith E. (1965) To be published.

Wronski A. & Fourdeux A. (1964) J.L-C. Metals 7 205.

Yamashita T. & Taneda Y. (1963) Jap.J.App.Phys. 2 266.

lbrecht W.M. ,Mallett M.W. and Goode W.D. (1959) J.Electrochem.Soc. 106 981

arris B. (1964) J. L-C. Met. 7 185.

ACKNOWLEDGEMENTS

The author is grateful to members of the Department for assistance during the course of this work. In particular he wishes to thank:

Dr. J.W. Christian for advice and encouragement;

Dr. J.W. Martin for supervision whilst Dr. Christian was in the U.S.A. (1962-63);

Mr. J. Lowell of the Clarendon Laboratory for the resistivity measurements;

Dr. K. Mendelssohn for loan of the Miles Hivolt E.B.U;

Mr. D.K. Bowen for loan of the computer programmes;

Mr. R. Clemons for photographic work;

The Ministry of Aviation for financial support.

List of Figure Captions

II. Twinning Shear in bcc lattice.

III1. Focussing arrangement for Mark I E.B.U.

III2 Cage focussing gun for Mark II E.B.U.

III3. Pumping system for U.H.V. annealing furnace.

III4. Circuit diagram for U.H.V. annealing furnace.

III5. Circuit diagram for oven (part U.H.V. furnace).

III6. Diagramatic section through U.H.V. furnace.

III7. Vacuum seal on electrical lead-throughs (U.H.V.furnace).

III8. Pyrometer calibration (U.H.V. furnace).

III9. Cutting jig for sawing single crystals.

III10. Rotating table for cutting jig.

III11. Tool holder arm for spark cutter.

III12. Collet tool holder for spark cutter.

III13. Acid saw, diagramatic.

III14. Grinding jig.

III15. Tensile specimen cutting jig.

III16. Anti-backlash device for mechanical testing machine.

III17. Circuit diagram for load measurement.

III18. Compression jig.

III19. Tension jig.

III20. Device for direct measurement of strain.

III21. Goniometer carrier (E.M.6).

III22. Goniometer stage E.M.6.

III23. Thermo-couple calibration (low temperatures).

III24.
III25. } Rotation of image with respect to diffraction pattern in E.M.6 microscope.

IV1. Macro photographs of specimens after deformation at room temperature. a) single glide b) double glide.

IV2. Macro photograph of specimen deformed at 77°K.

IV3. Stress distribution on specimen during deformation.

IV4. Orientations of niobium crystals.

IV5. Division of standard triangle into regions on the basis of Schmid factor for the different glide systems.

IV6. Laüe photograph homogeneous double glide.

IV7. Laüe photograph heterogeneous double glide.

IV8. Rotation of tensile axis during deformation of Nb23C.

IV9. Rotation of compression axis during deformation of Nb(F.P.)6.

IV10. Laüe photograph of Nb29.

IV11. Stereogram of deformation of Nb29.

IV12. Shear stress v. strain curve for room temperature slip on $(\bar{2}11)$.

IV13. Load-time chart showing stage I for $(\bar{2}11)$ slip.

IV14. Load-time chart showing end of compression test.

IV15. Shear stress-strain curve for room temperature double glide on $\{211\}$ planes, primary and critical, in compression.

IV16. } Slip lines on Nb19D. (see caption for fig. IV 15).
IV17. } Screw face (16) and 45° to screw face (17).

IV18. Shear stress-strain curve room temperature single glide on $(\bar{2}11)$ in tension.

IV19. Shear stress-strain curve room temperature double glide in tension on $\{211\}$ planes.

IV20. Shear stress-strain curve for room temperature single glide in compression on $(\bar{1}01)$.

IV21. } Shear stress-strain curves for room temperature 'single'
IV22. } glide in tension on $(\bar{1}01)$. (21), assuming glide on primary system only; (22), assuming double glide at the symmetry boundary.

IV23. Shear stress-strain curve for room temperature double glide in compression on primary and critical $\{110\}$ planes.

IV24. Shear stress-strain curve for room temperature single glide in compression on $(1\bar{1}2)$ plane.

IV25. Axial stress-strain curve for double glide in tension on $(1\bar{1}2)$ and $(\bar{1}01)$ planes. (room temperature).

IV26. Shear stress-strain curve for single glide in compression at 158°K on $(\bar{2}11)$.

IV27. Shear stress-strain curve for double glide in compression at 158°K on primary and critical $\{211\}$ planes.

IV28. Shear stress-strain curve for tension tests at 158°K.
IV29. Axial stress-strain curve for Nb3A, deformed at 77°K.
IV30. Axial stress-strain curve for Nb6A, deformed at 77°K.
IV31. Optical micrograph of twins in 9D (unpolished).
IV32. Optical micrograph of twins in 14A (polished).
IV33. Axial stress-strain curve Nb.2C, pre-strained at room temperature and then at 77°K.
IV34. Axial stress-strain curves for 77°K deformation showing stress drops associated with zonal glide.
IV35. Axial stress-strain curves for specimens cut from Nb28
IV36. showing the effect of temperature on the work hardening curve.
IV37. Yield stress-temperature curve for Nb28.
IV38. Flow stress-temperature curve for Nb28.
IV39. Stress-strain curves of Nb19 showing the effects of U.H.V. anneal.
IV40. Orientation of tantalum crystals.
IV41. Shear stress-strain curve of Nb56 - $(\bar{2}11)$ slip at room temperature.
IV42. Initial part of (41) with expanded strain scale and theoretical elastic line E.
IV43. } Shear stress-strain curves for Nb56 tested at 158°K.
IV44. } and theoretical elastic line E (IV44).
IV45. Axial stress-strain curve for Nb56 tested at 77°K (up to the first large 'twin drop') and theoretical line E.
IV46. Axial stress-strain curve after a large twin drop (tested at 77°K).
IV47. Stereogram for cubic lattice showing $\{111\}$ planes.
IV48. Stereogram for cubic lattice showing $(\bar{2}11)$ and $(\bar{1}01)$ planes.
IV49. Electron micrograph showing thickness fringes.
IV50. Electron micrograph showing dislocations at an angle to the foil (used for estimating foil thickness).
IV51. Dislocations running in from the edge of the foil.

IV52. a-j. Composite photograph of dislocations on the ($\bar{1}01$) plane after 9.8% deformation (γ). Section parallel ($\bar{1}01$).

IV 53 a and b. Burgers vector determination, section parallel to slip plane, ($\bar{1}01$) γ = 9.8%.

IV54. Section parallel ($\bar{1}01$), the slip plane, showing braids. made up largely of dipoles and edge dislocations.

IV55. Section parallel to slip plane, ($\bar{1}01$) after γ = 15.9%.

IV56. Area from same foil as fig. IV55 showing region with smaller proportion of dipoles.

IV57. Section parallel to ($\bar{1}01$) slip plane after a shear strain of 0.203. - cell structure.

IV58. a + b. Composite showing cell structure and density variation.

IV59. Section parallel to the slip plane ($\bar{2}11$). Shows structure at the start of stage II. (γ = 0.196).

IV60. a + b. Part of IV 59 enlarged and using different reflections for Burgers vector determination.

IV61. Sections parallel to the glide plane ($\bar{2}11$) γ = 0.196. a, b + c show same area under different reflections.

IV63. Section perpendicular to the glide directionn Primary dislocations may be giving transverse displacement contrast.

IV64. Section perpendicular to the glide directions showing black and white contrast across boundaries. (γ = 0.32).

IV65. Section perpendicular to the glide direction. Tilts across

IV66. boundaries detailed in text (P.183).

IV67. Section perpendicular to the glide direction, a, b + c taken with different reflections for B.V. and density determinations.

IV68. Section parallel to ($\bar{2}11$) plane after γ = 0.083. Double glide on ($\bar{2}11$) + (211) planes.

IV69. Typical long, narrow braid after double glide as in IV68.

IV70. Section parallel ($\bar{2}11$) (after γ = 0.083, double glide) showing braids collapsing into narrow walls.

IV71. Sections parallel ($\bar{2}11$) showing relationship between braids.

IV72. Section as IV71. Shows amalgamation of two braids, tilt across both, 10'.

IV73. Same area as IV 70, but $g = [0\bar{1}1]$. Most dislocations invisible.

IV74. Same area 72. $g = [0\bar{1}1]$. Double braid almost invisible.

IV75. Section parallel to ($\bar{2}11$) after 25% shear strain on ($\bar{2}11$) and (211). Shows well developed corridor structure.

IV76. Burgers vector determination shows that walls still made up of $[111]$ or $[\bar{1}11]$ dislocations. (Section as IV75).

IV77. a + b. Shows that only one braid is made invisible under a $[0\bar{1}1]$ reflection. Section as IV75.

IV78. Section as IV75. Tilt measured across boundary (P.186).

IV79. a + b. Increasing the shear strain from 25% to 50% results in a large increase in $[\bar{1}11]$ and $[1\bar{1}1]$ dislocations. Section as IV 75.

IV80. Section as 45° to (211). $[111]$ dislocations show glide

IV81. polyganisation. Shear strain = 0.24.

IV82. Section parallel ($0\bar{1}1$). Shear strain = 0.889, double glide ($\bar{2}11$) + (211). Typical low magn. micrograph.

IV83. Part of 82 enlarged. Rotations across boundaries A-B = 26°, A-C = 20° and B-C = 6°.

IV84. Section as 82, network probably contains $[111]$, $[1\bar{1}\bar{1}]$ and $[100]$ (invisible) dislocations

IV85. Section as 82; Moiré pattern due to a cross-grid of screw dislocations with a spacing of 61 Å.

IV86. Typical area after shear strain of 0.118 at 158°K.

IV87. Same section as 86. Burgers vector determination.

IV88. Same section as 86. Adjacent screws are of opposite sign and also very 'joggy'.

IV89. Same section as 86. Micrograph shows a dragging jog.

IV90. a + b Section parallel to the slip plane. Deformed 2% at room temperature and then at 77°K. Shows a mixture of the two types of deformation described above, Primary dislocations invisible in b.

IV91. Micrograph of a twin boundary. Adjacent areas contain a high density of dislocations.

IV92. Diffraction patterns from either side of the twin boundary shown in IV91.

IV93. Dislocation structures seen inside twins. Slip plane is {110} and probably perpendicular to the foil.

IV94. Sections cut from specimen which had twinned, showing that some areas were not deformed.

IV95. Niobium, niobium oxide plates in thin foil.

IV96. Diffraction pattern of area from 95.

V1. The solubility of nitrogen in niobium as a function of pressure and temperature.

V2. Activation enthalpy v. temperature.

V3. Activation volume v. temperature.

V4. Heat capacity and enthalpy of niobium v. temperature.

V5. Plot of stress increase v. sq. root of dislocation density.

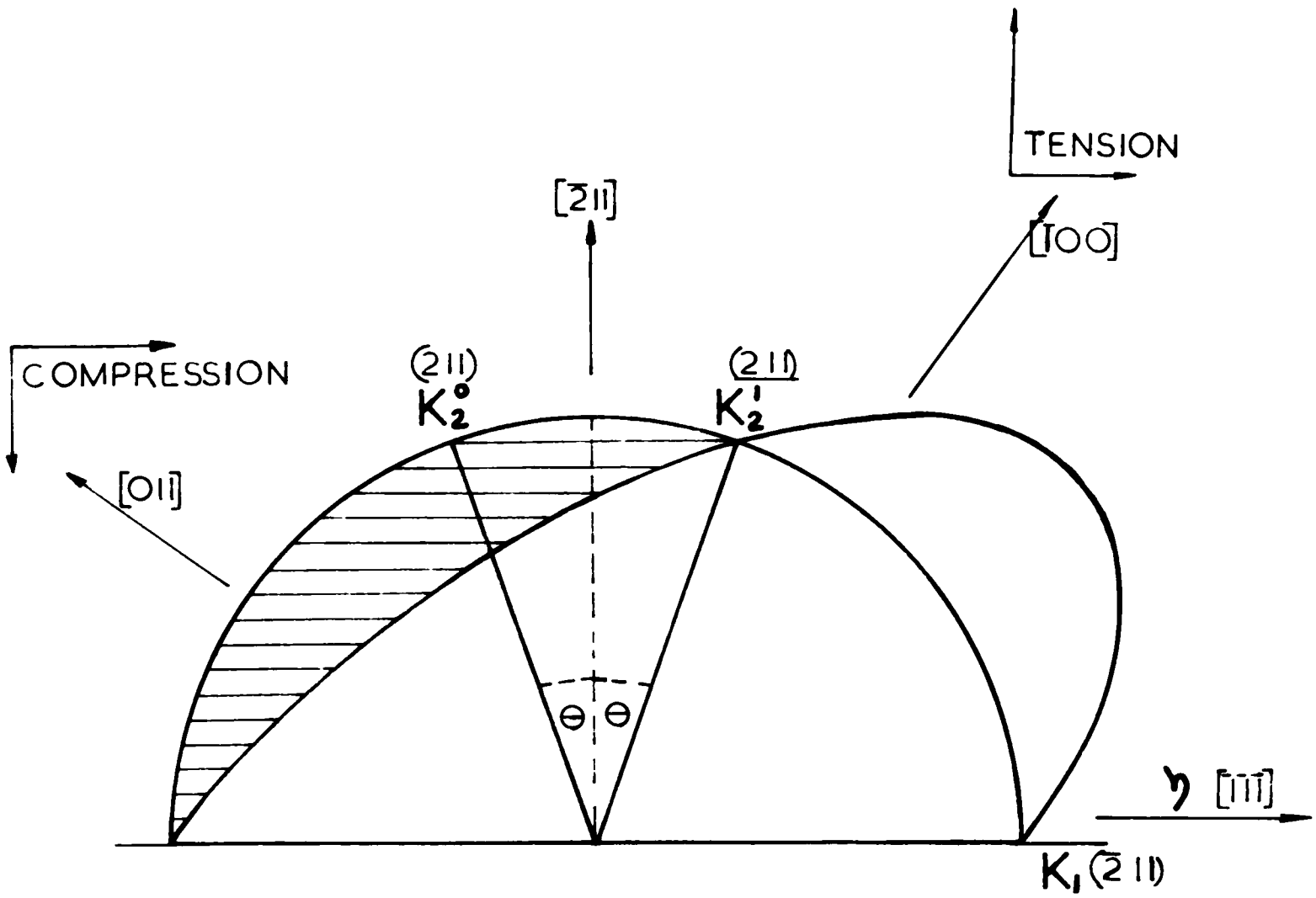


FIG.1.1.

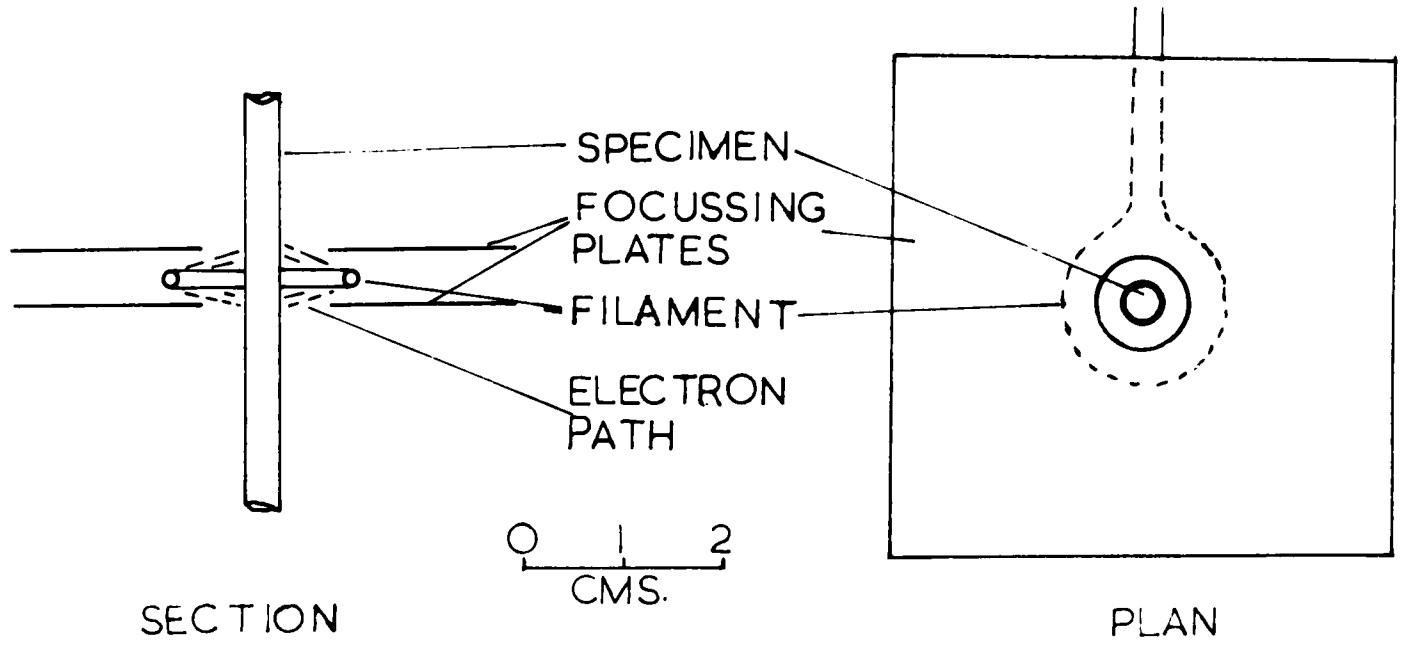
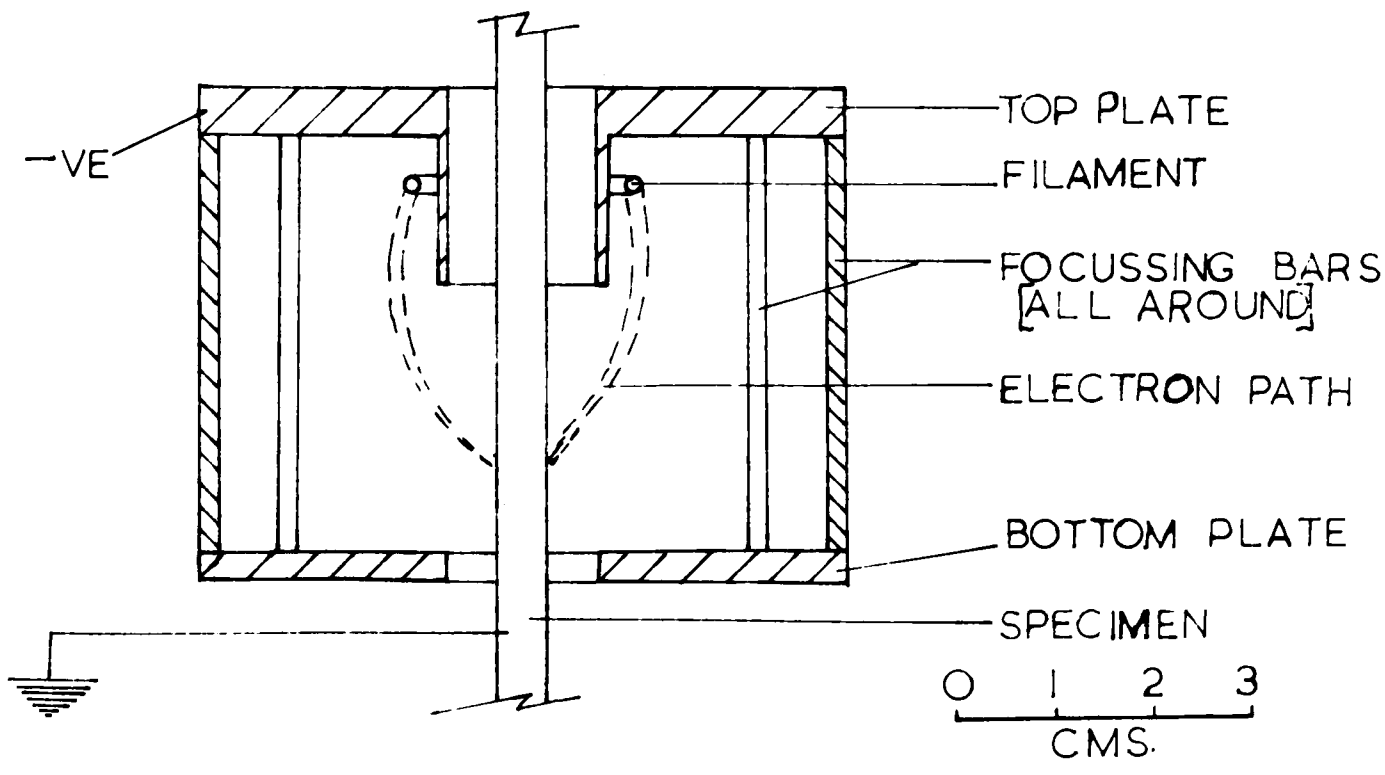


FIG. III.1.



SECTION-CAGE CATHODE

FIG. III.2.

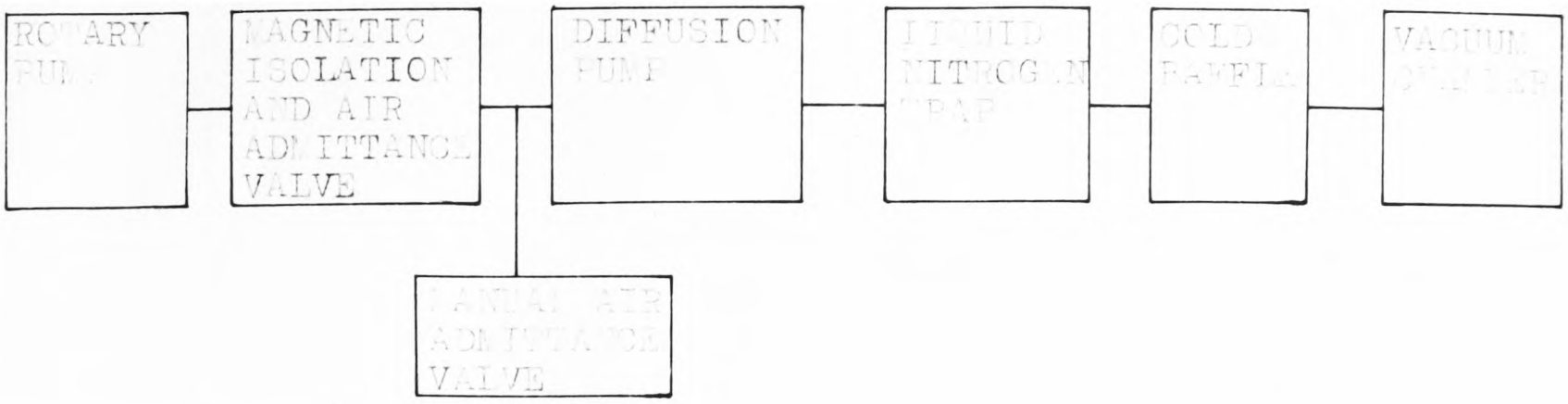


FIG.III.3.

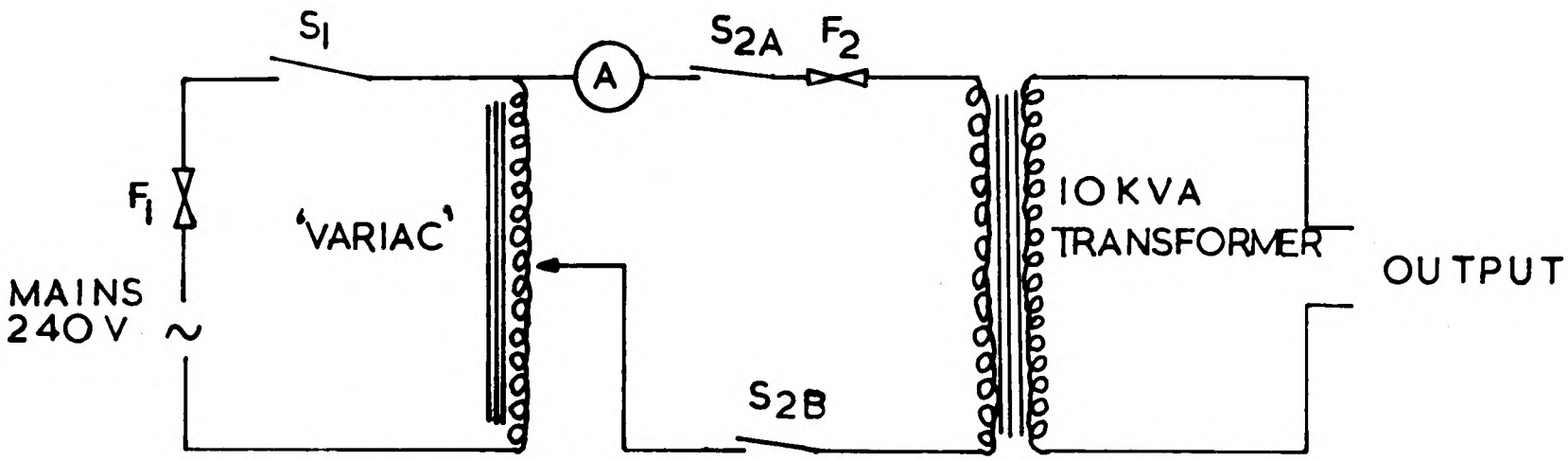


FIG.III.4.

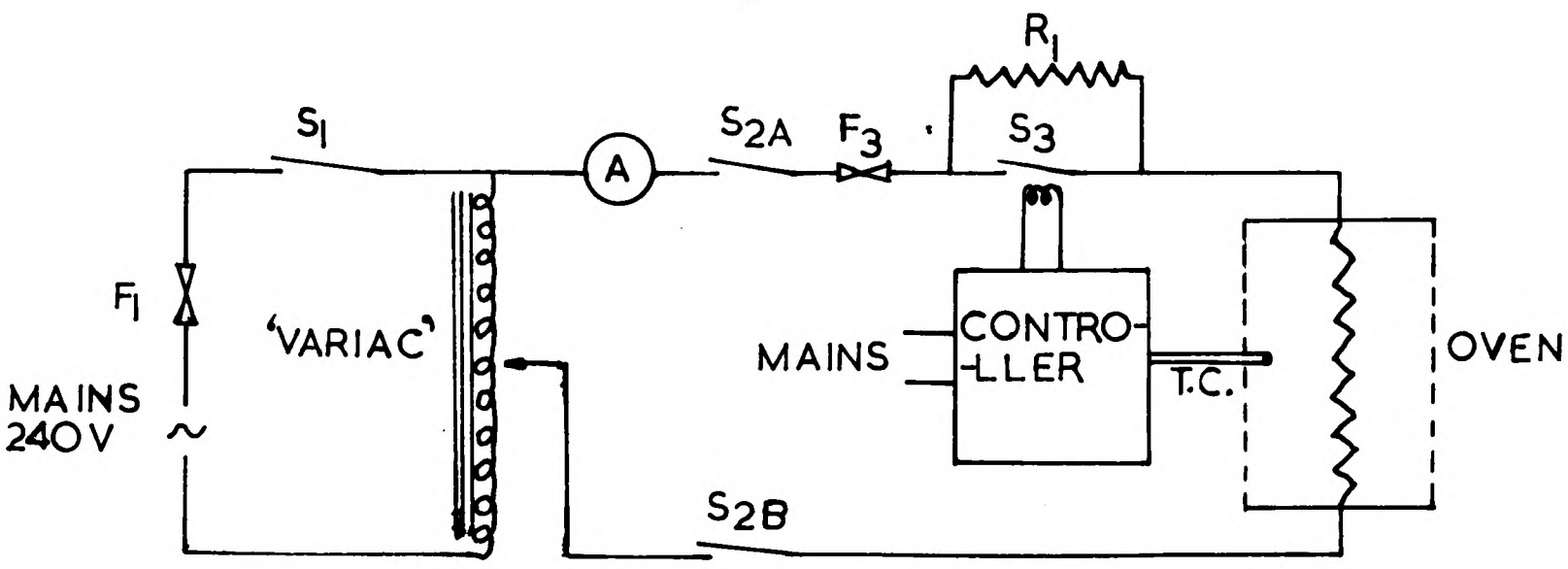
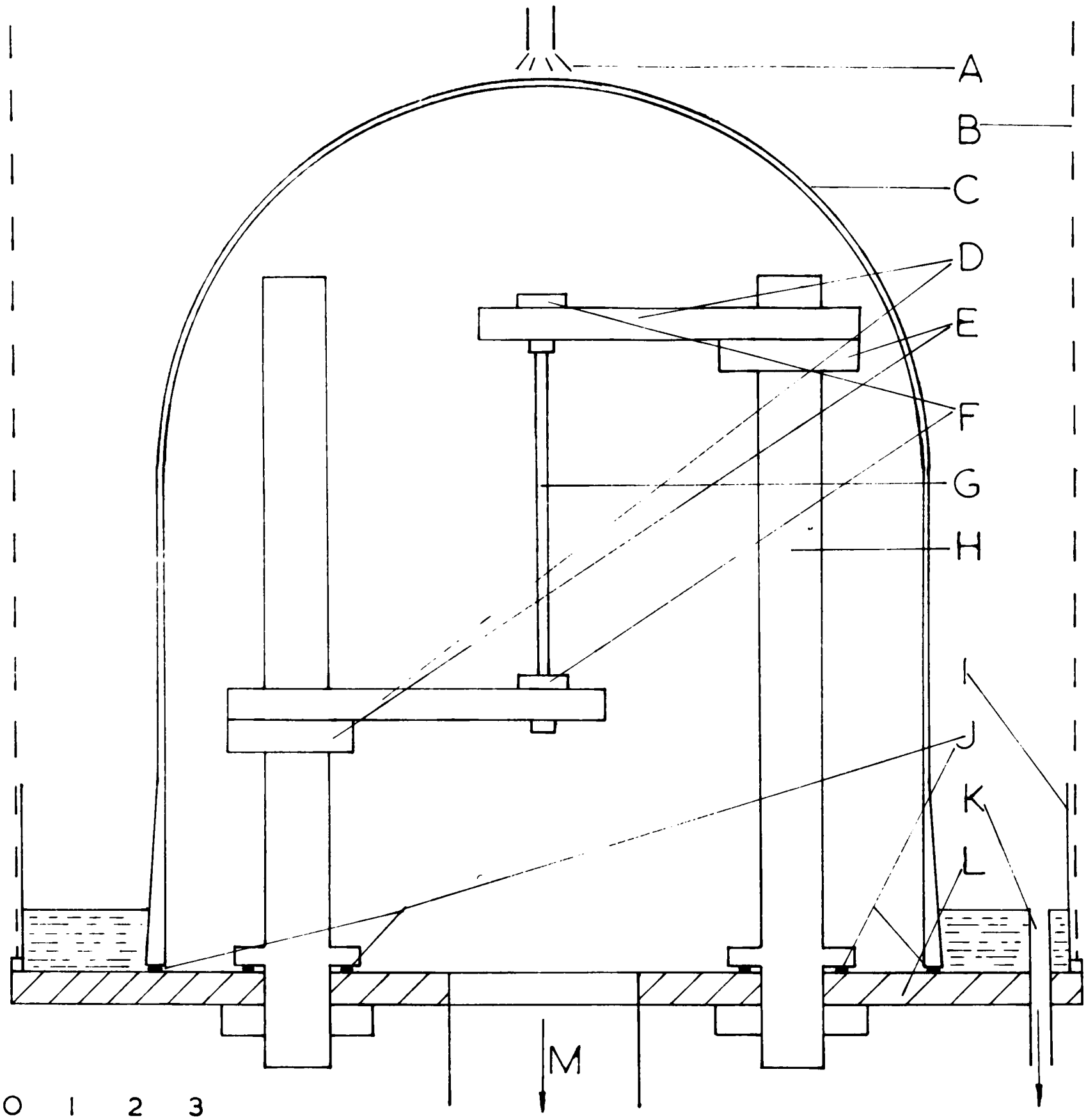


FIG.III.5.



SECTION U.H.V. FURNACE

A WATER SPRAY
B SAFETY SCREEN
C GLASS BELL JAR
D CROSS-ARMS
E COLLARS
F CHUCKS
G SPECIMEN
H ELECTRICAL LEAD-THROUGH
I DETACHABLE WALLS
J VITON 'O' RINGS
K WATER OUTLET
L BASE PLATE
M TO PUMPS

FIG. III.6.

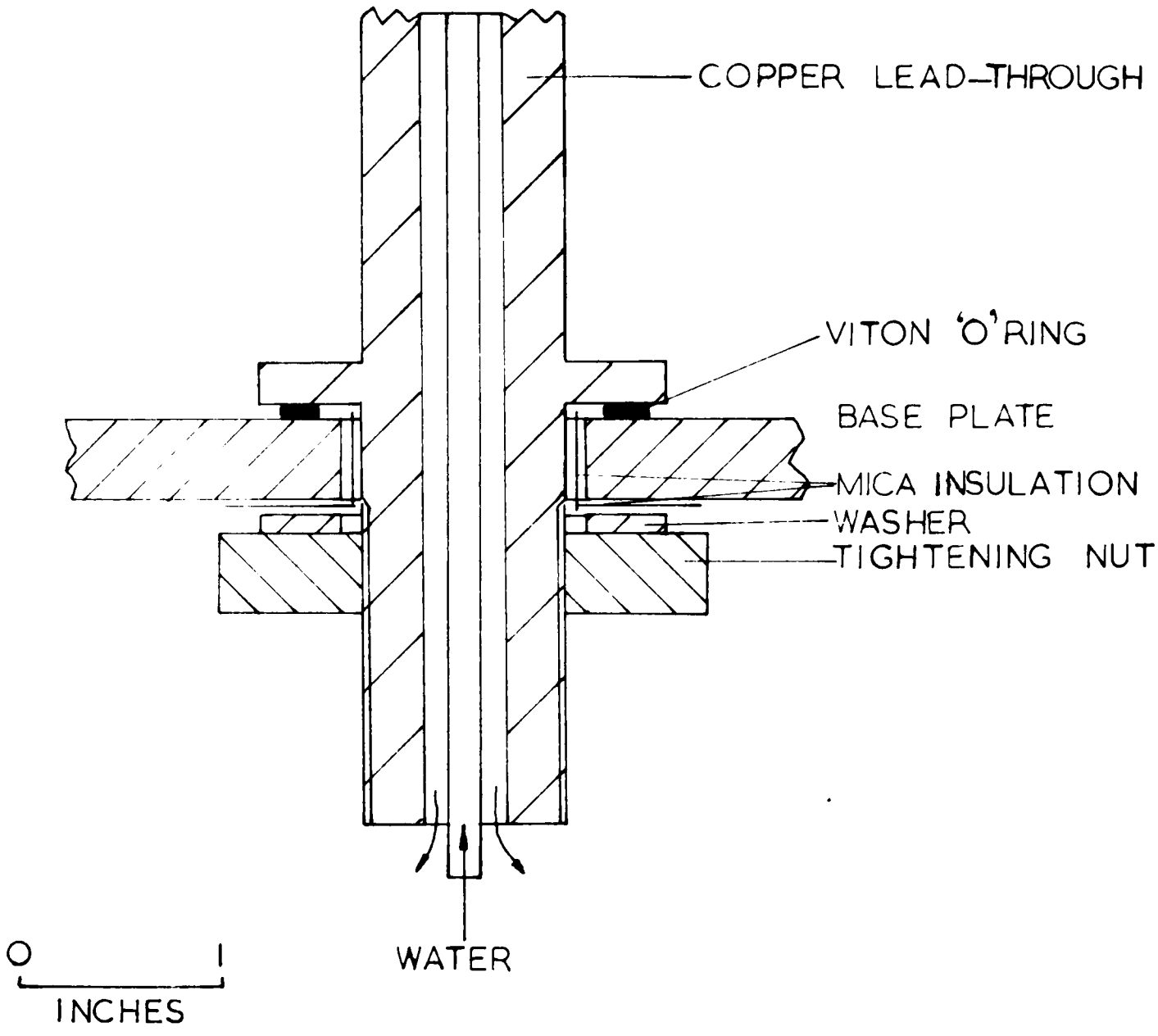

COPPER LEAD-THROUGH
VITON 'O' RING
BASE PLATE
MICA INSULATION
WASHER
TIGHTENING NUT
WATER
0
1
INCHES

FIG. III. 7.

TEMPERATURE CALIBRATION FOR U.H.V. FURNACE

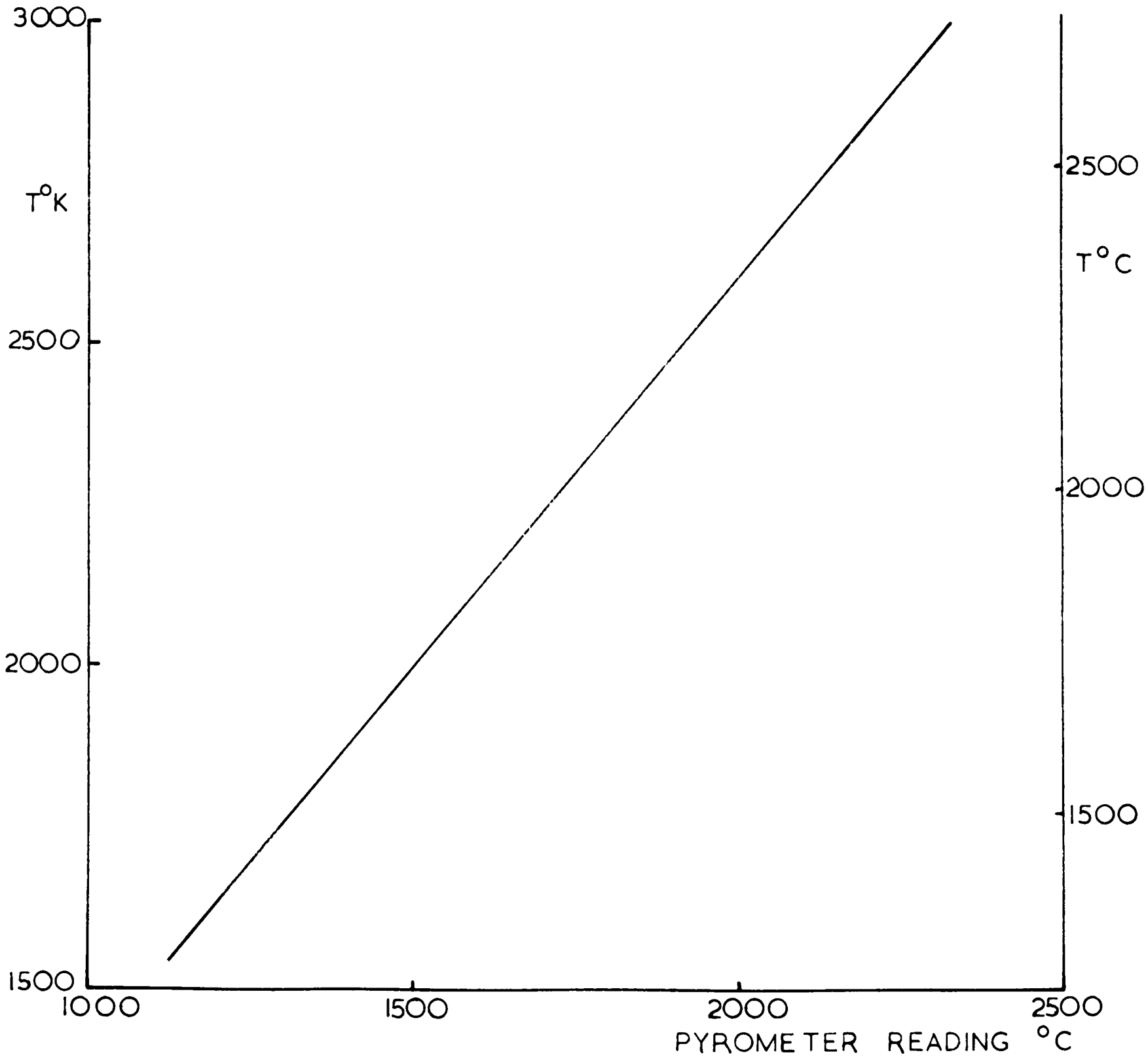


FIG.III.8.

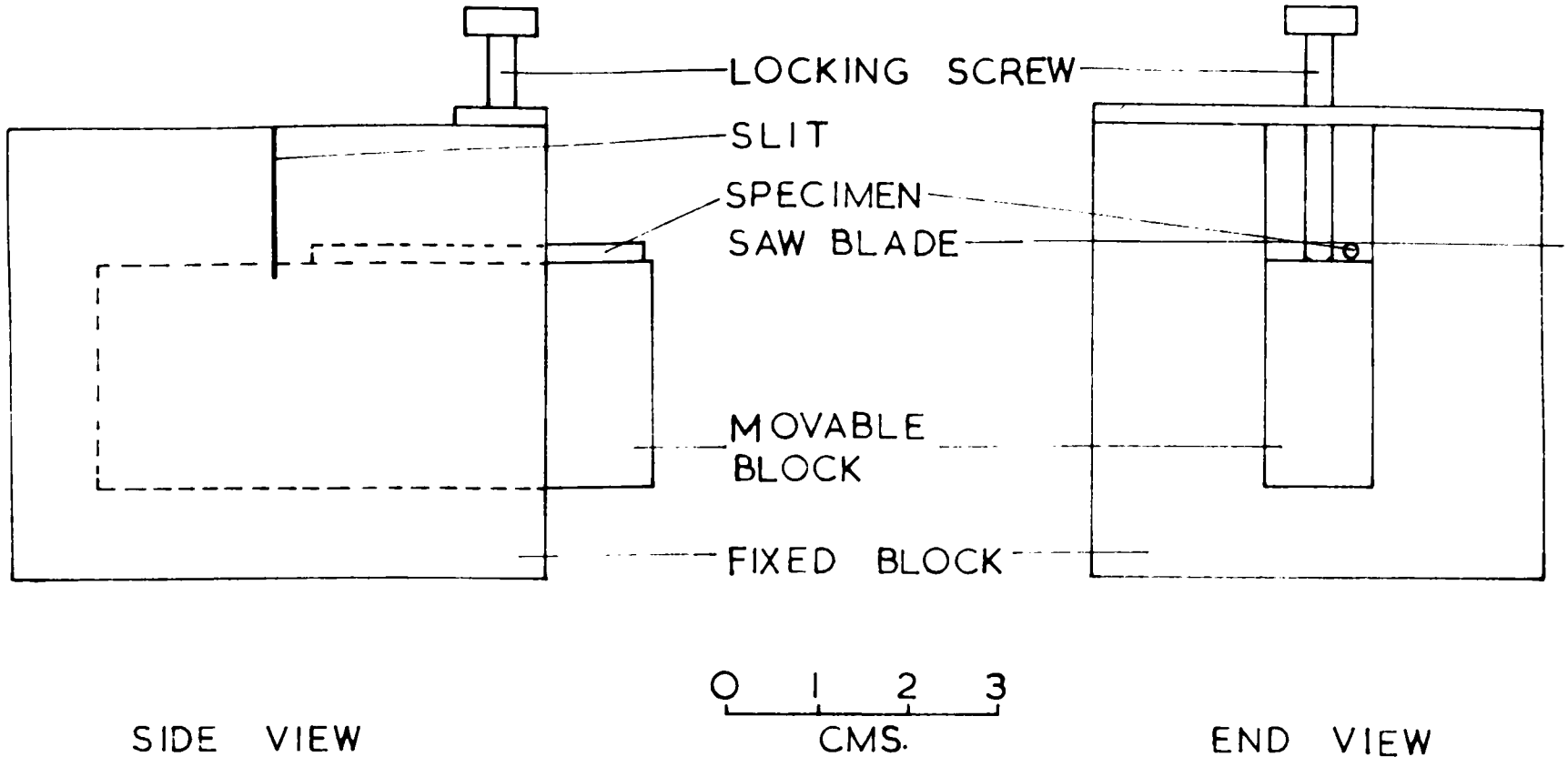


FIG. III.9.

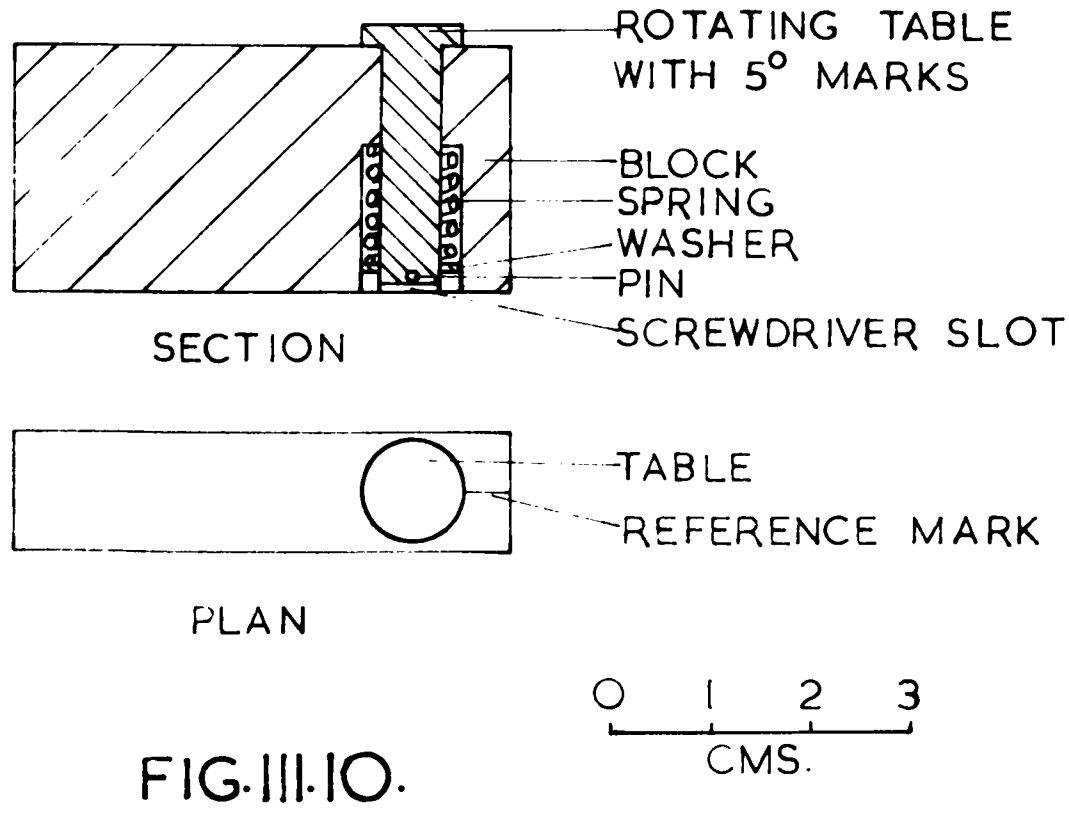
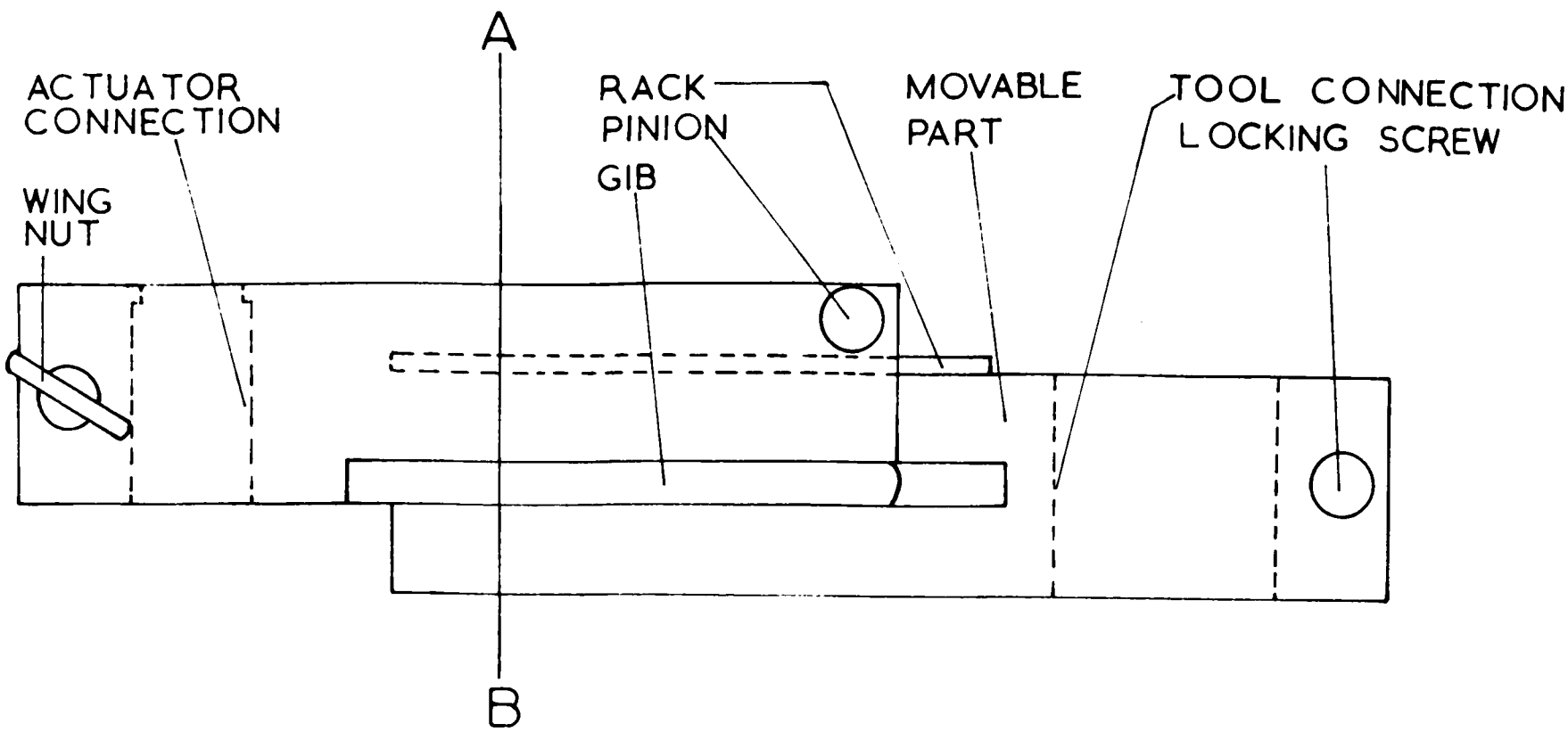
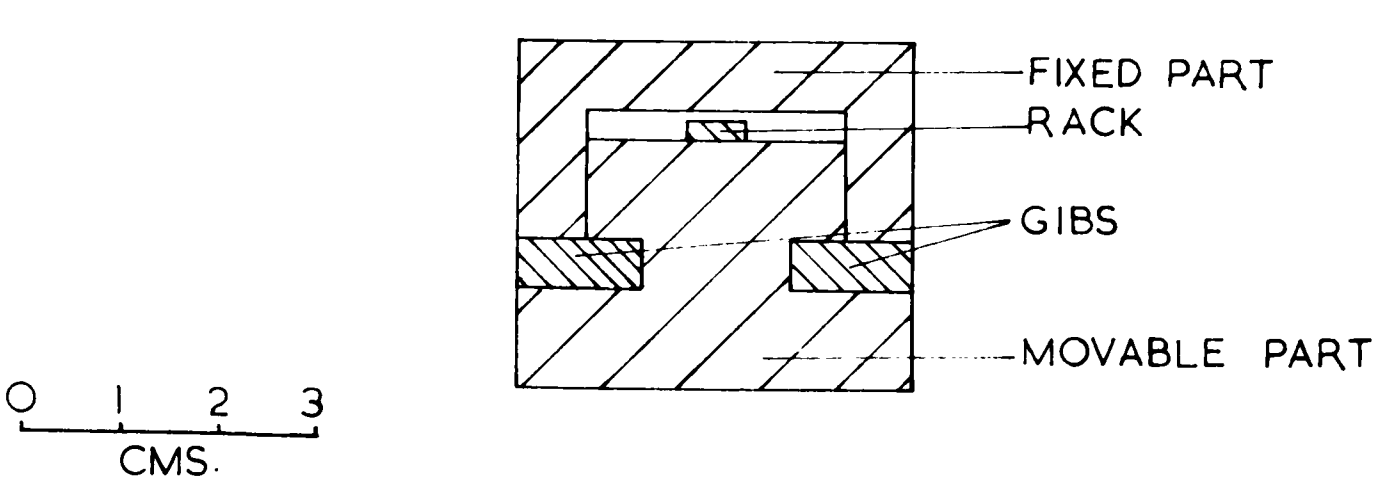


FIG. III.10.

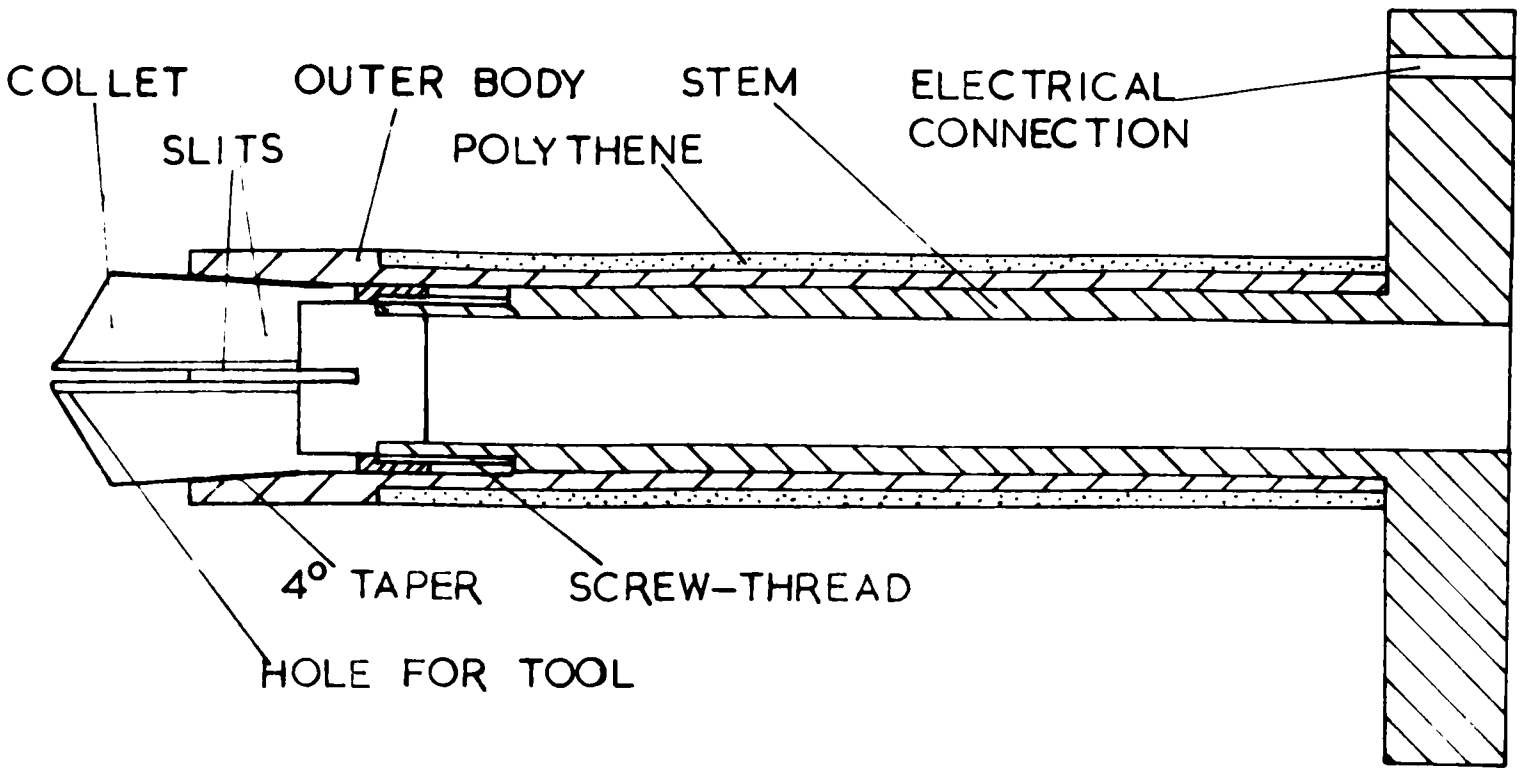


SIDE VIEW

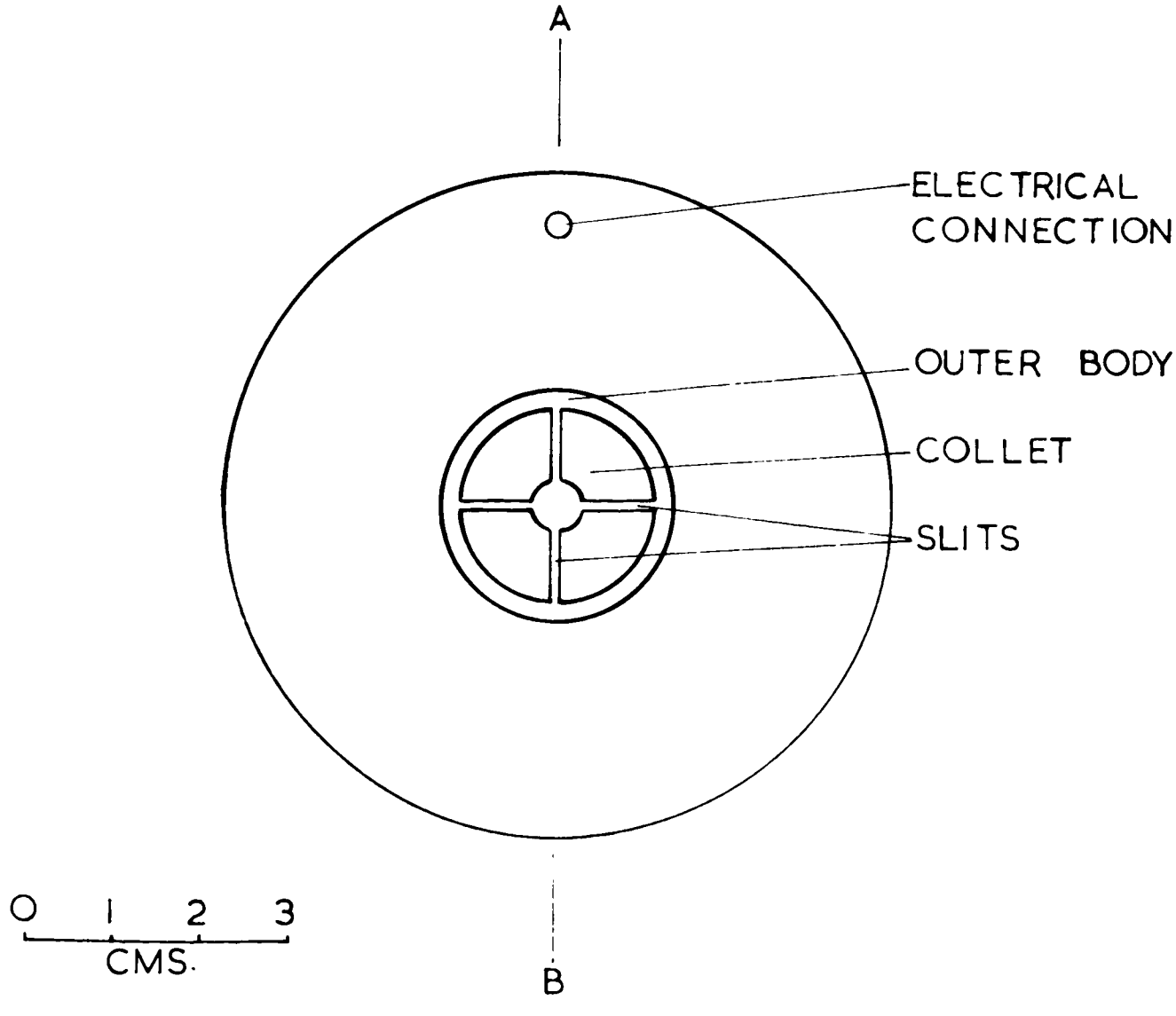


SECTION A-B

FIG. III.II.



SECTION A–B



END VIEW

FIG. III·12.

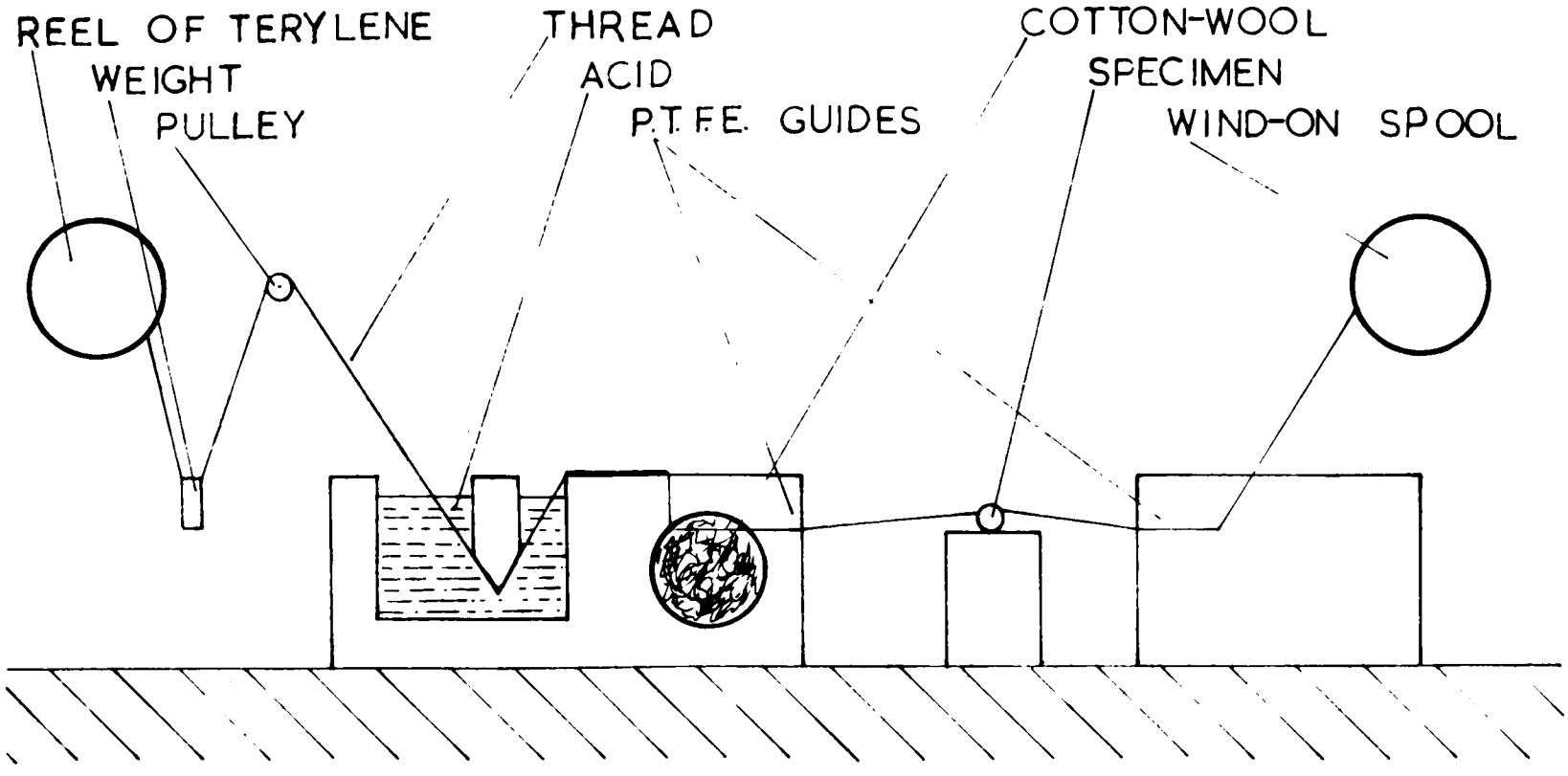
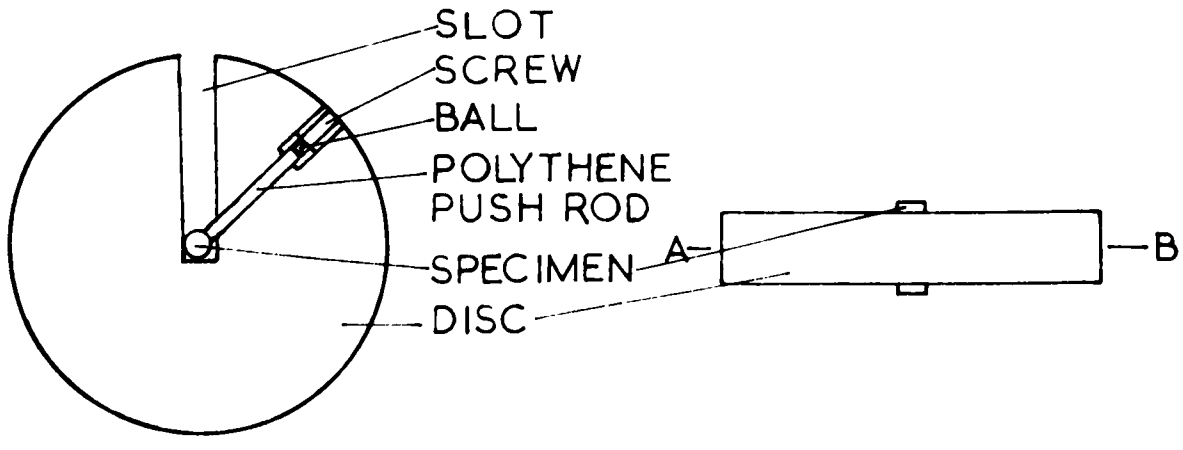


FIG.III.13.



SECTION A–B PLAN

FIG.III.14.

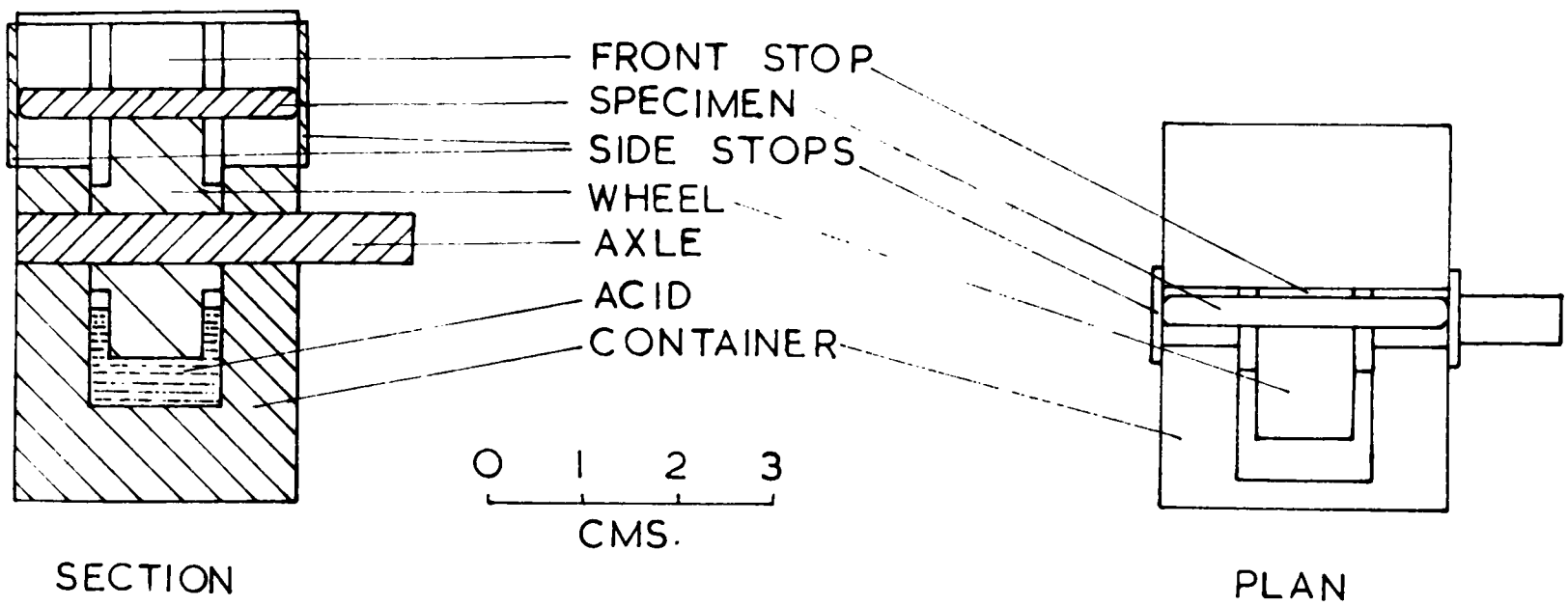


FIG.III.15.

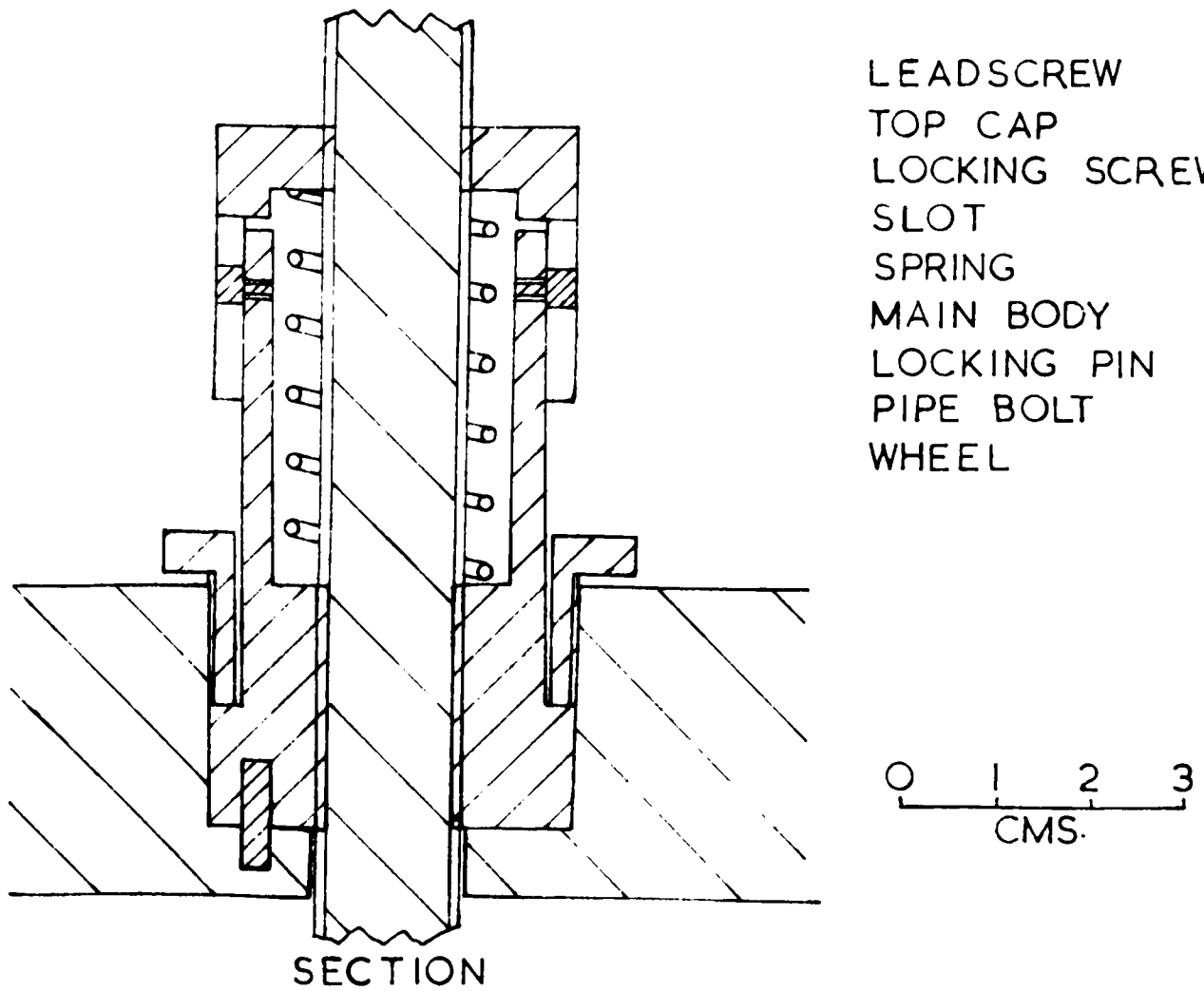


FIG.III.16.

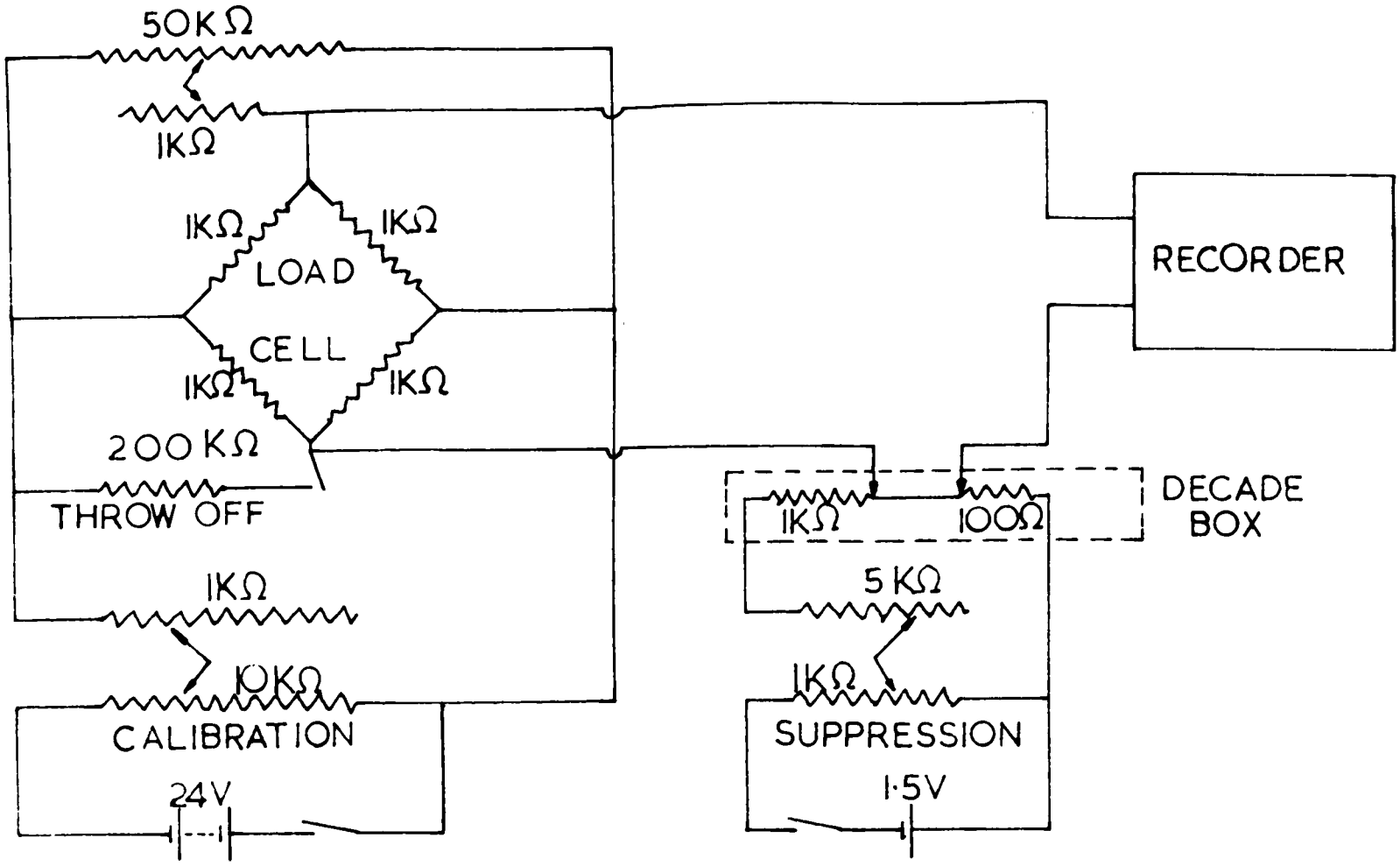


FIG.III.17.

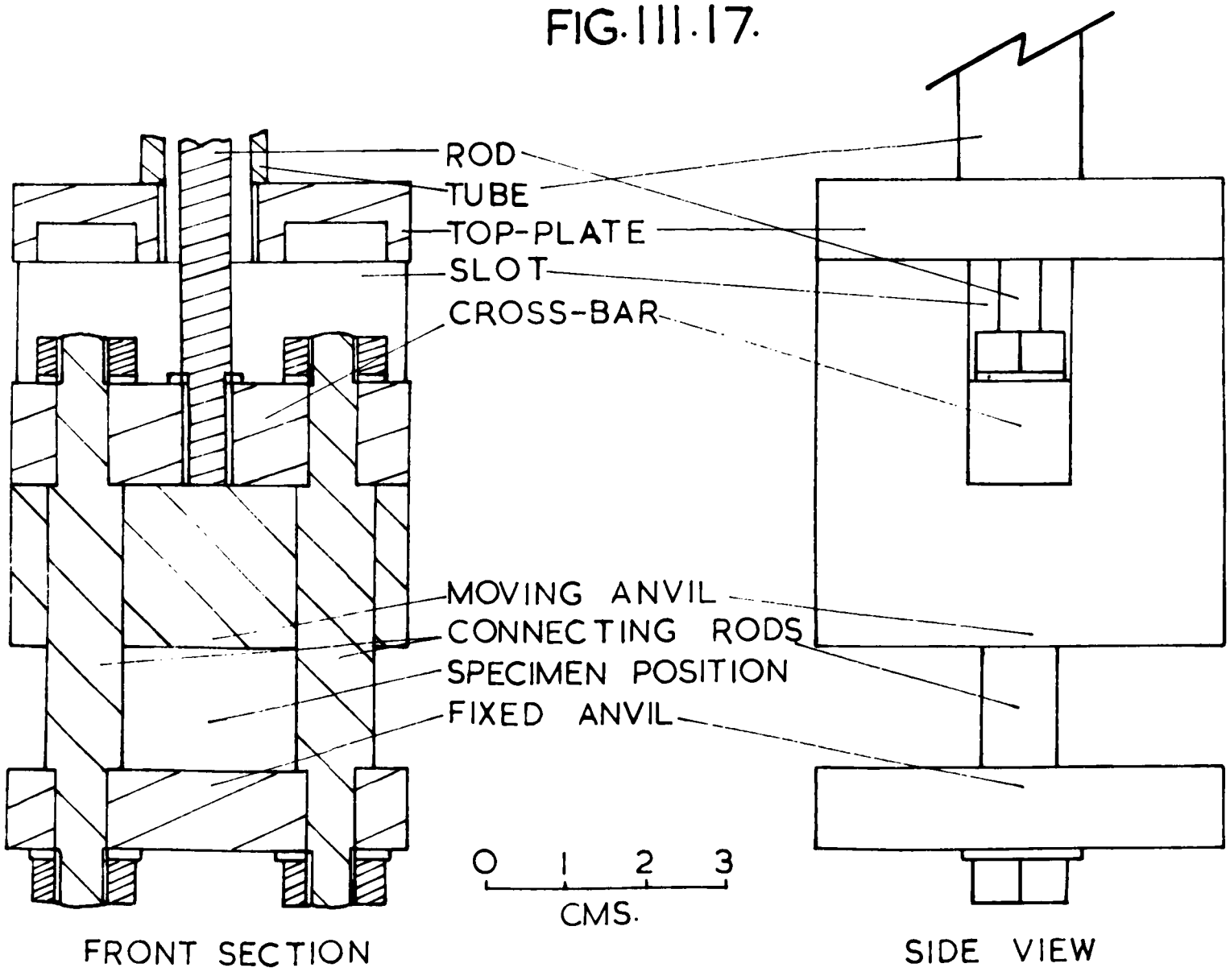
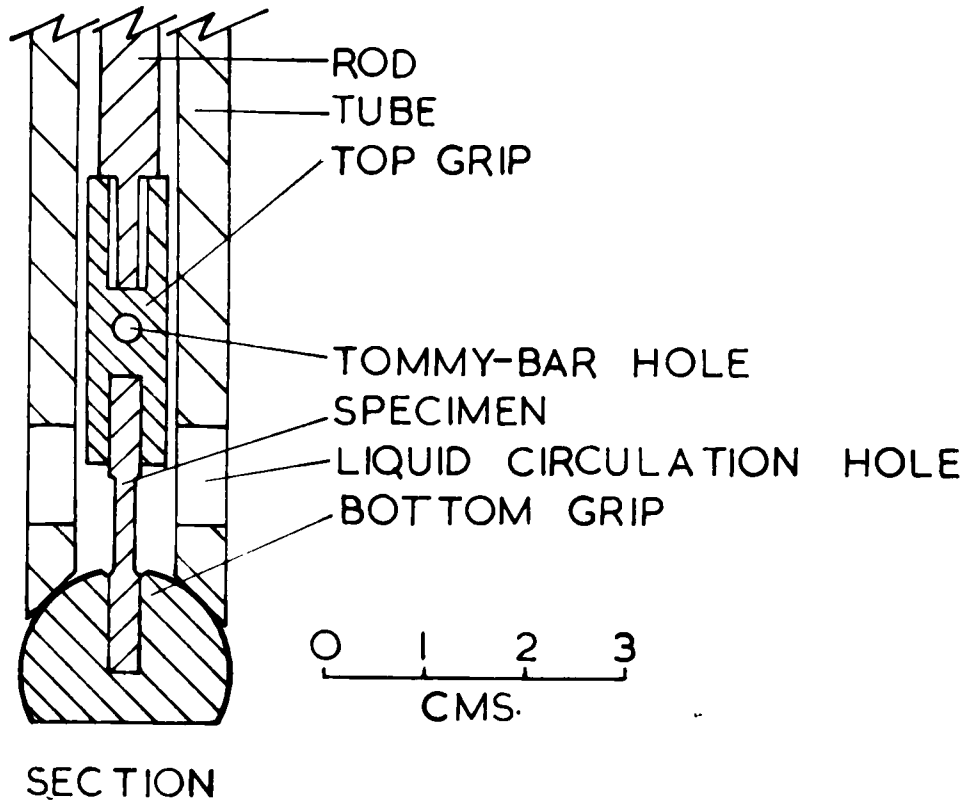
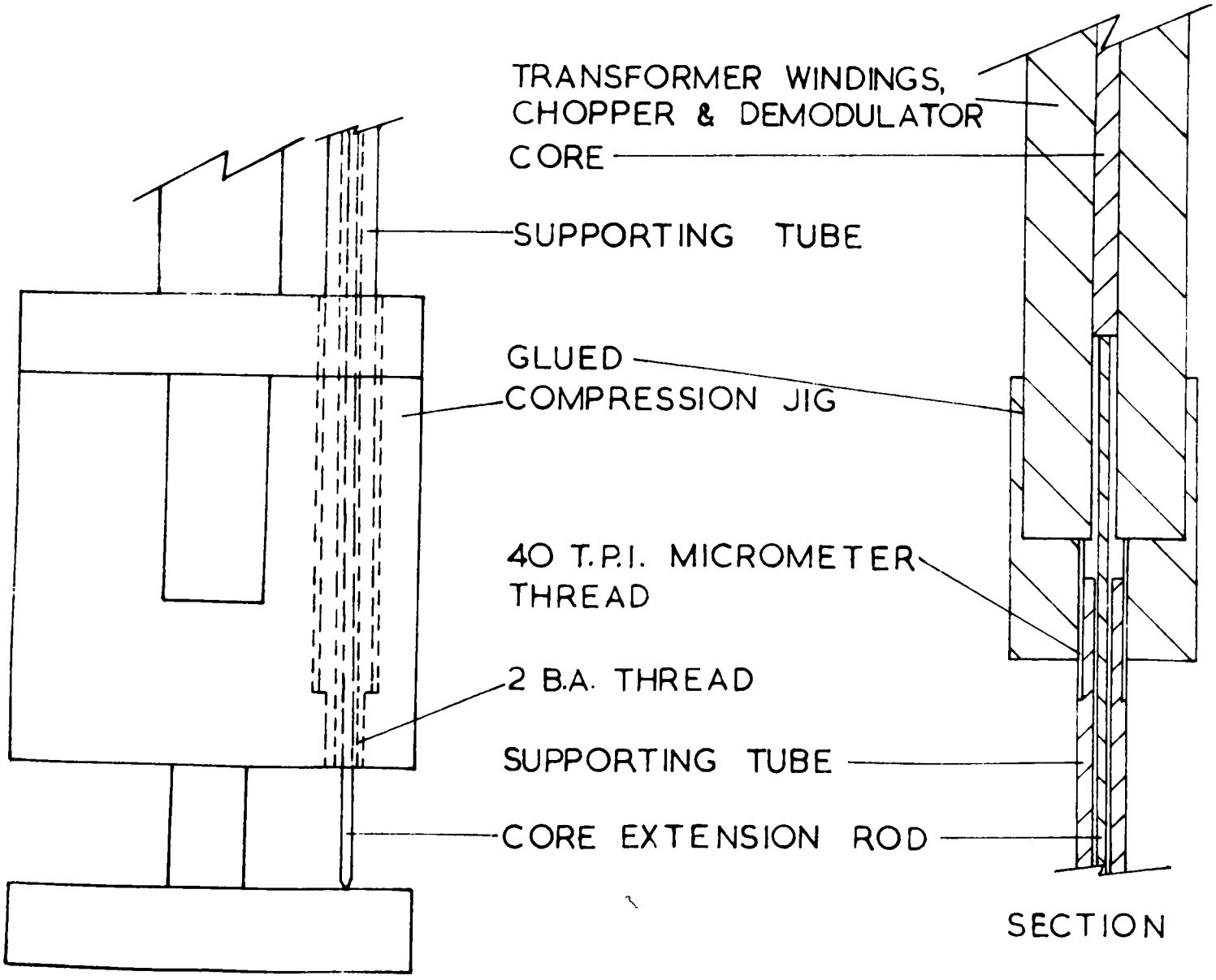


FIG.III.18.



SECTION

FIG.III.19.

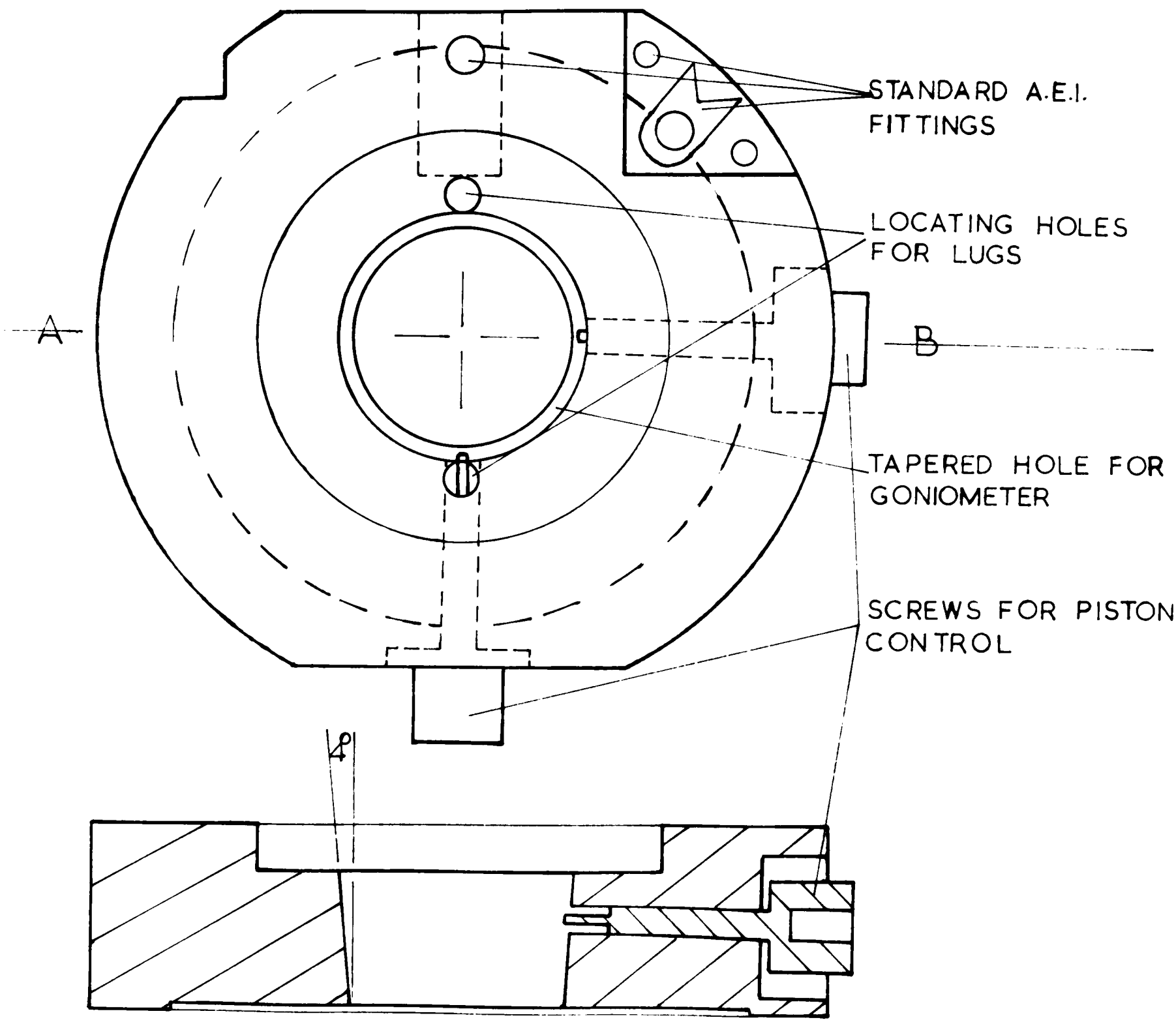


SECTION

FIG.III.20.

GONIOMETER CARRIER

PLAN

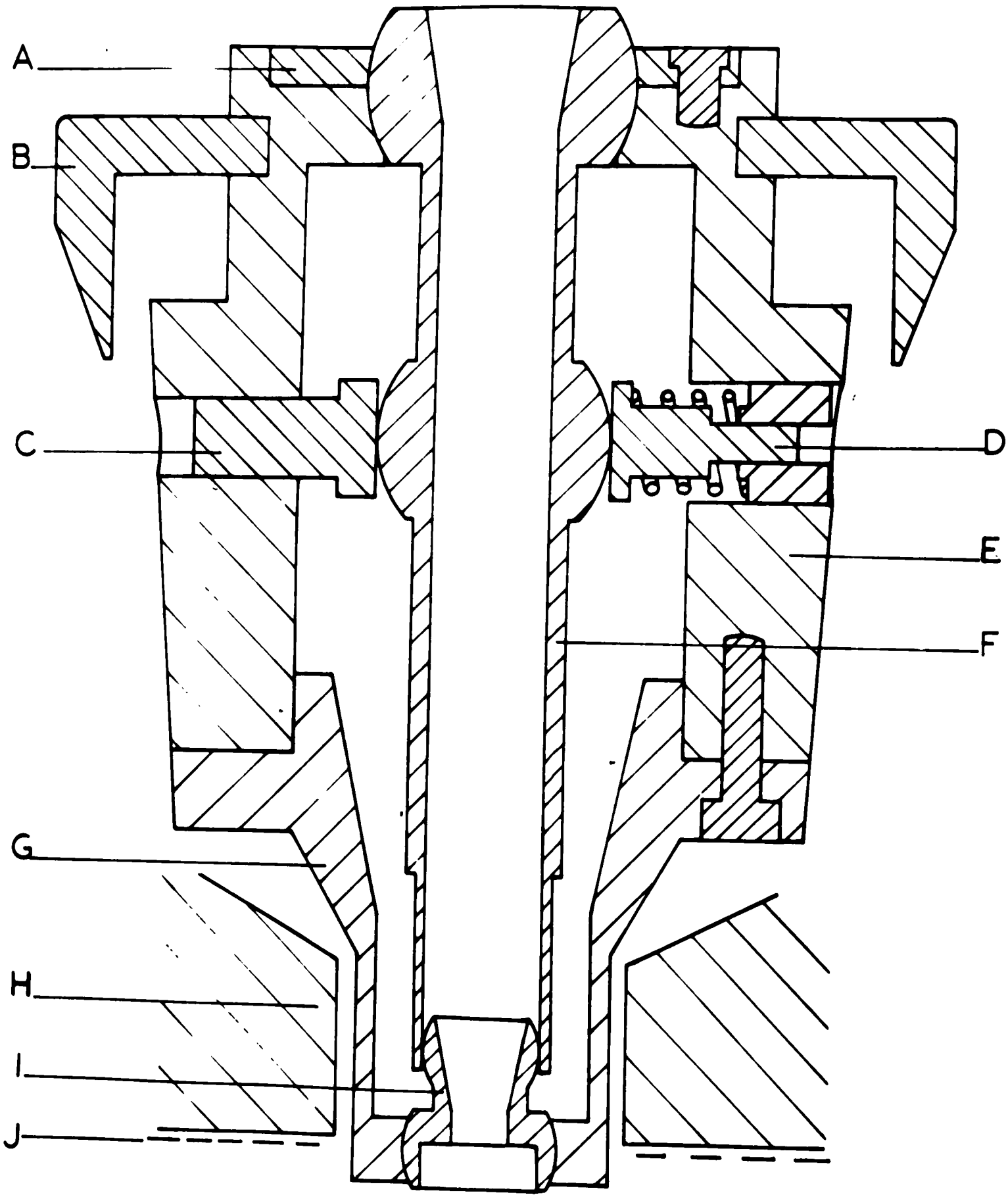


SECTION A-B

0 0·5 1·0
INCHES

FIG·III·21·

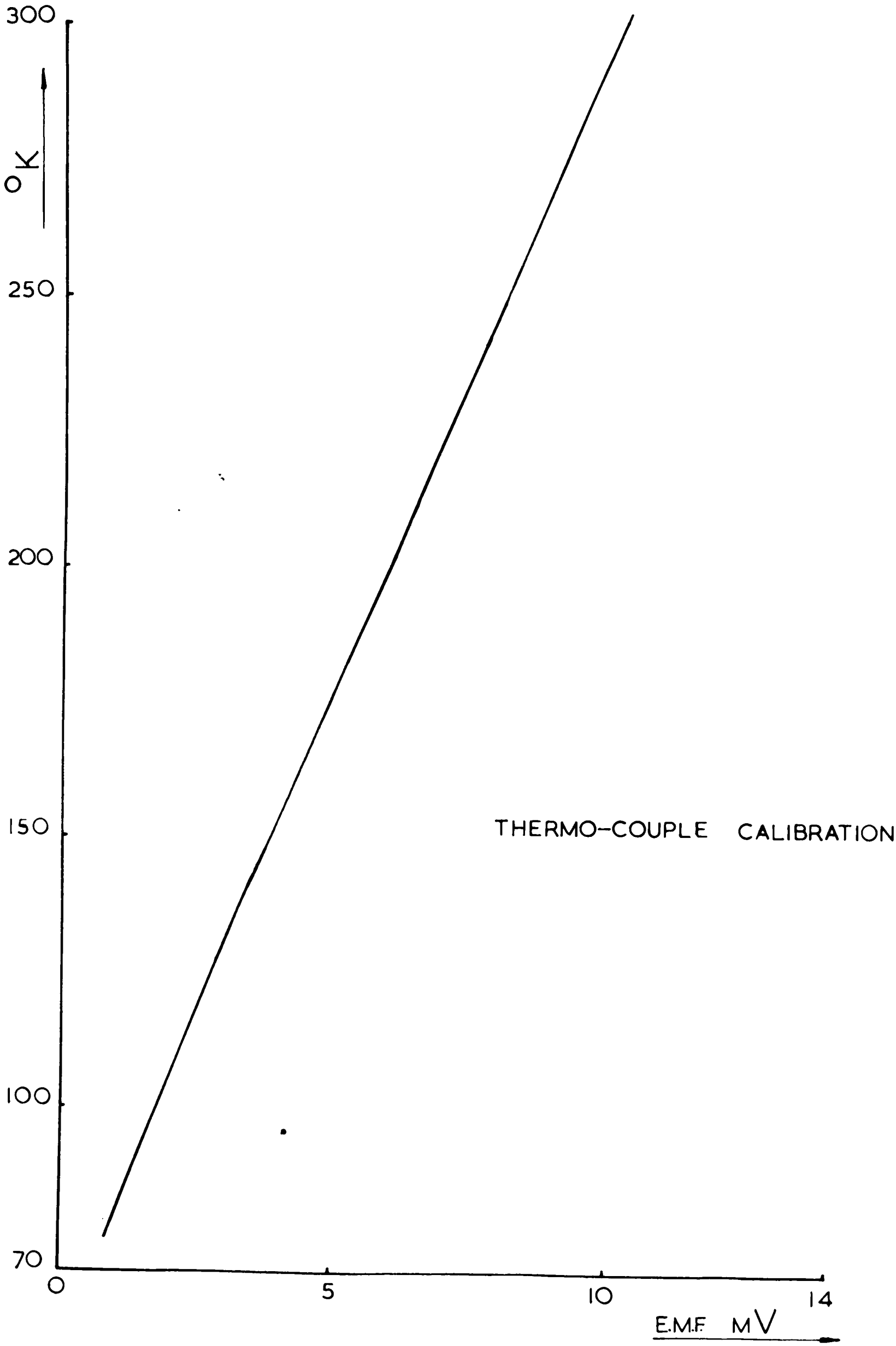
GONIOMETER STAGE E.M. 6.



0 1 2 3
MM.

SECTION

A TOP PLATE
B LUG
C PISTON
D SPRING LOADED PISTON
E MAIN BODY 4° TAPER SEMI-ANGLE
F TUBULAR LEVER
G LOWER BODY
H POLE PIECE OF OBJECTIVE LENS
I TILTING HEAD
J PLANE OF SPECIMEN


300
°K
250
200
150
100
70
0
5
10
14
E.M.F mV
THERMO-COUPLE CALIBRATION

FIG·III·23·

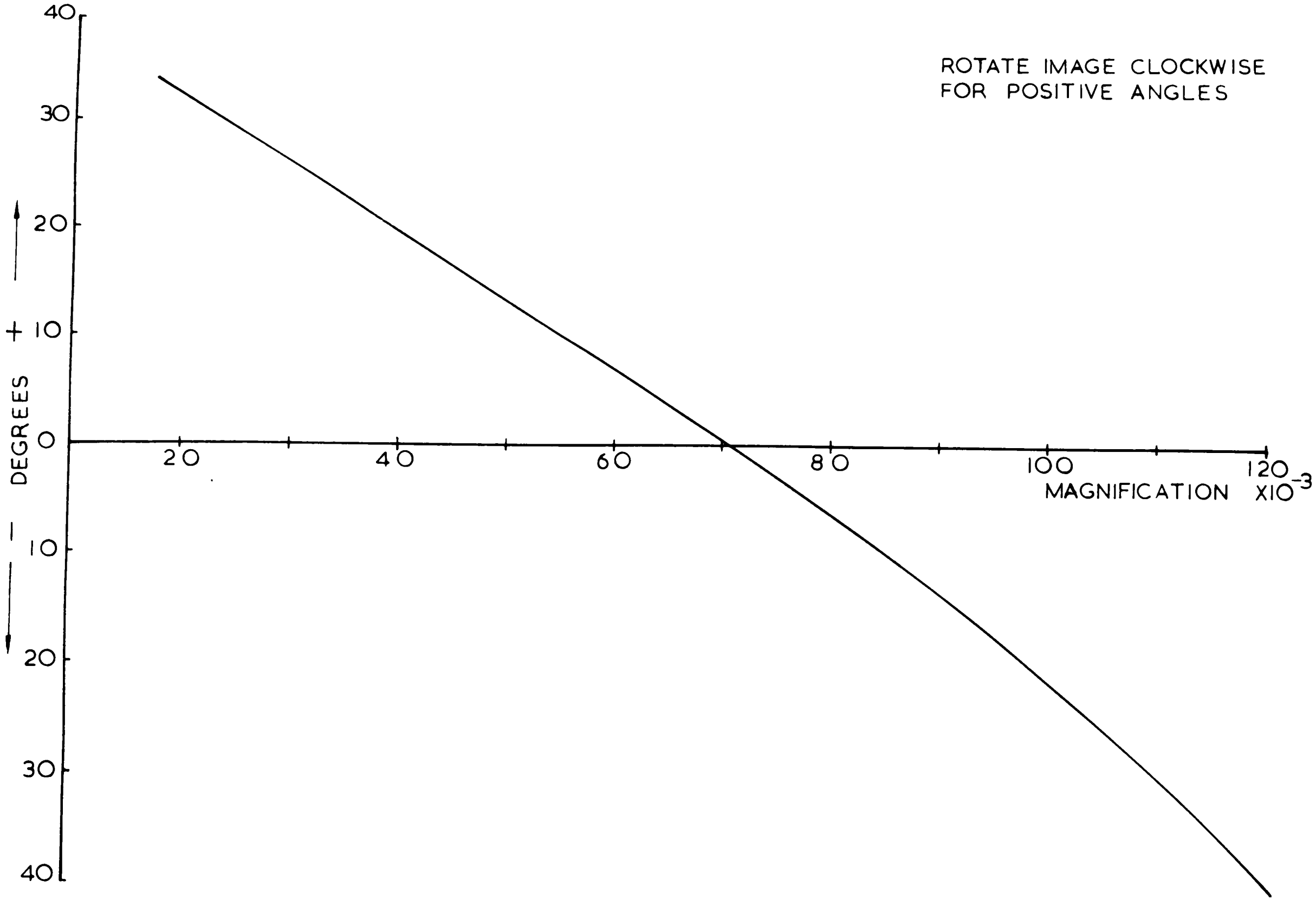

ROTATE IMAGE CLOCKWISE
FOR POSITIVE ANGLES
40
30
20
+ 10
0
10
20
30
40
DEGREES
20
40
60
80
100
120
MAGNIFICATION X10⁻³

FIG. III.24.

ROTATE IMAGE CLOCKWISE

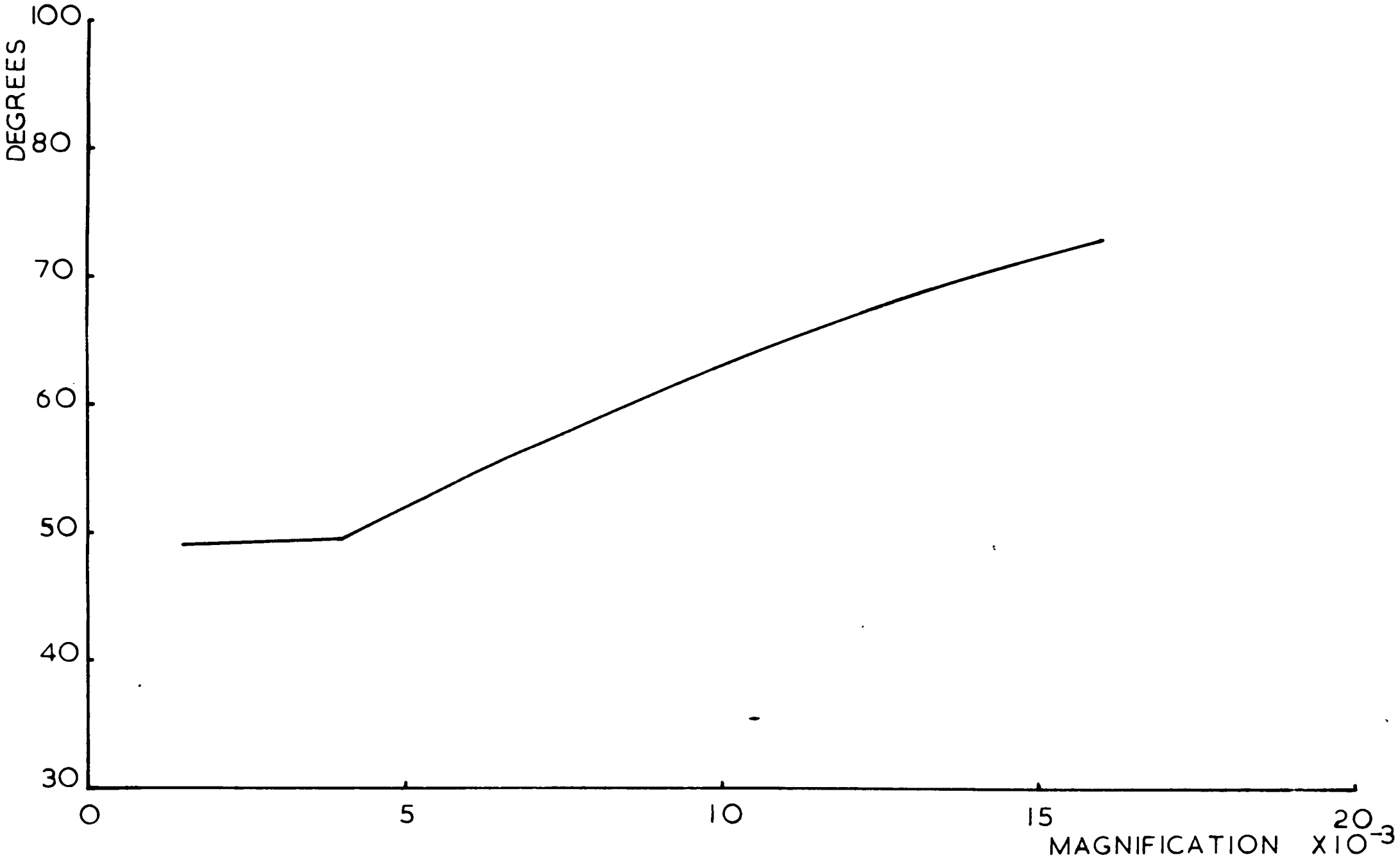


FIG. III.25.

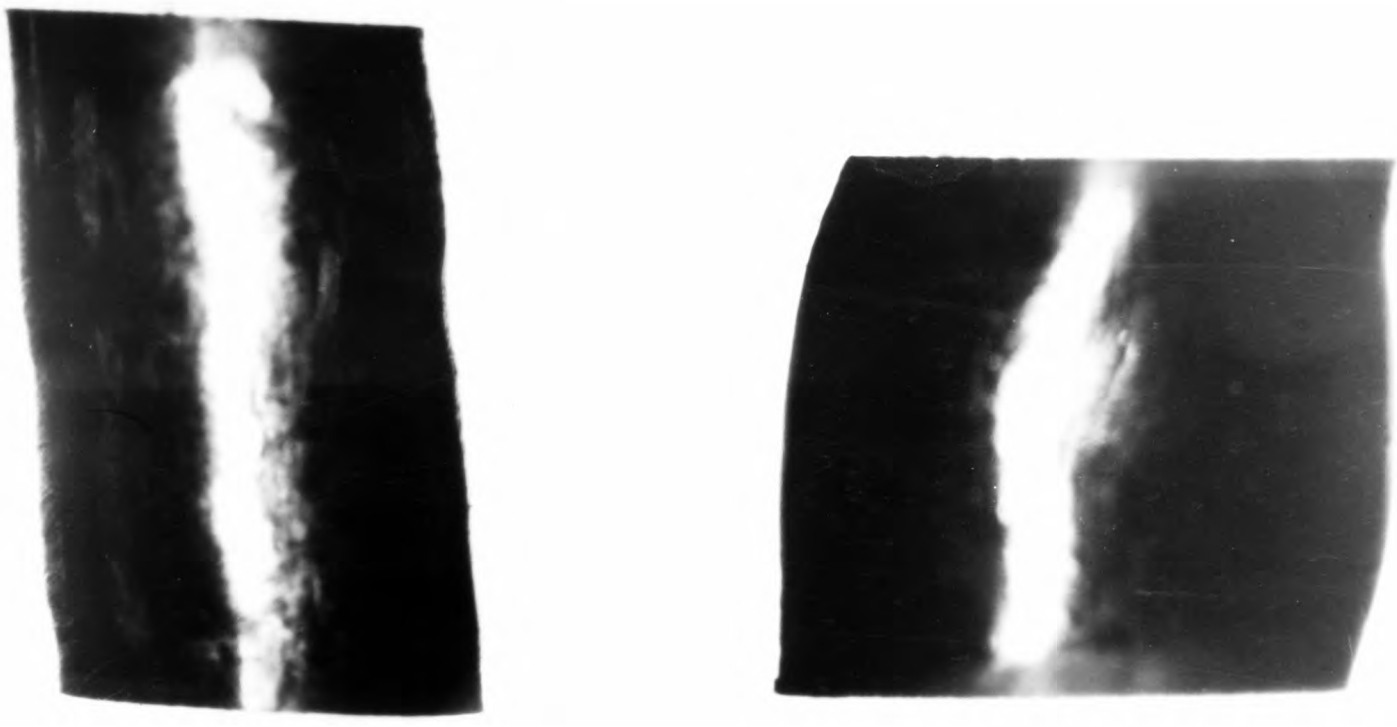
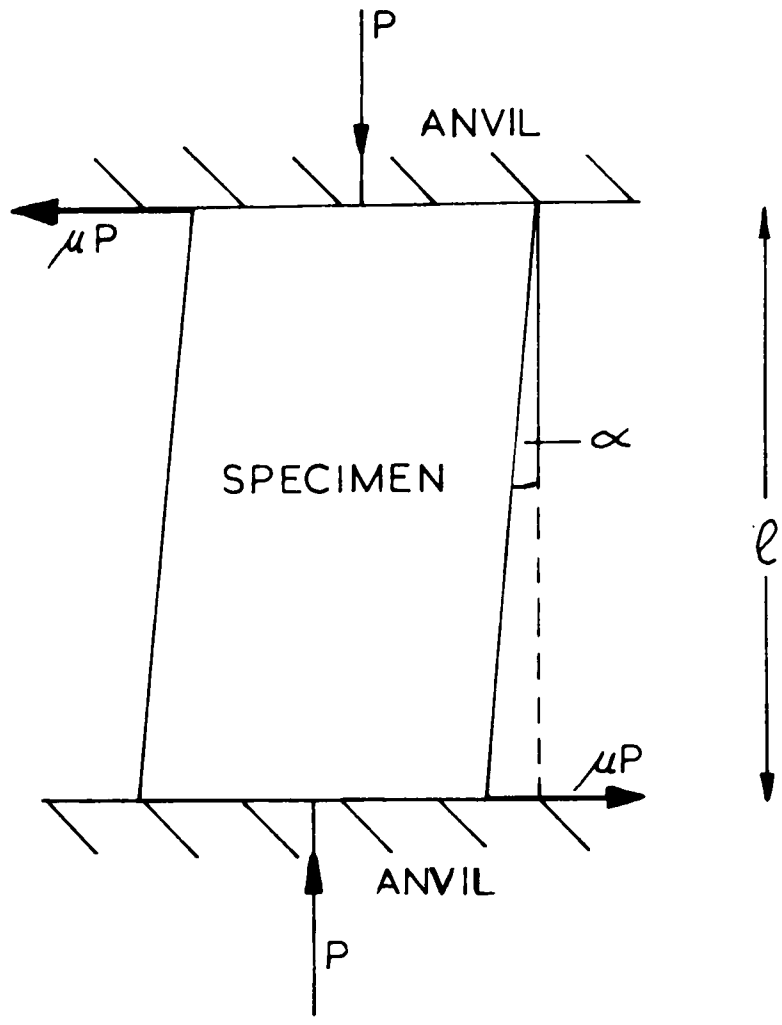


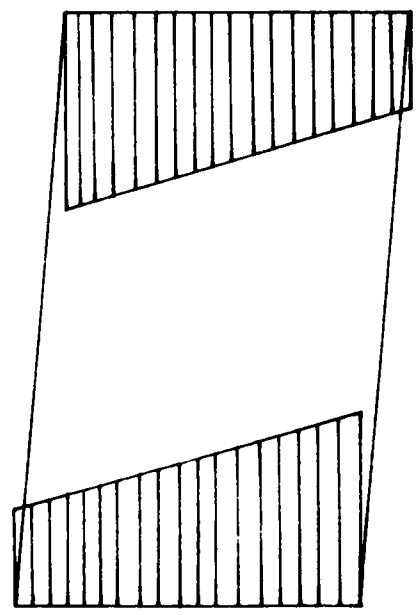
FIG. IV 1



FIG. IV 2



(a)



(b)

STRESS DISTRIBUTION ON SPECIMEN ENDS
FOR TAN $\alpha > \mu$

FIG.IV: 3

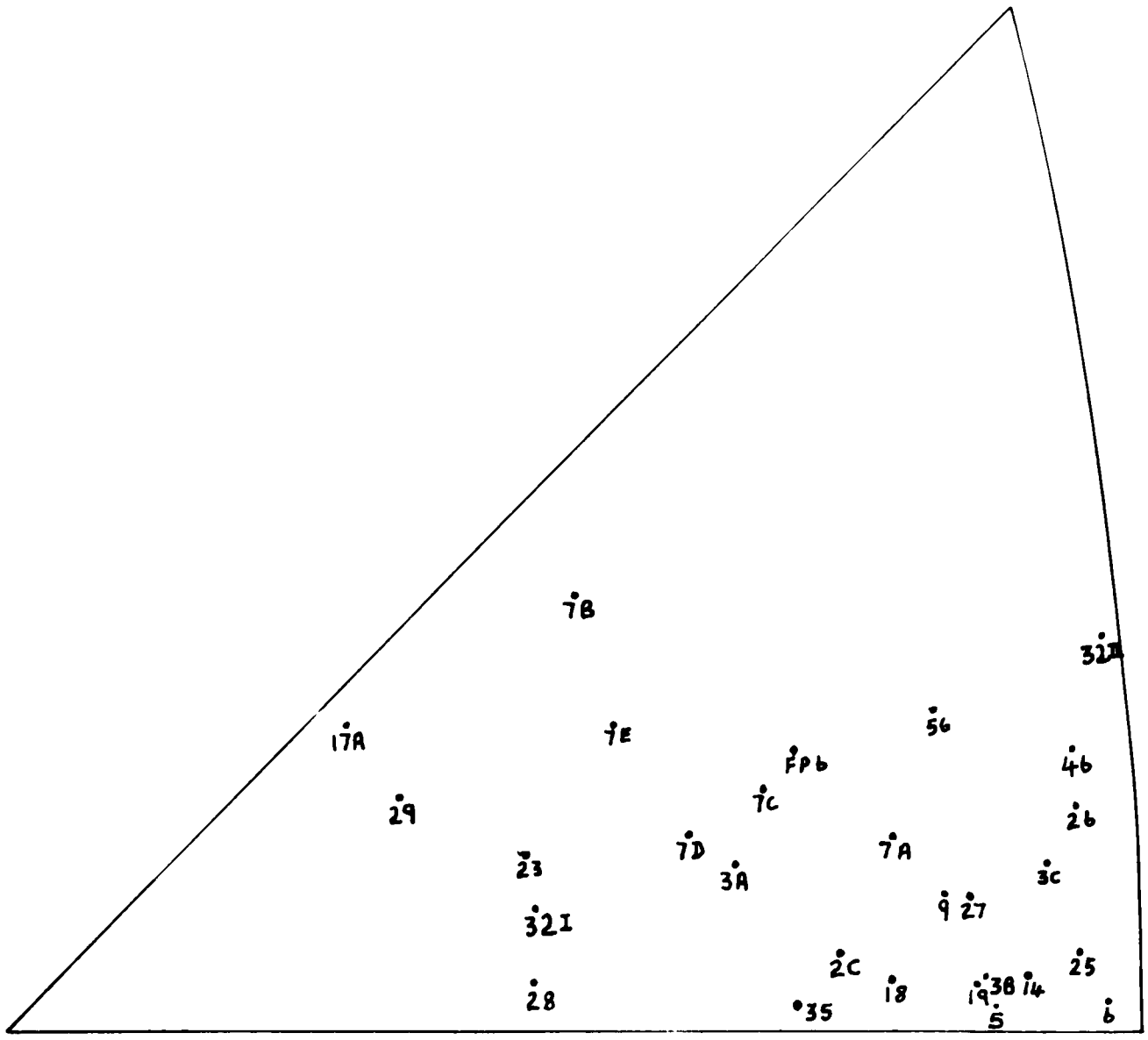


FIG. IV. 4.

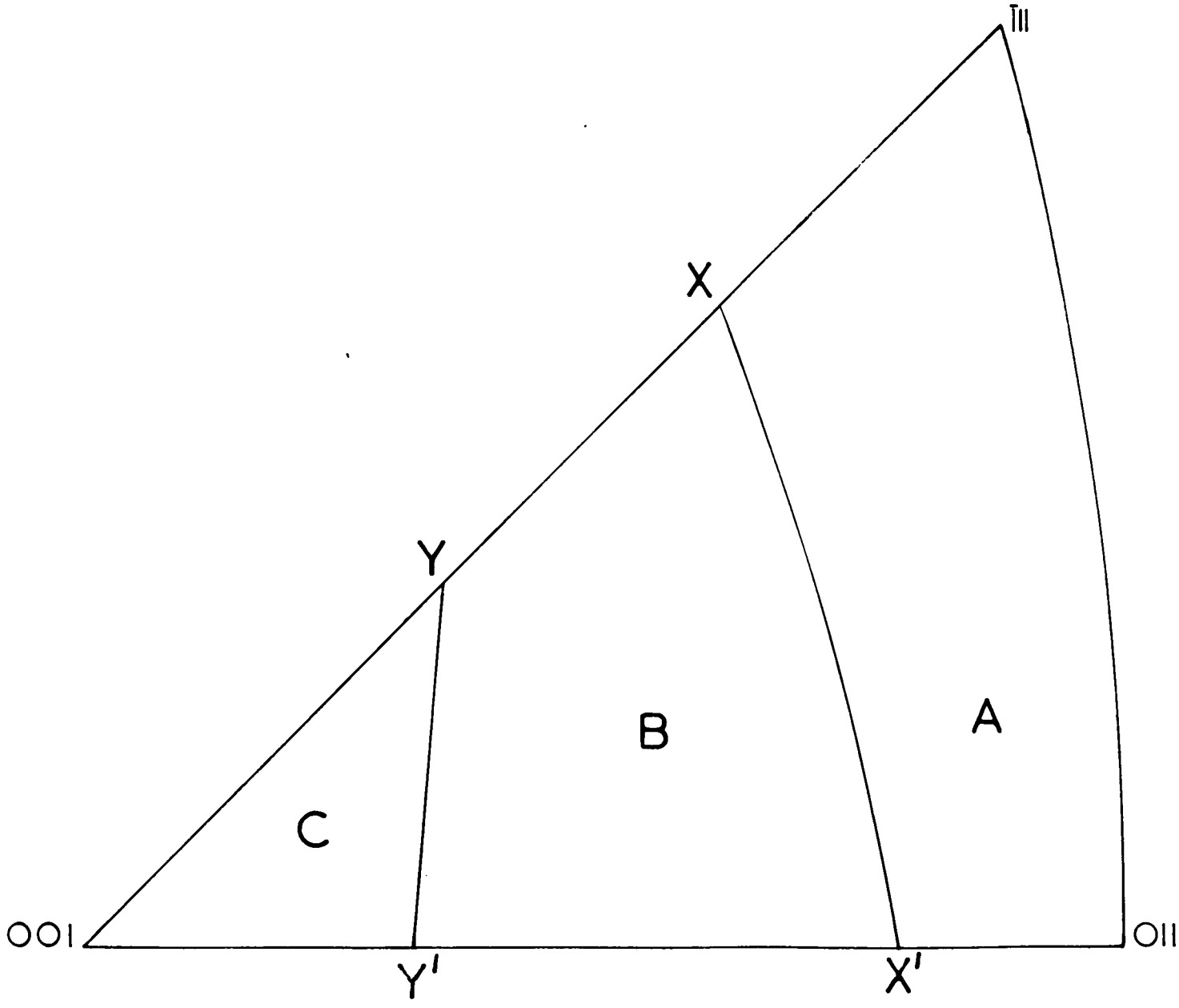


FIG. IV. 5.



FIG. IV 6

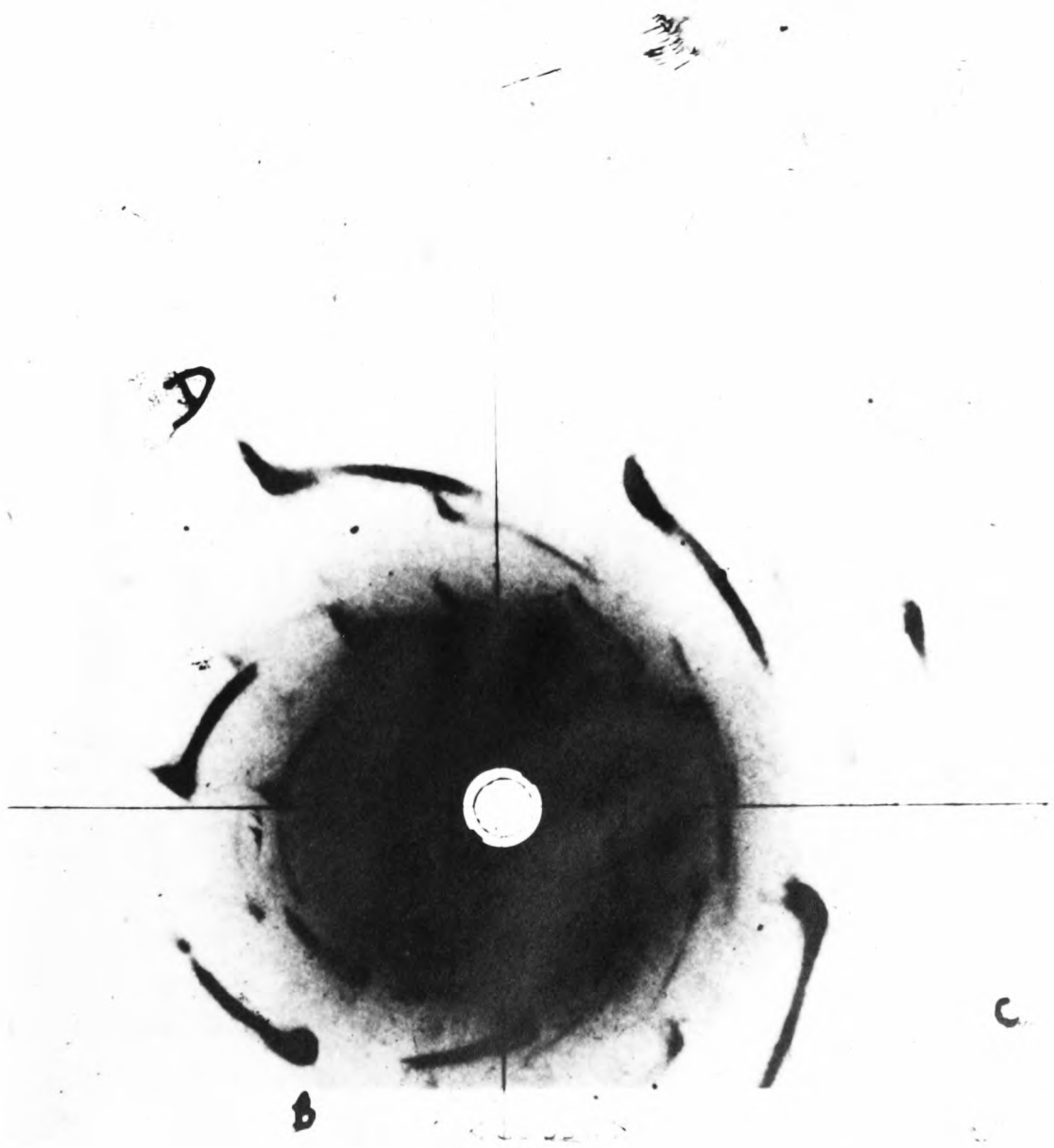


FIG. IV 7

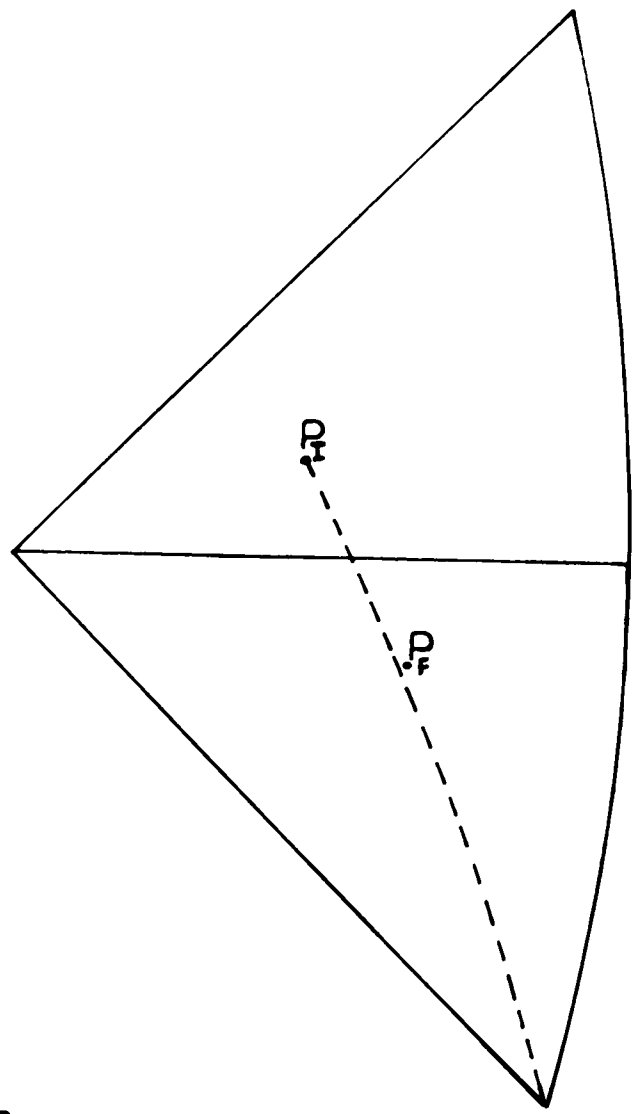


FIG.IV. 8.

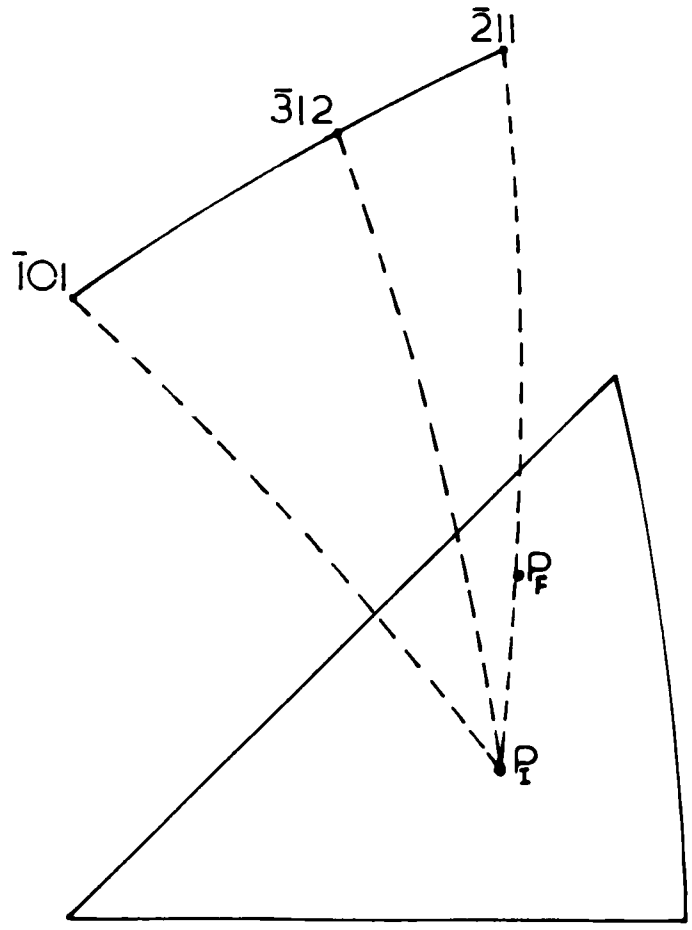


FIG.IV. 9.

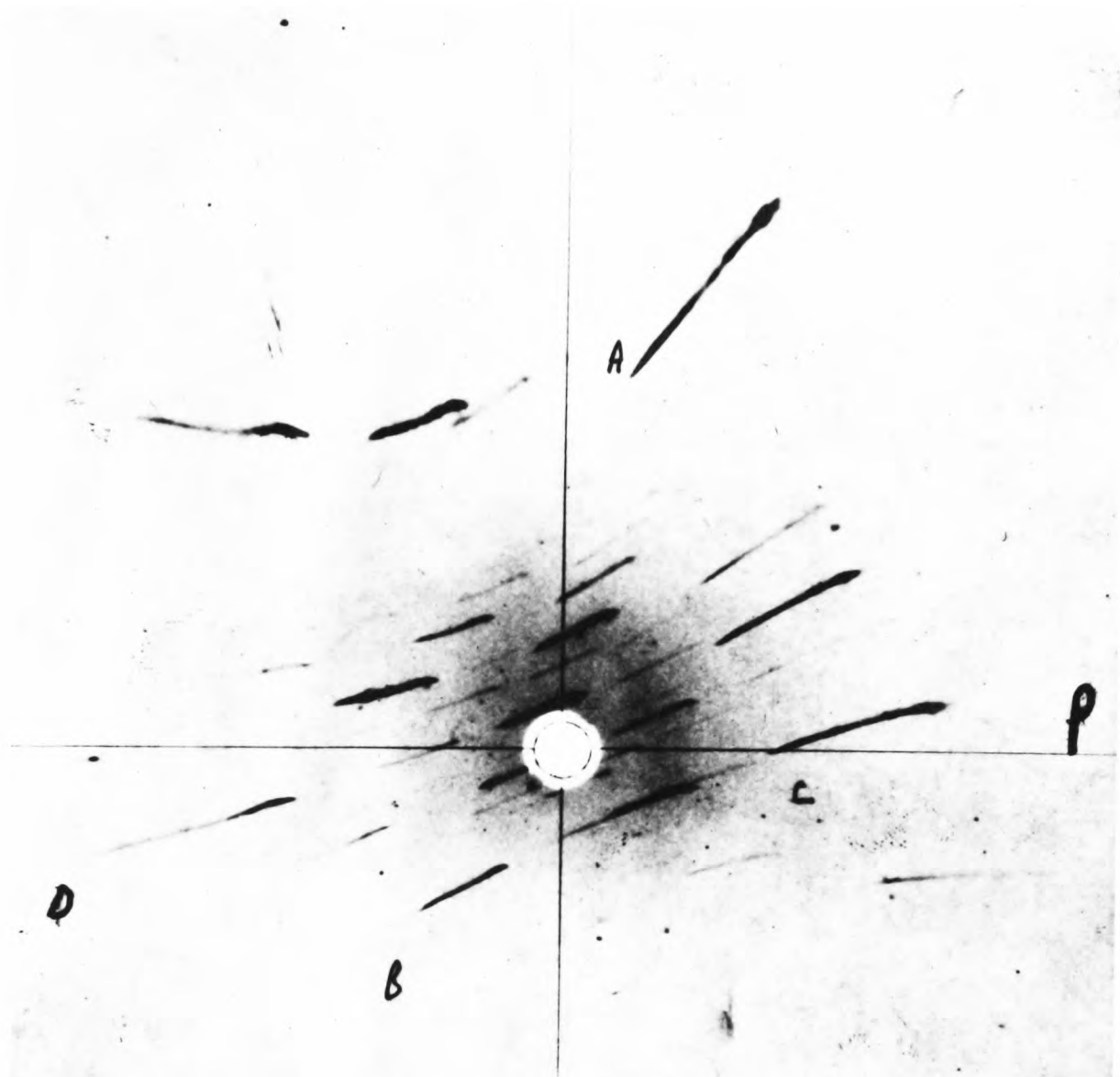


FIG.IV.10 LAUE PHOTOGRAPH Nb 29.

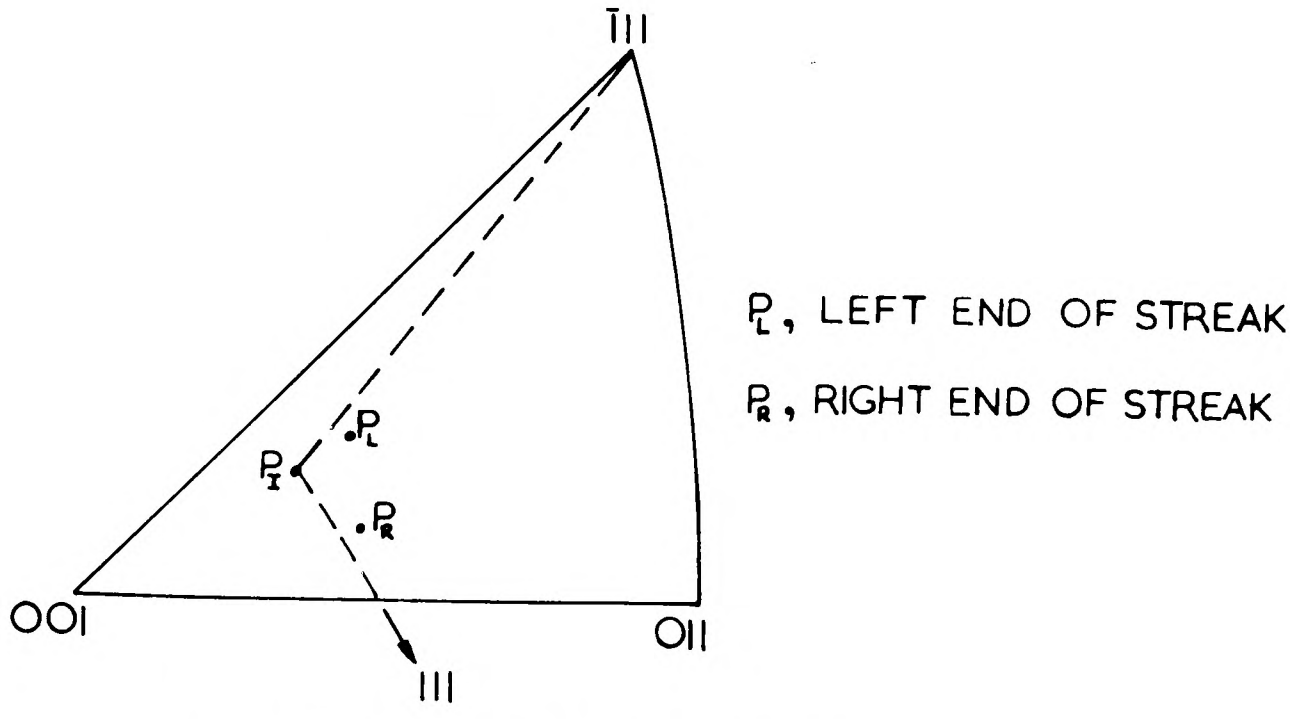


FIG.IV.11 STEREOGRAM Nb 29.

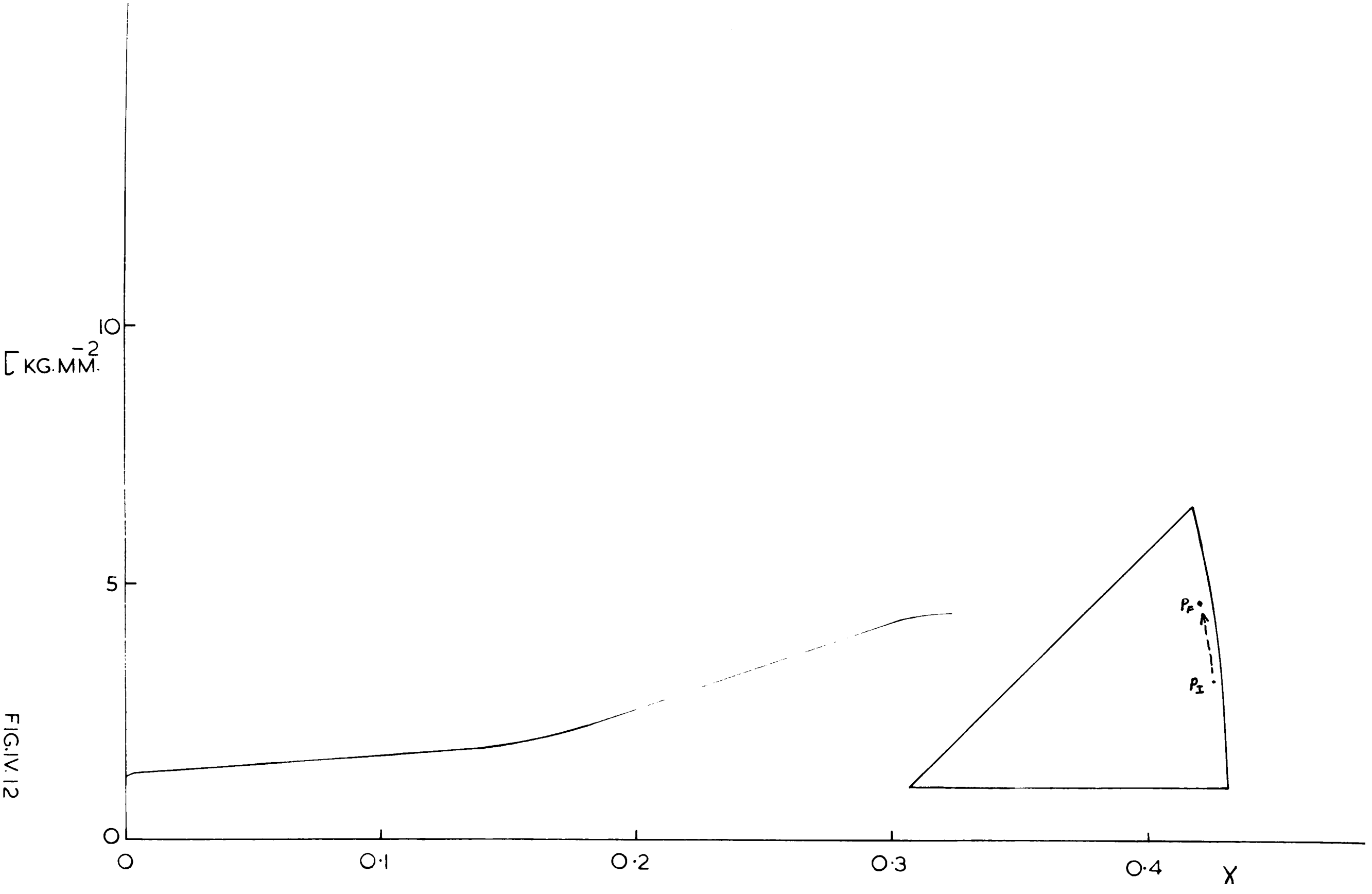


FIG.IV.12

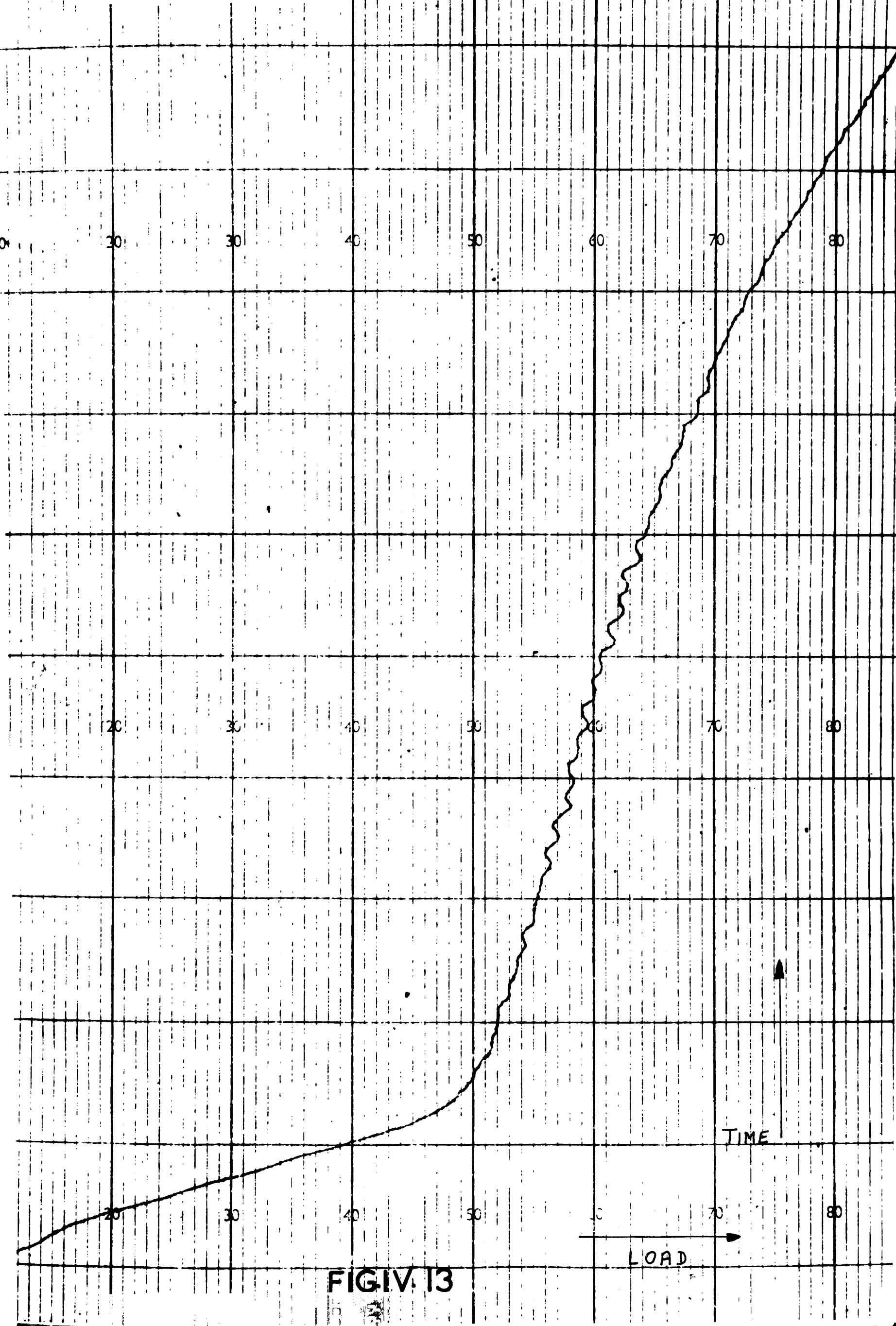


FIG.IV.13

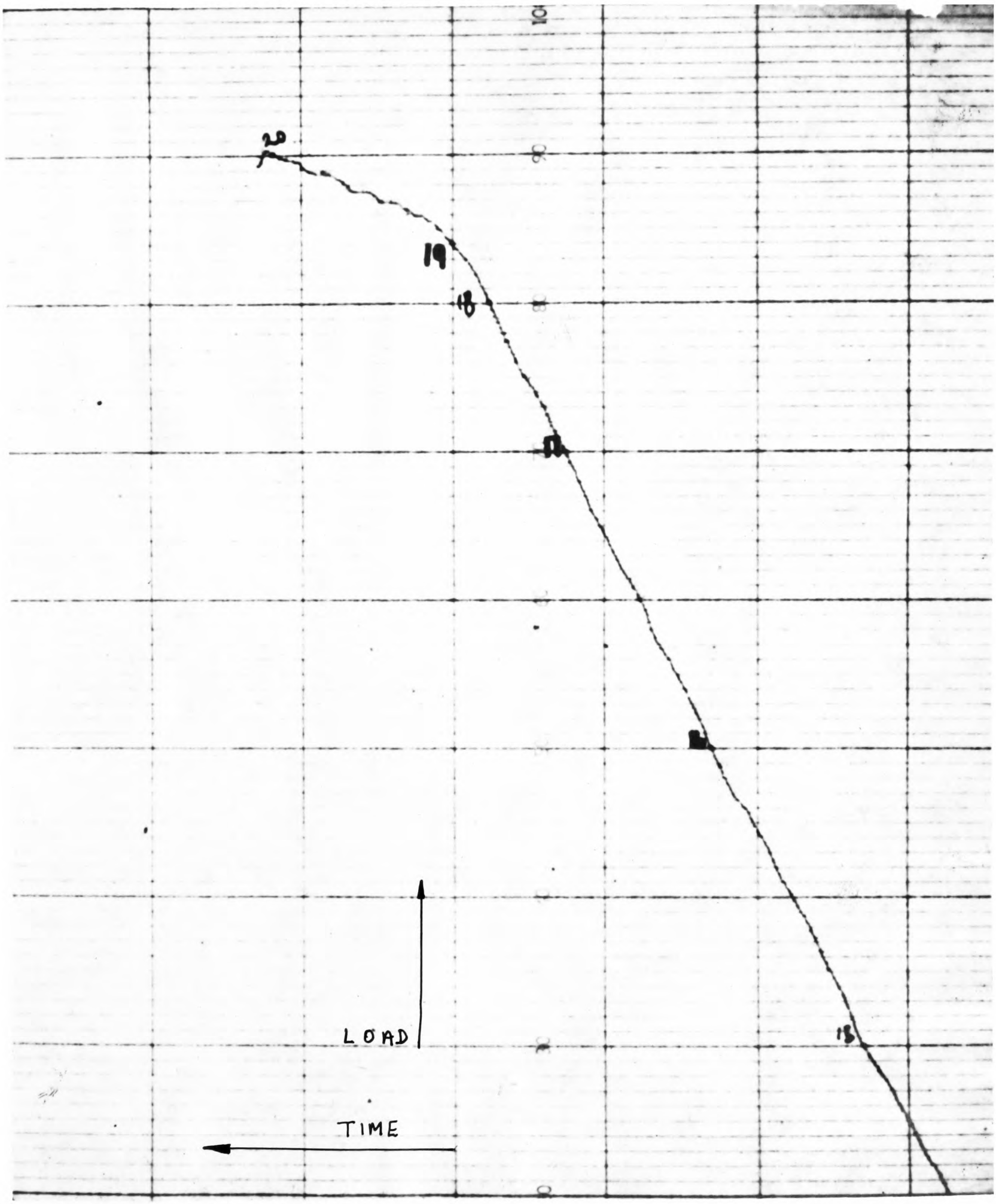


FIG. IV 14

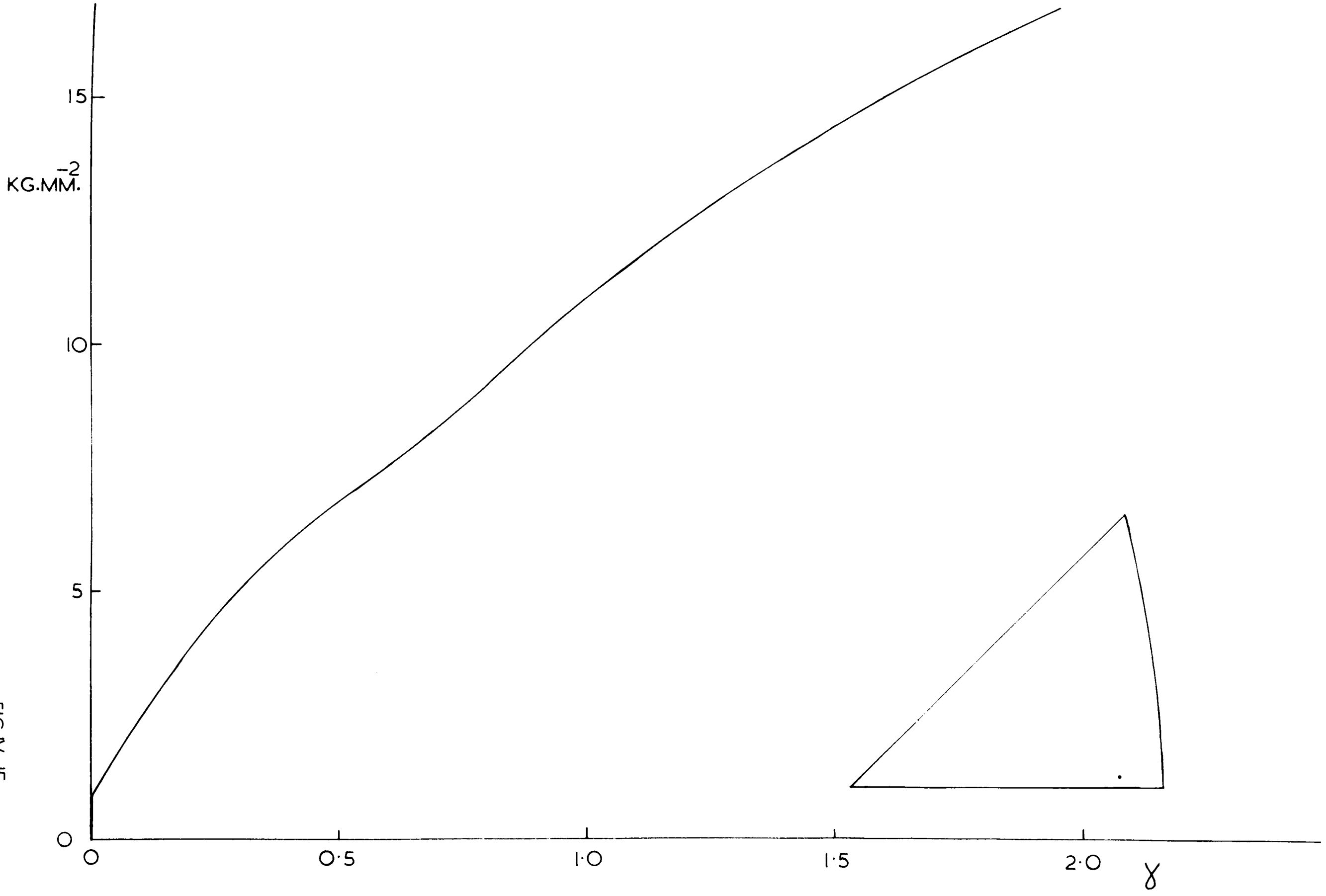


FIG. V. 15



FIG. IV 16

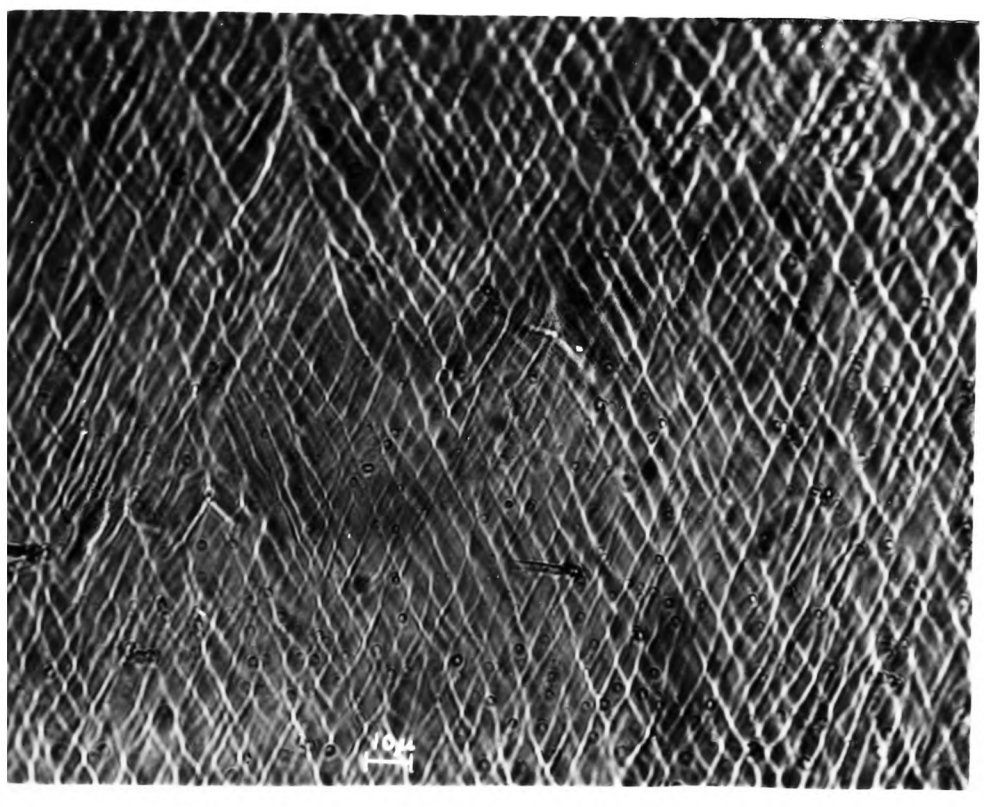


FIG. IV 17

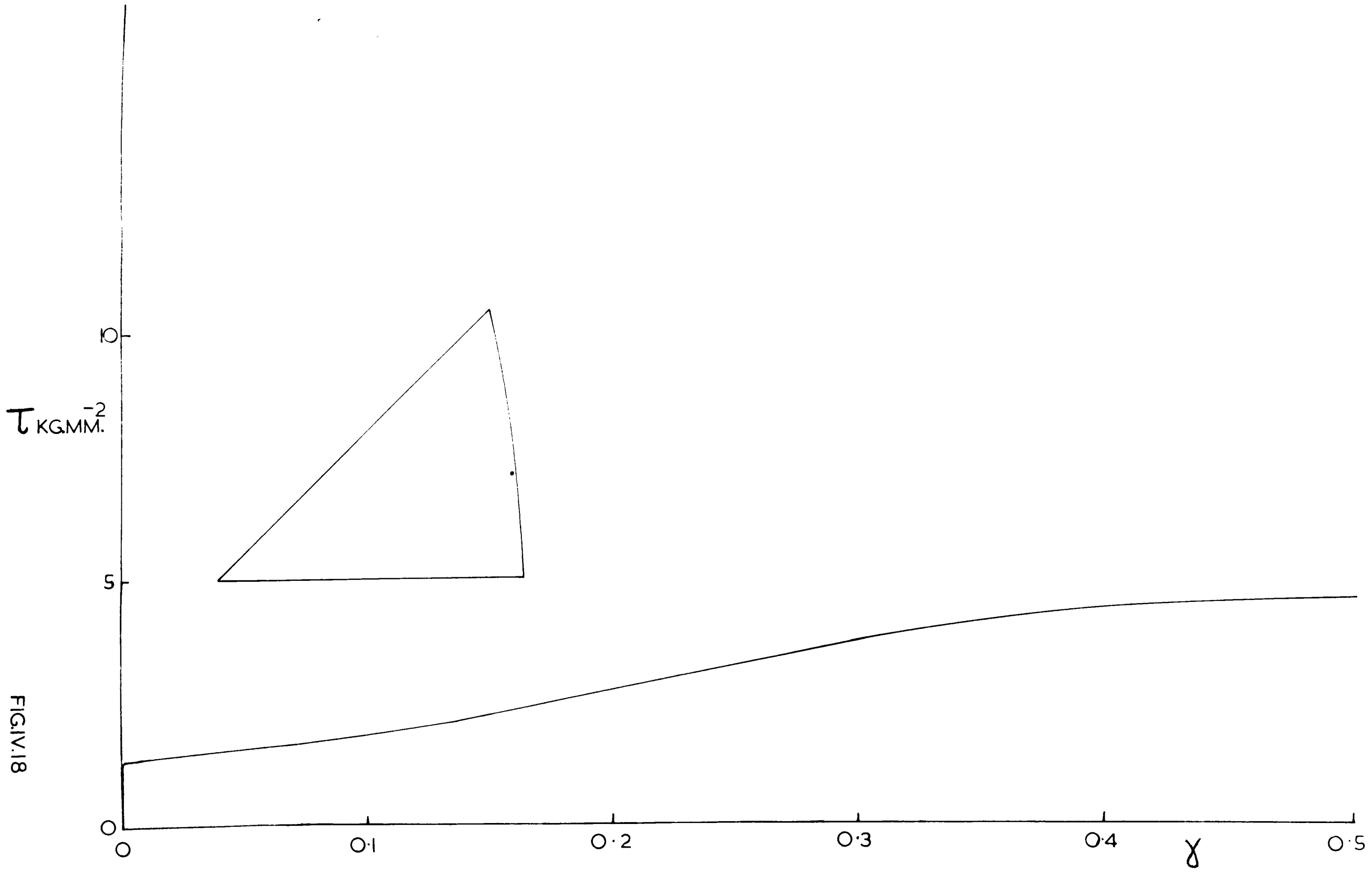


FIG.IV.18

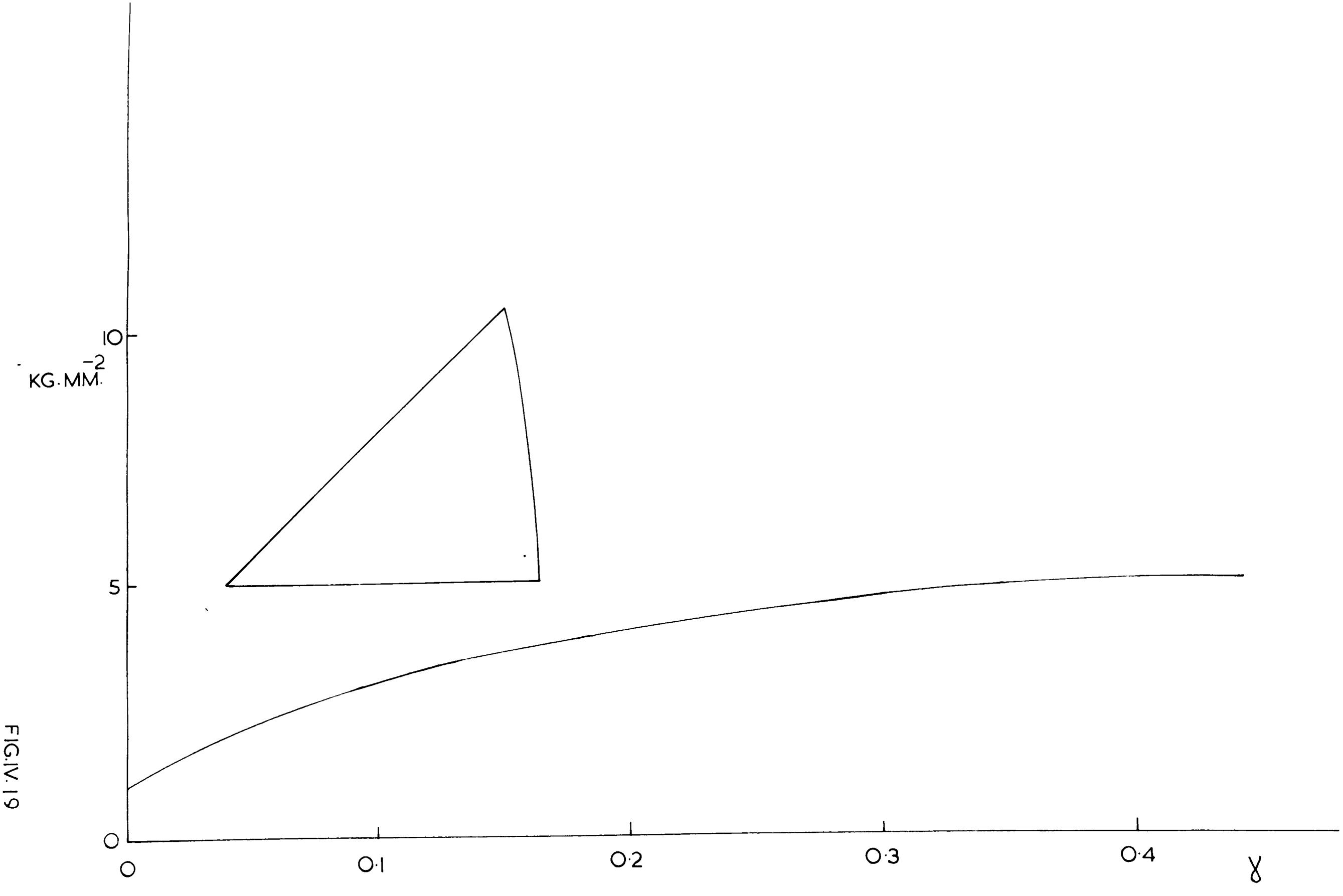


FIG.IV.19

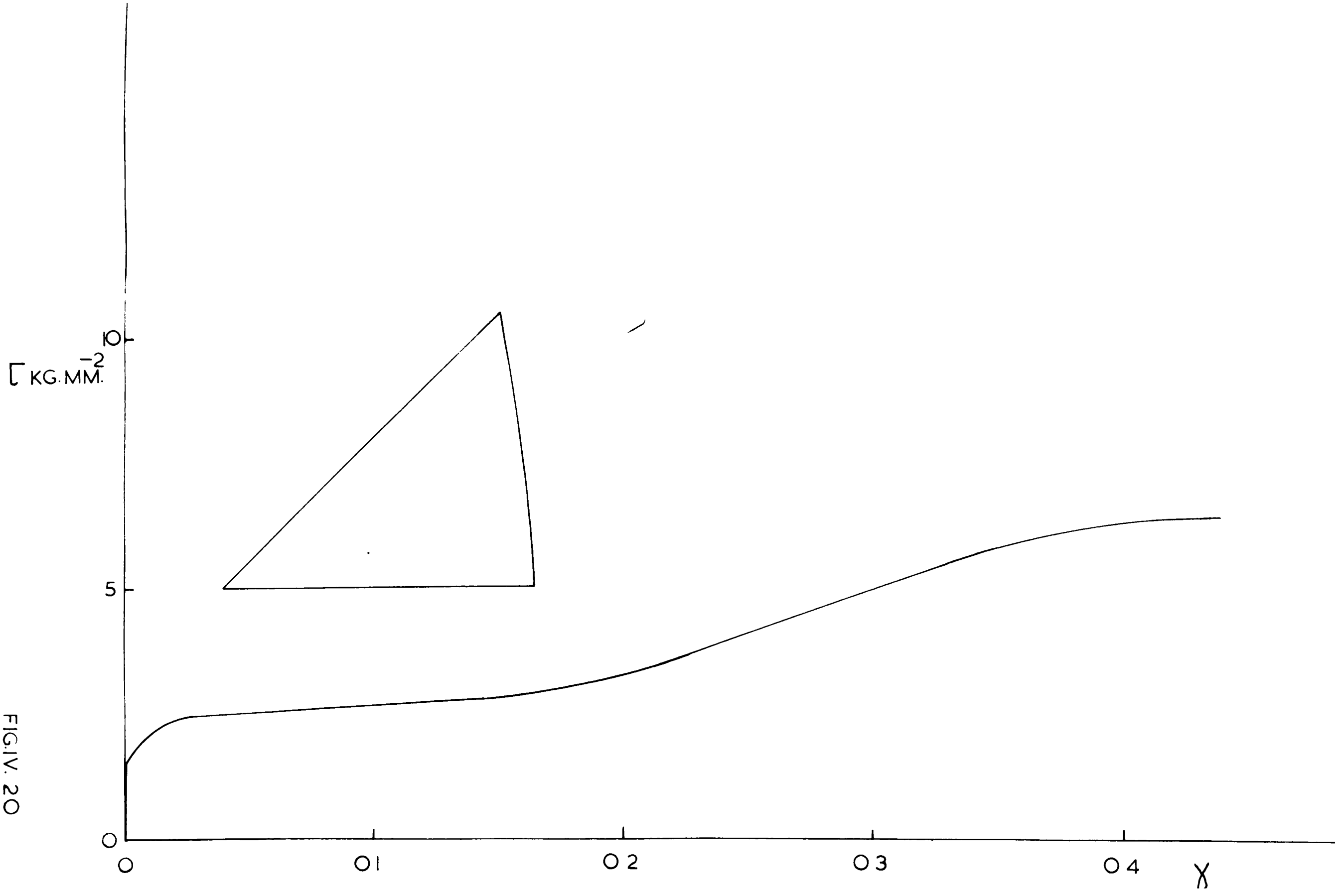


FIG.IV. 20

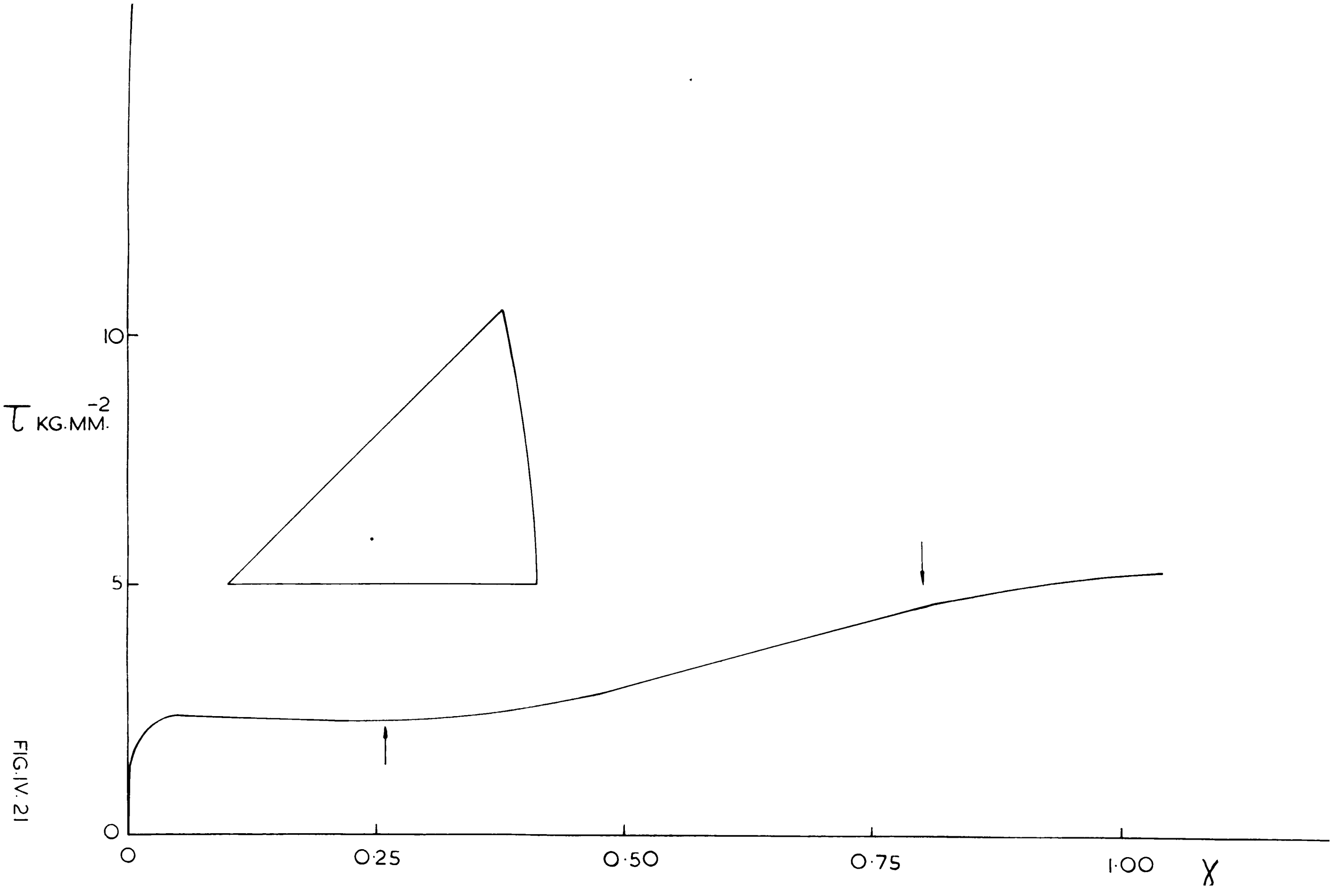


FIG. IV. 21

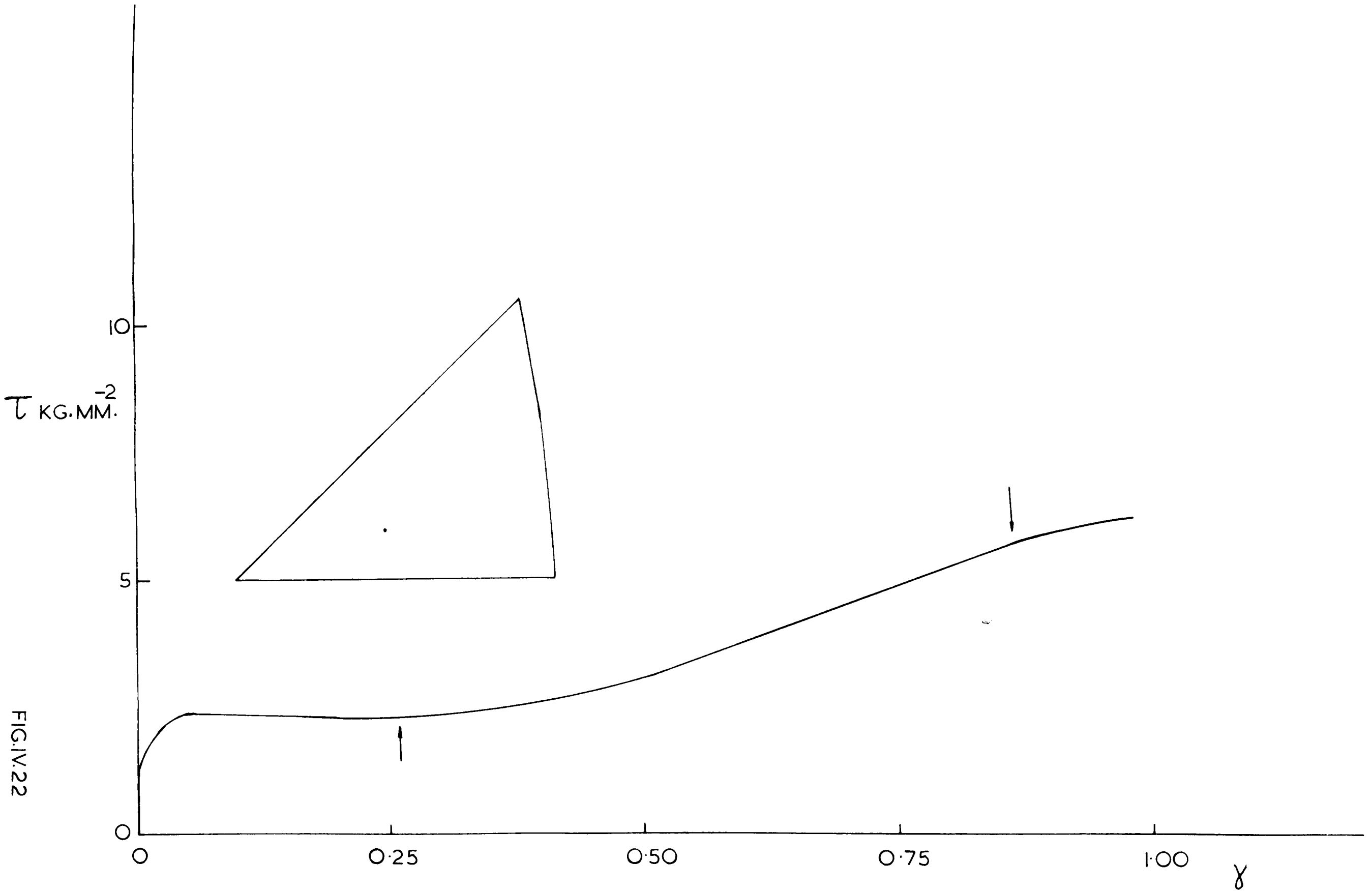


FIG.IV.22

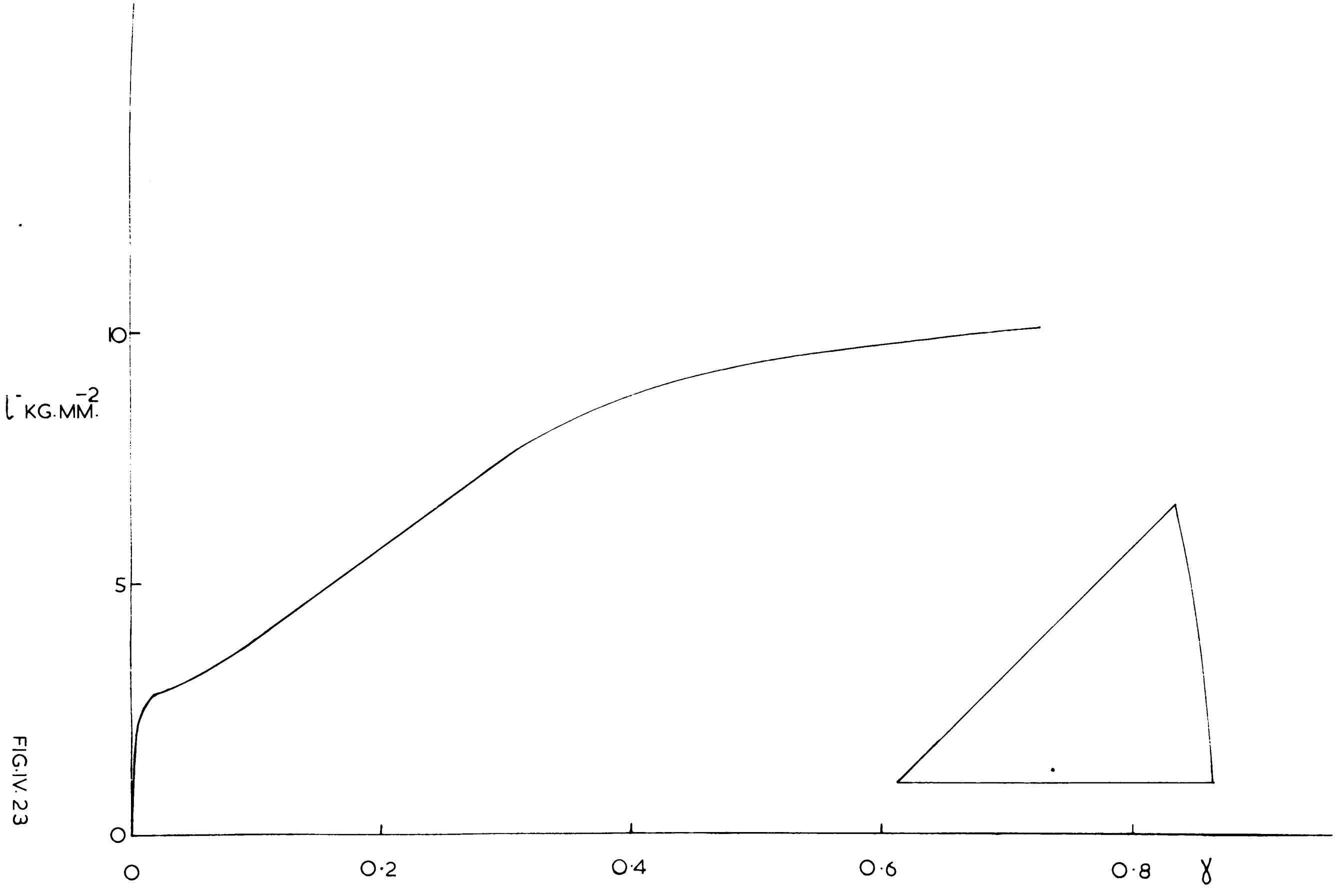


FIG.IV.23

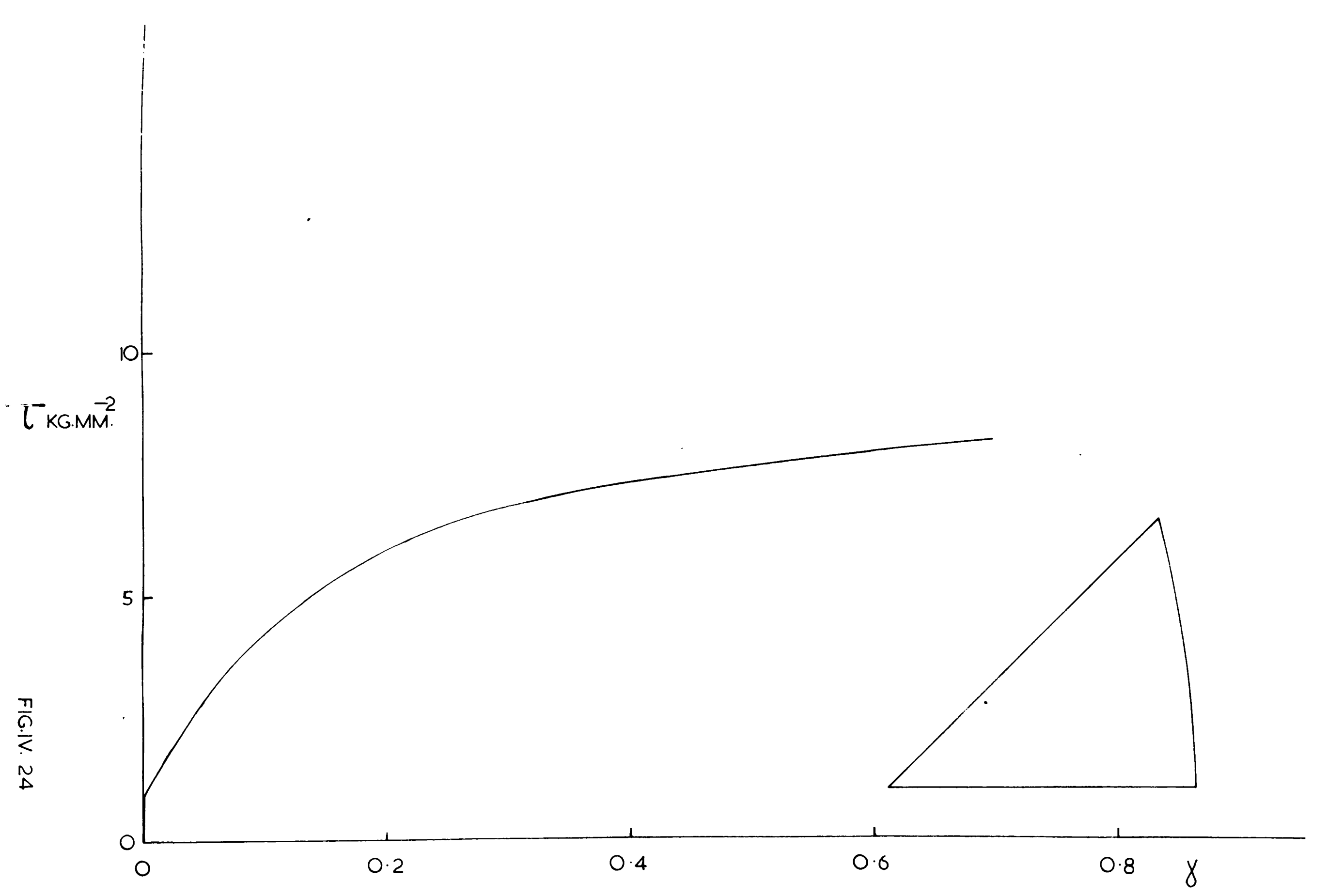


FIG. IV. 24

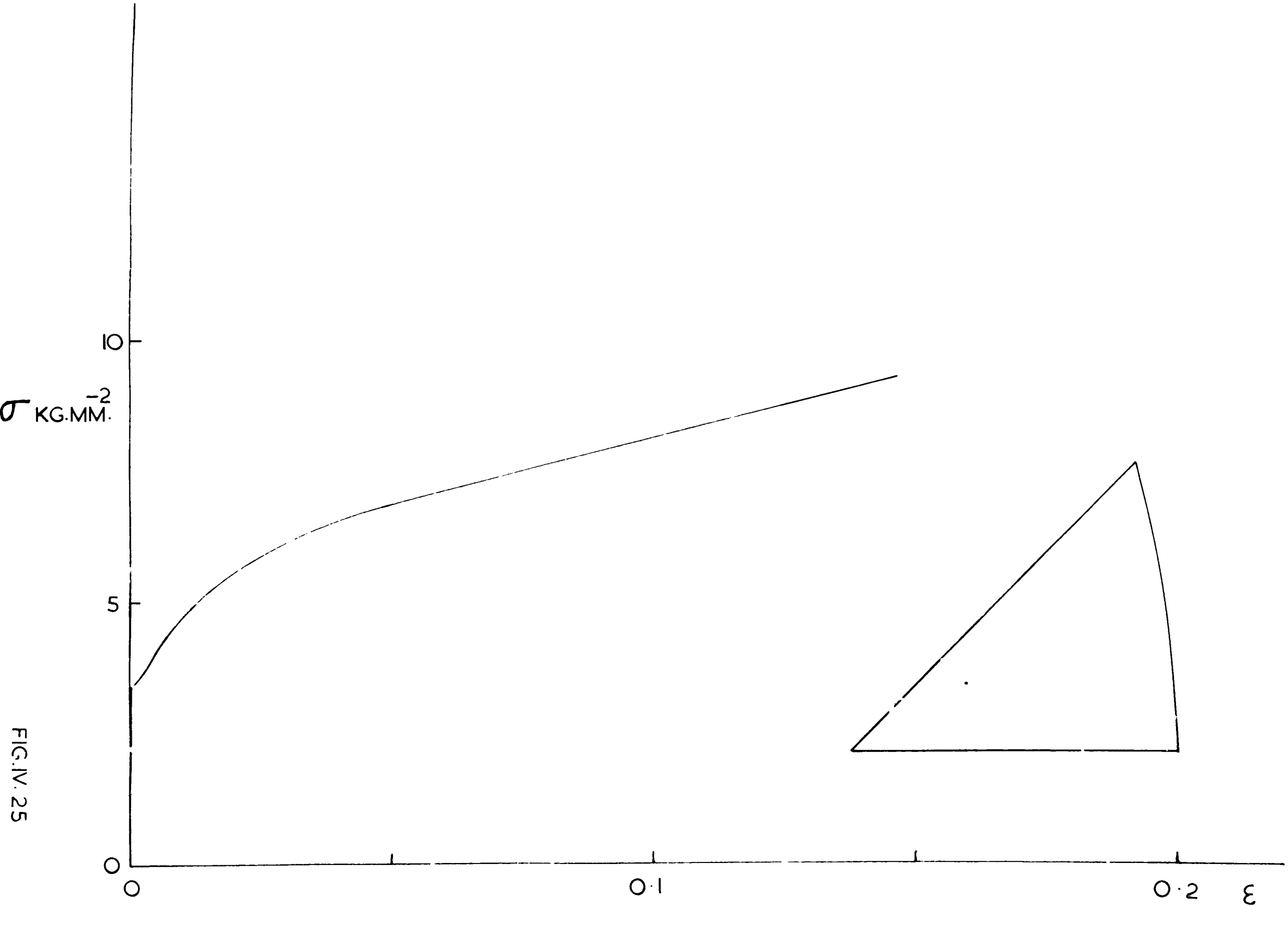


FIG. IV. 25

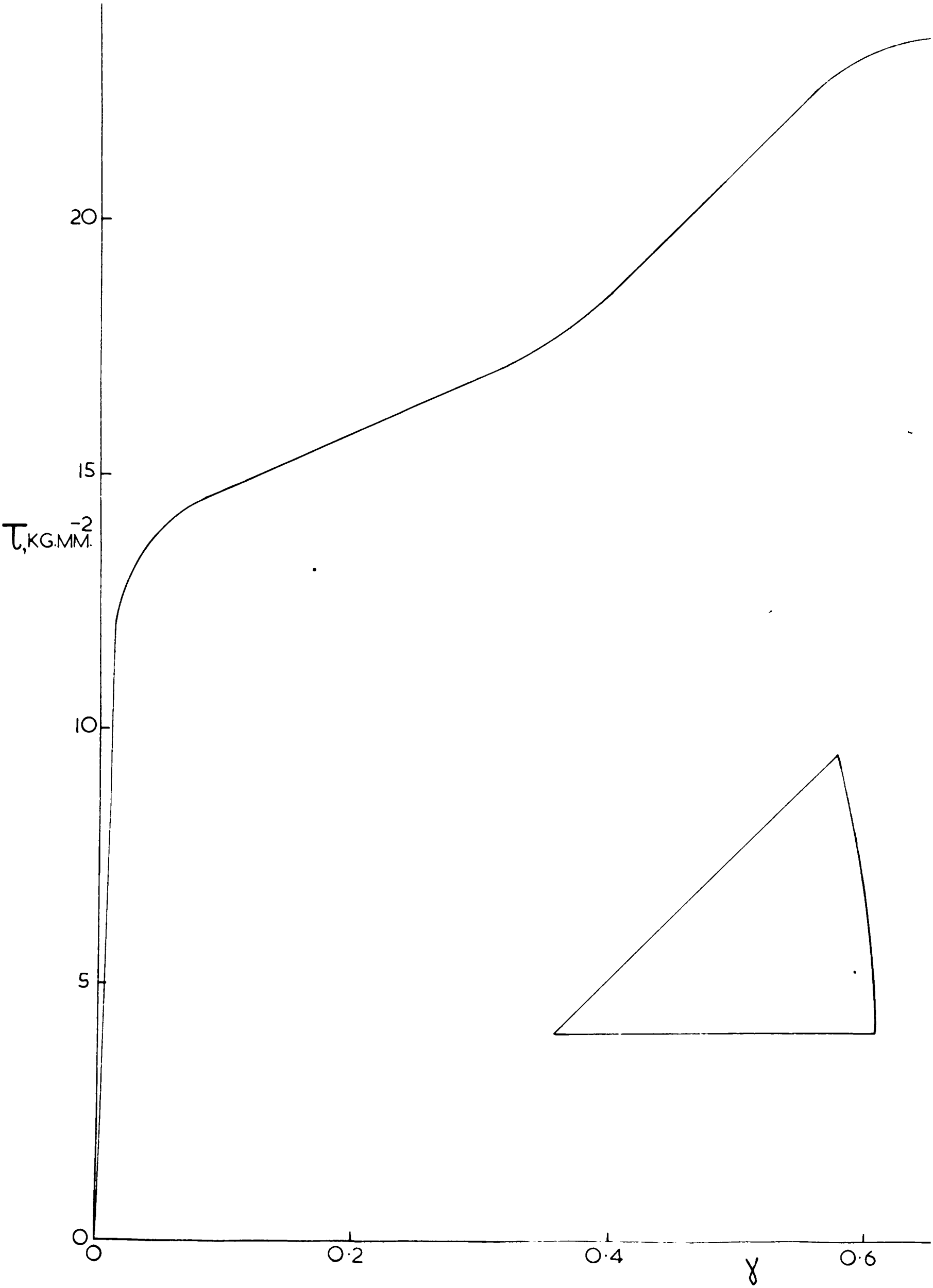


FIG.IV. 26

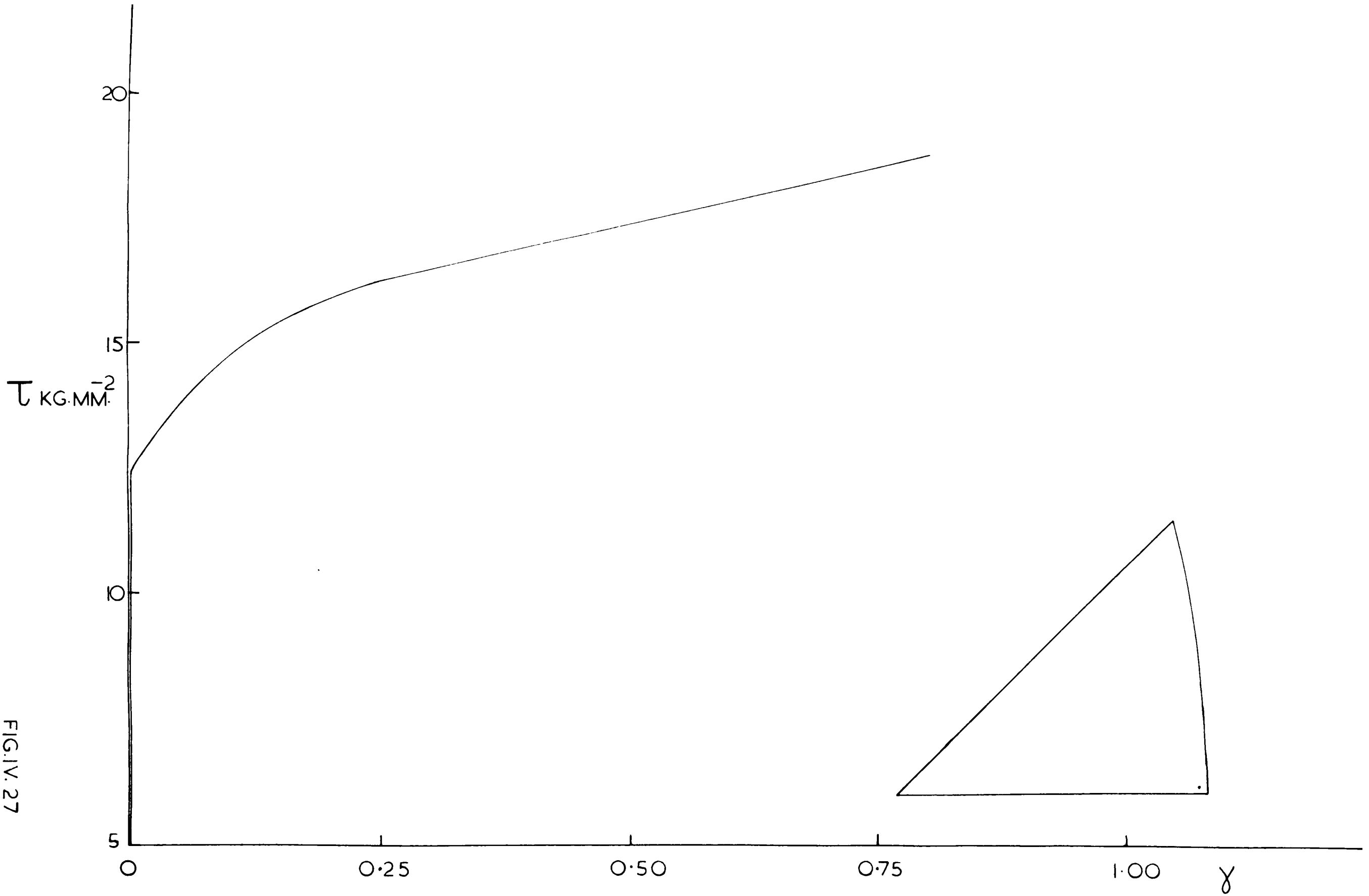


FIG. IV. 27

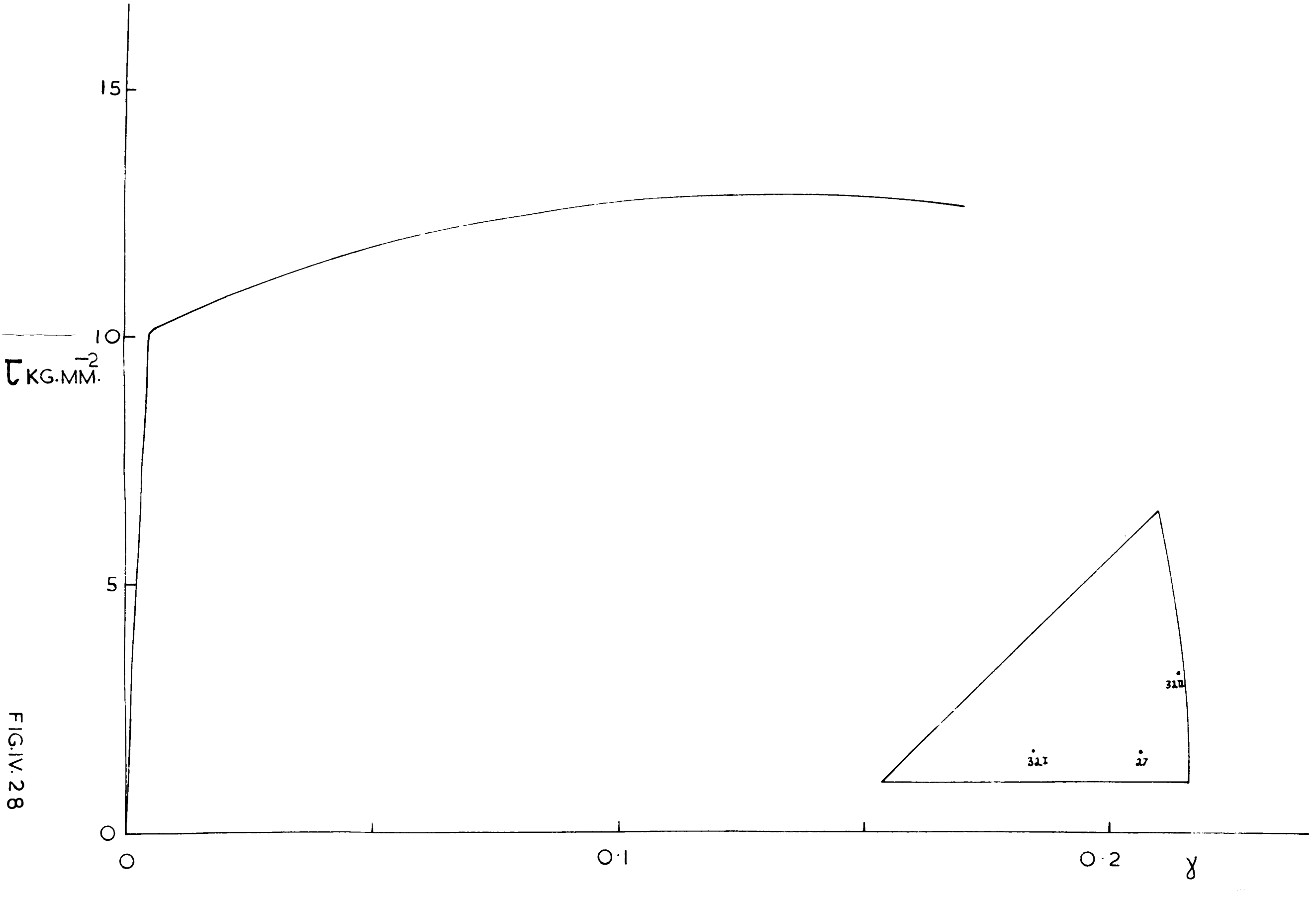


FIG. IV. 28

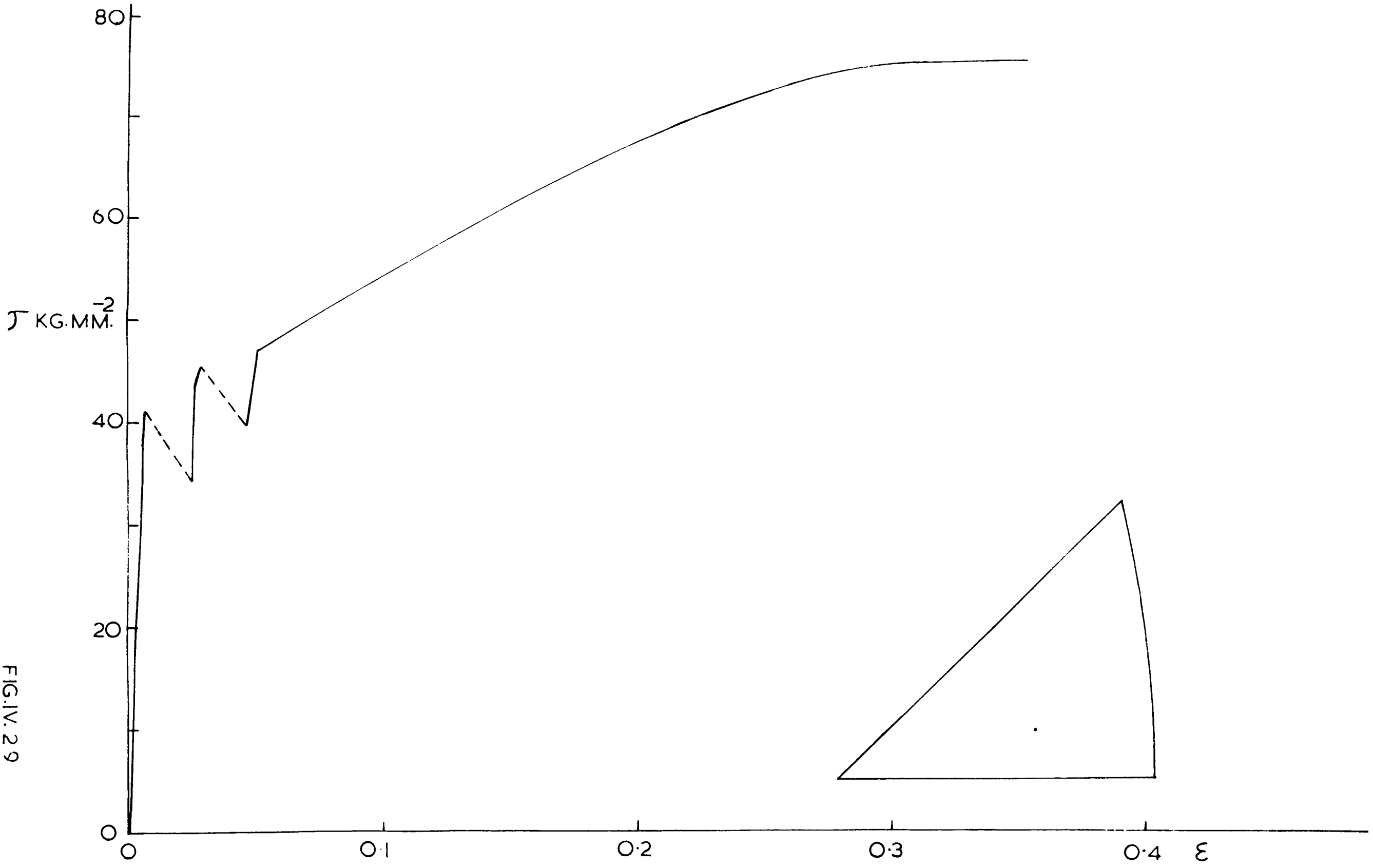


FIG.IV. 29

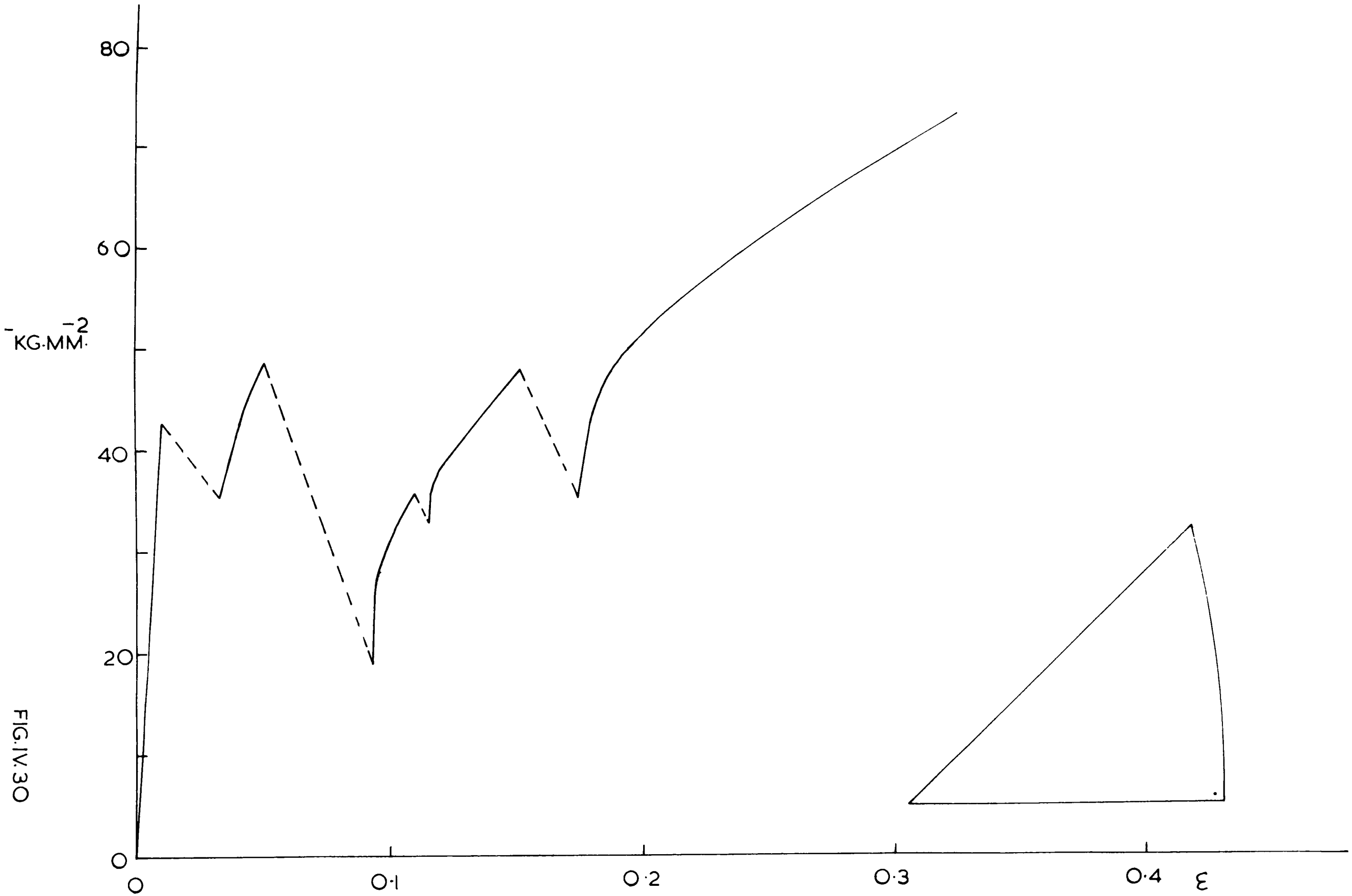


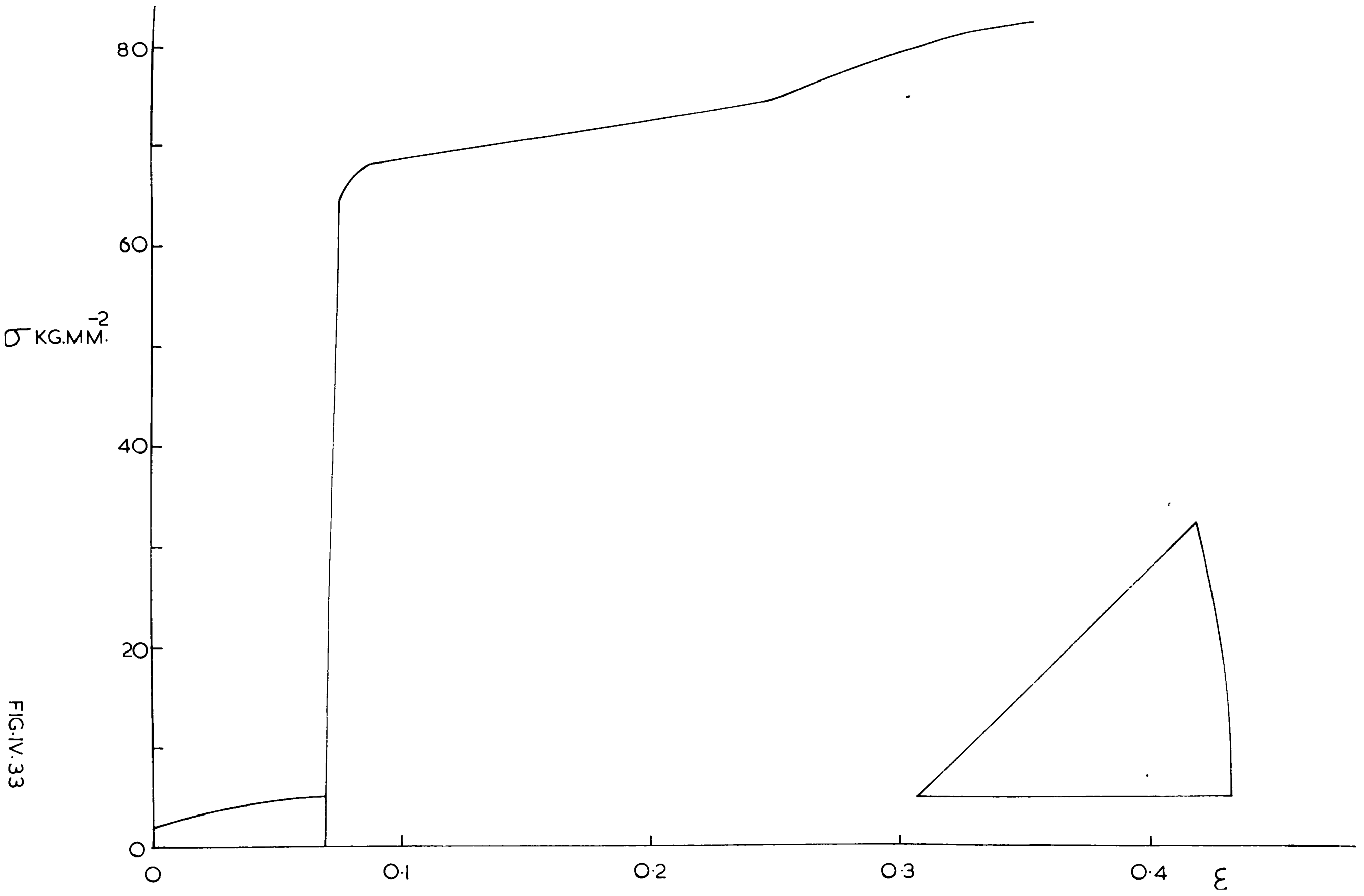
FIG. IV. 30



FIG. IV 31



FIG. IV 32



FIG·IV·33

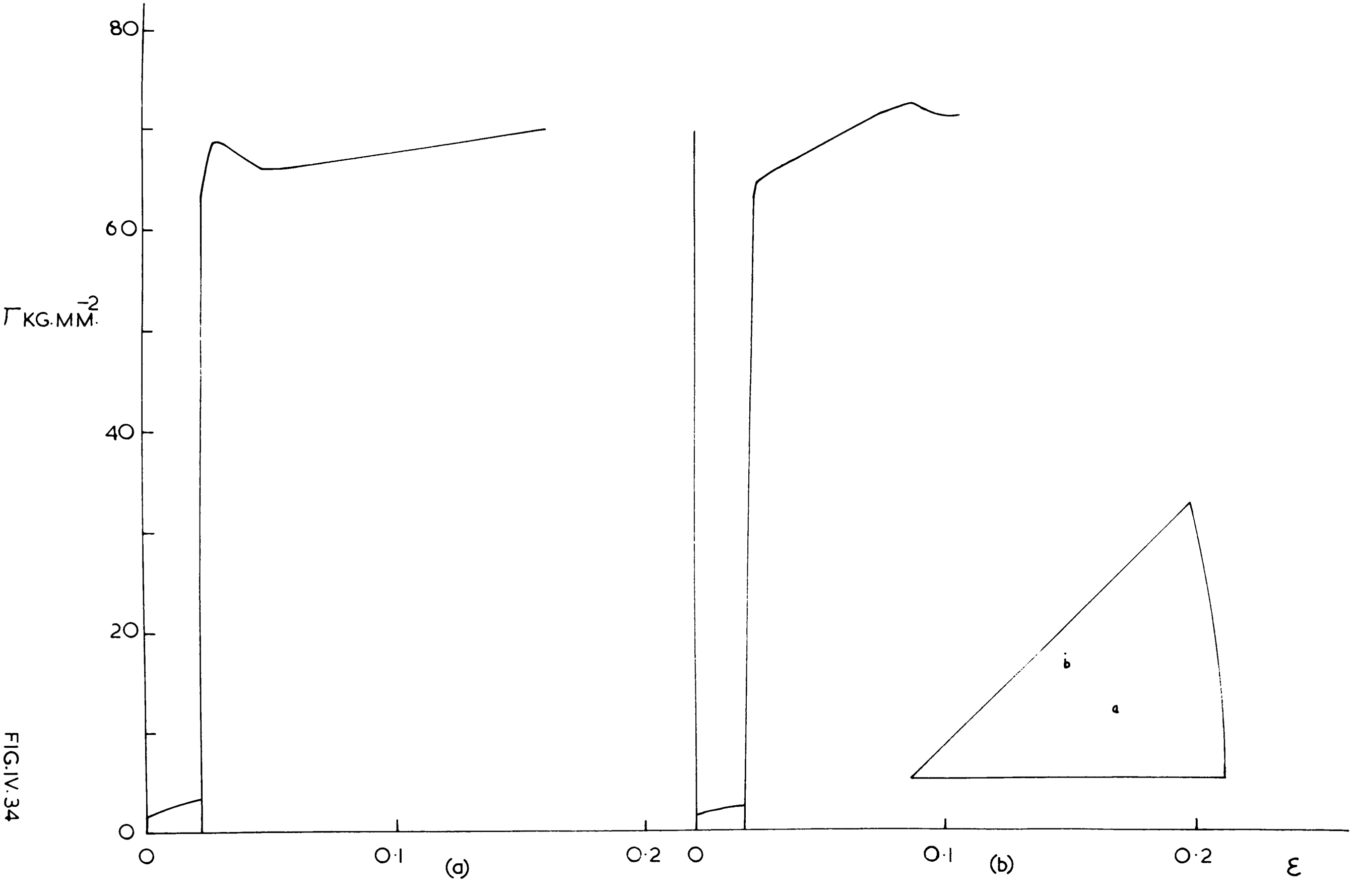


FIG.IV.34

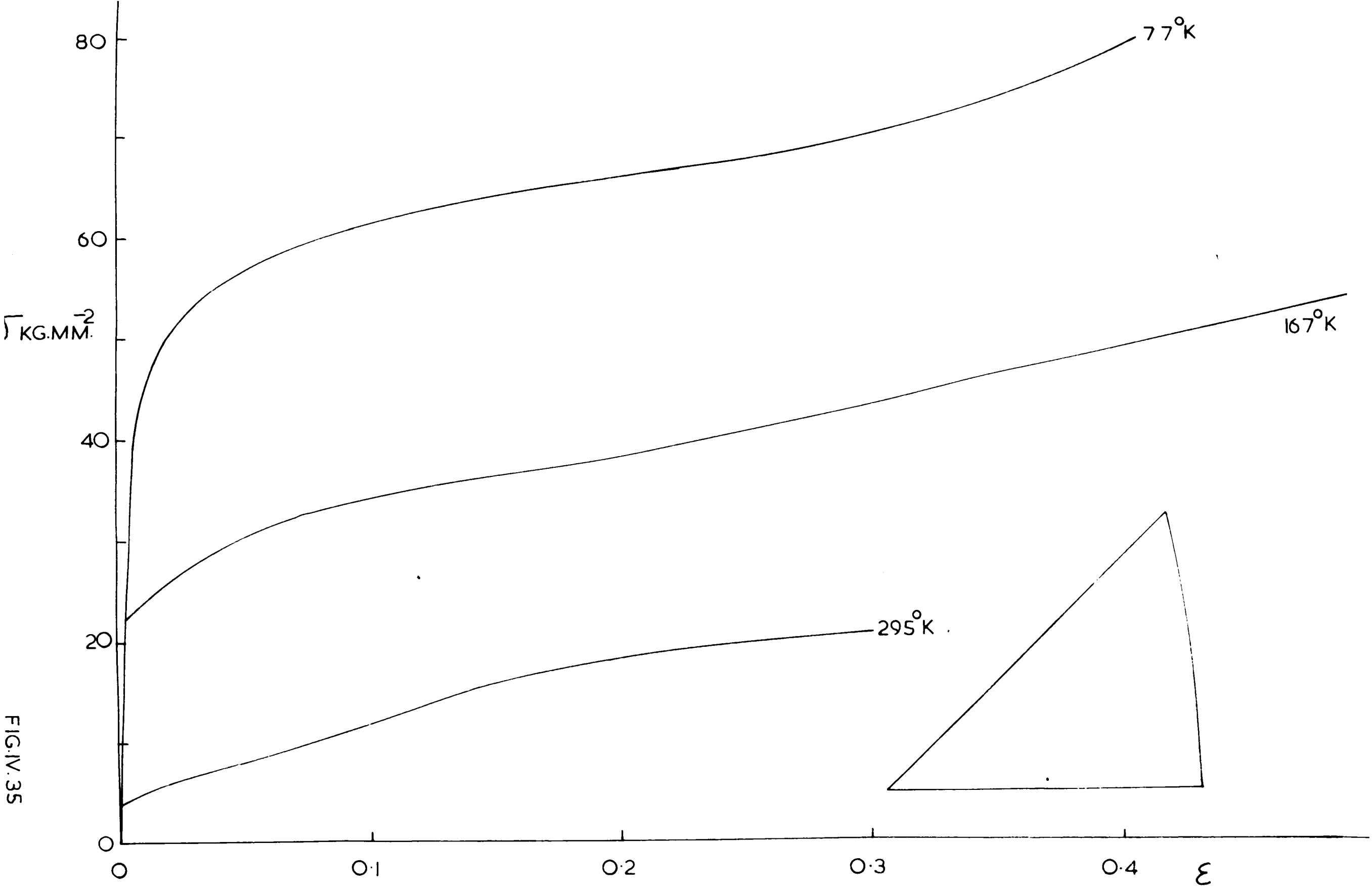


FIG.IV.35

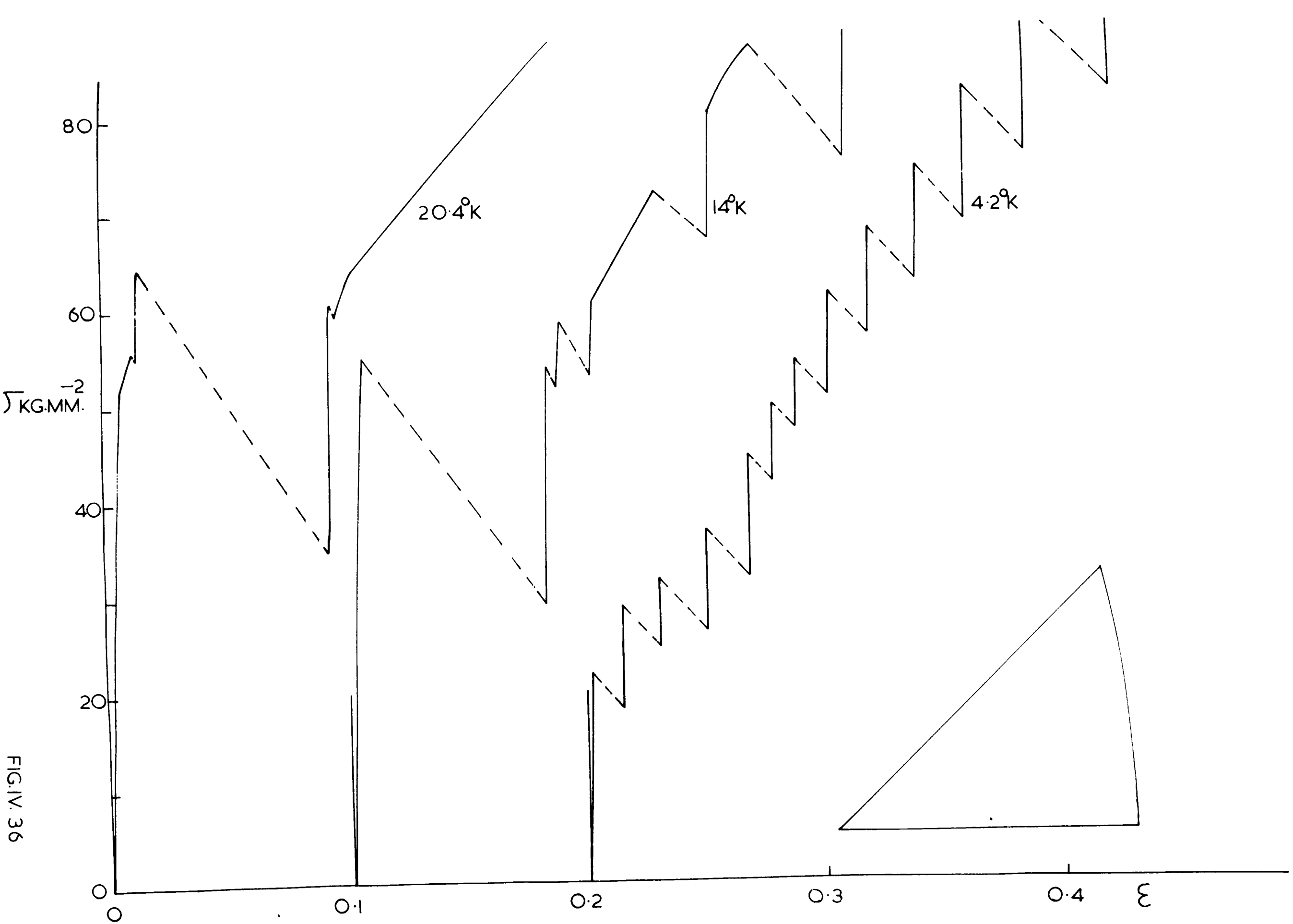


FIG. IV. 36

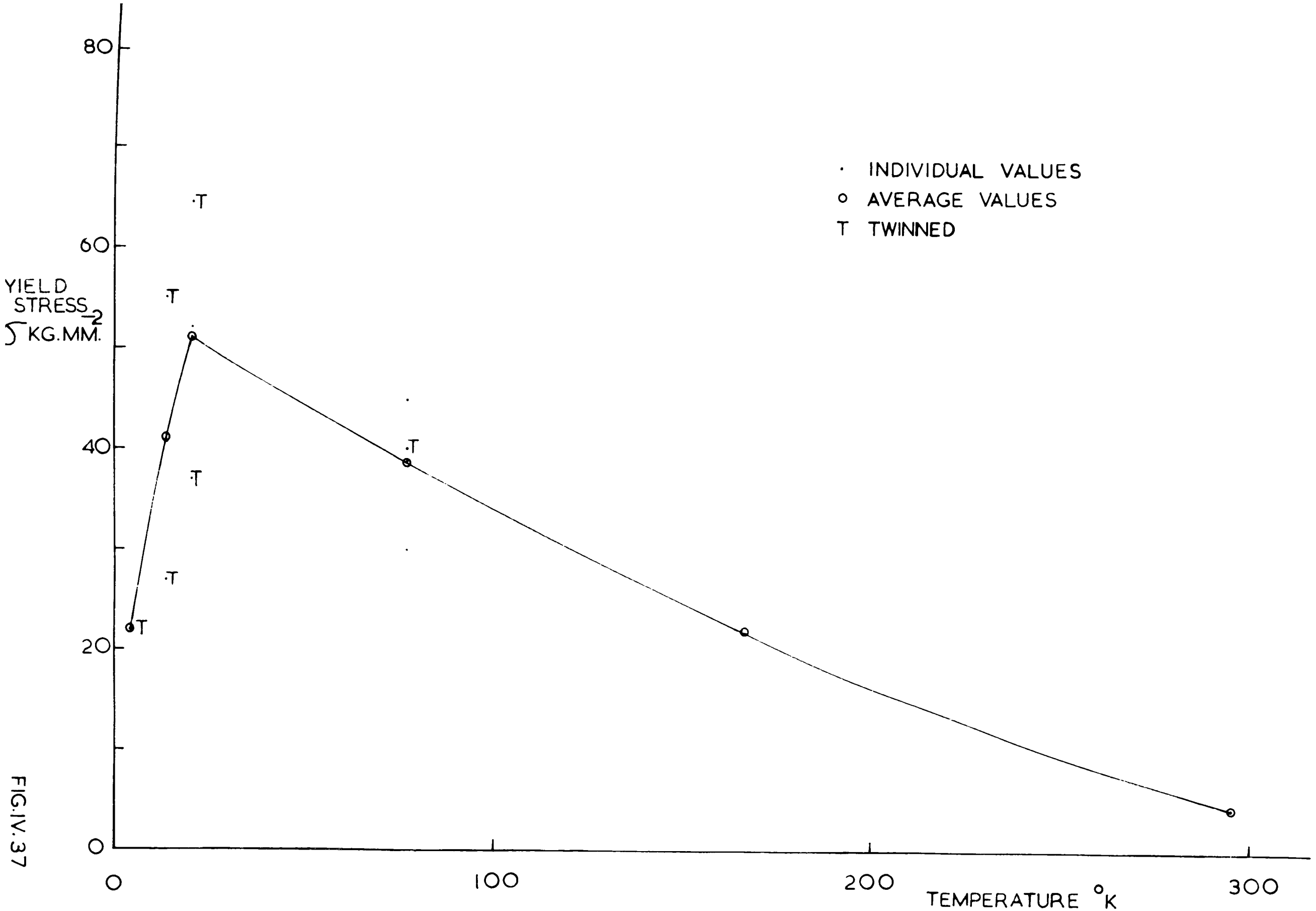

80
60
40
20
0
YIELD STRESS σ KG.MM.$^{-2}$
T
0
100
200
300
TEMPERATURE °K
· INDIVIDUAL VALUES
o AVERAGE VALUES
T TWINNED

FIG.IV.37

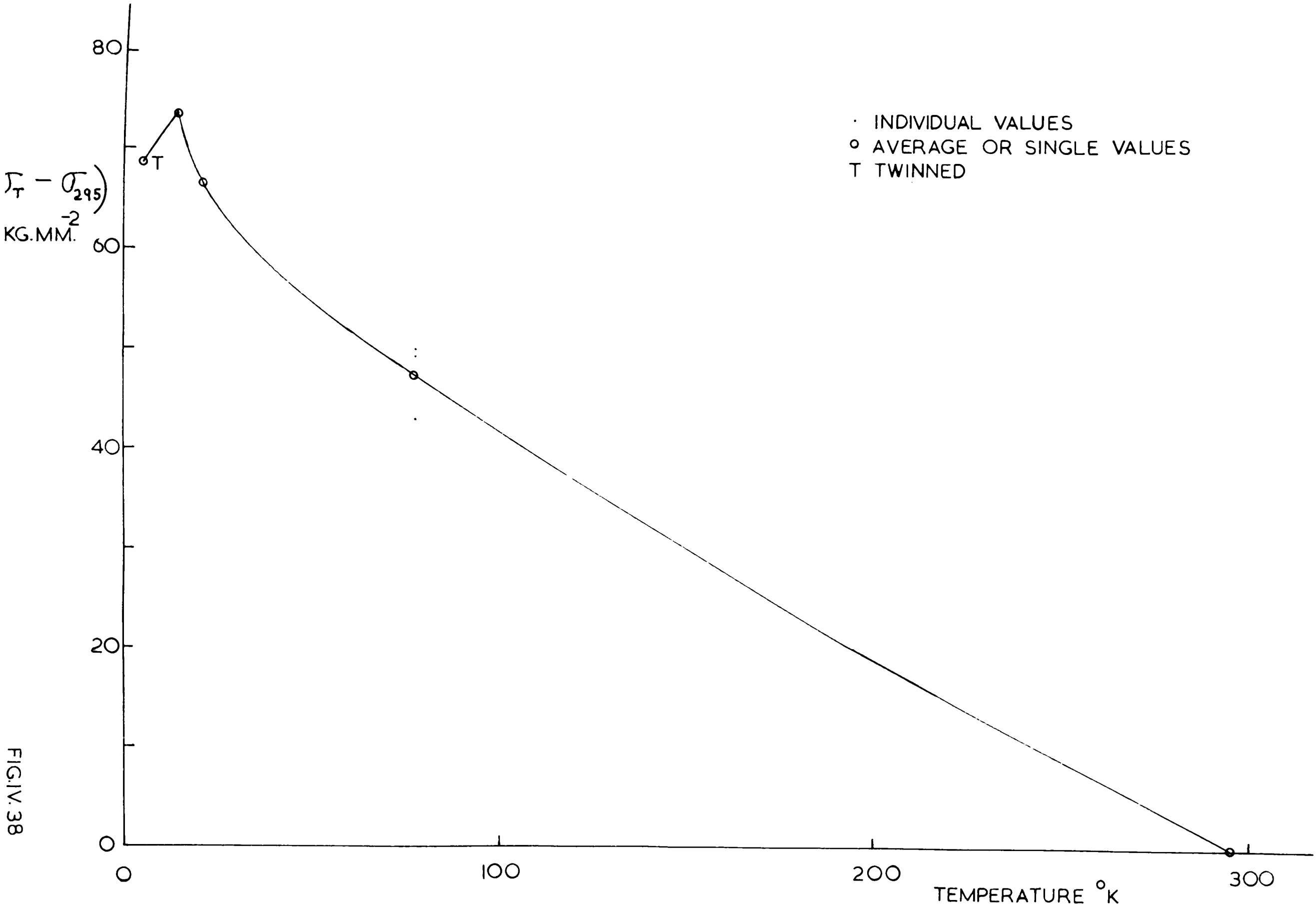

80
60
40
20
0
$(\sigma_T - \sigma_{295})$
KG.MM.$^{-2}$
T
0
100
200
300
TEMPERATURE °K
· INDIVIDUAL VALUES
o AVERAGE OR SINGLE VALUES
T TWINNED

FIG.IV.38

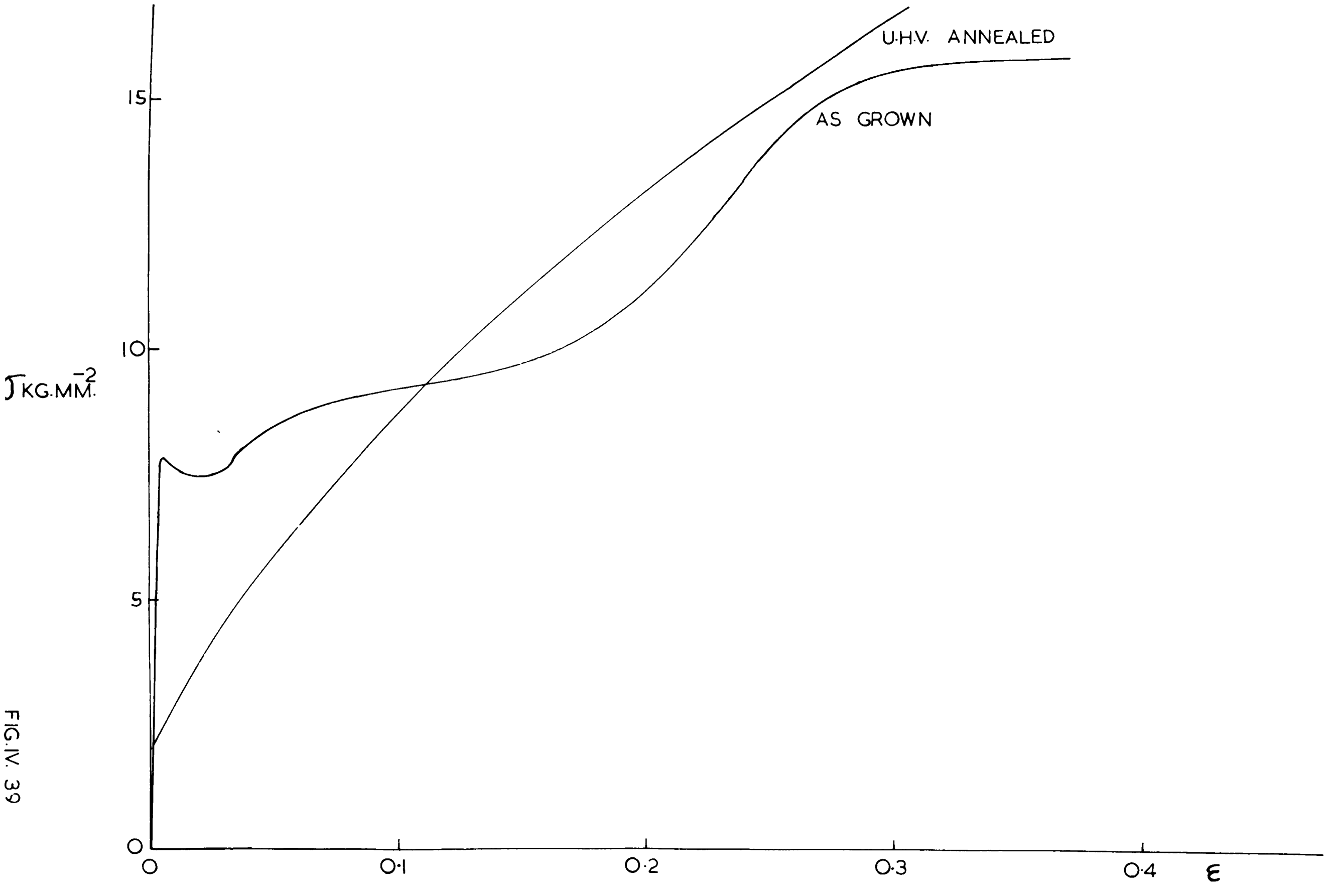

U·H·V· ANNEALED
AS GROWN
15
10
5
0
σ KG.MM^{-2}
0
0·1
0·2
0·3
0·4
ε

FIG. IV. 39

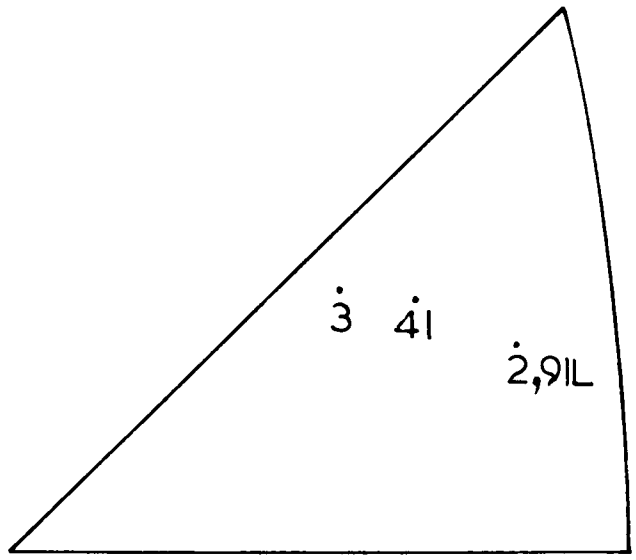


FIG.IV. 40

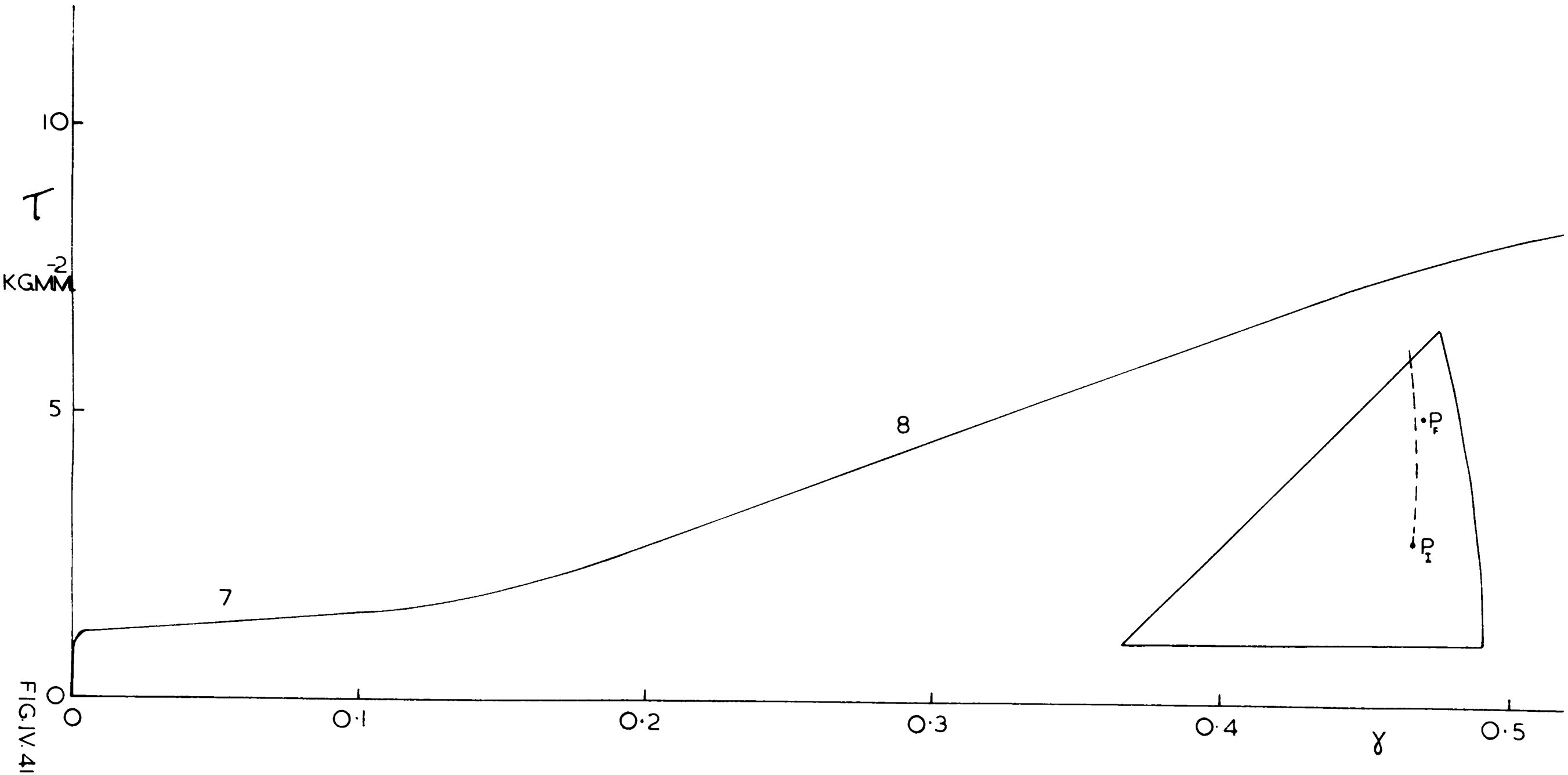


FIG. IV. 41

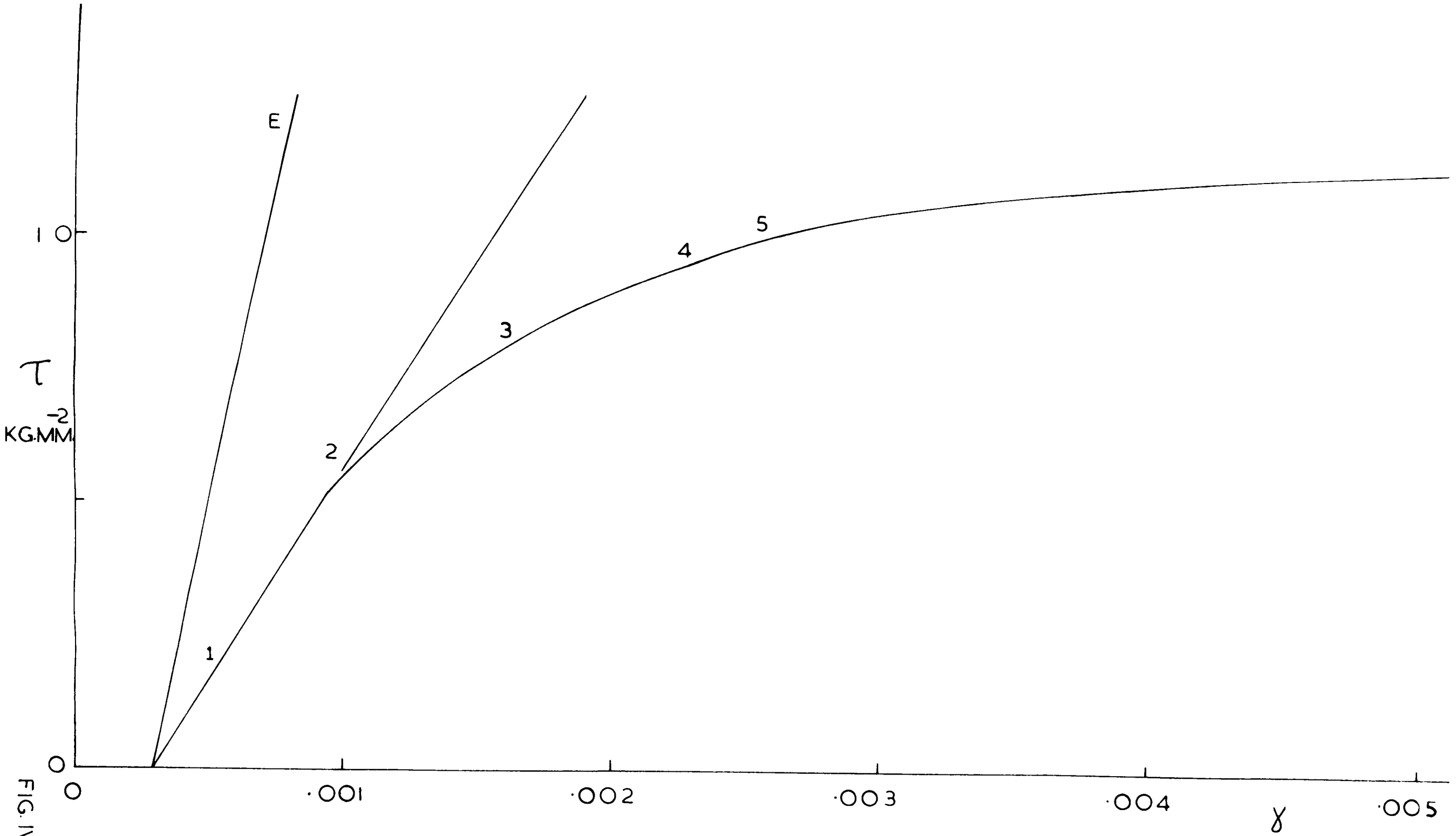


FIG. IV.42

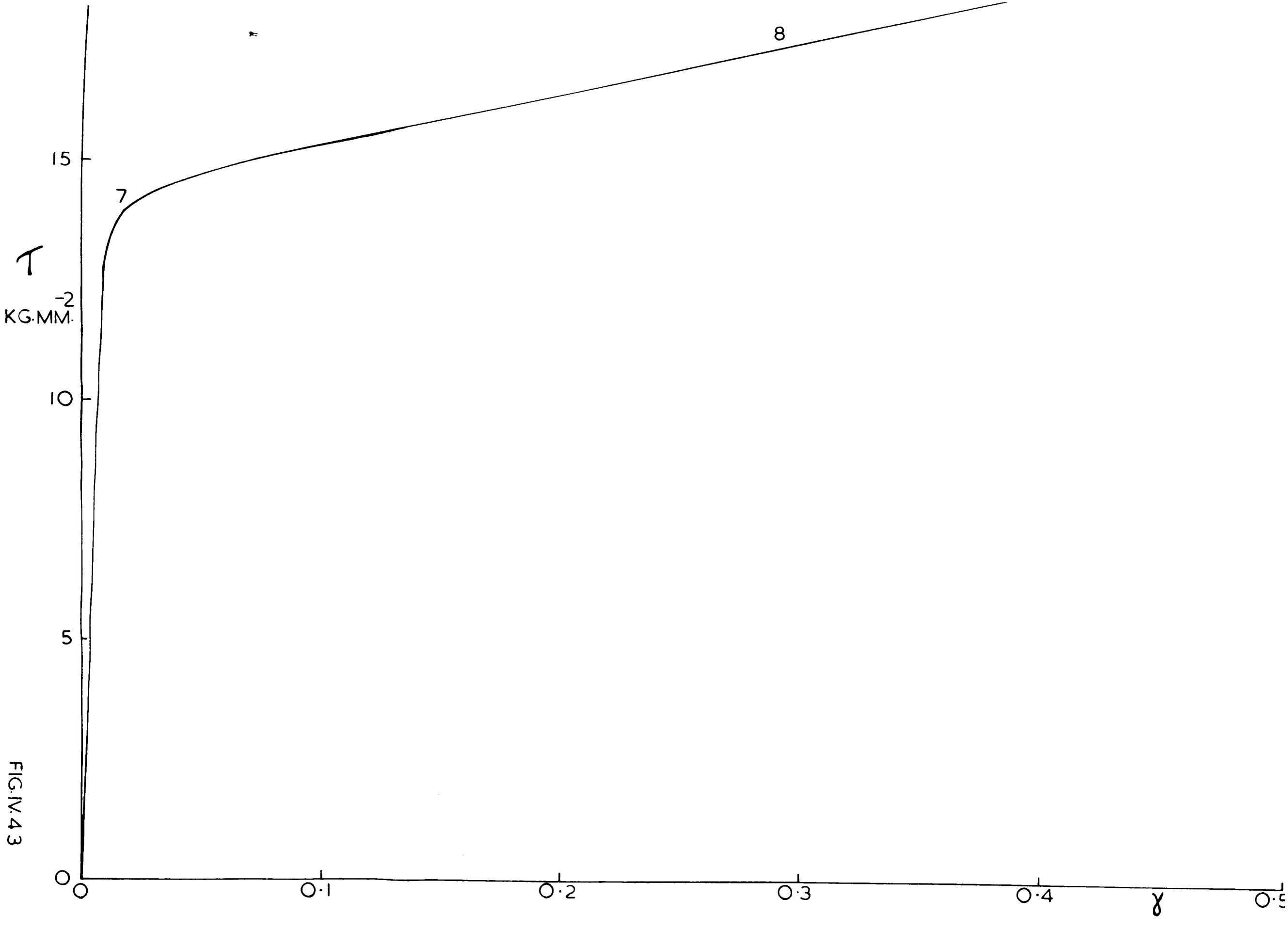


FIG. IV. 43

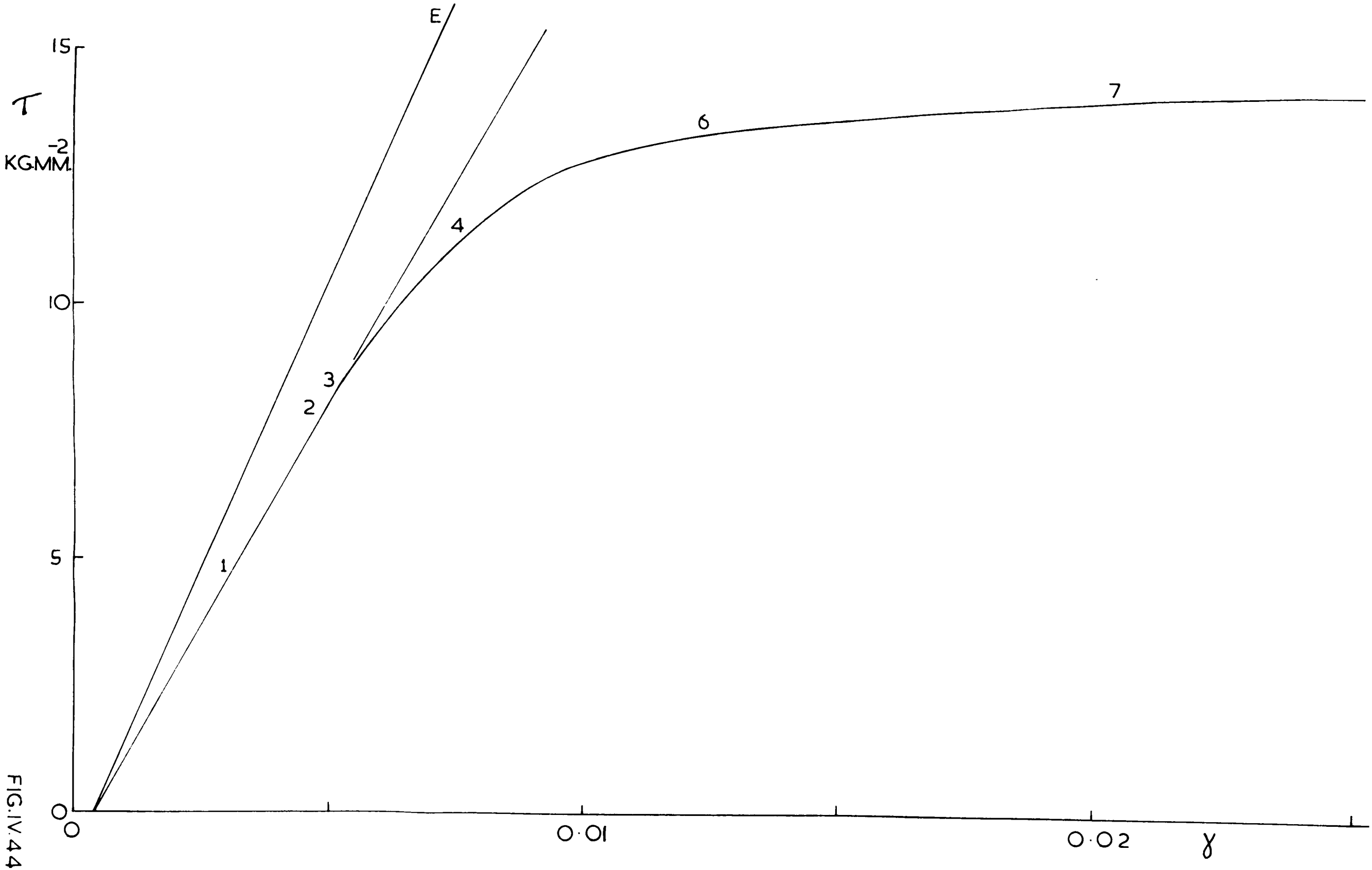


FIG.IV.44

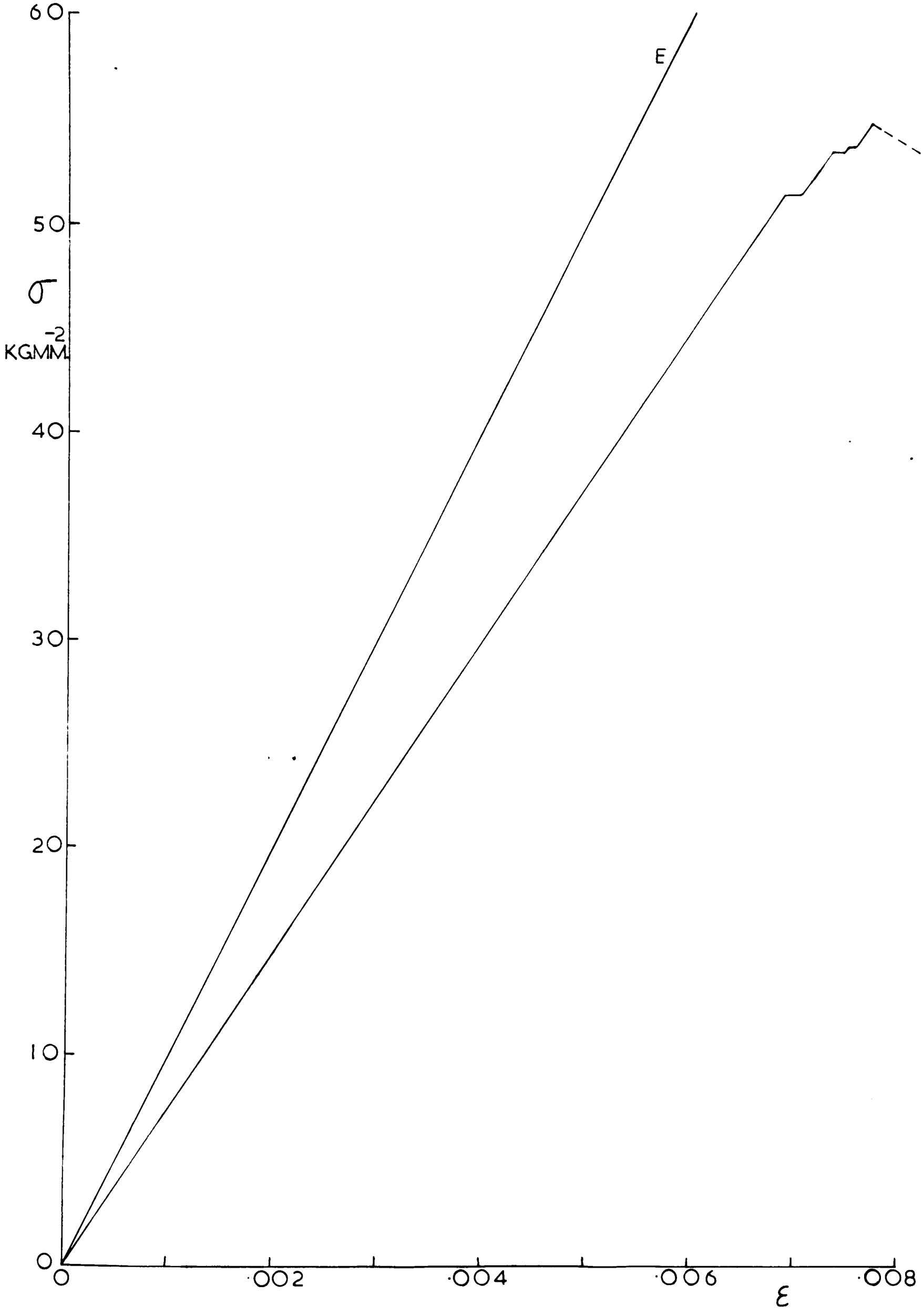


FIG. IV. 45

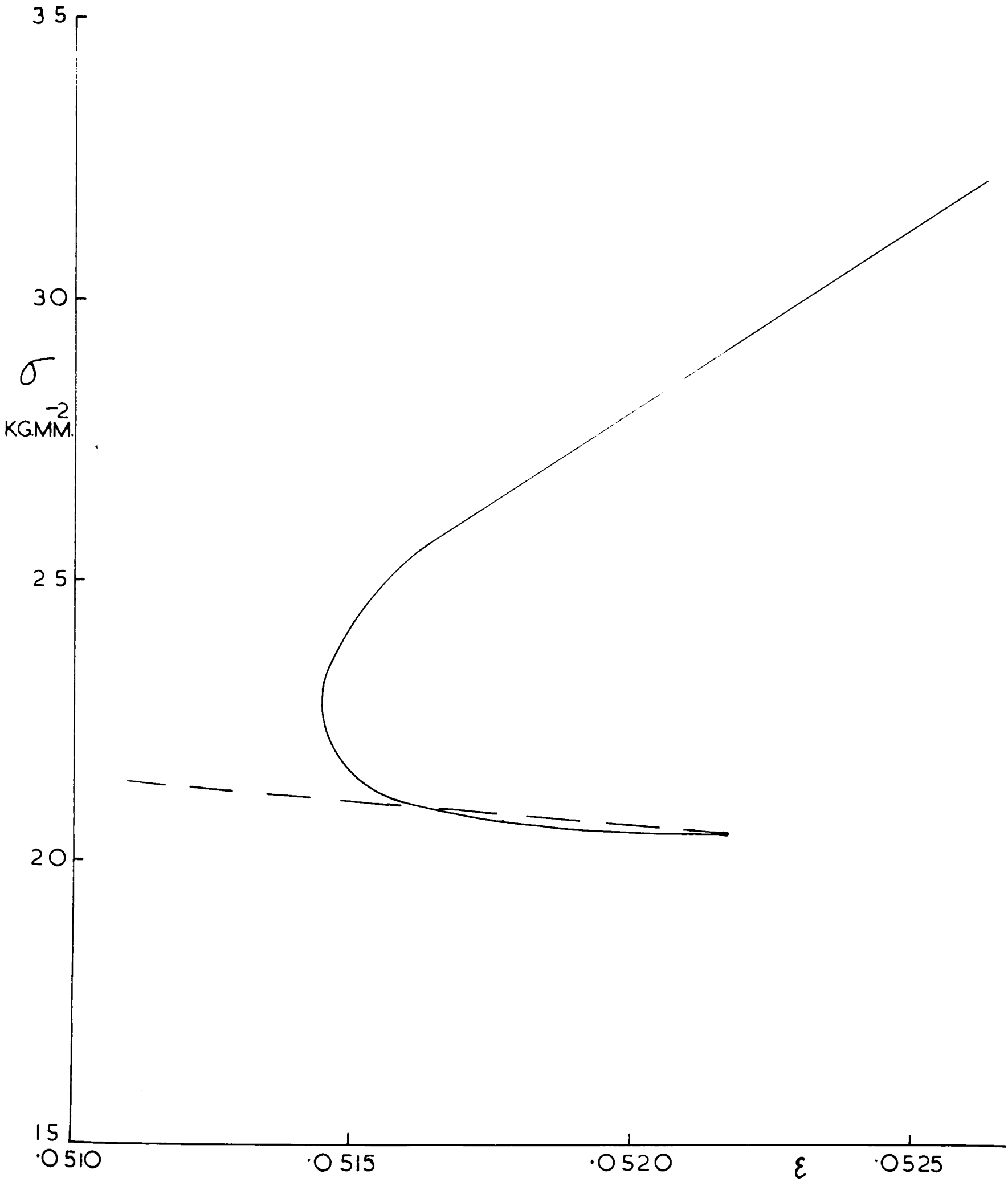


FIG.IV.46

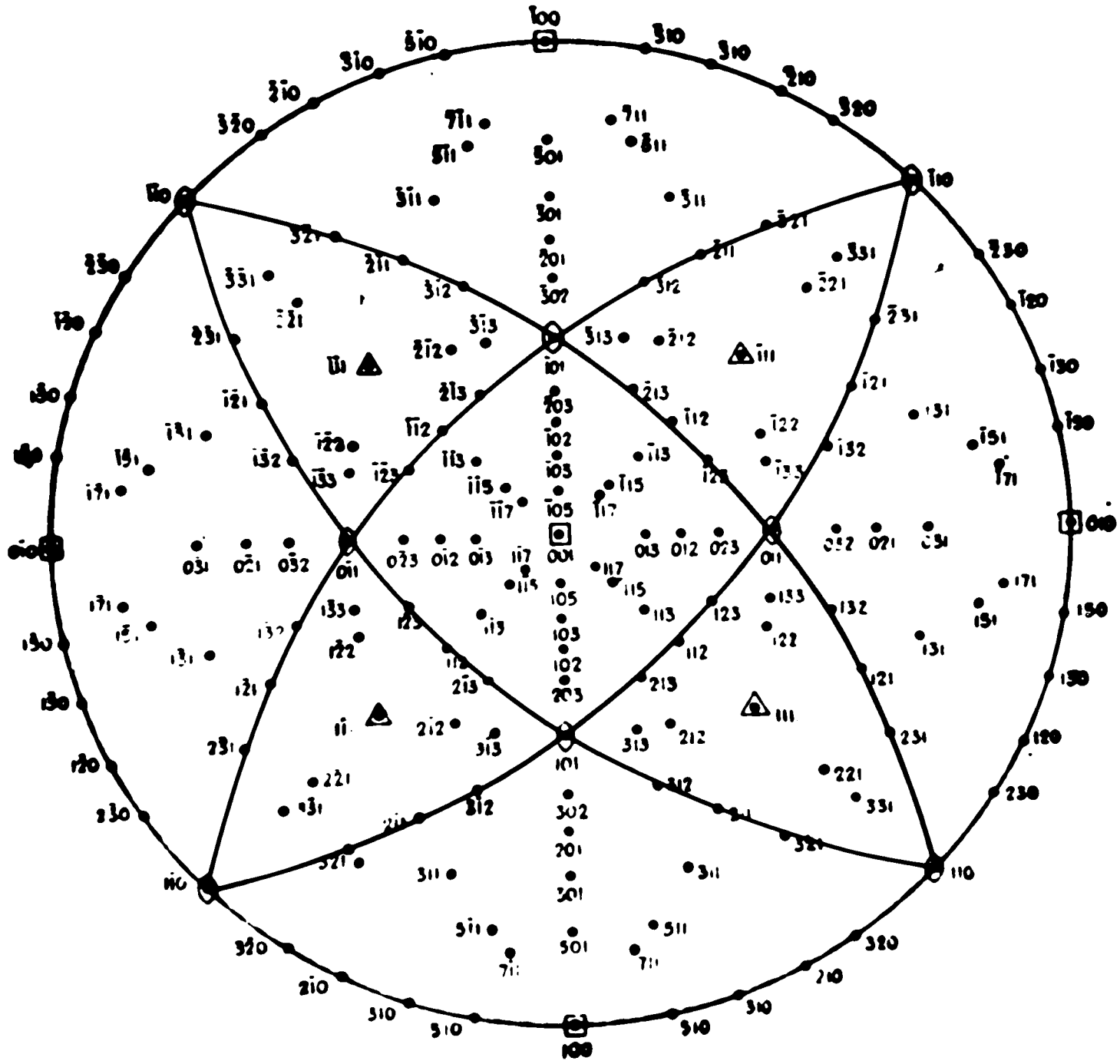


FIG IV47

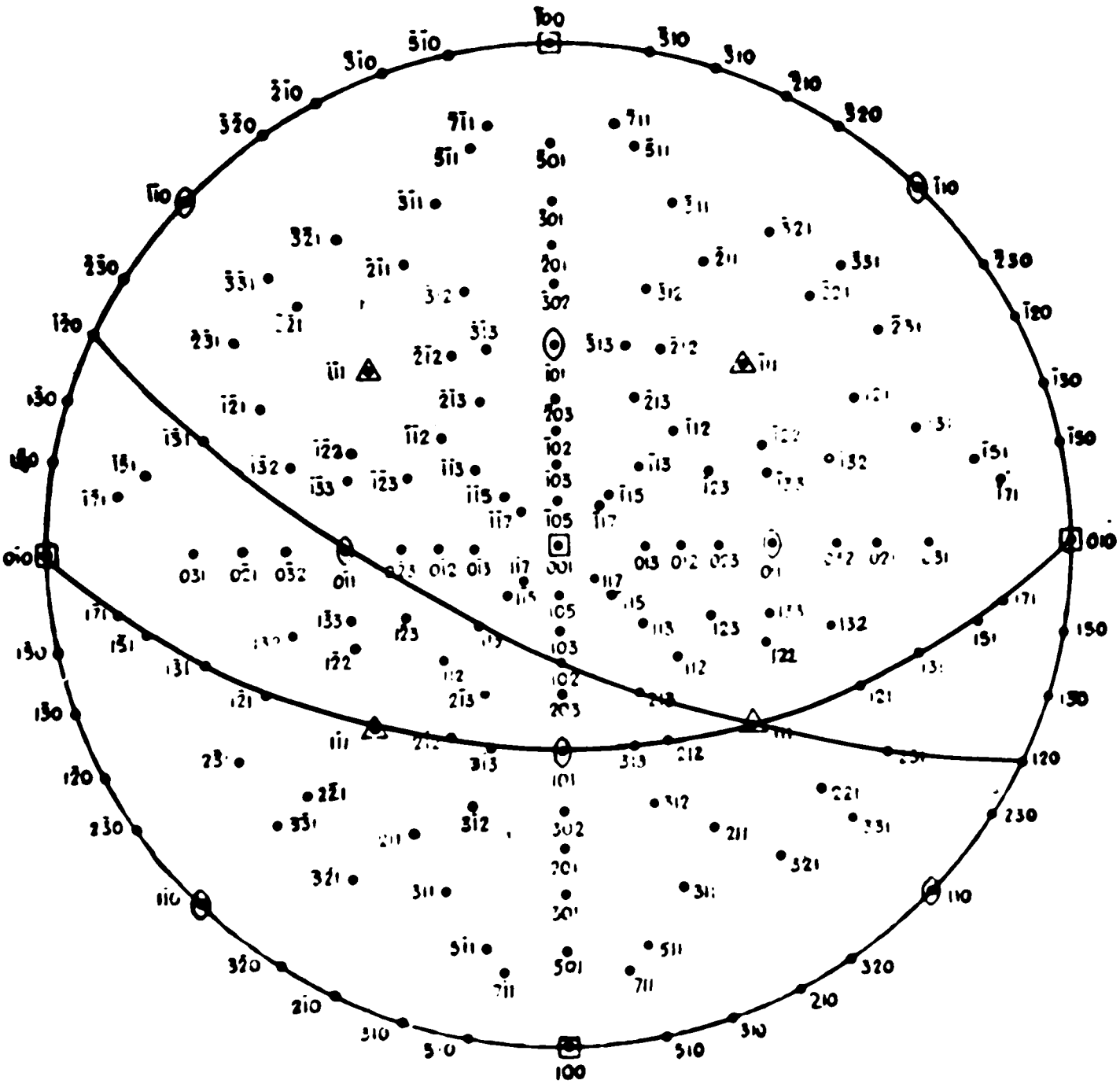
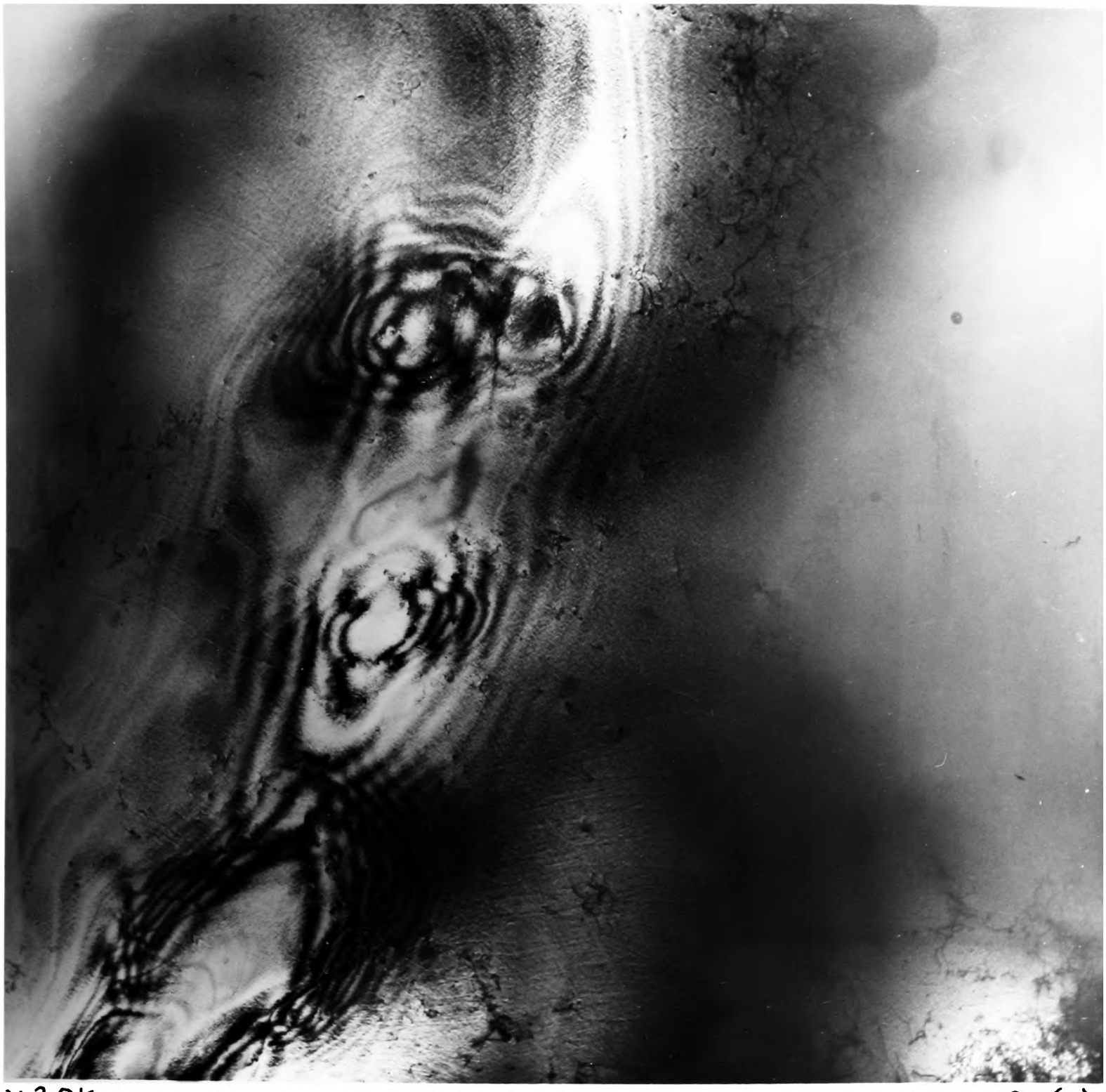


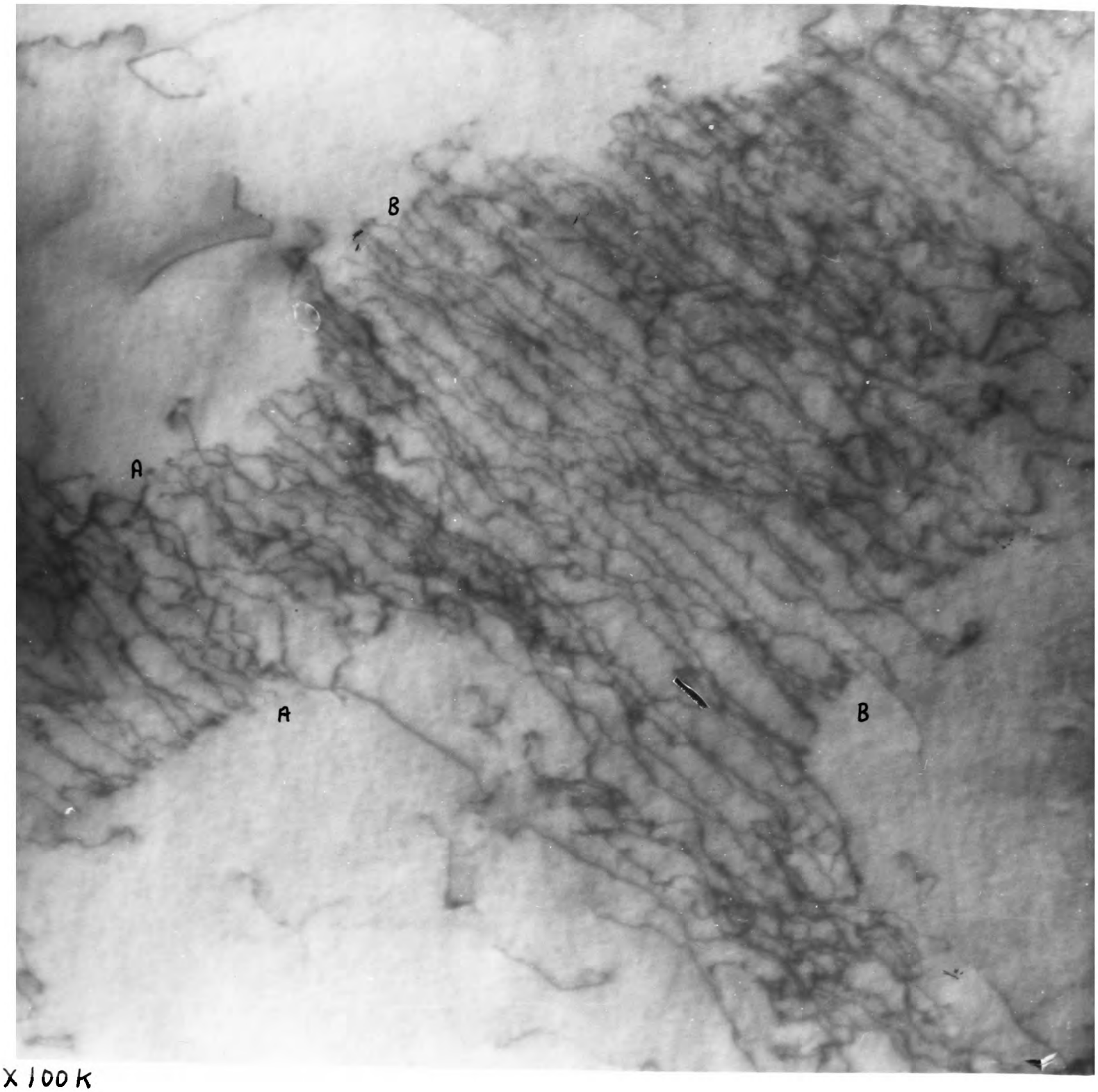
FIG.IV48



x 20K

g=⟨110⟩

FIG. IV 49



X 100 K

FIG. IV 50

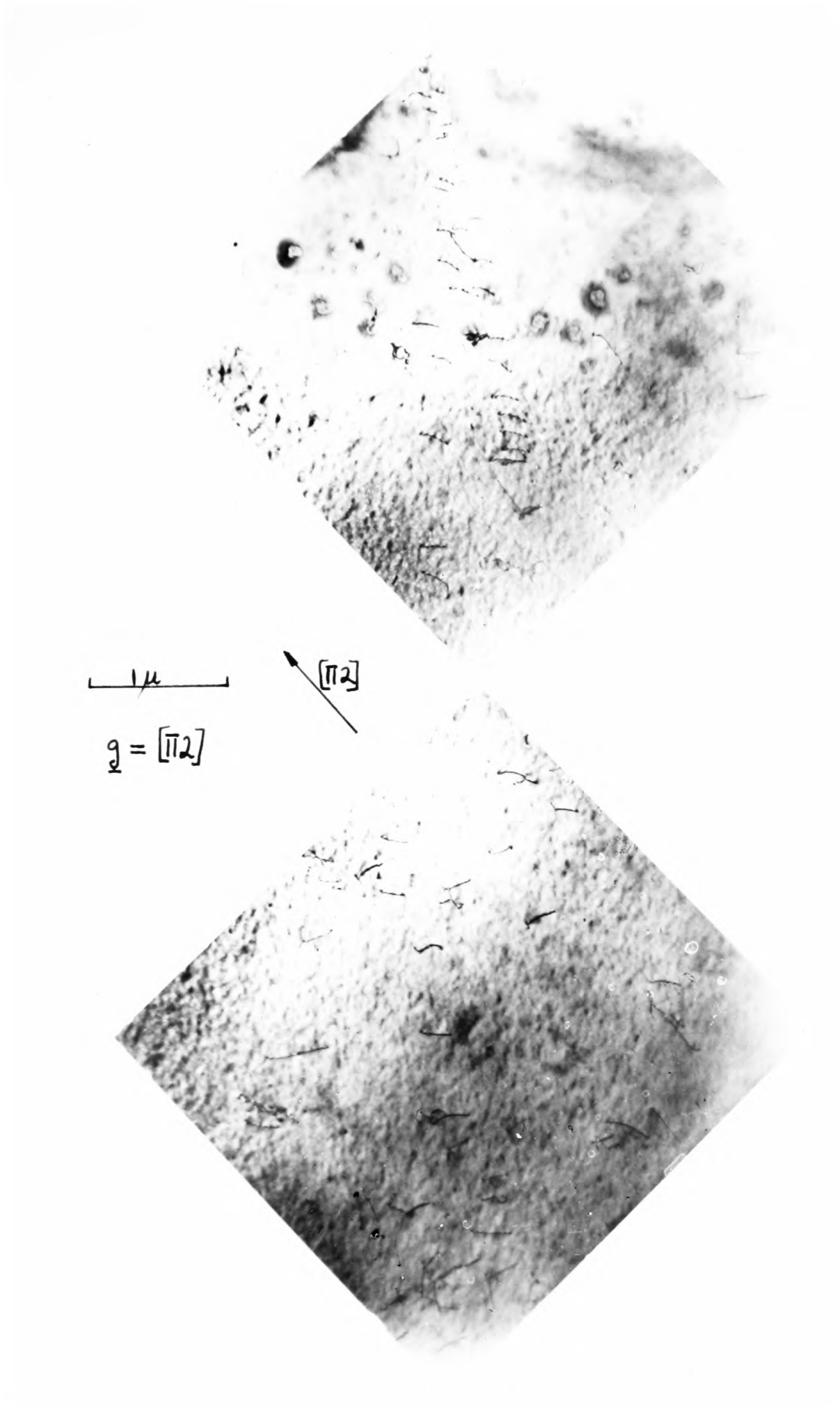
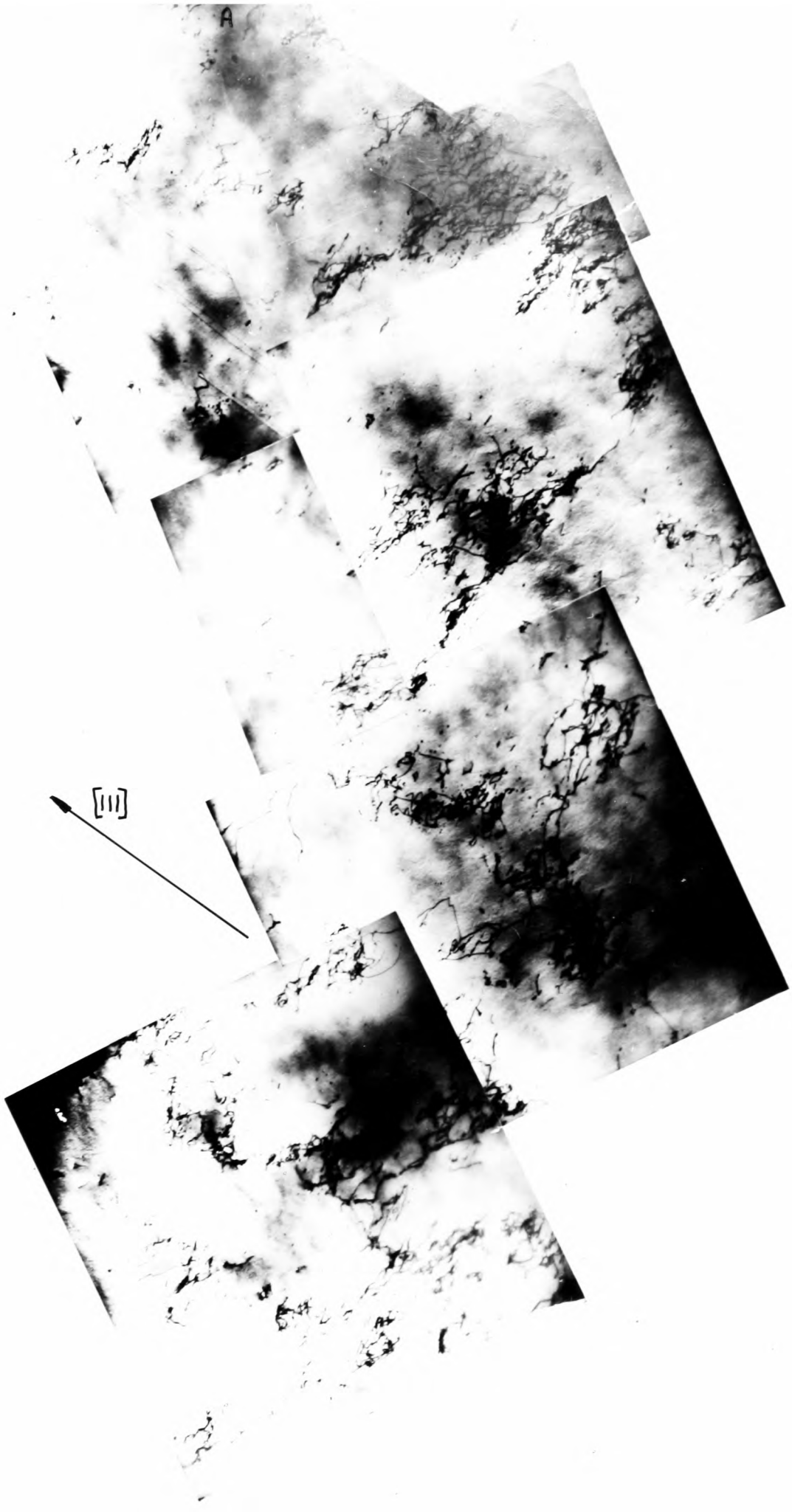


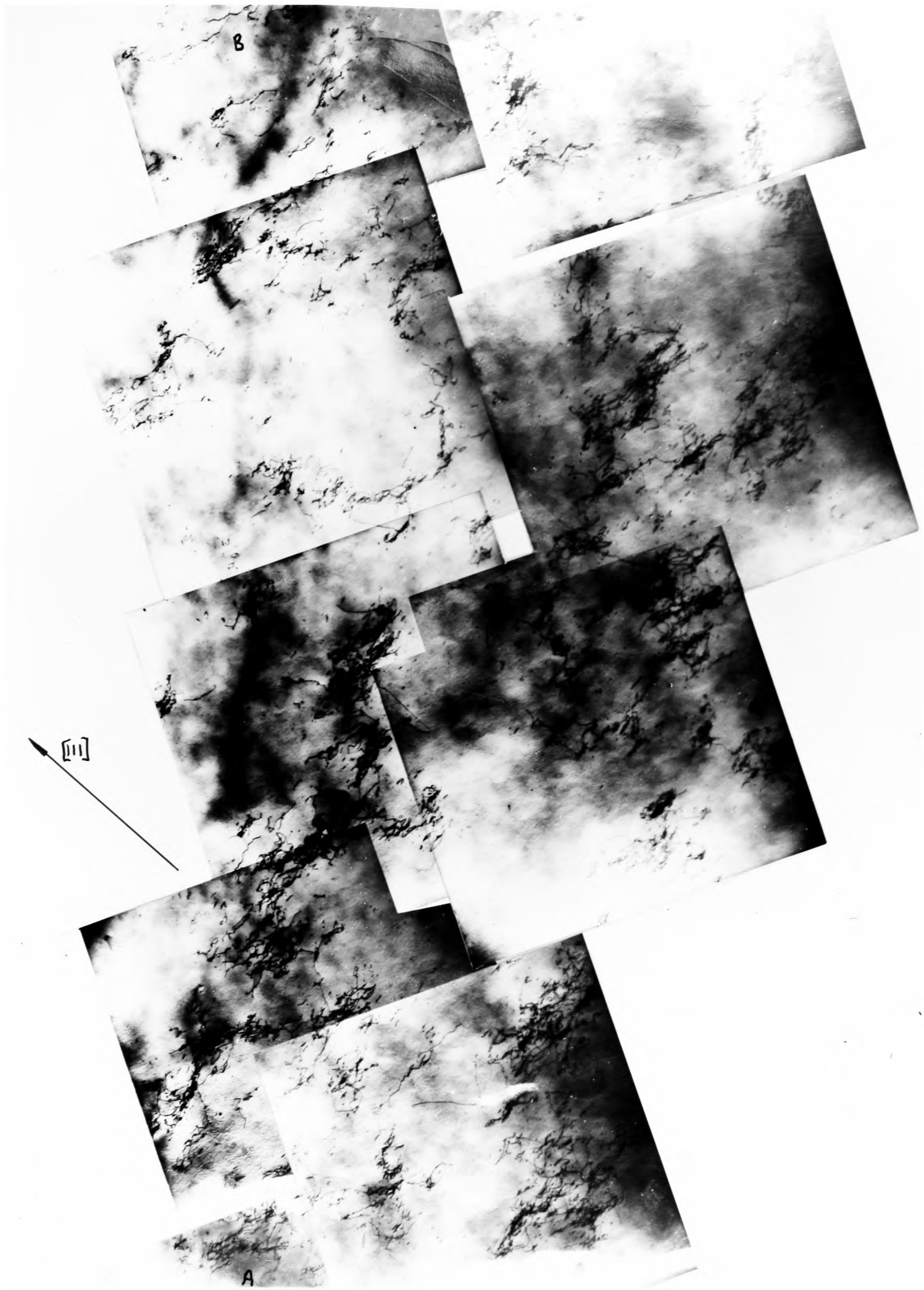
FIG IV 51



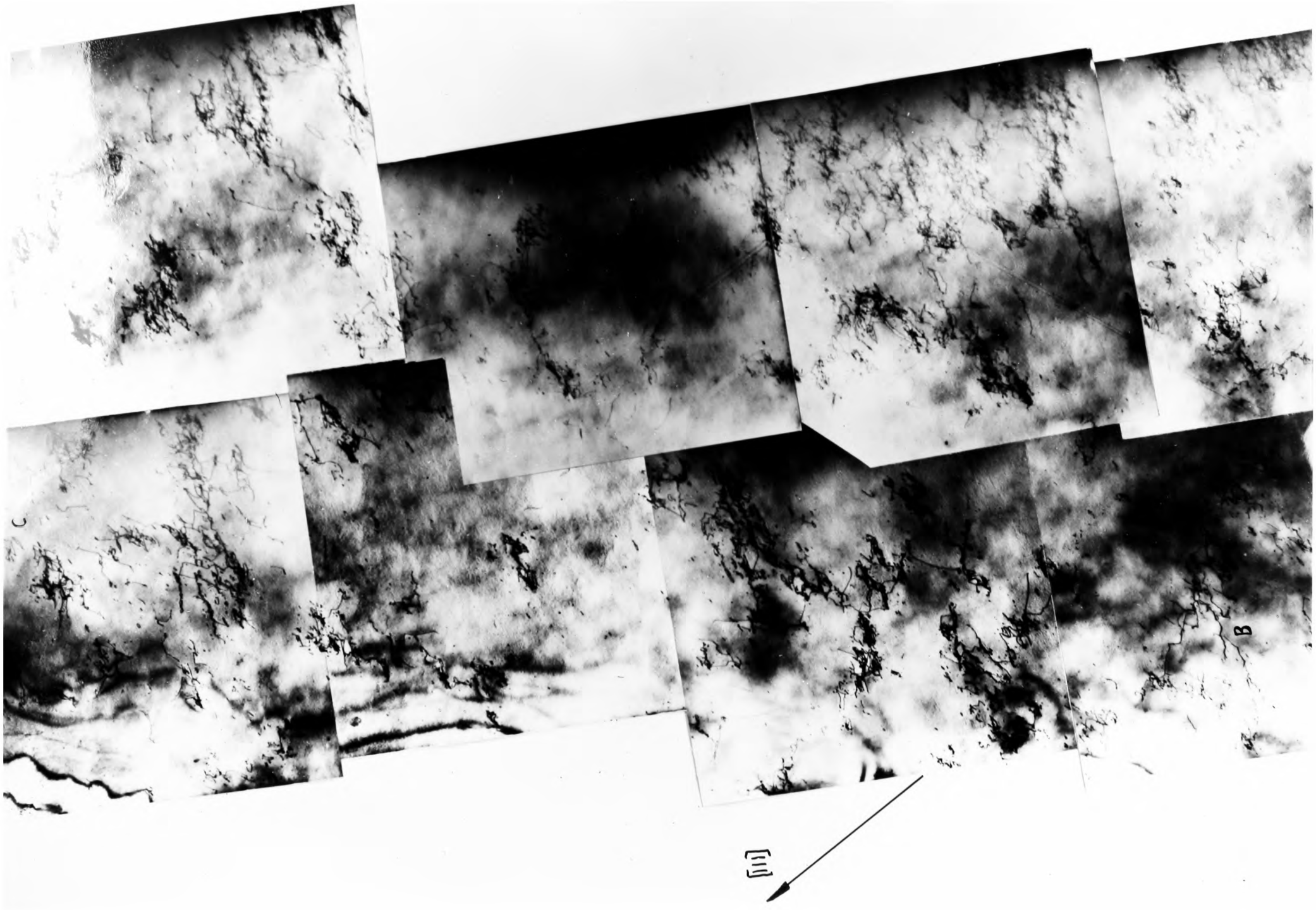
X8000

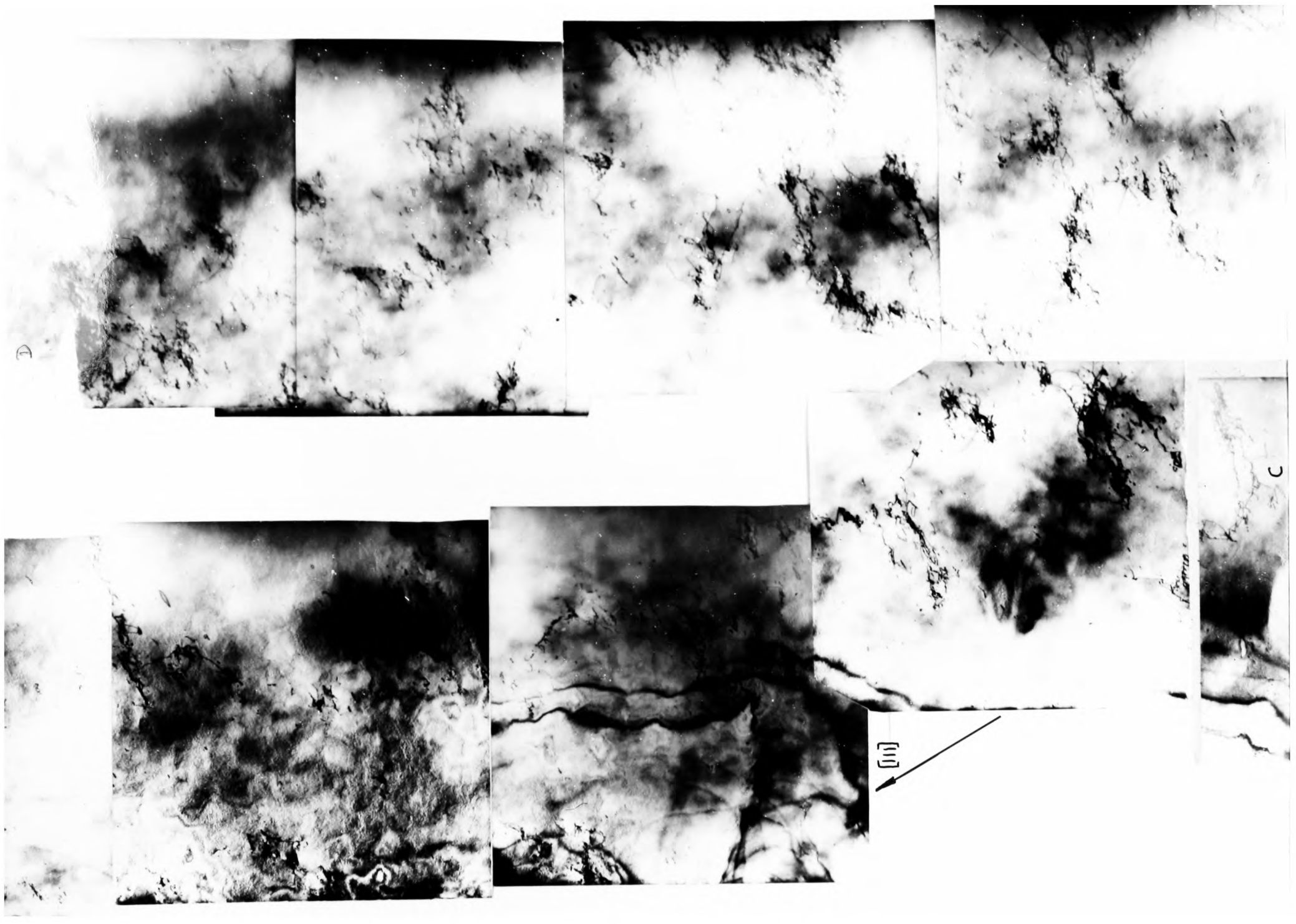
$\underline{g} = [101]$

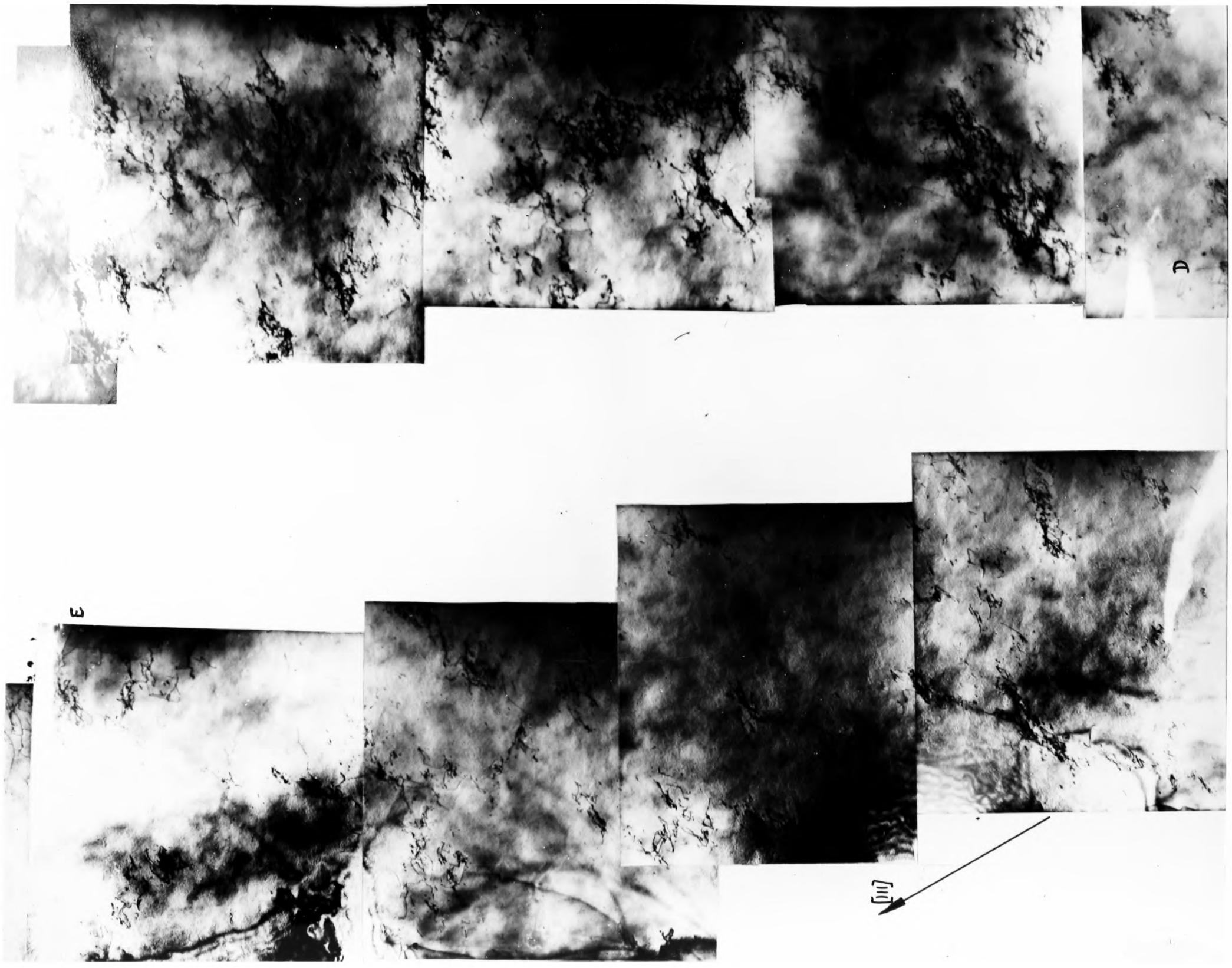
FIG. IV 52 a

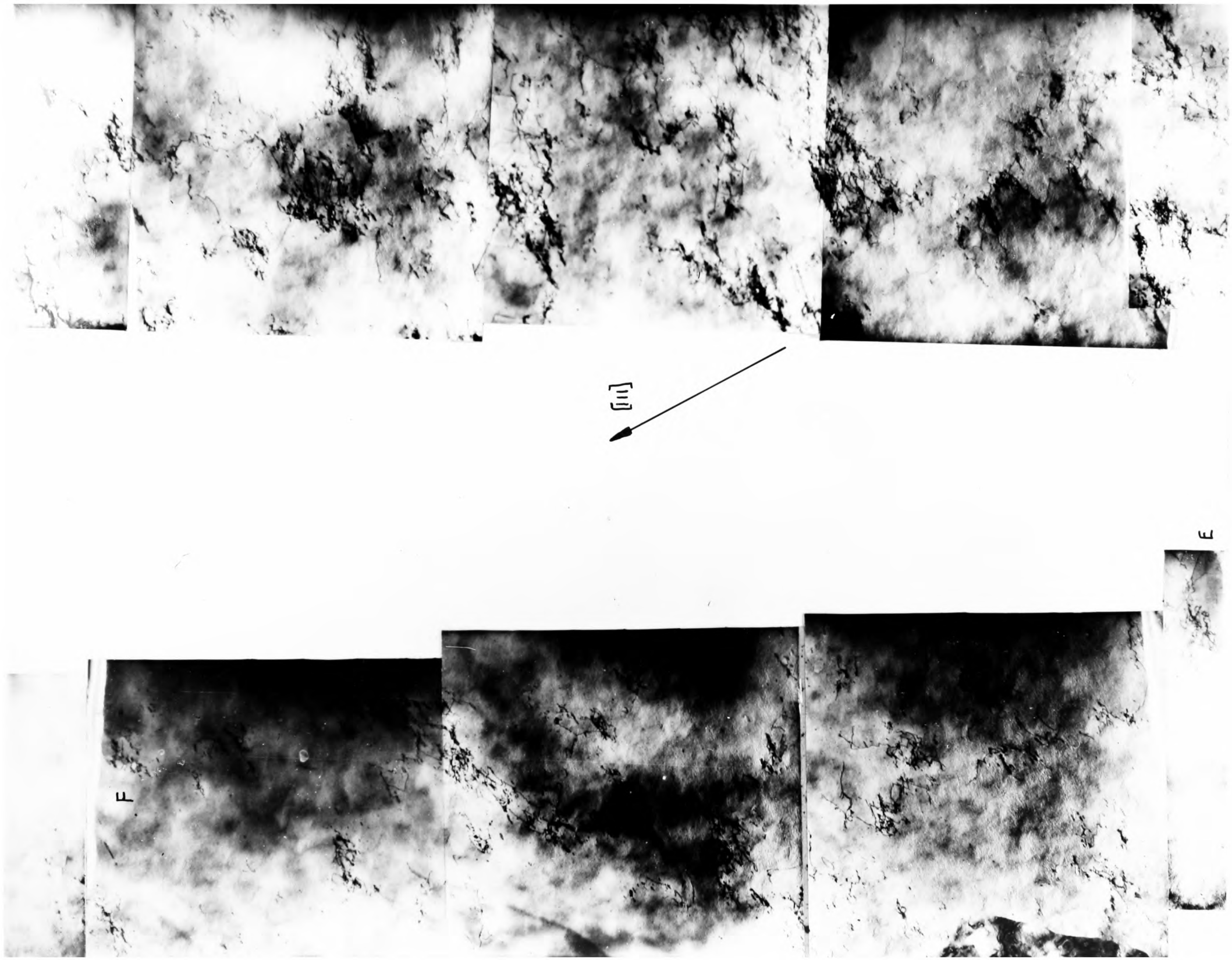


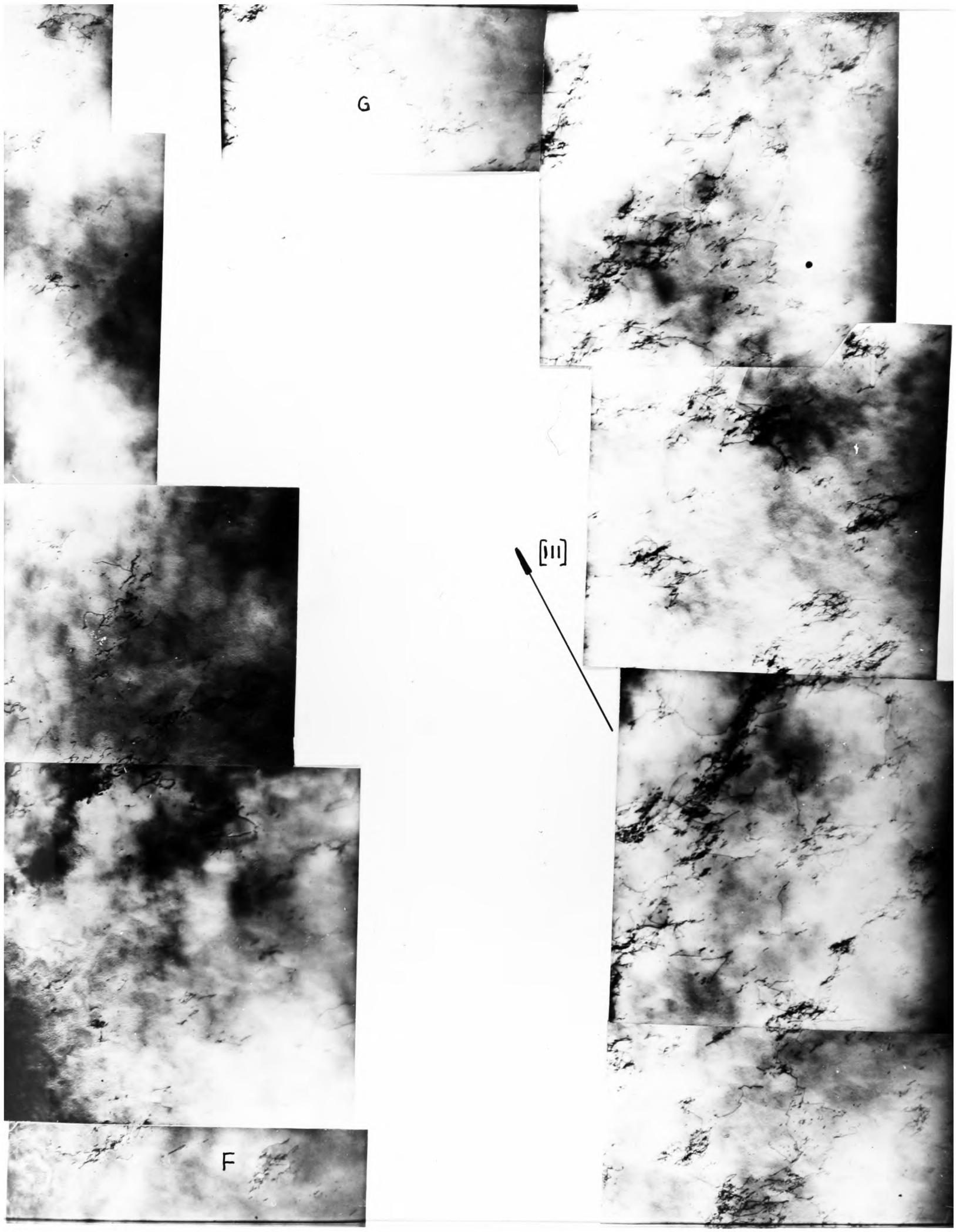
b

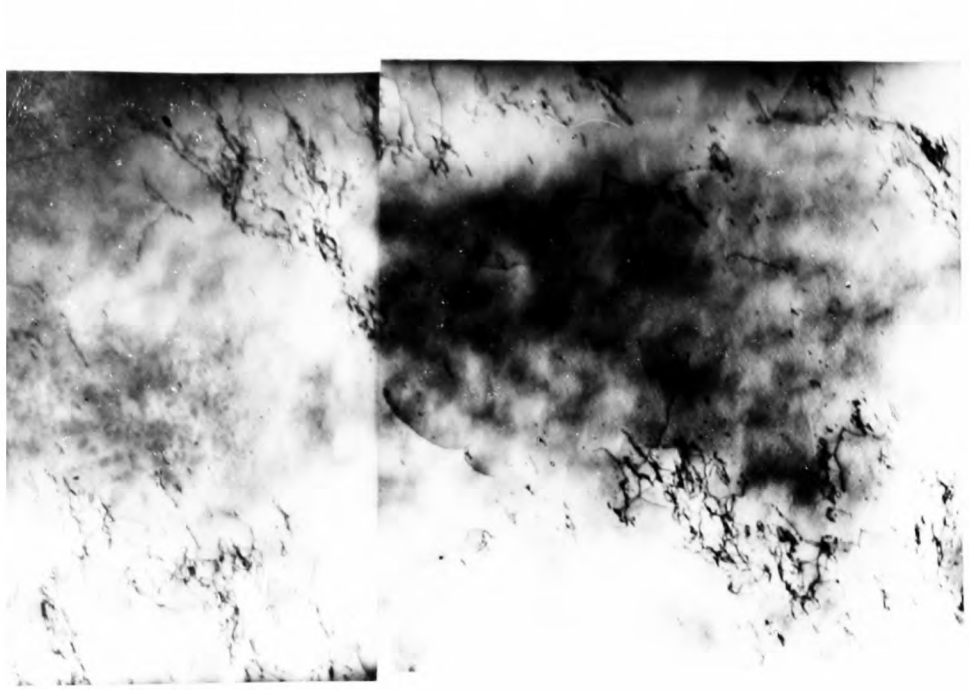

C
B
C


A
B
C
[111]

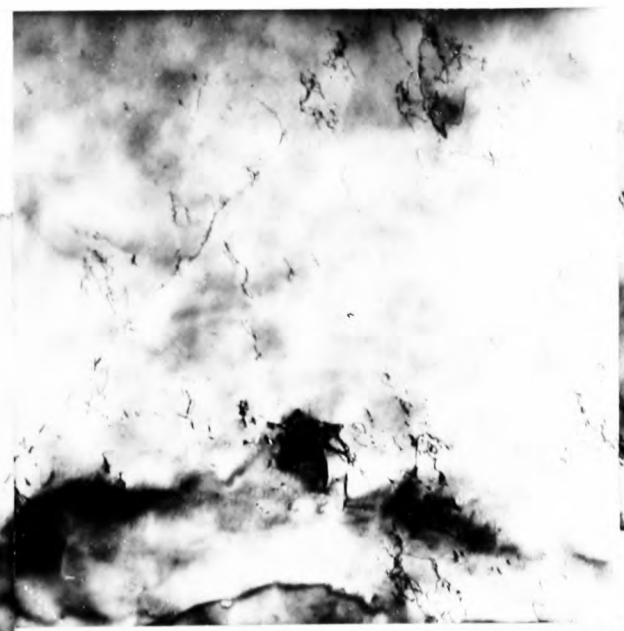

A
B
[111]


E
F

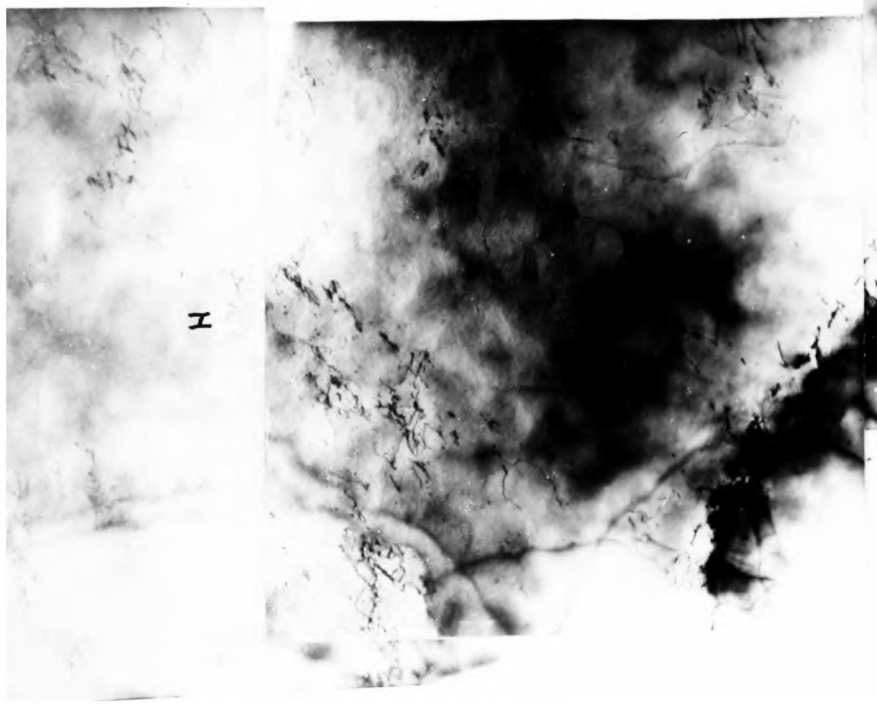

G
[11]
F

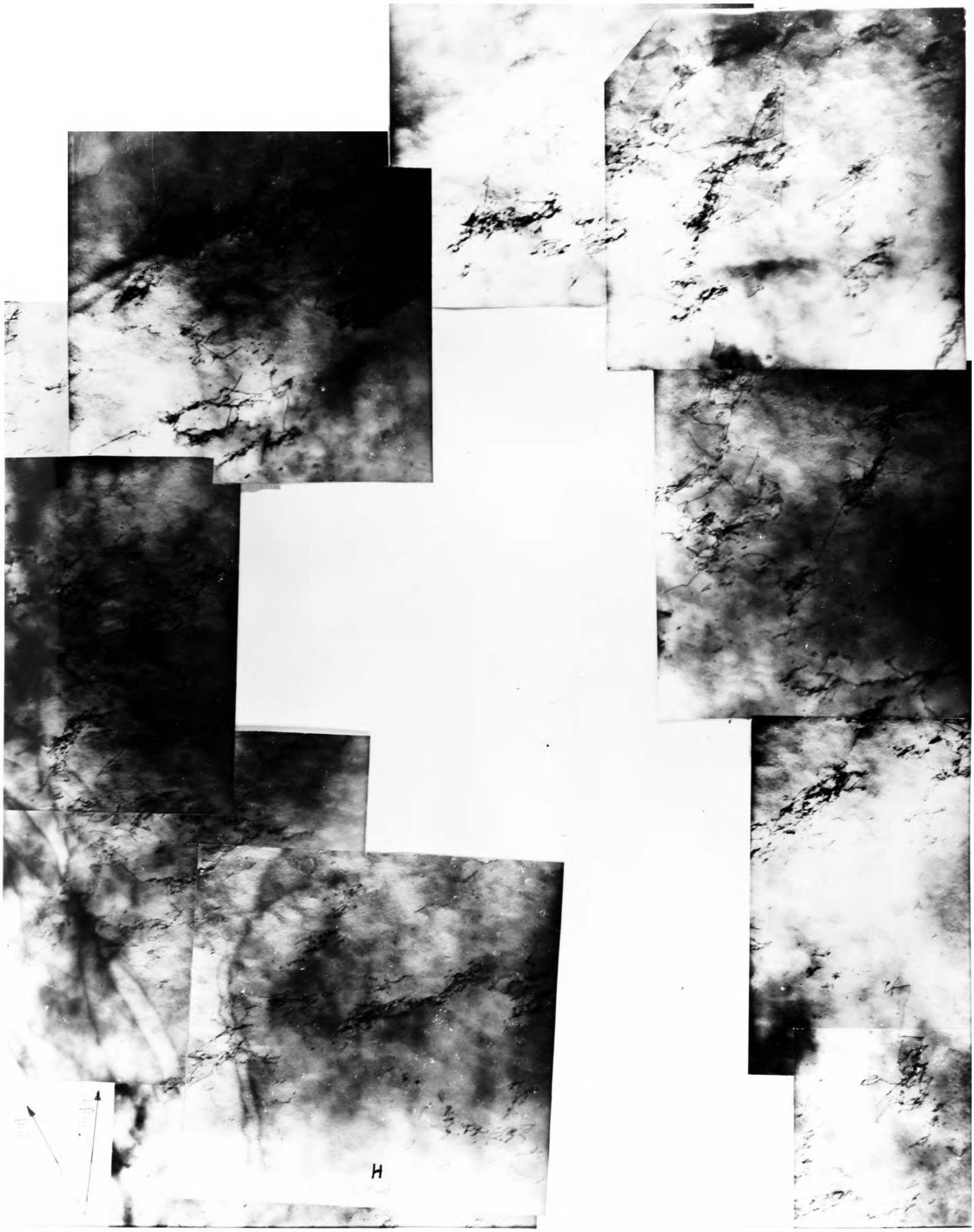


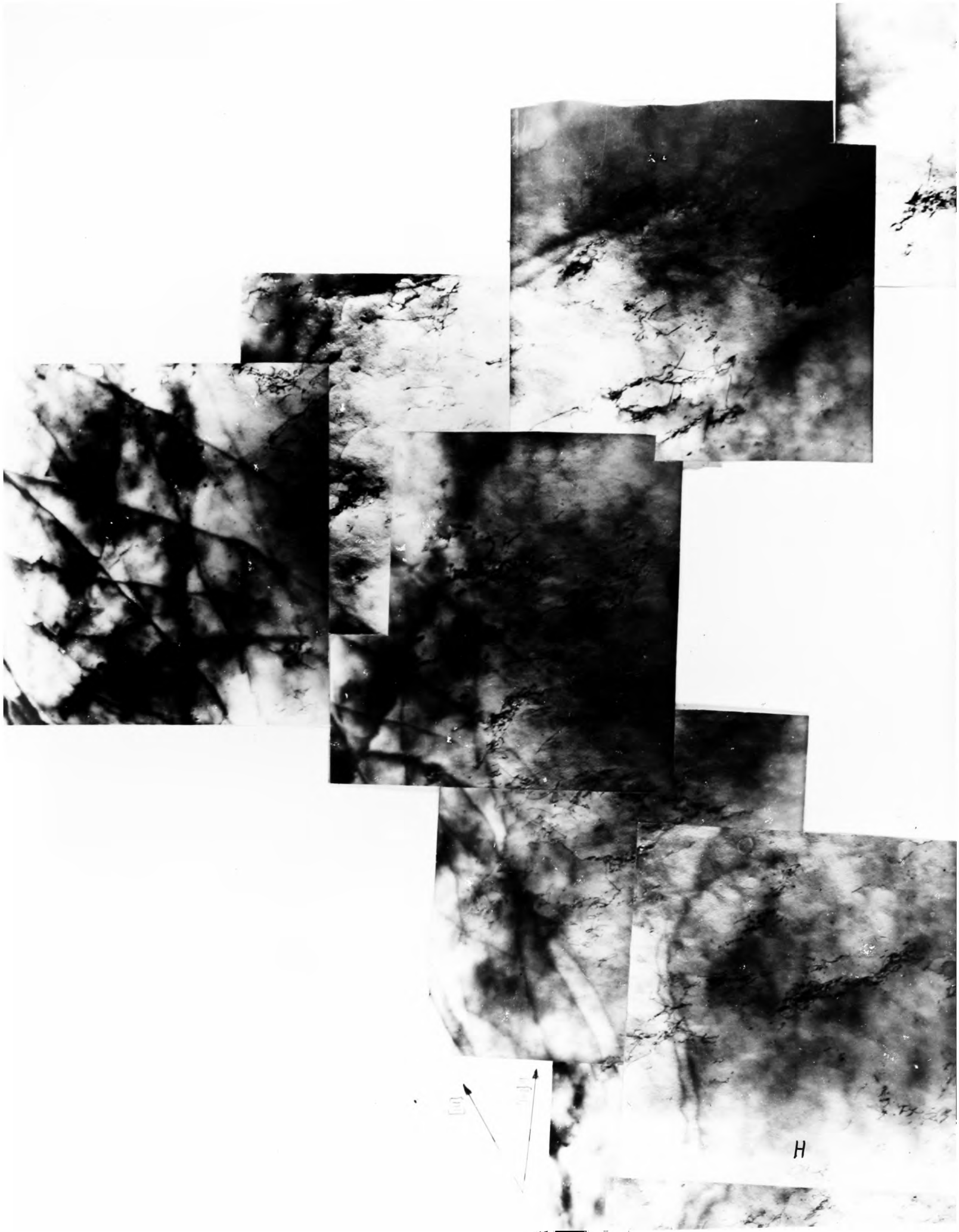


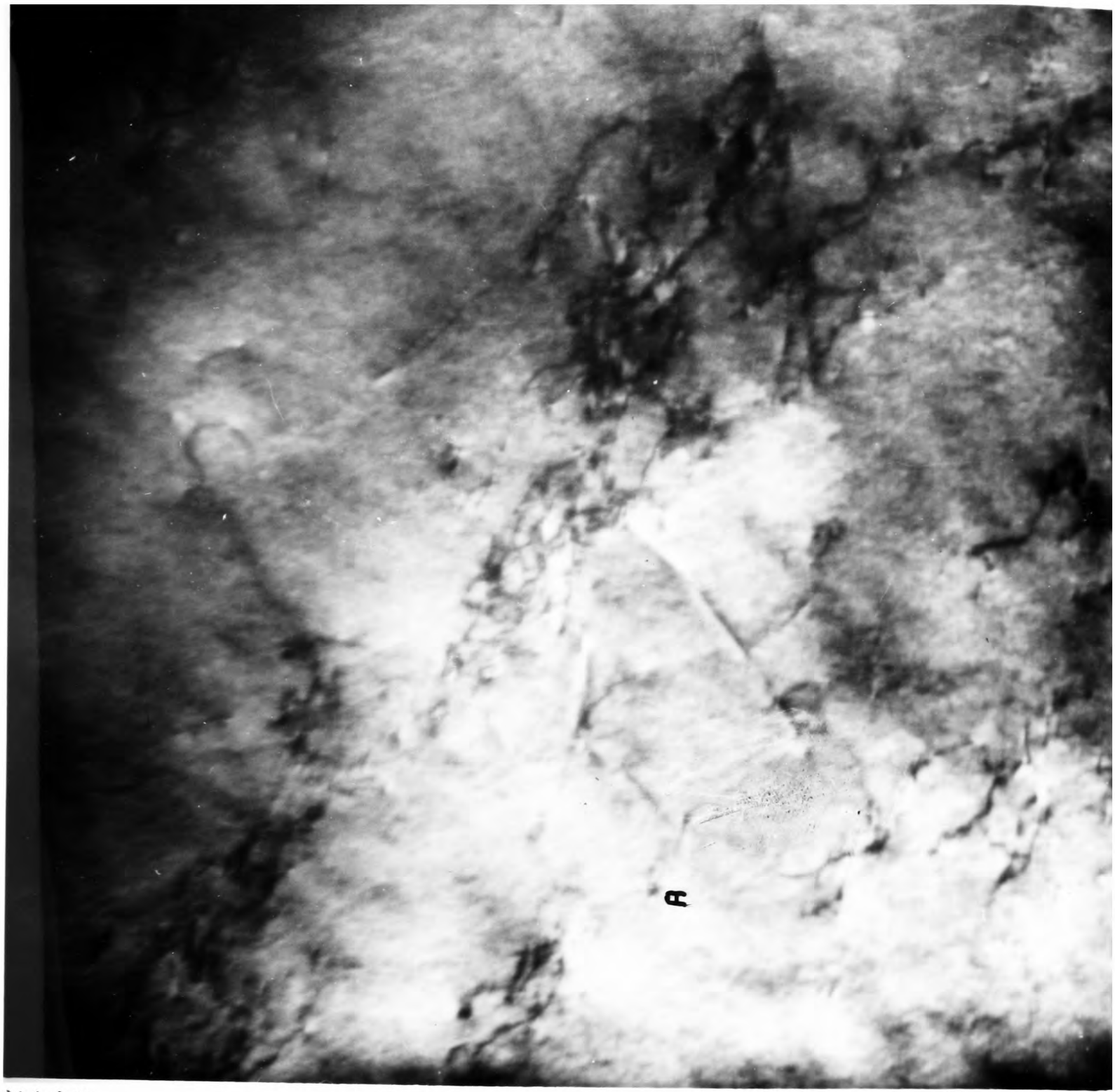







H

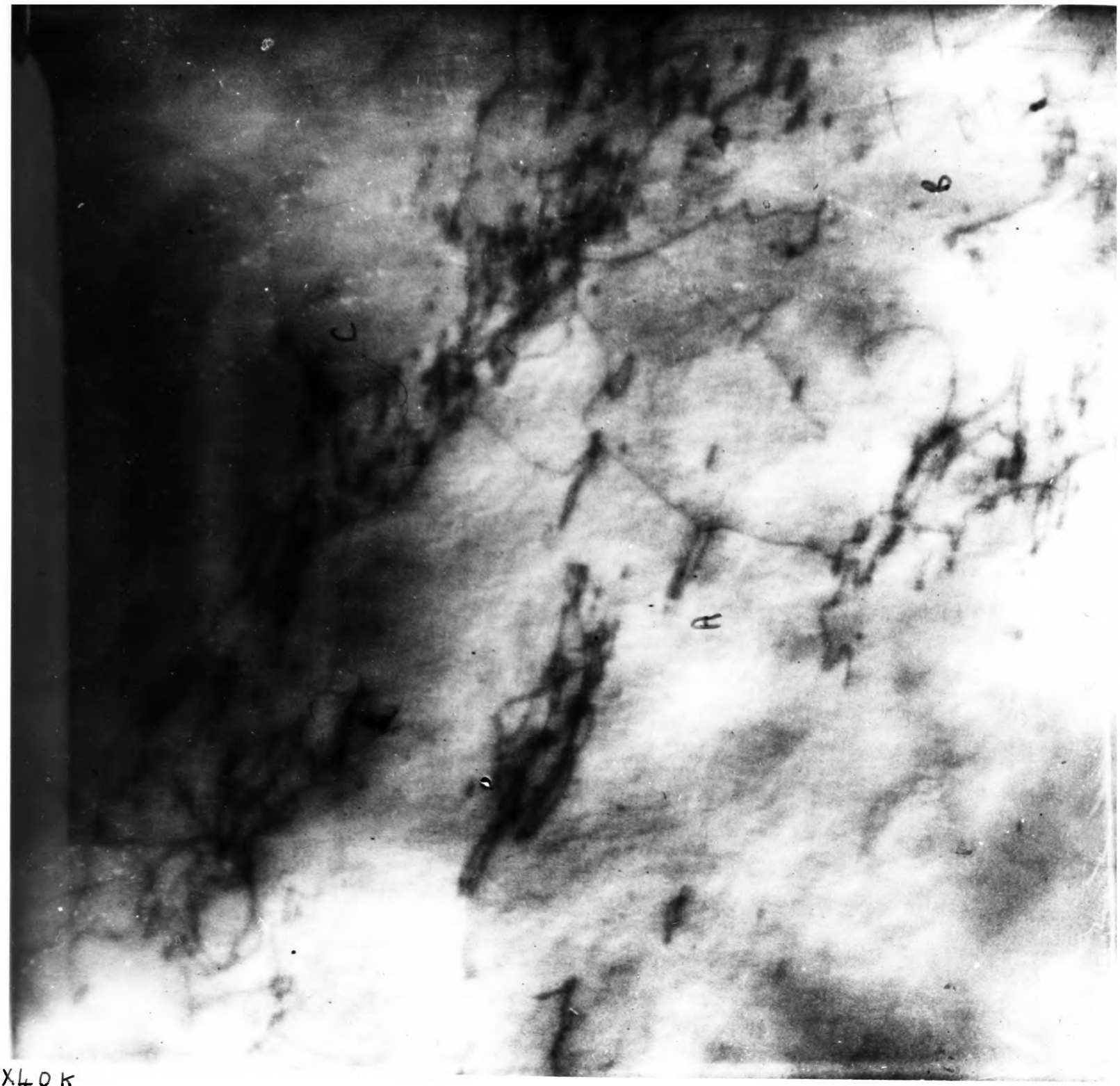

H



X40K

$\underline{g} = [1\bar{2}]$

FIG. IV 53a

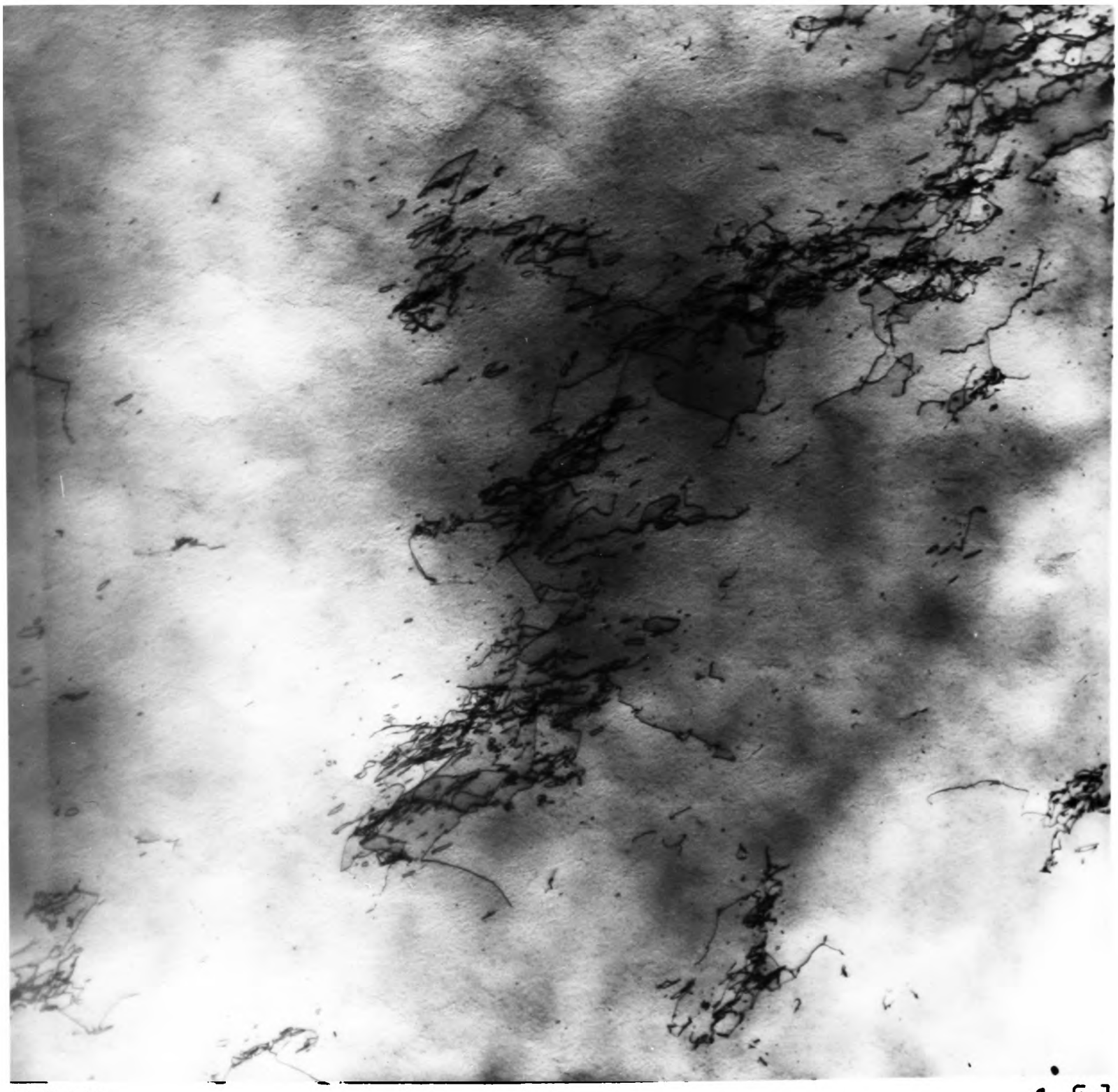


X40K

$\underline{g} = [101]$

[111]

FIG. IV 53 b



X 20K

g = [101]

[111] = b

FIG. IV 54

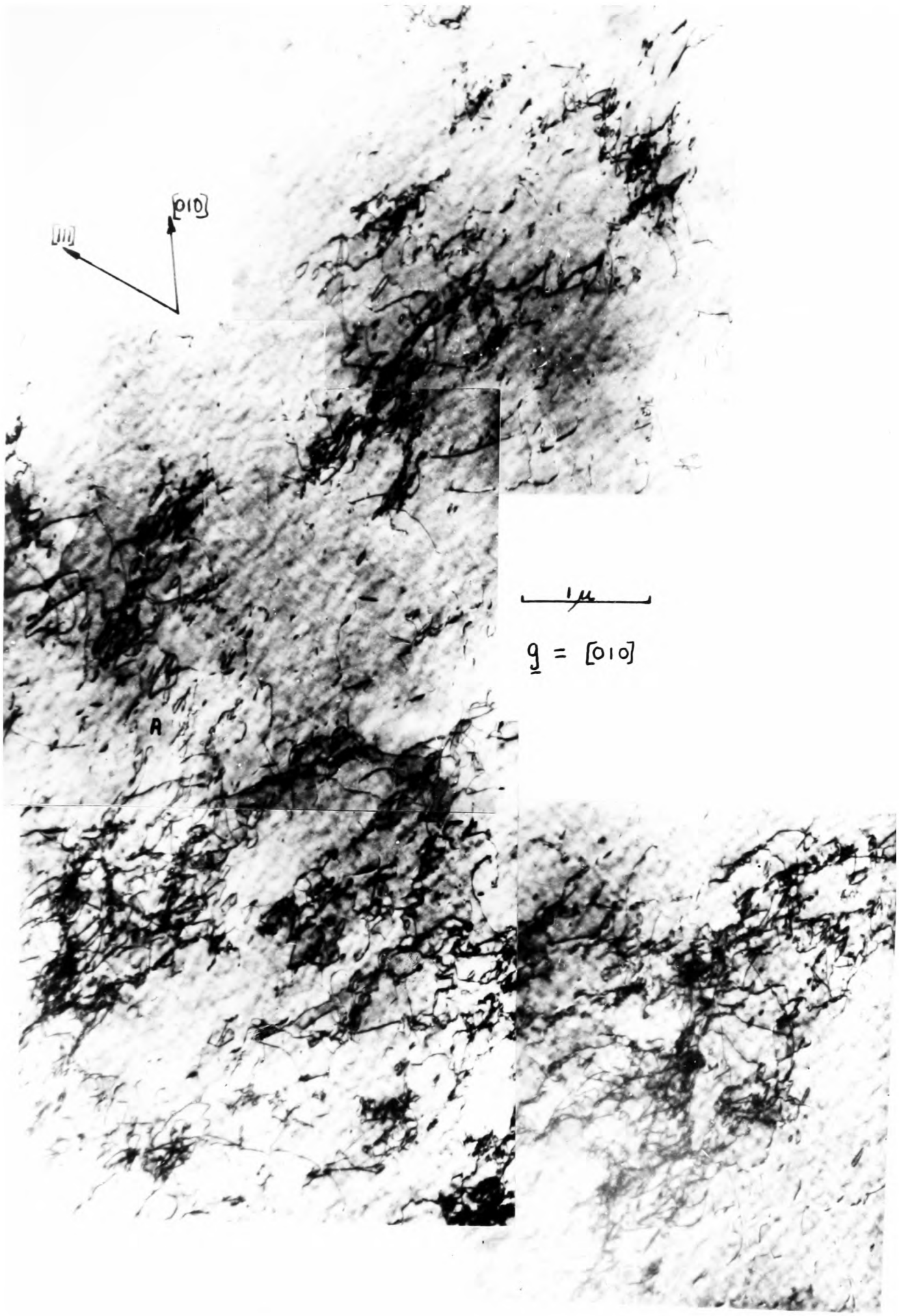
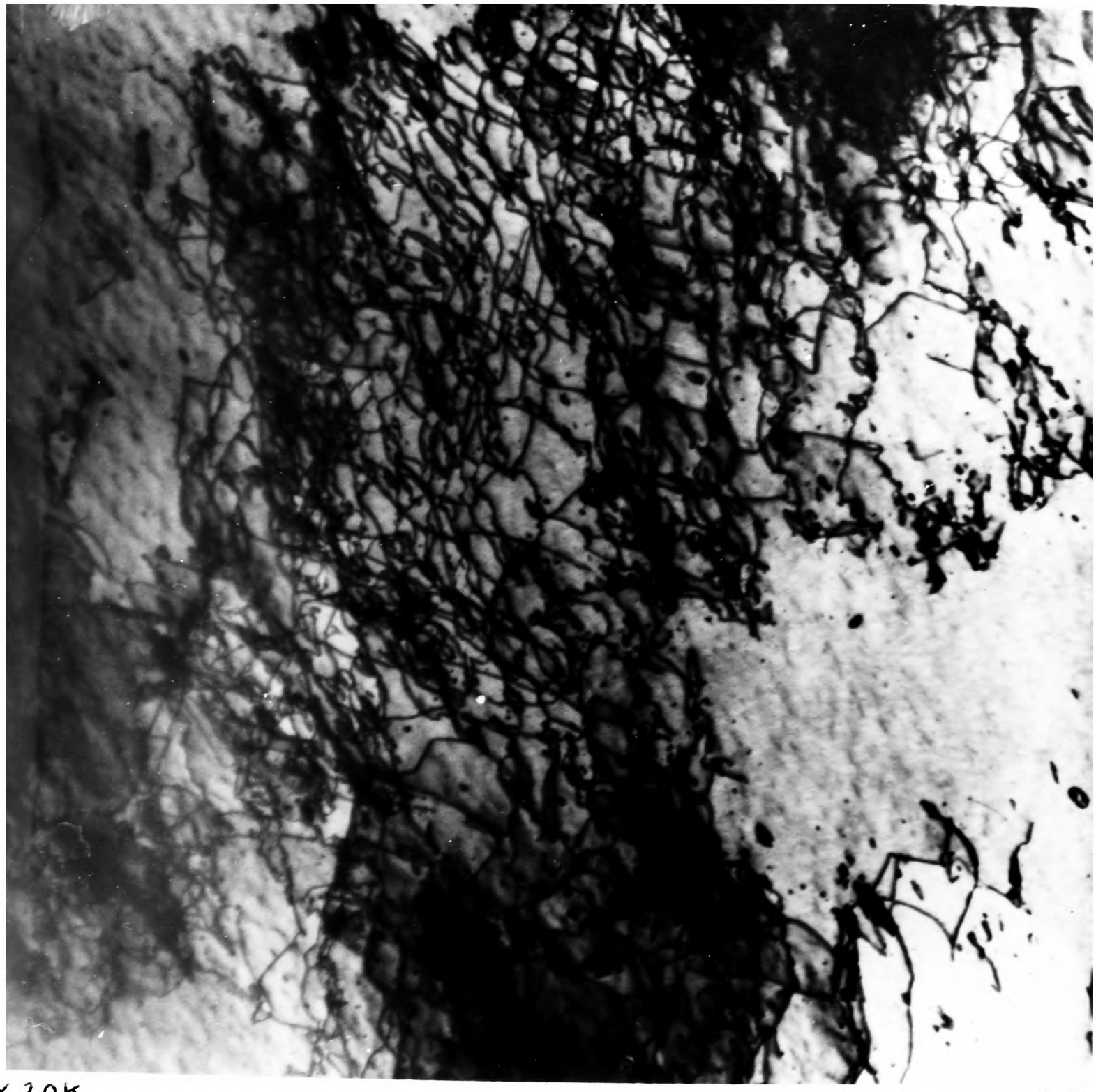


FIG. IV'55



X 20K

$\underline{g} = [101]$

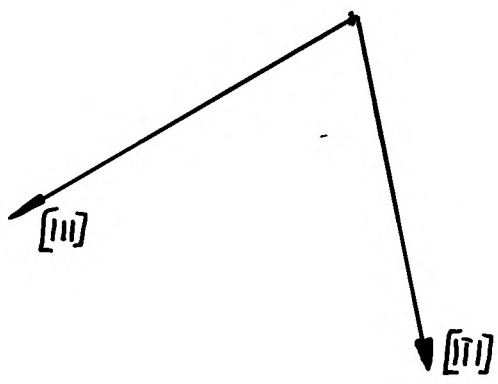
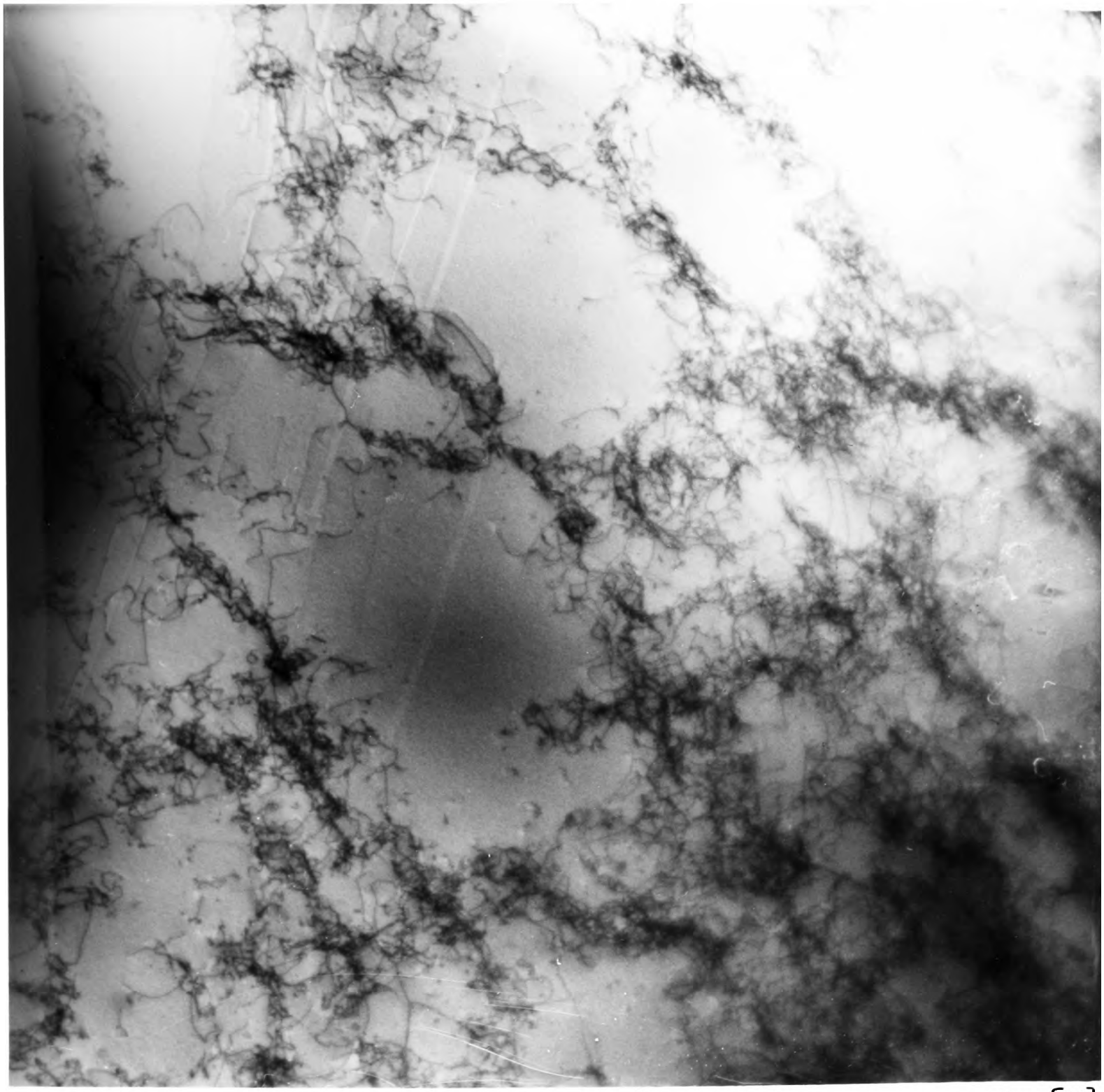


FIG. IV 56



X 20K

$\underline{g}$ = [101]

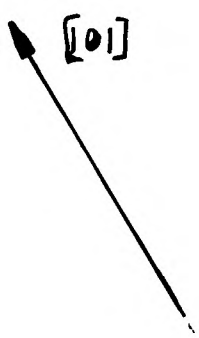


FIG. IV 57

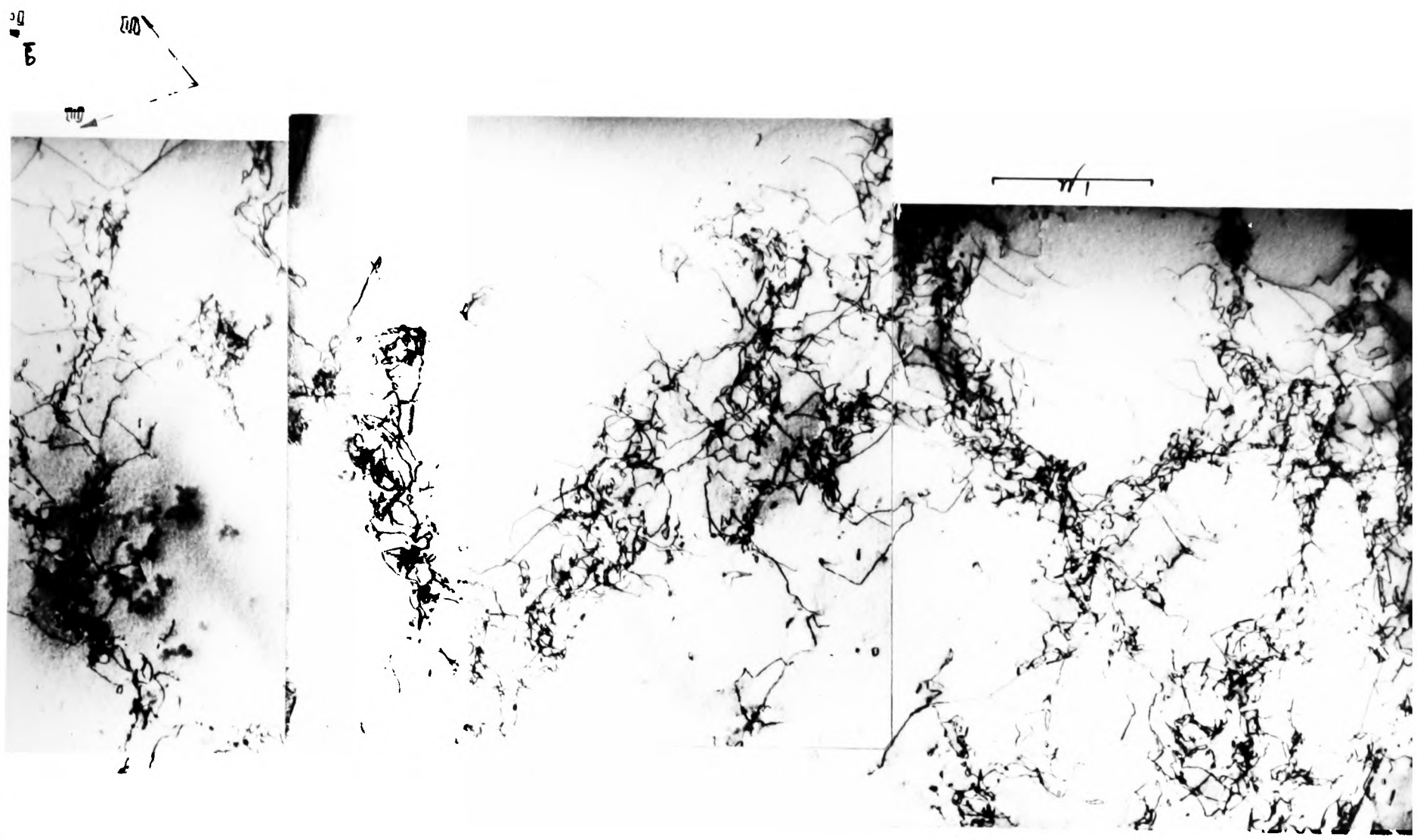
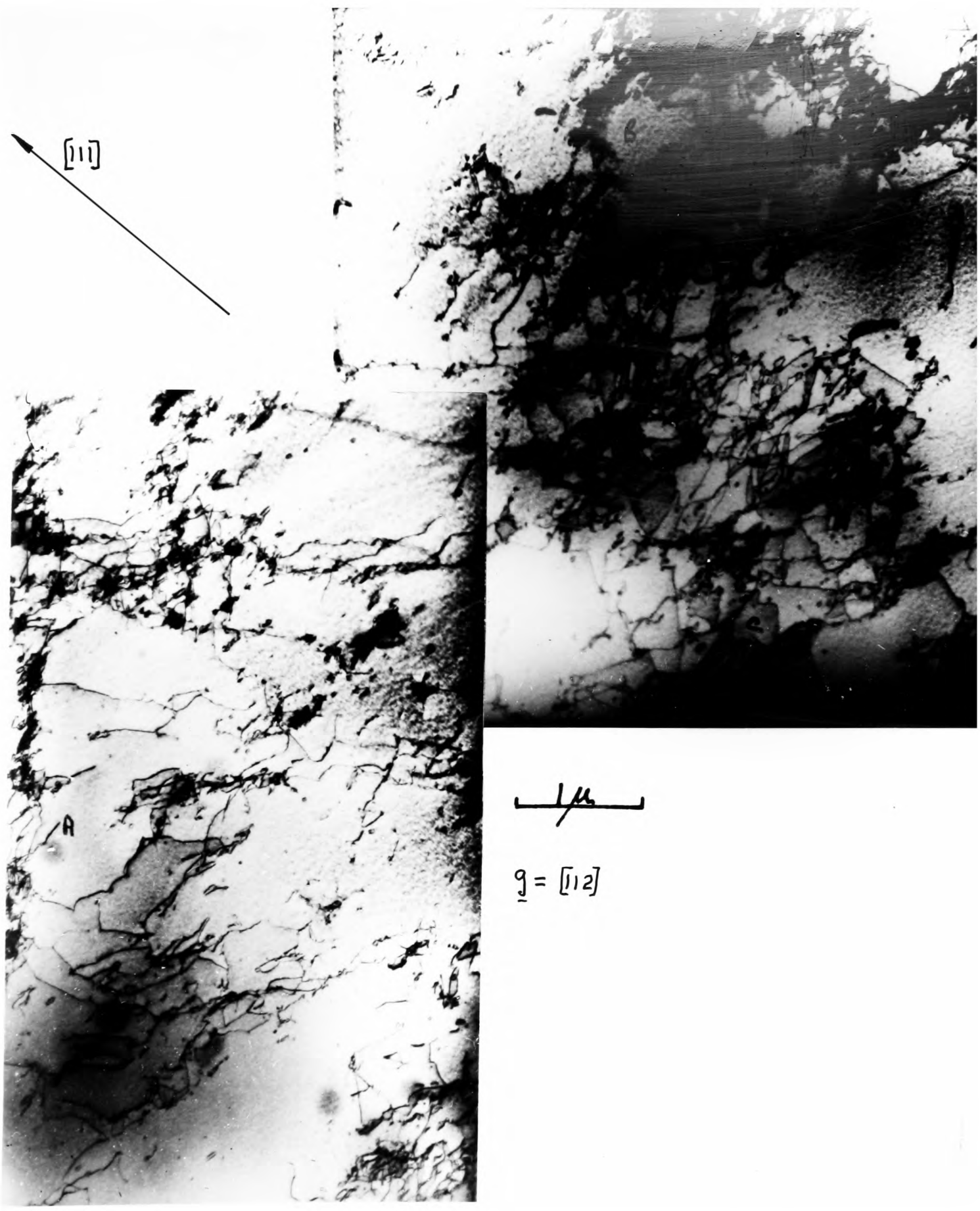


FIG. 1 V 584

FIG. IV 59

$\underline{g} = [11\bar{2}]$

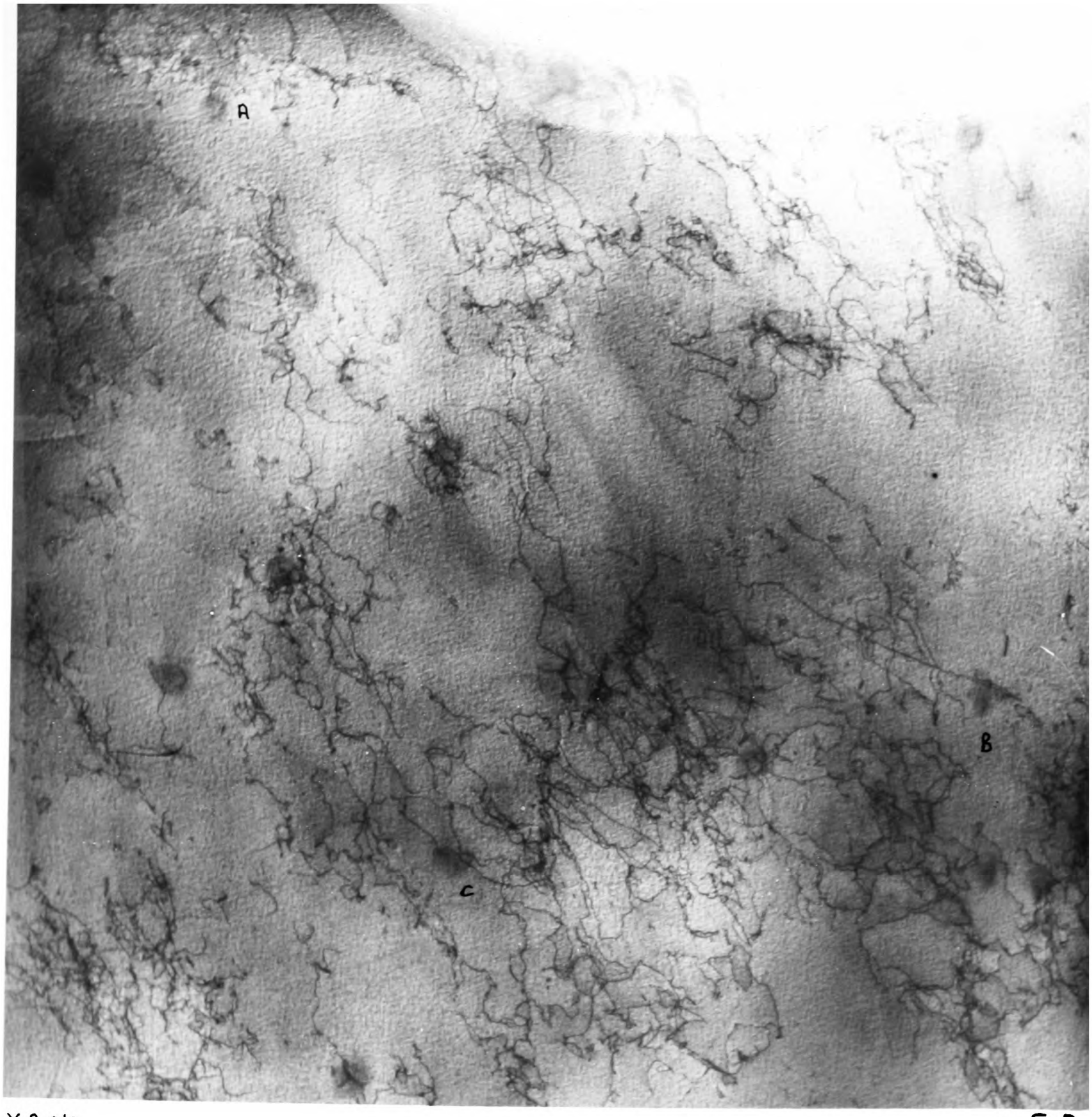




1μ

$\underline{g}$ = [112]

FIG. IV 60a



X20K

$\underline{g} = [0\bar{1}1]$

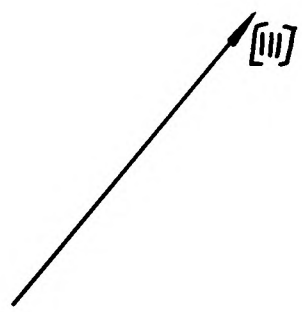
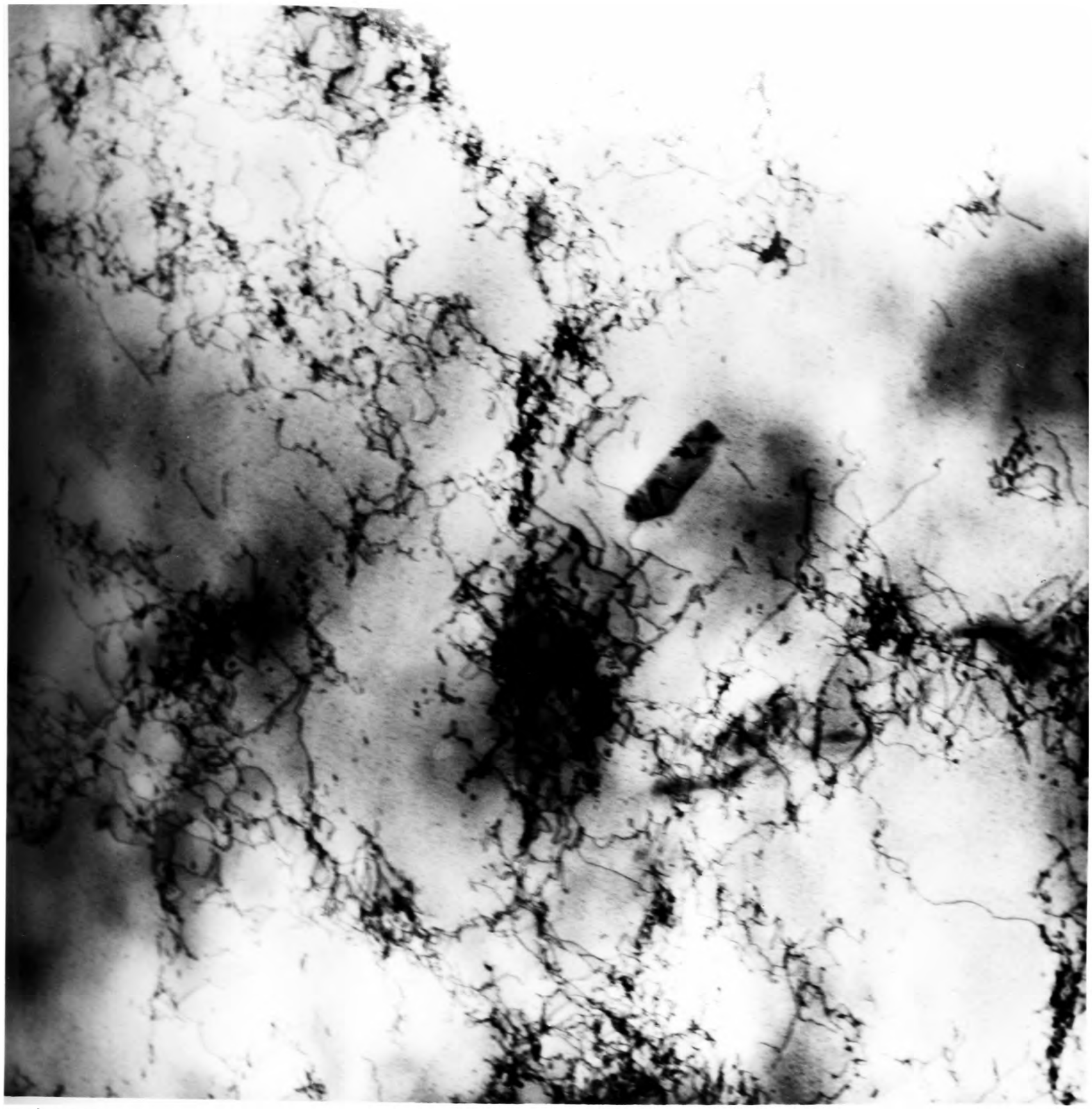


FIG. IV 60b



x 20K

$\underline{g} = [101]$

[111]

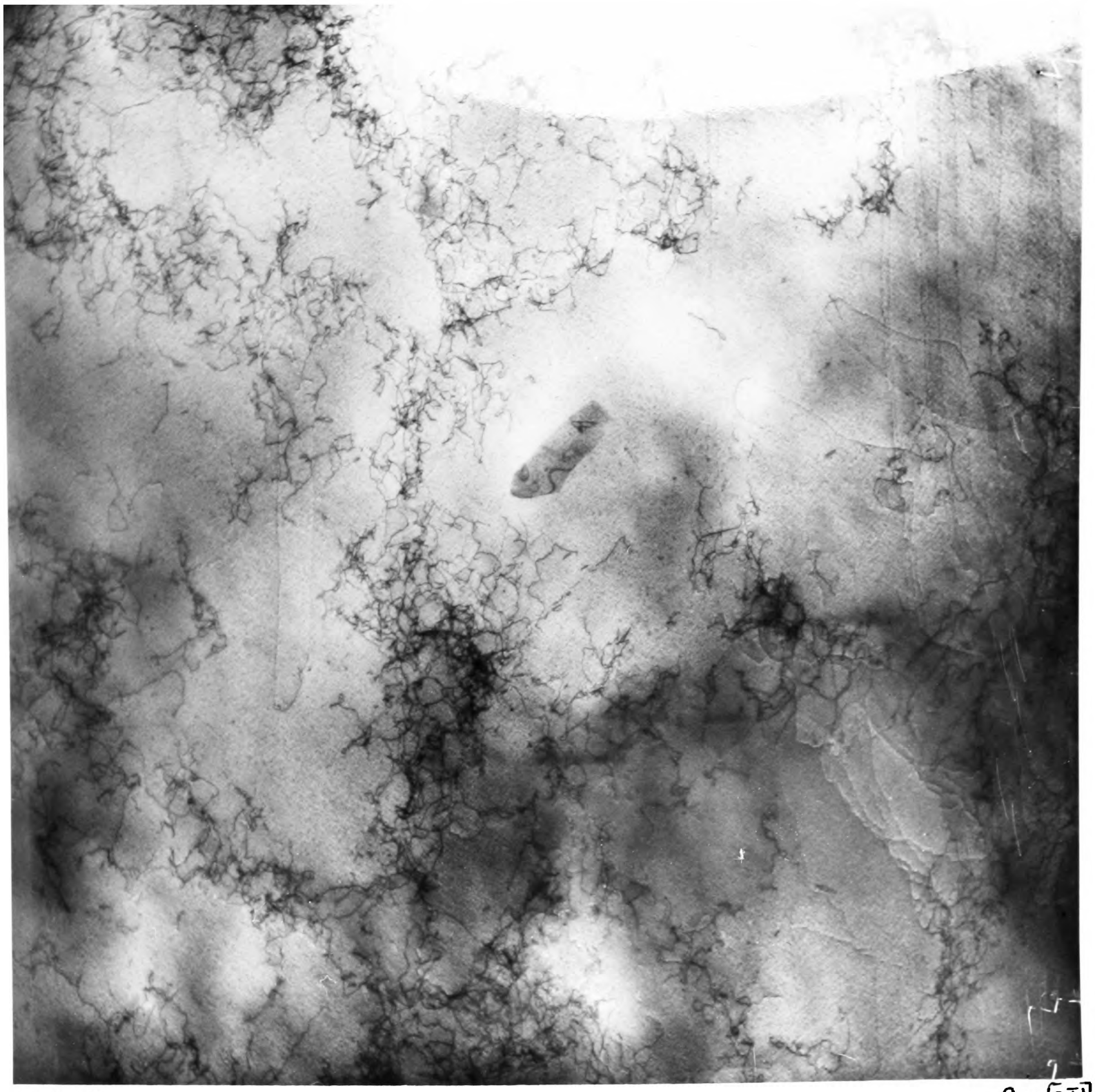
FIG. IV 6a



X20K

$\underline{g} = [11\bar{9}]$

FIG. IV 616



x 20 K

$\underline{g} = [0\bar{1}1]$

FIG. IV 6/c

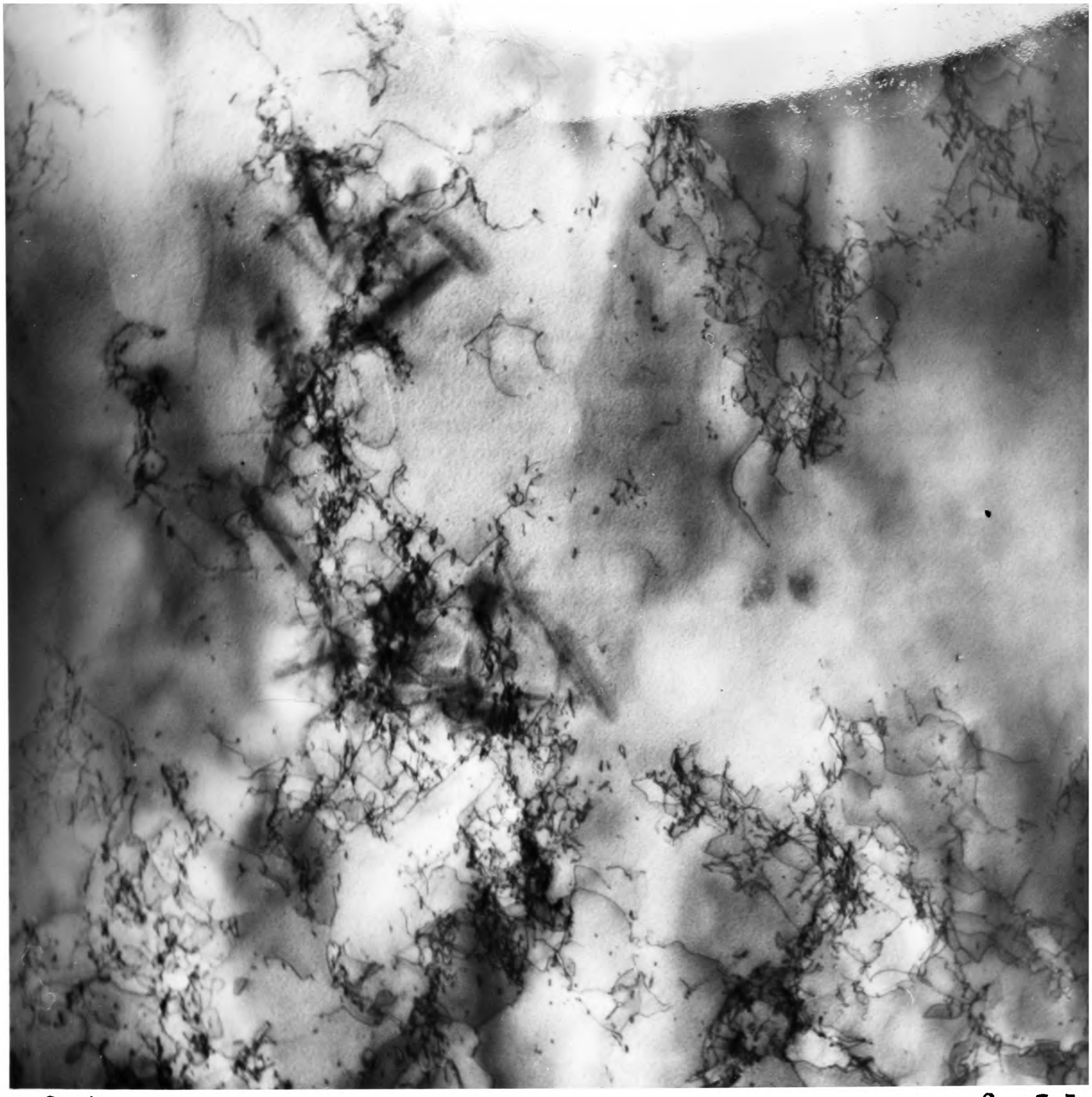


X 20K

$\underline{g}$ = [110]

[111]

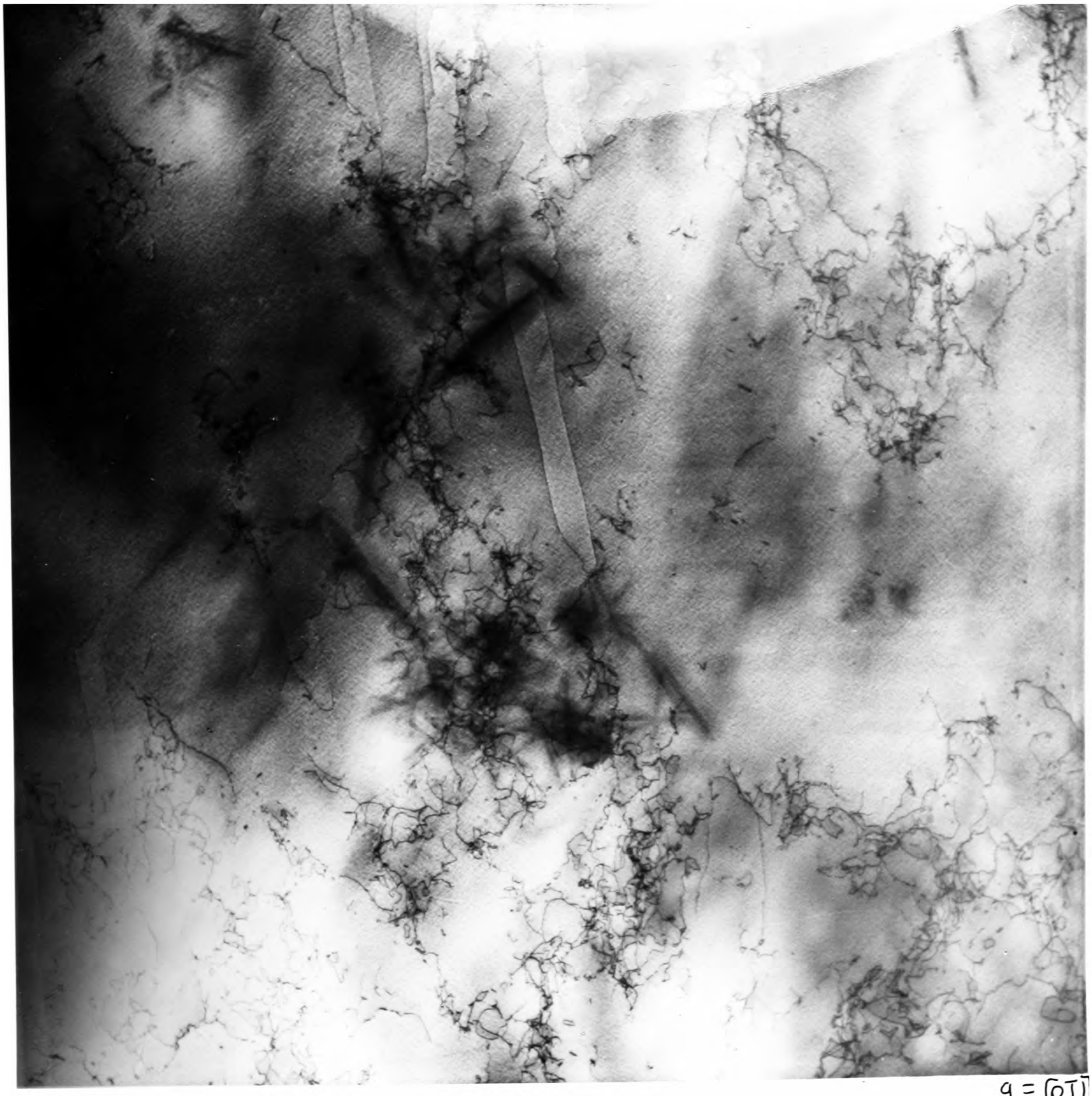
FIG. IV 62a



×20K

$\underline{g} = [101]$

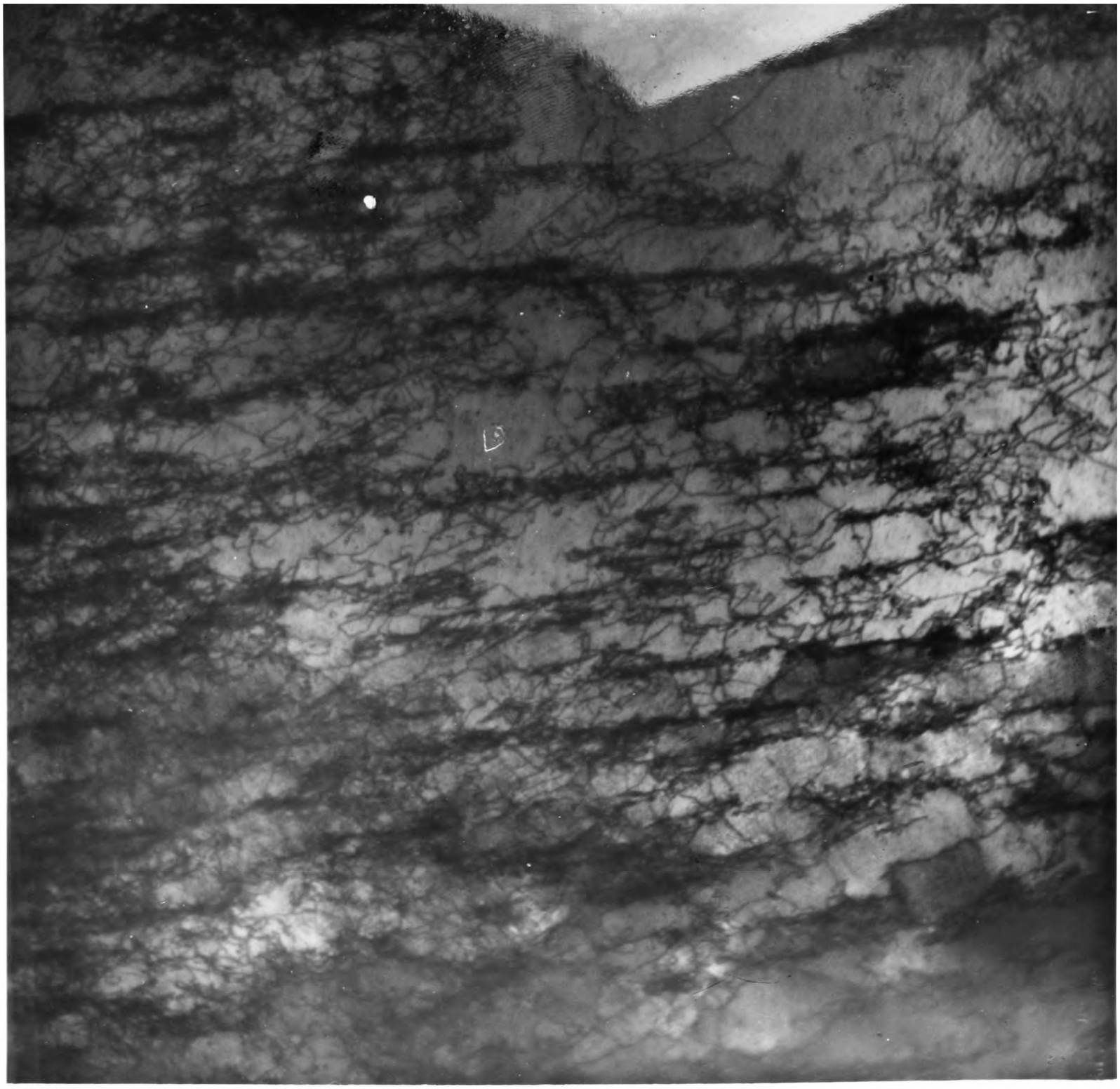
FIG. IV 62b



X20K

$\underline{g} = [0\bar{1}]$

FIG. 1V 62c



x20K

FIG. IV 63



X20K

$\underline{g} = [0\bar{1}1]$

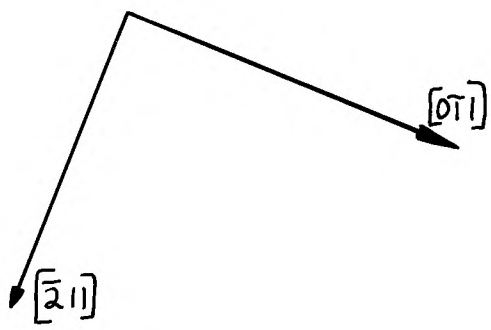
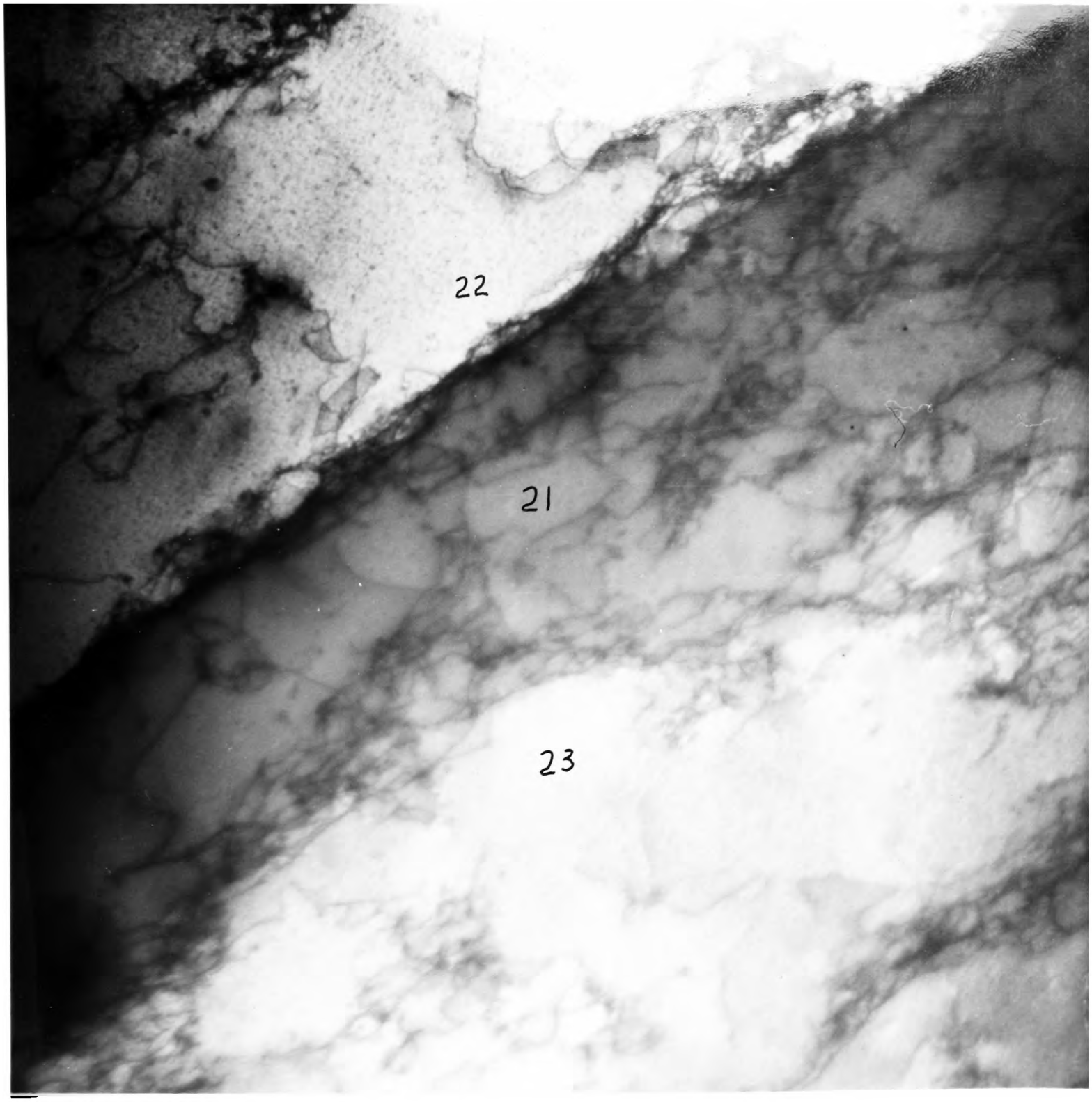
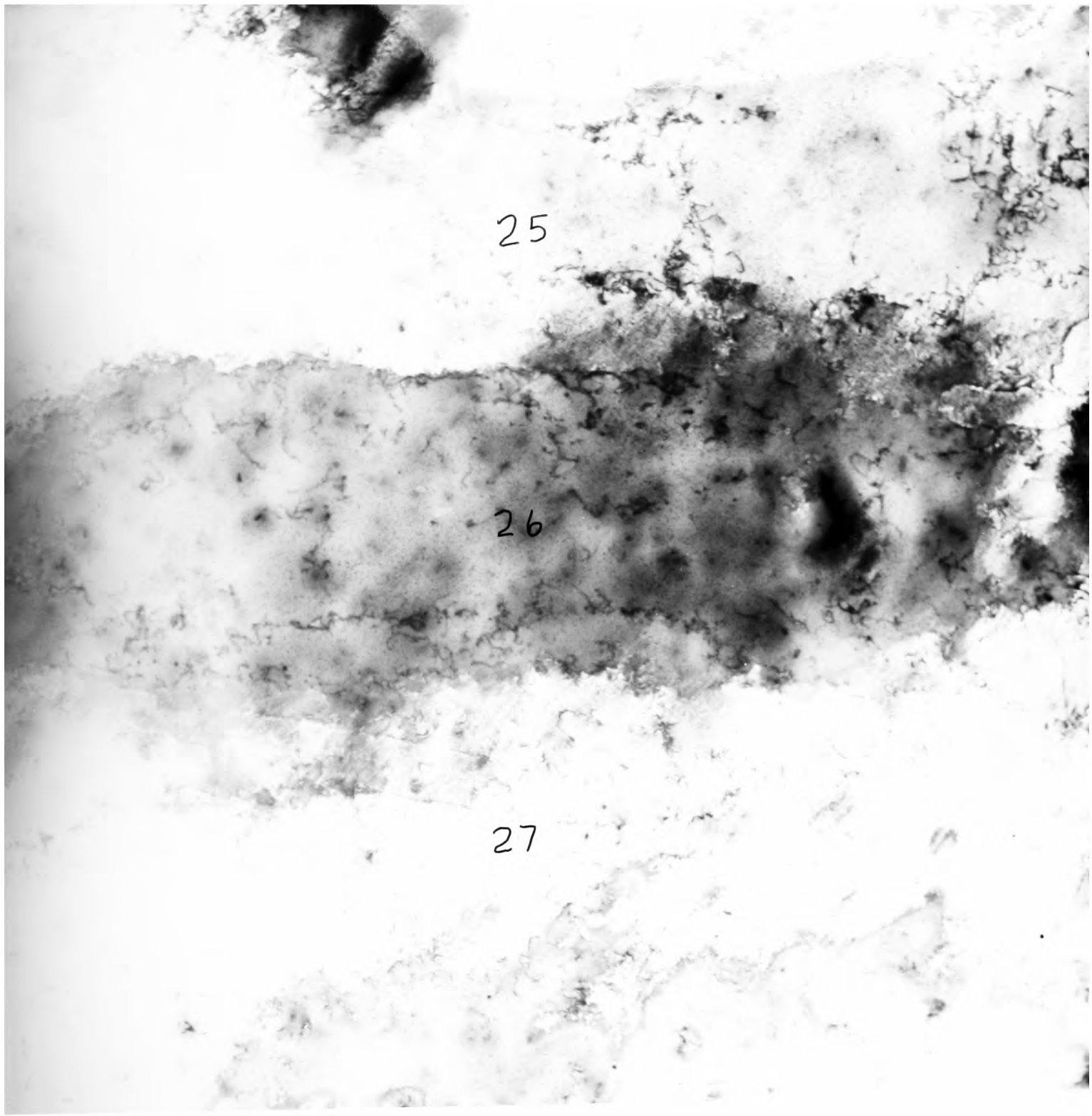


FIG. IV 64



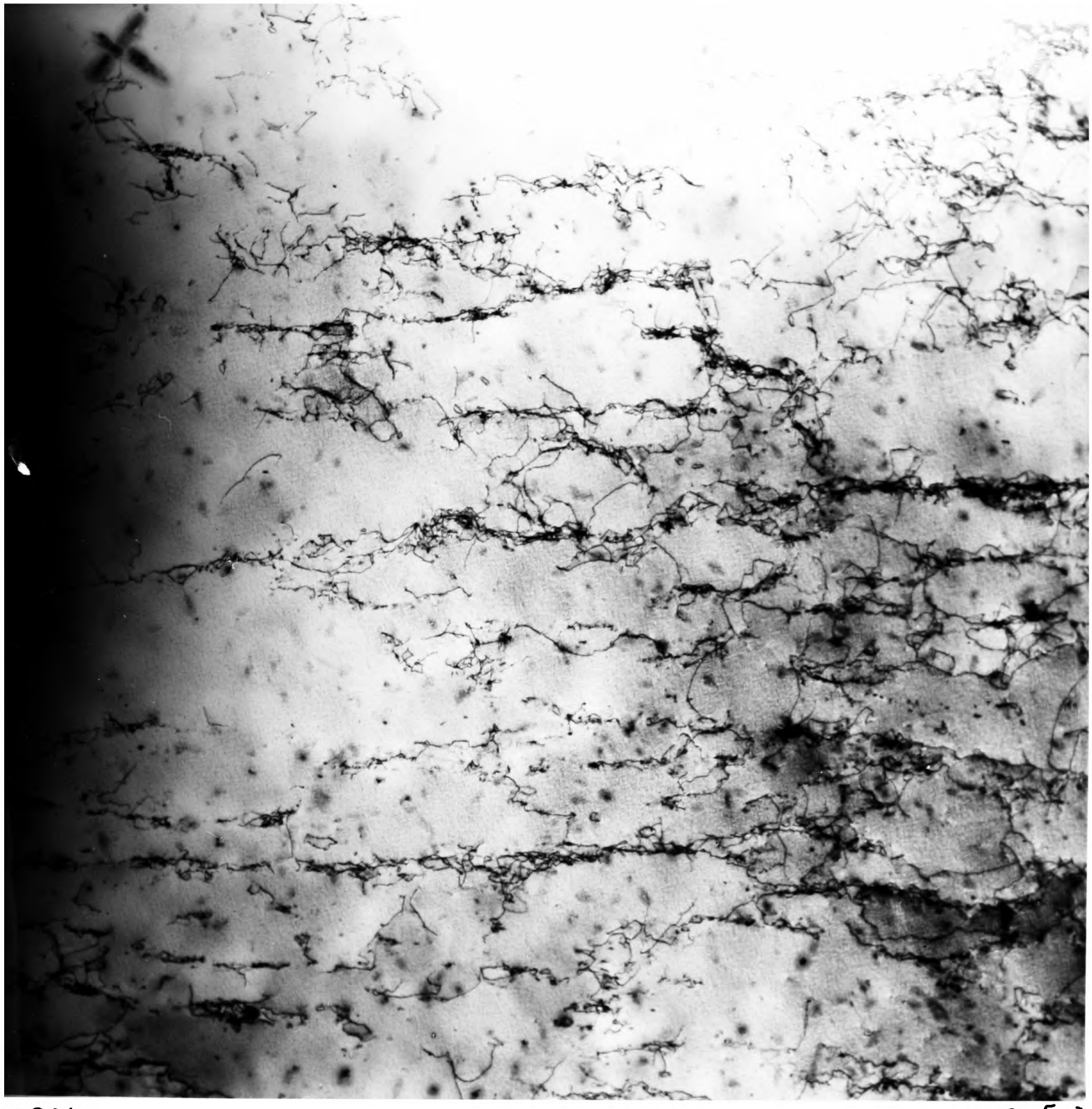
X 40K

FIG. IV 65



X 20K

FIG. IV 66

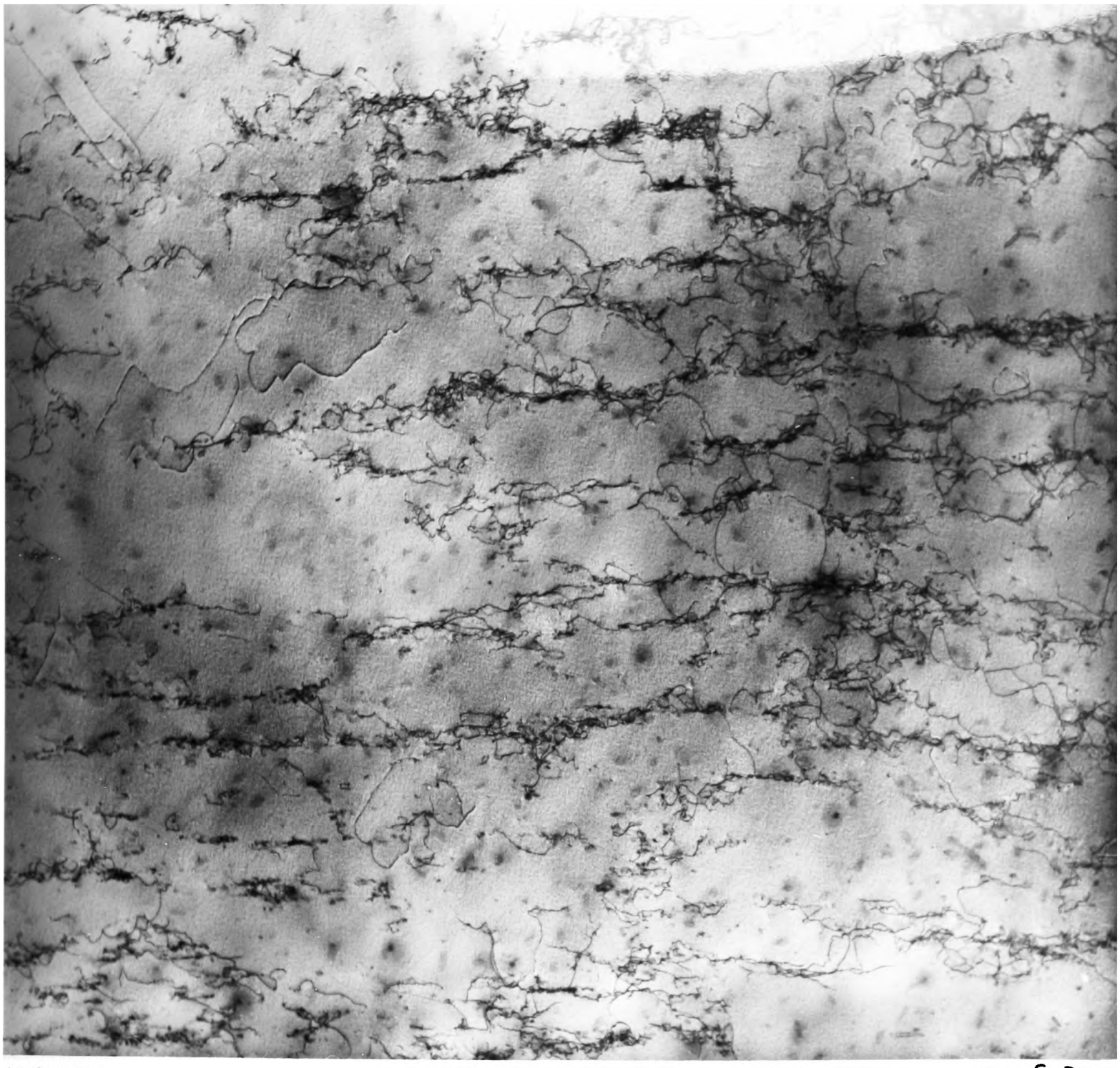


× 20K

$\underline{g} = [1\bar{1}0]$

$[\bar{2}11]$

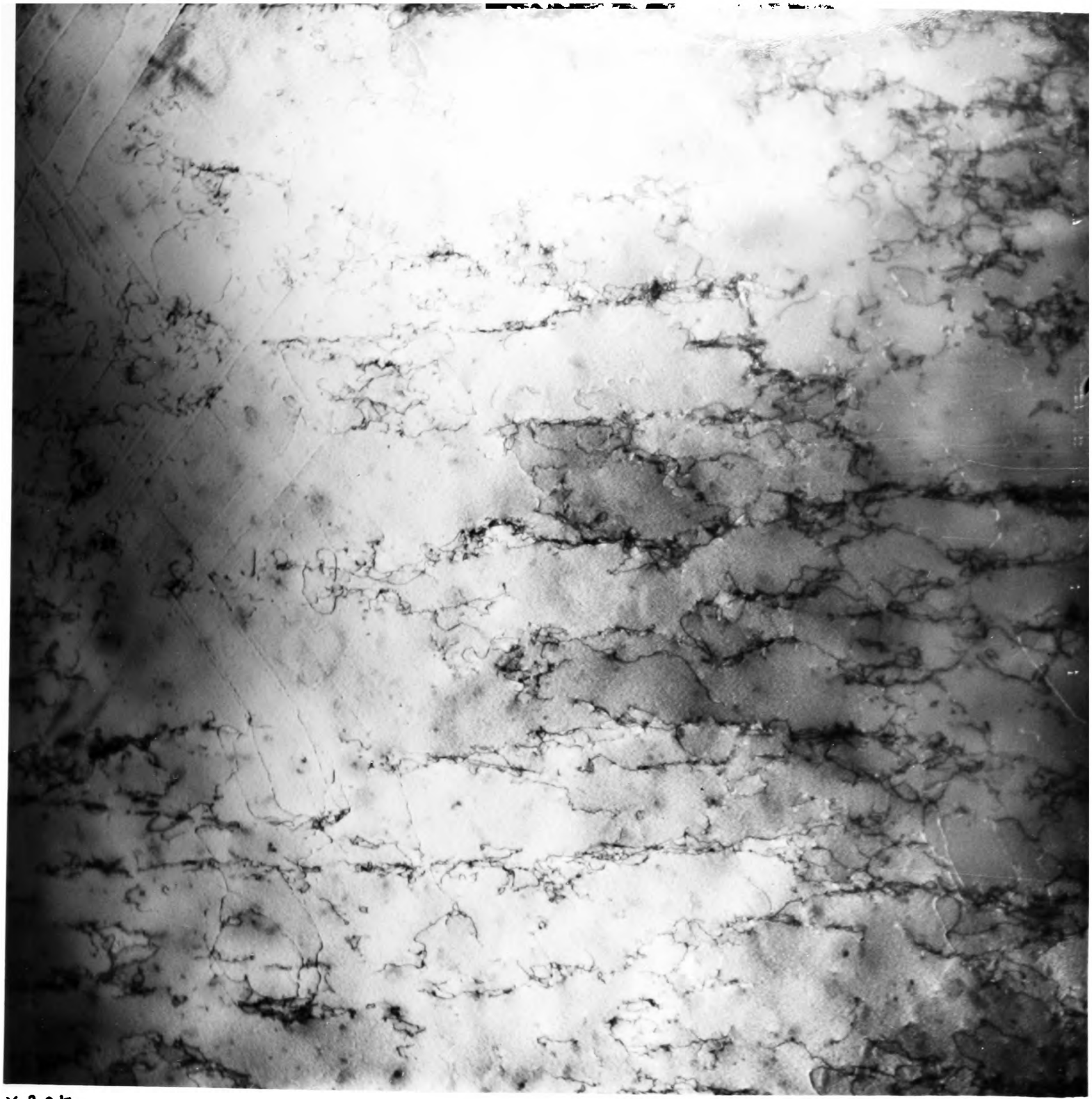
FIG. IV 67a



X 20K

$\underline{g} = [\bar{1}01]$

FIG. IV 67b

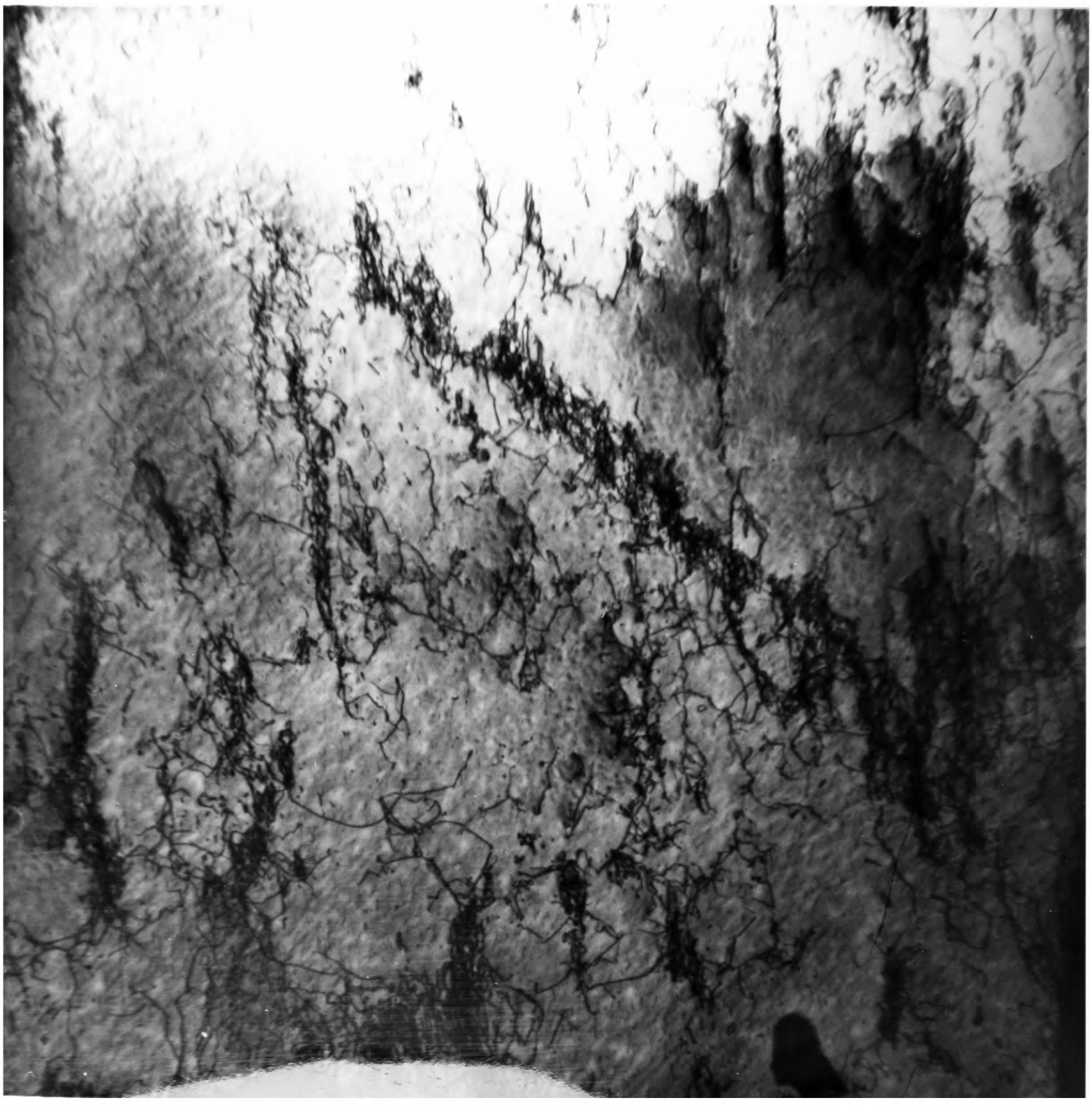


×20K

$\underline{g}=[0\bar{1}1]$

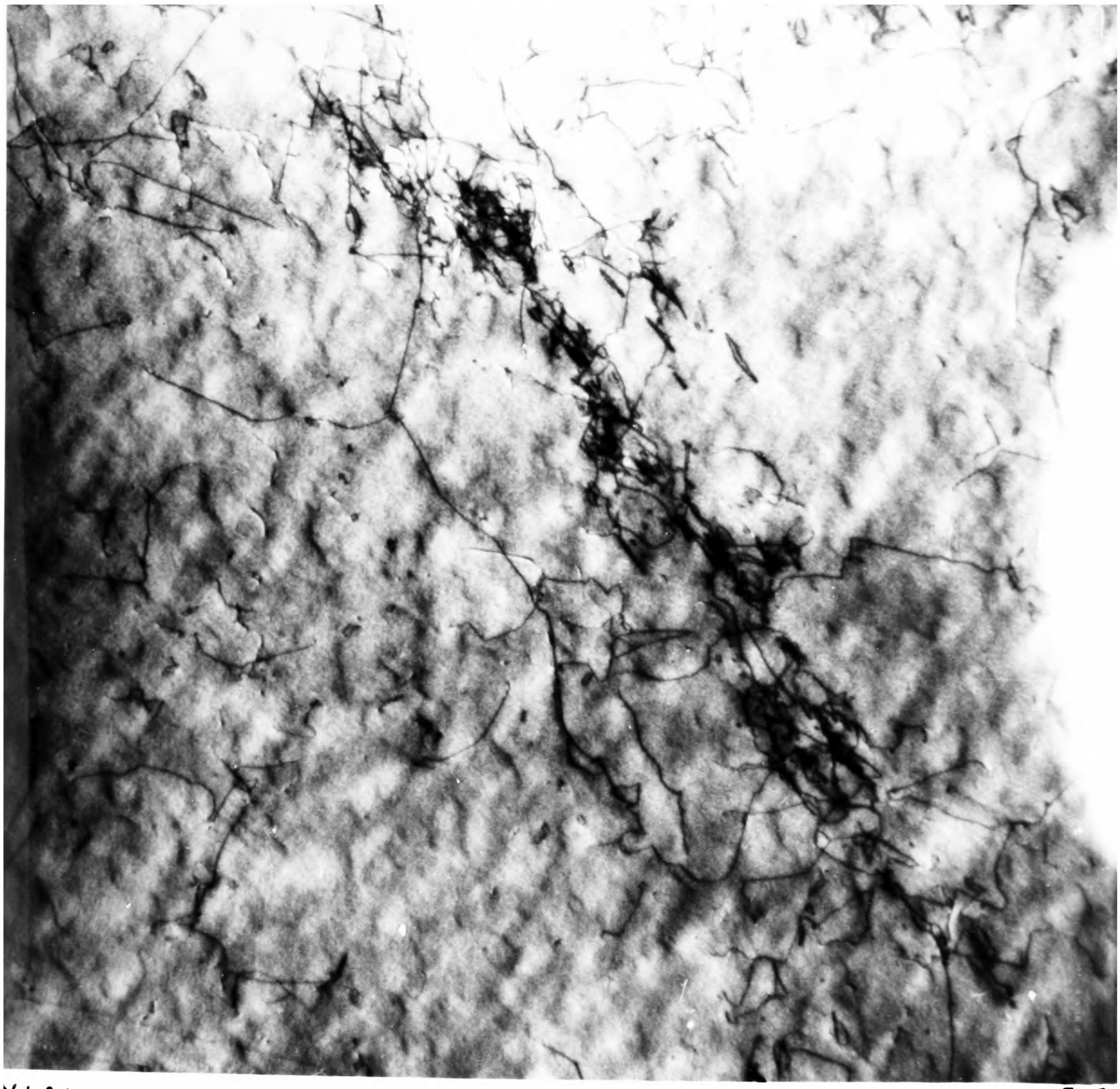
FIG. IV 67c

X 8K



[110]

FIG. 1V68



X40K

$\underline{g}$ = [110]

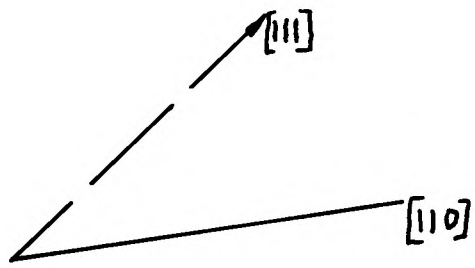


FIG. IV 69

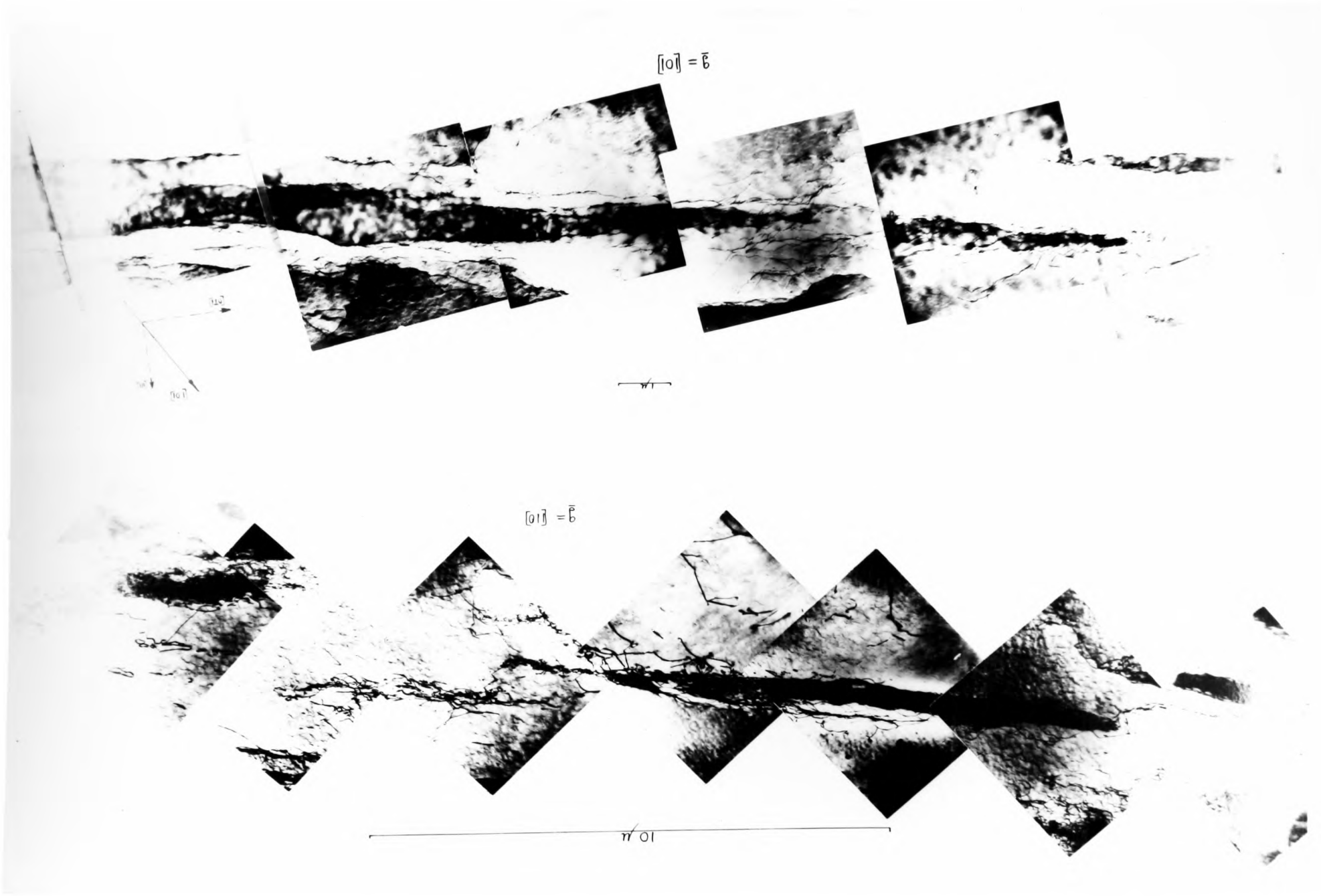
70

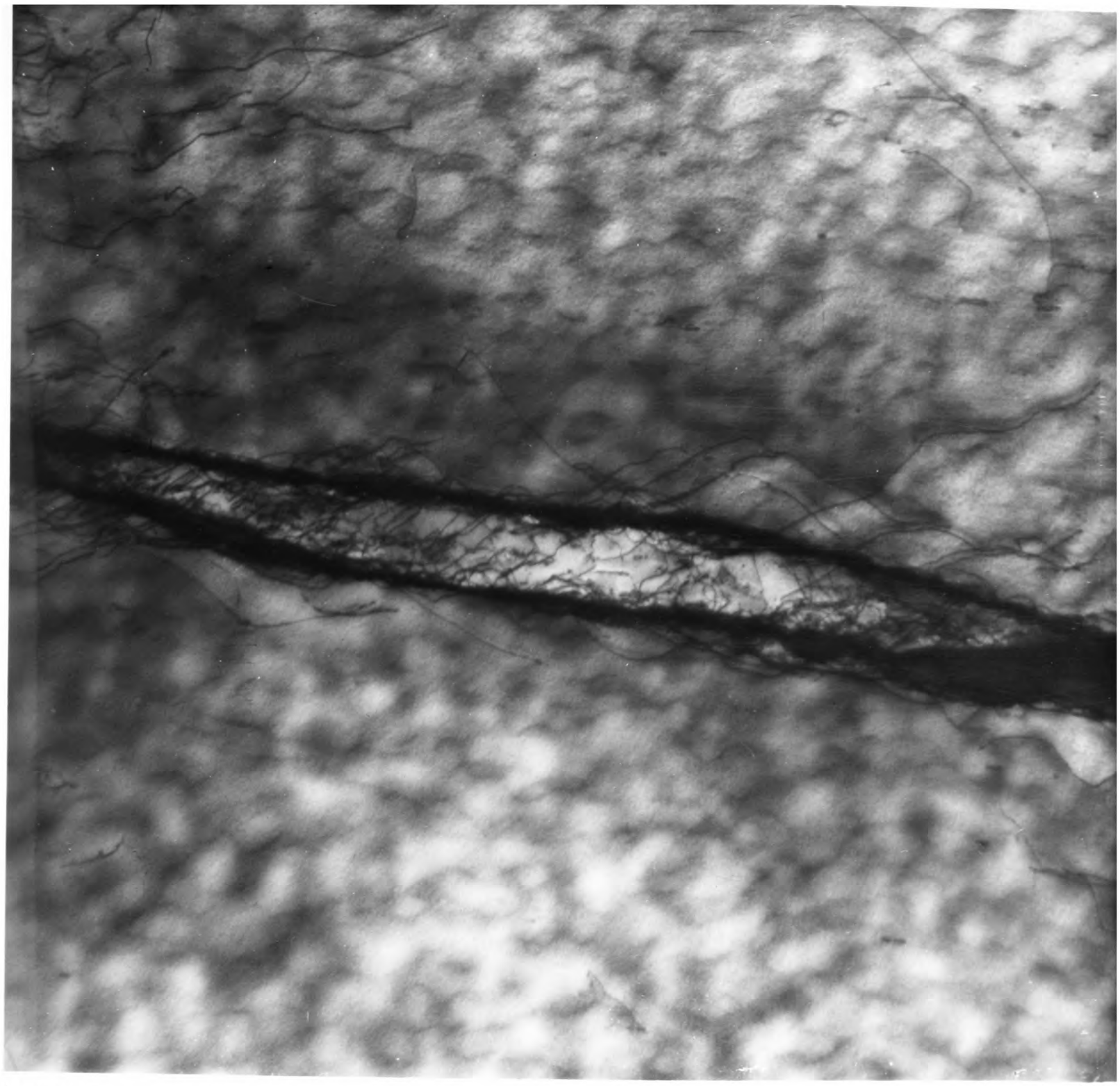
[011]

$\underline{g} = [101]$

X40K




$\underline{g} = [\bar{1}01]$
$\underline{g} = [01\bar{1}]$
10 μ



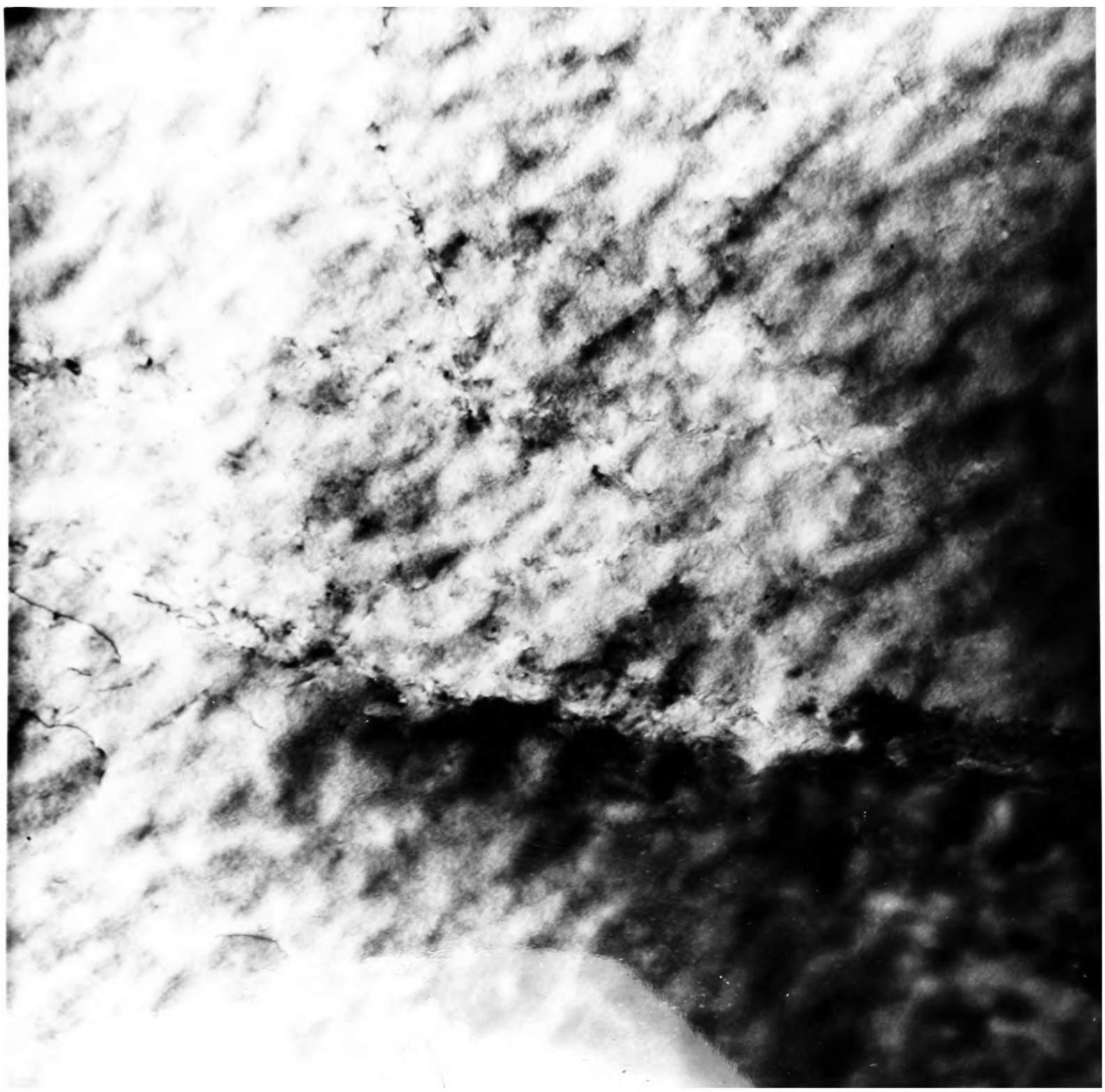
X 40K

$\underline{g} = [10\bar{1}]$

[0$\bar{1}$1]

FIG. IV 72

PTO.1V 73



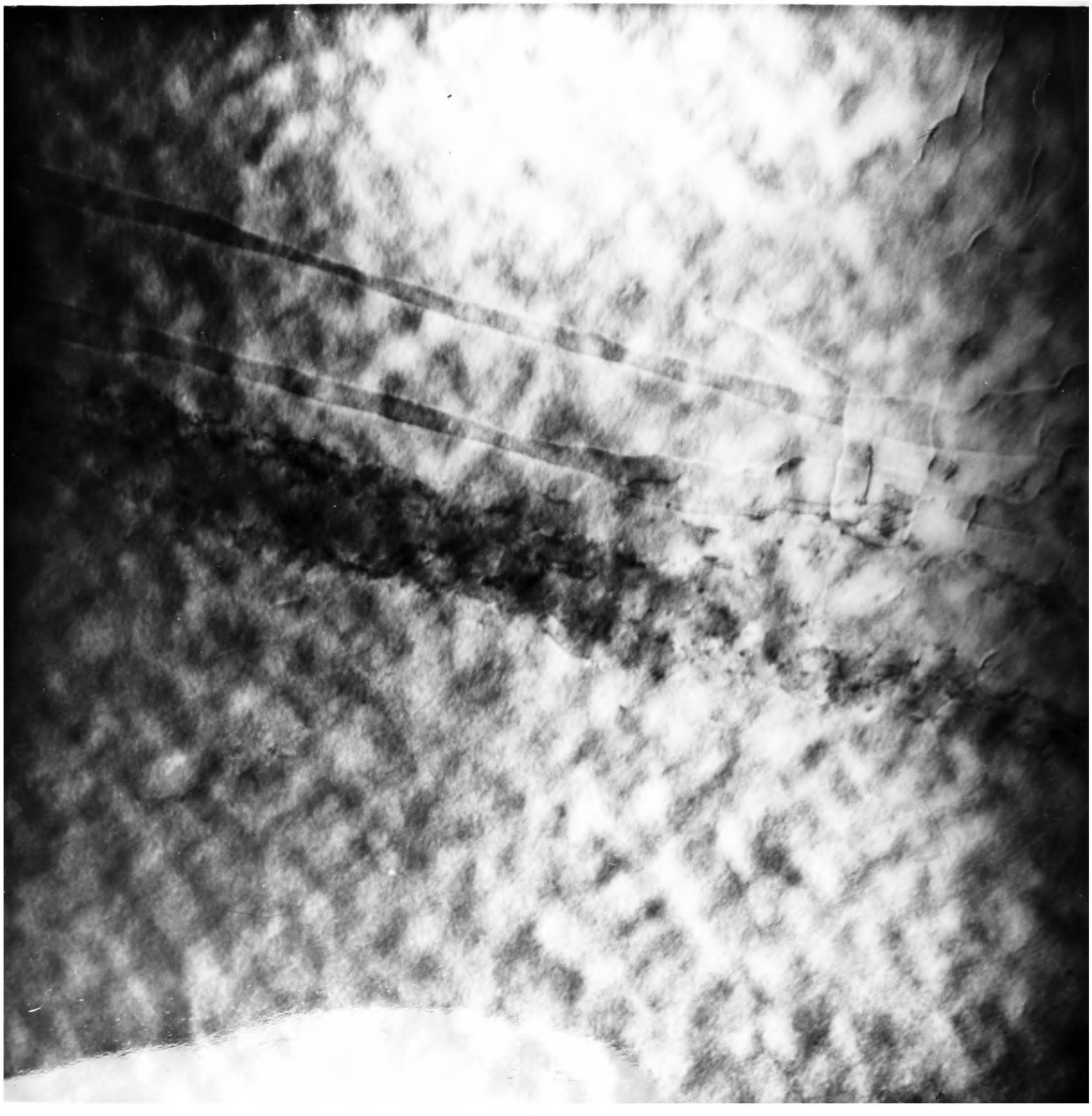
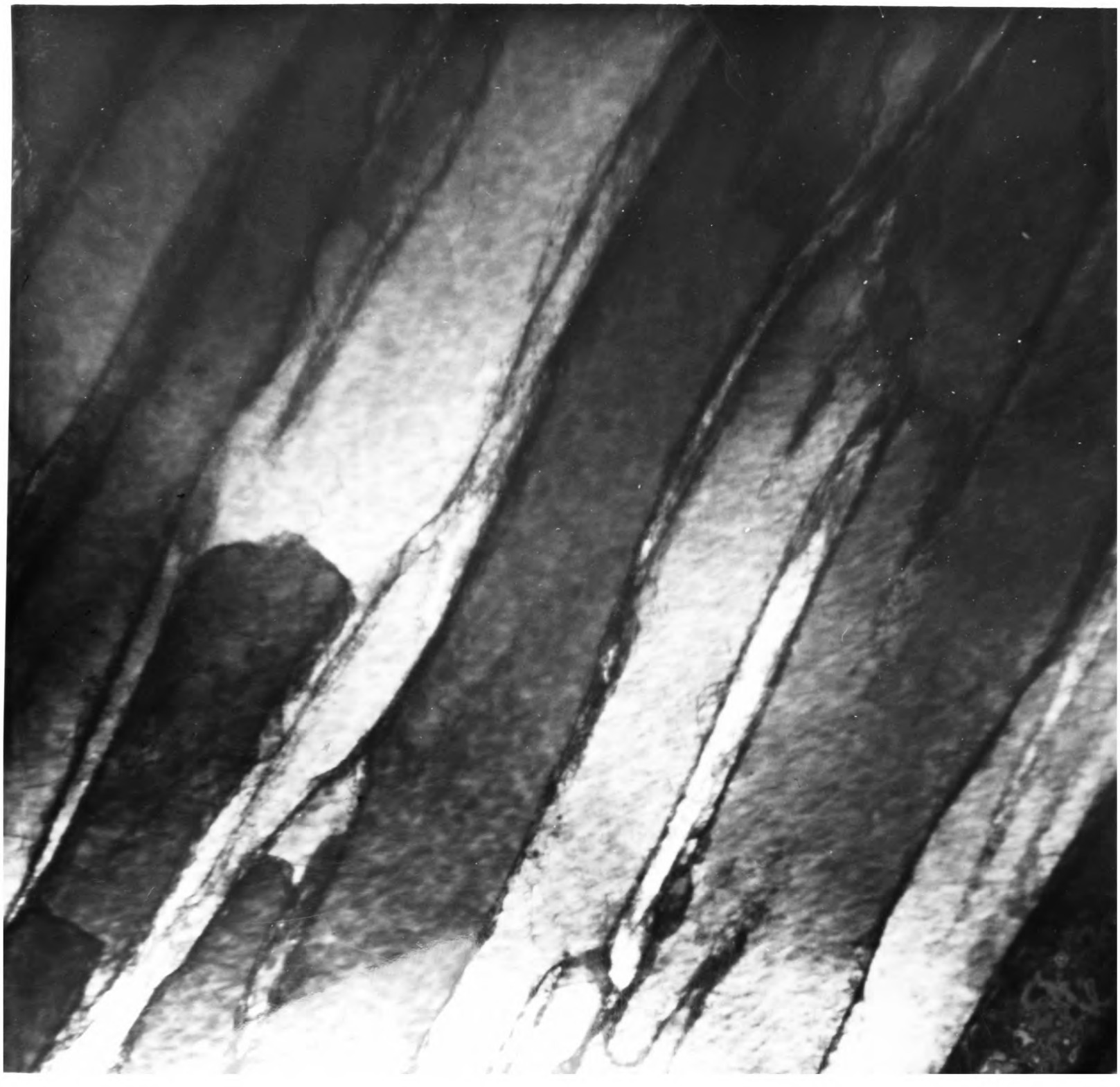

$\bar{q} = [0\bar{1}1]$
X40K

FIGURE 75

[61]

X8K



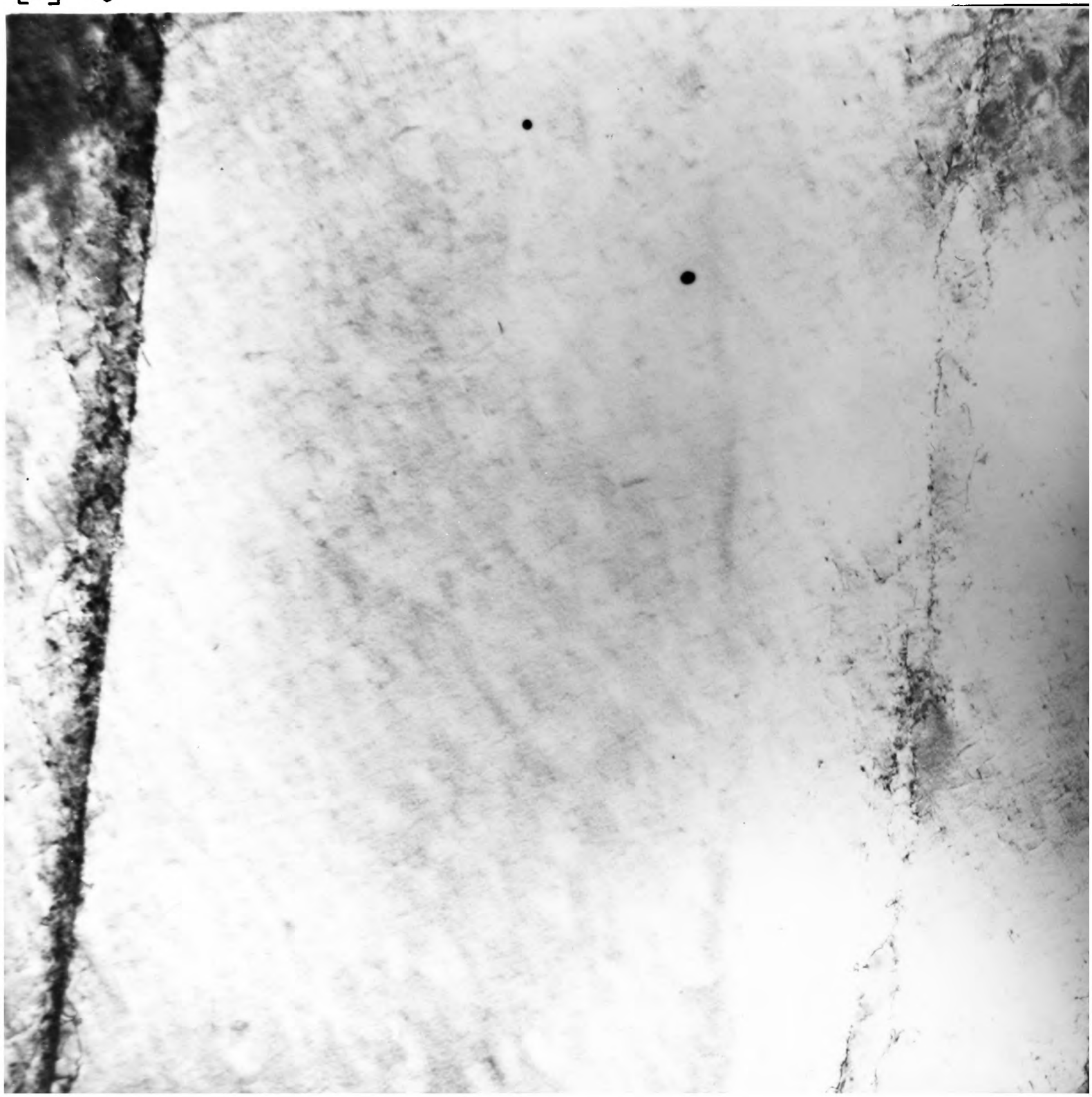


FIG. IV. 76

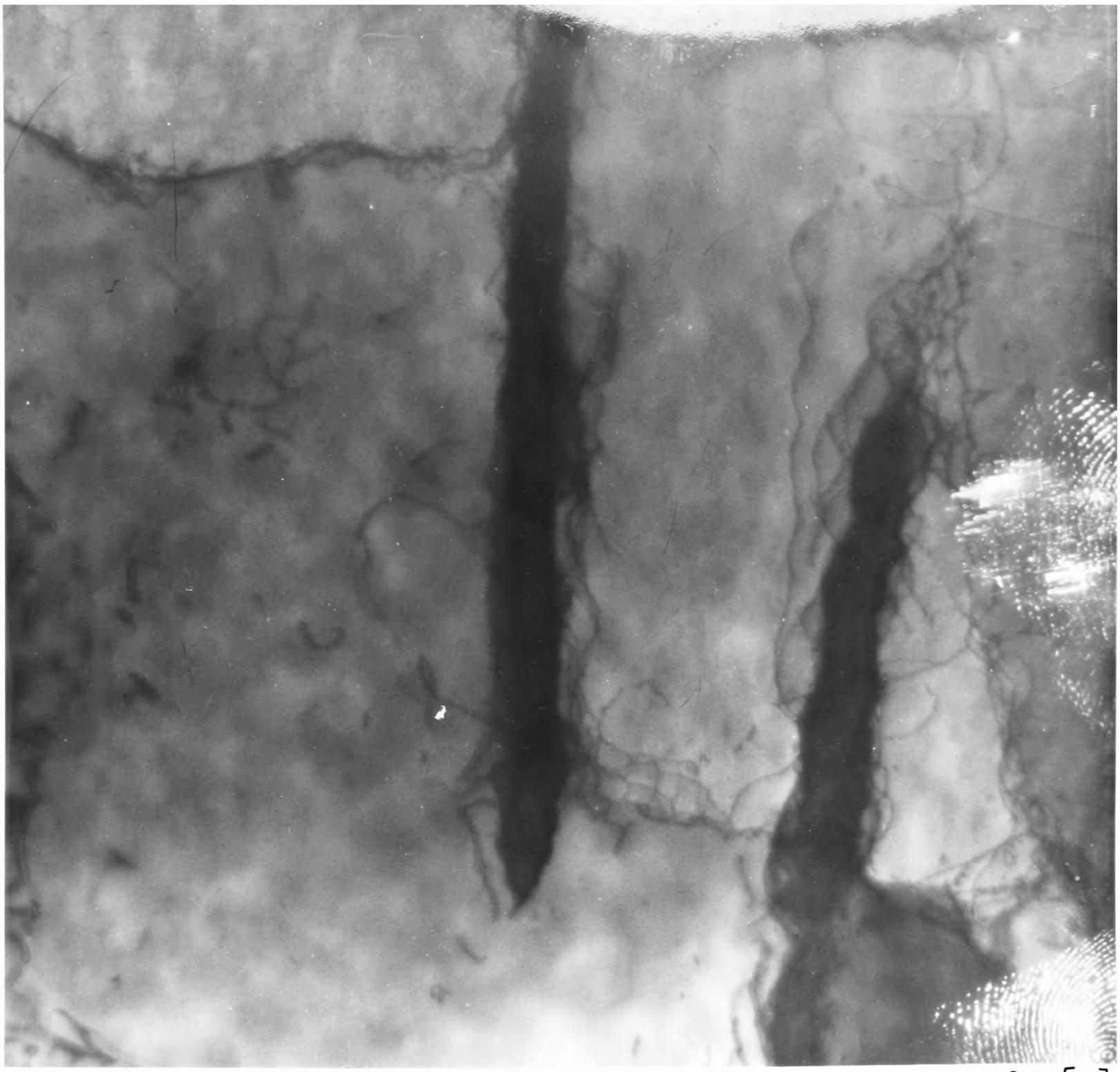
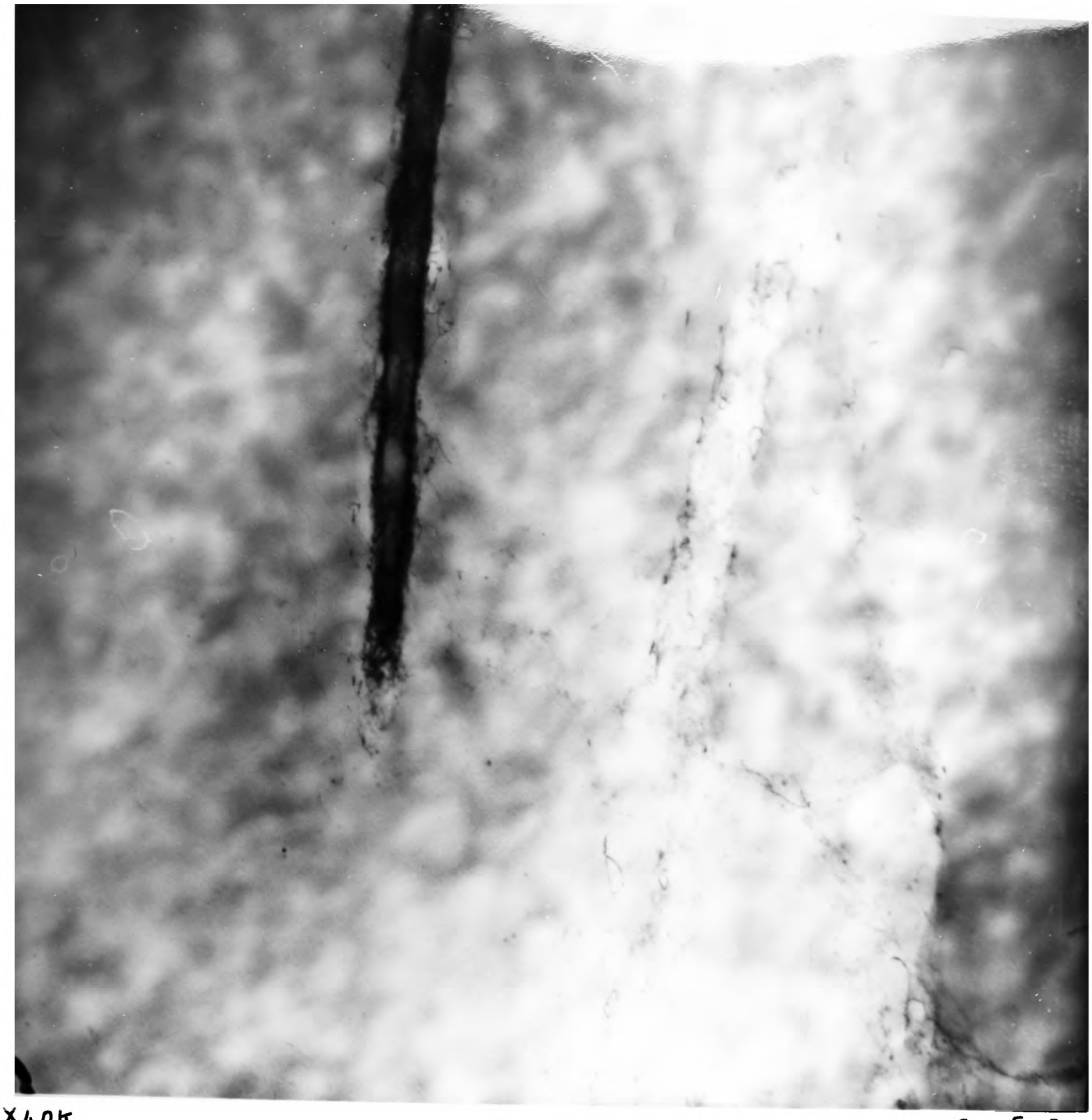


FIG. IV 77a



X40K

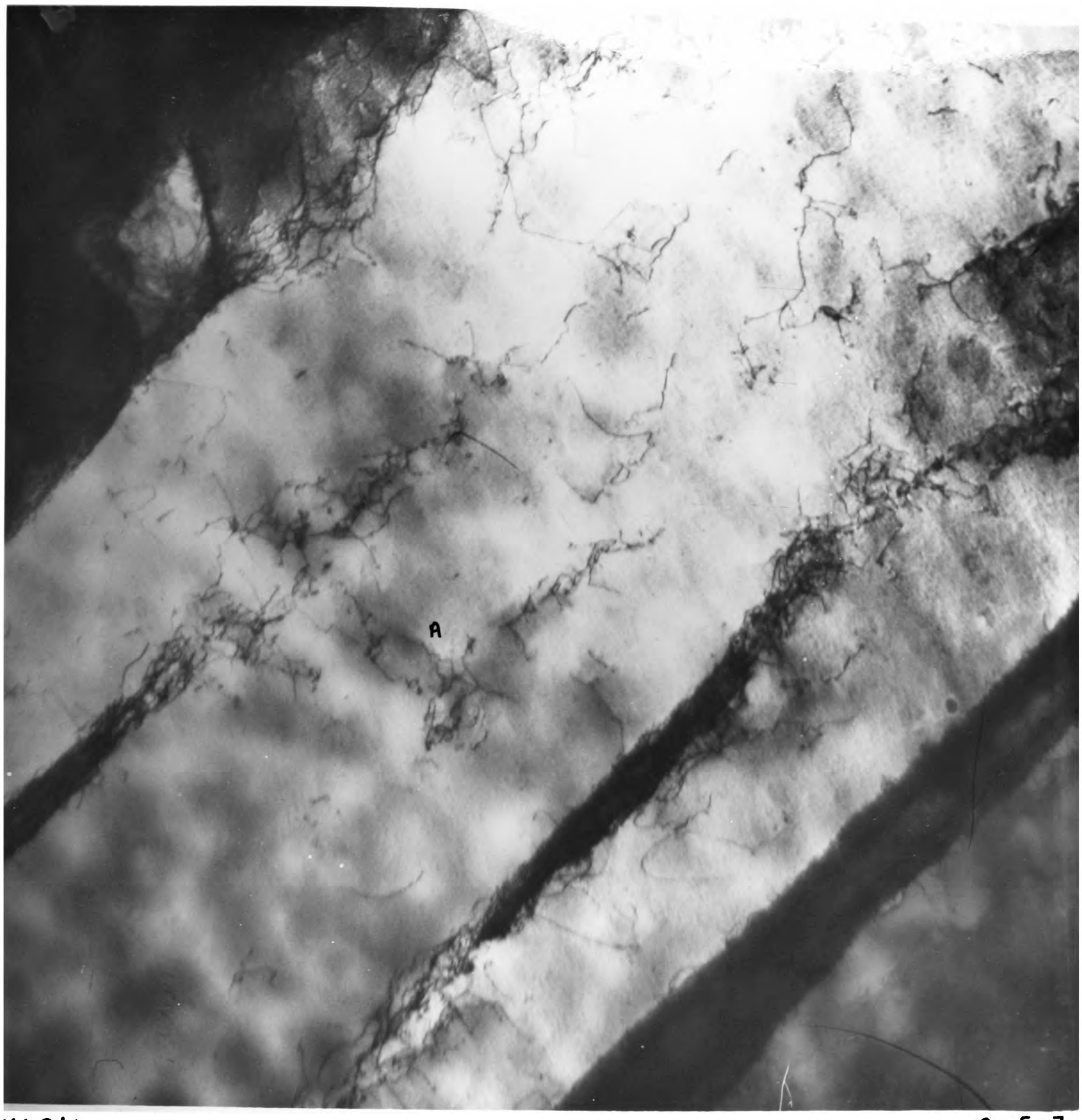
$\underline{g} = [\bar{2}0\bar{1}]$

FIG. IV 77b



X40K

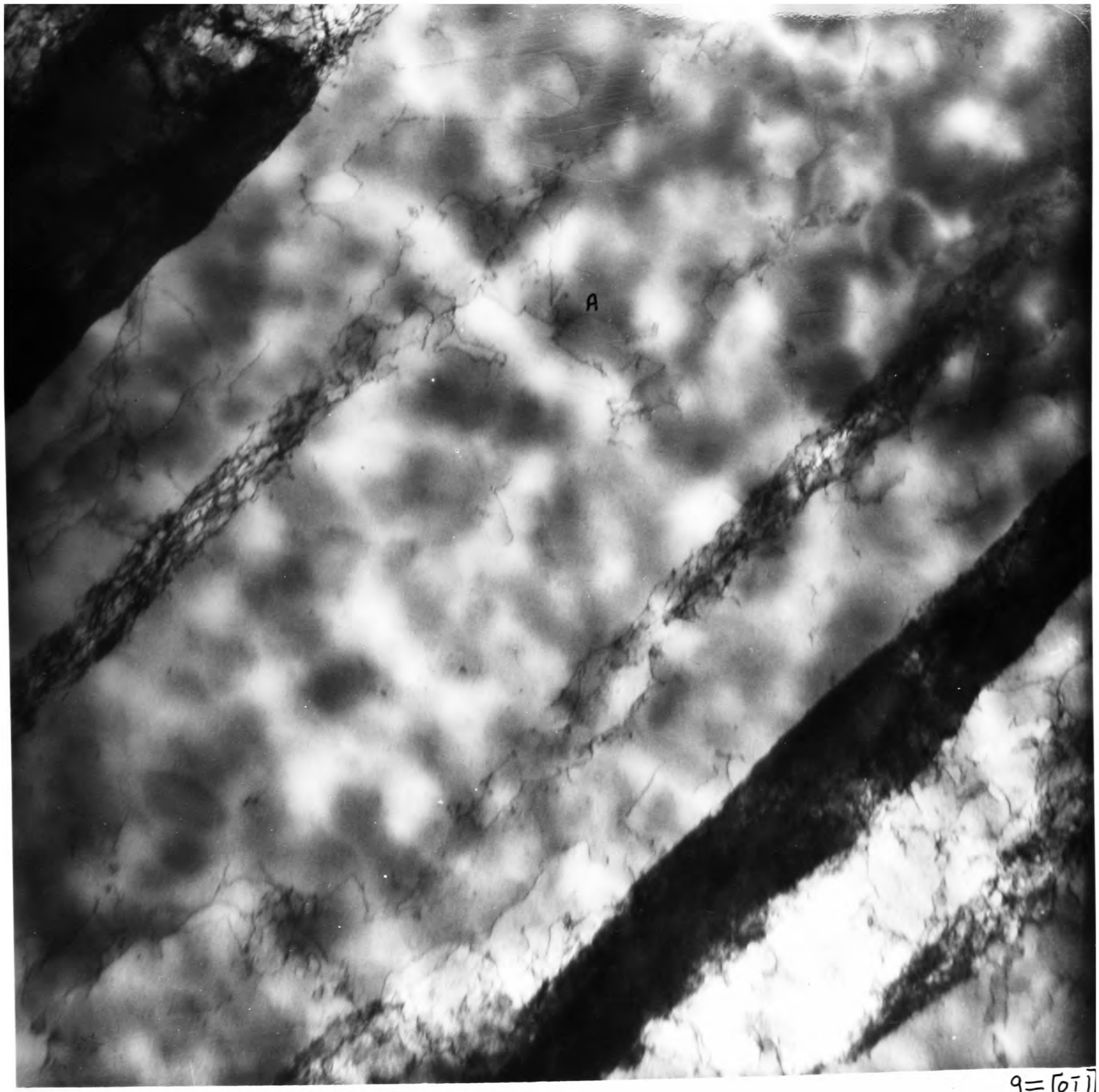
FIG. IV 78



X40K

$\underline{g} = [\bar{1}01]$

FIG. IV 79a



X40K

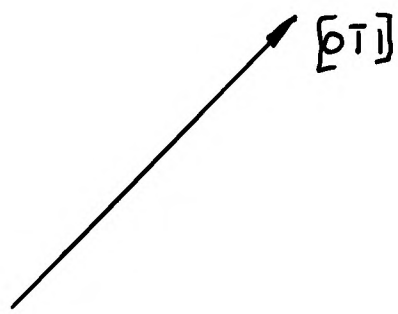
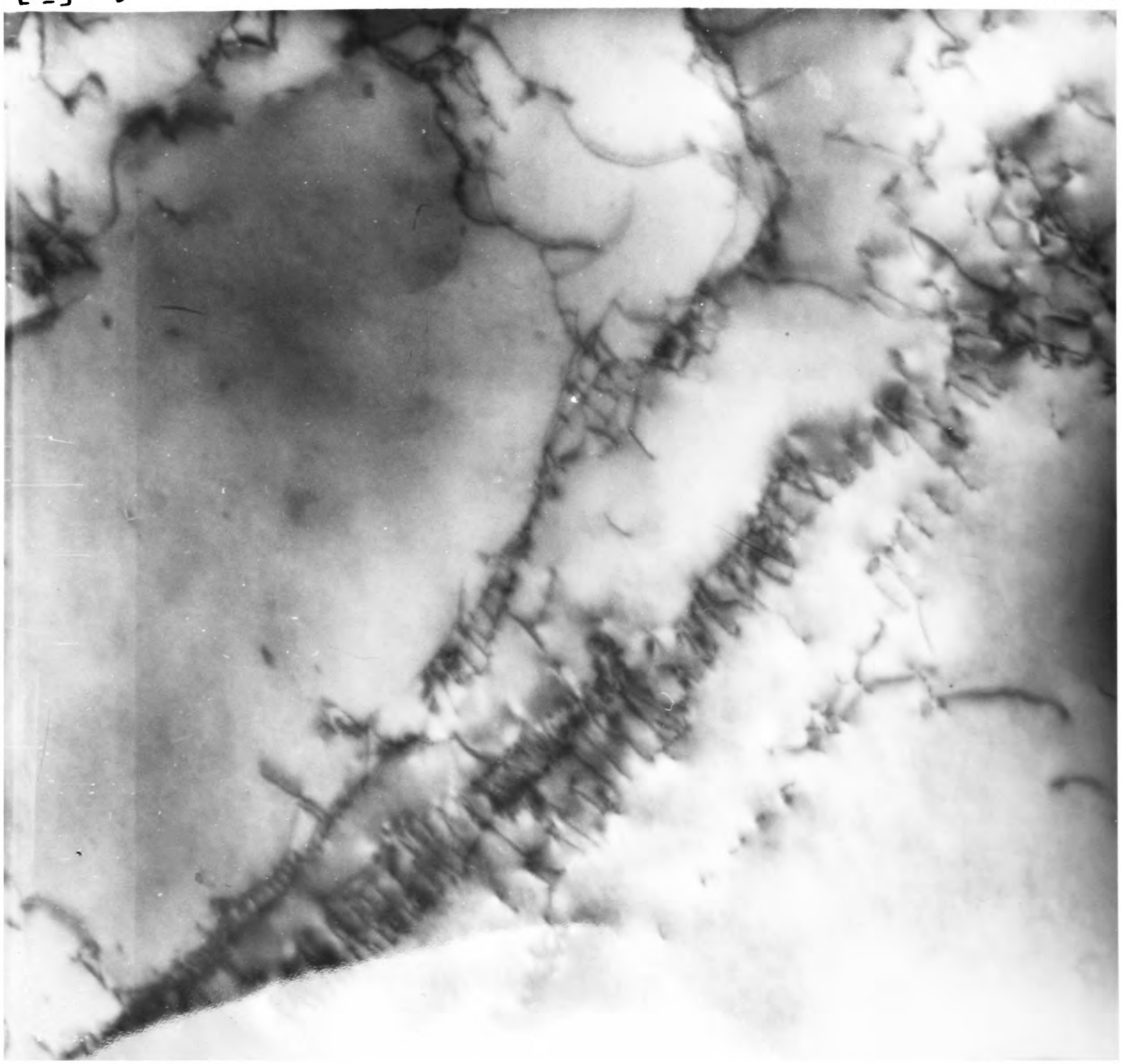
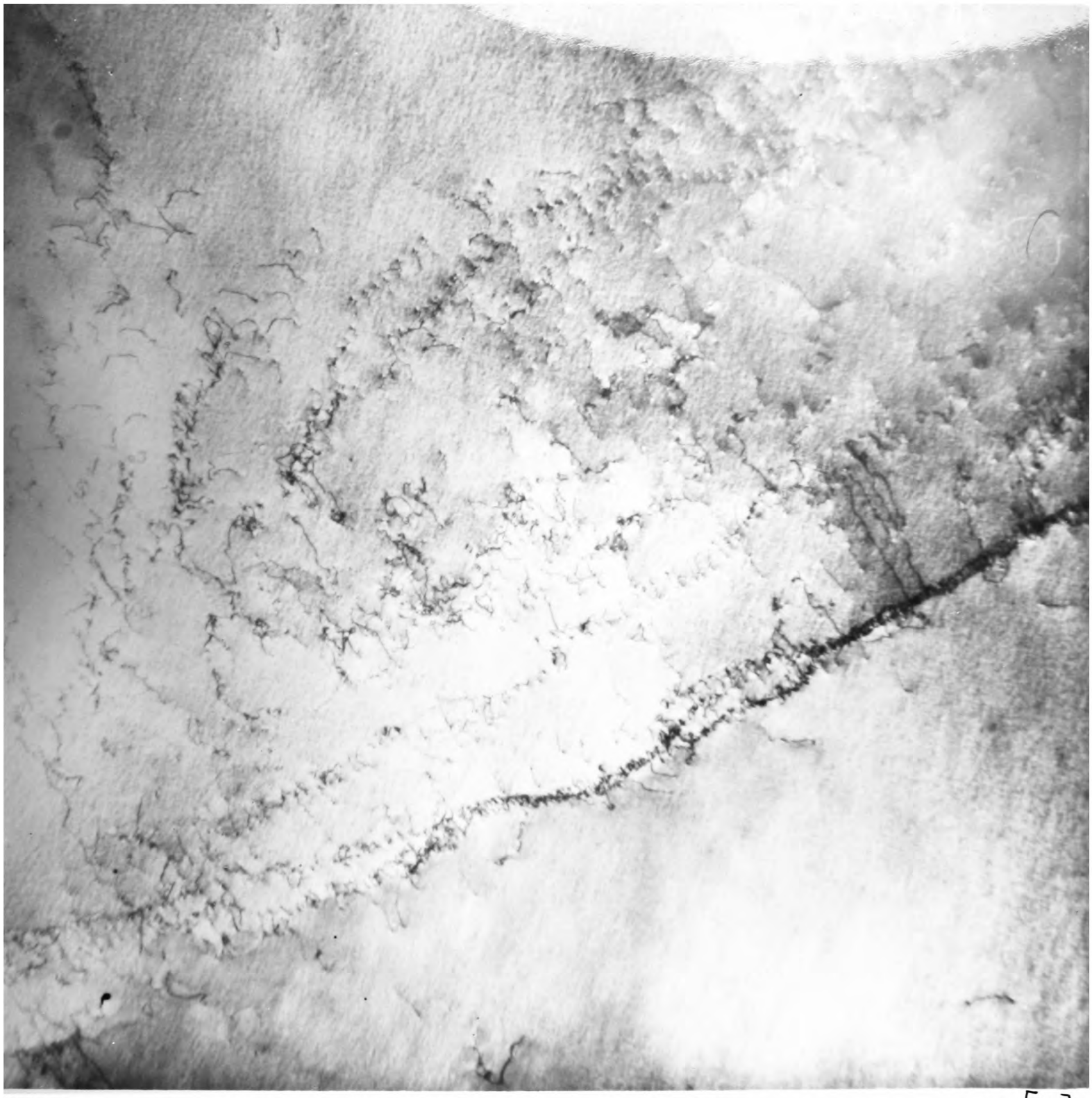


FIG. IV 79b

FIGURE 80

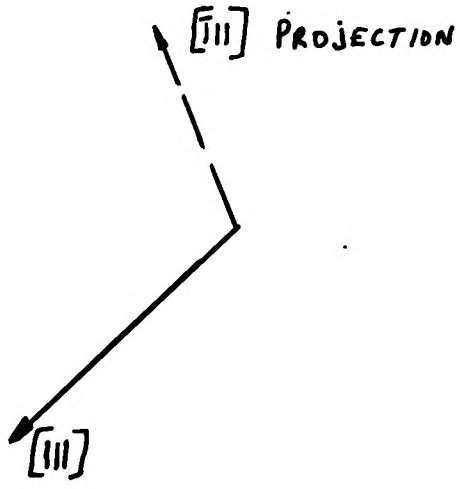
X100K $\bar{g} = [\bar{1}30]$





X40K

$\underline{g} = [\bar{1}10]$



SEE DISCUSSION

$\underline{g} = [110]$

$[111] \rightarrow [\bar{1}11]$ (INVISIBLE)

$[\bar{1}11] \rightarrow [111]$

FIG. IV 81



12 K

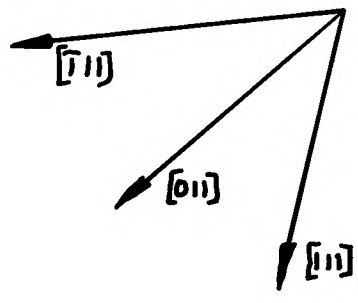
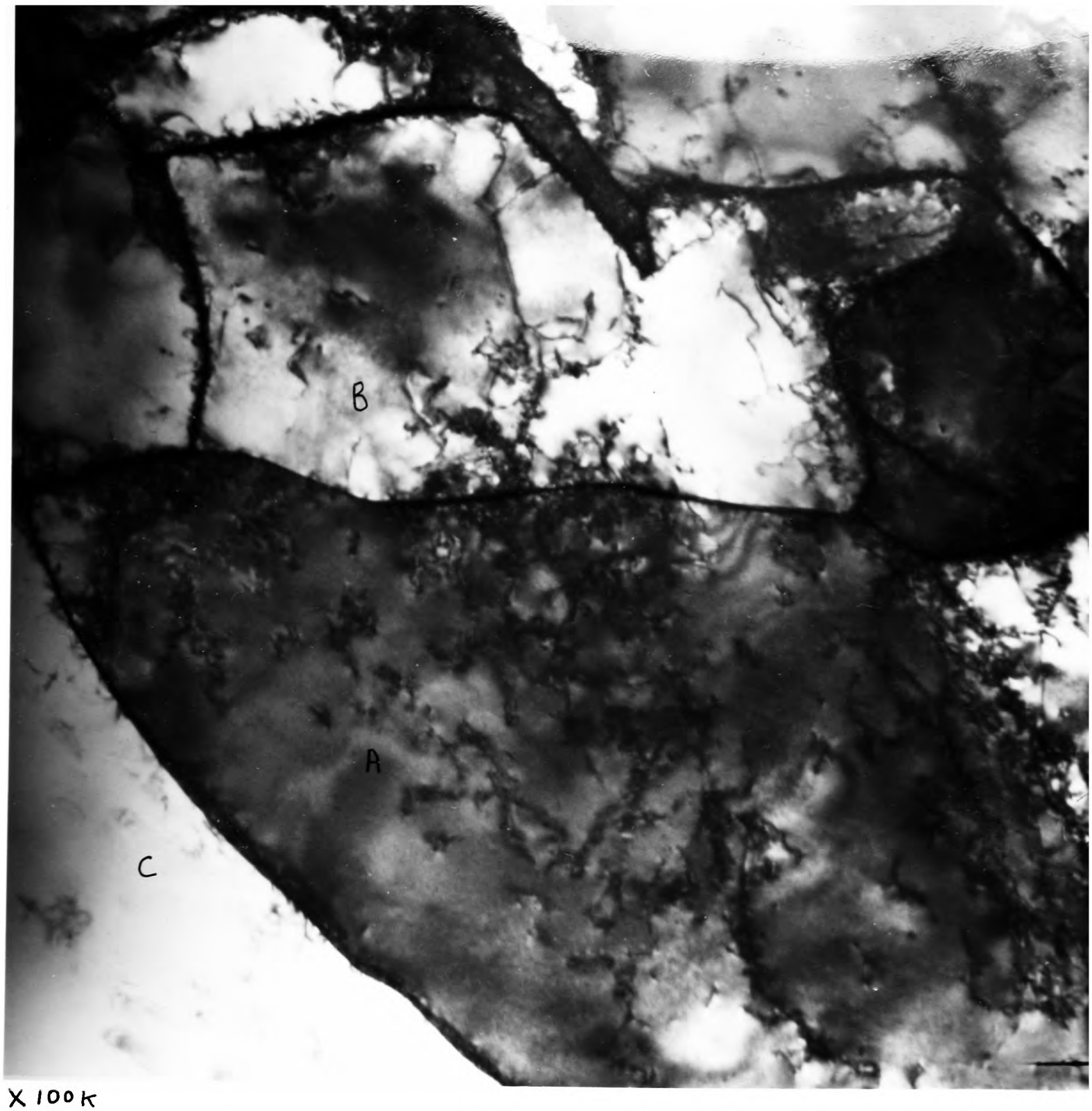


FIG. IV 82



X 100K

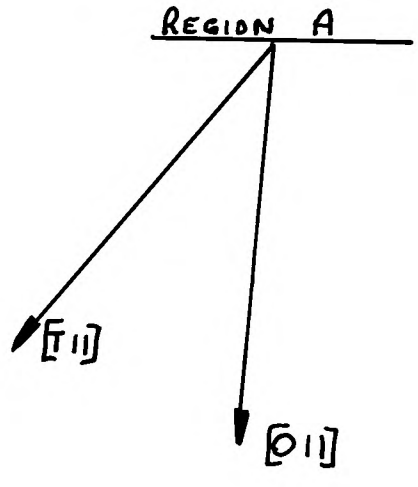
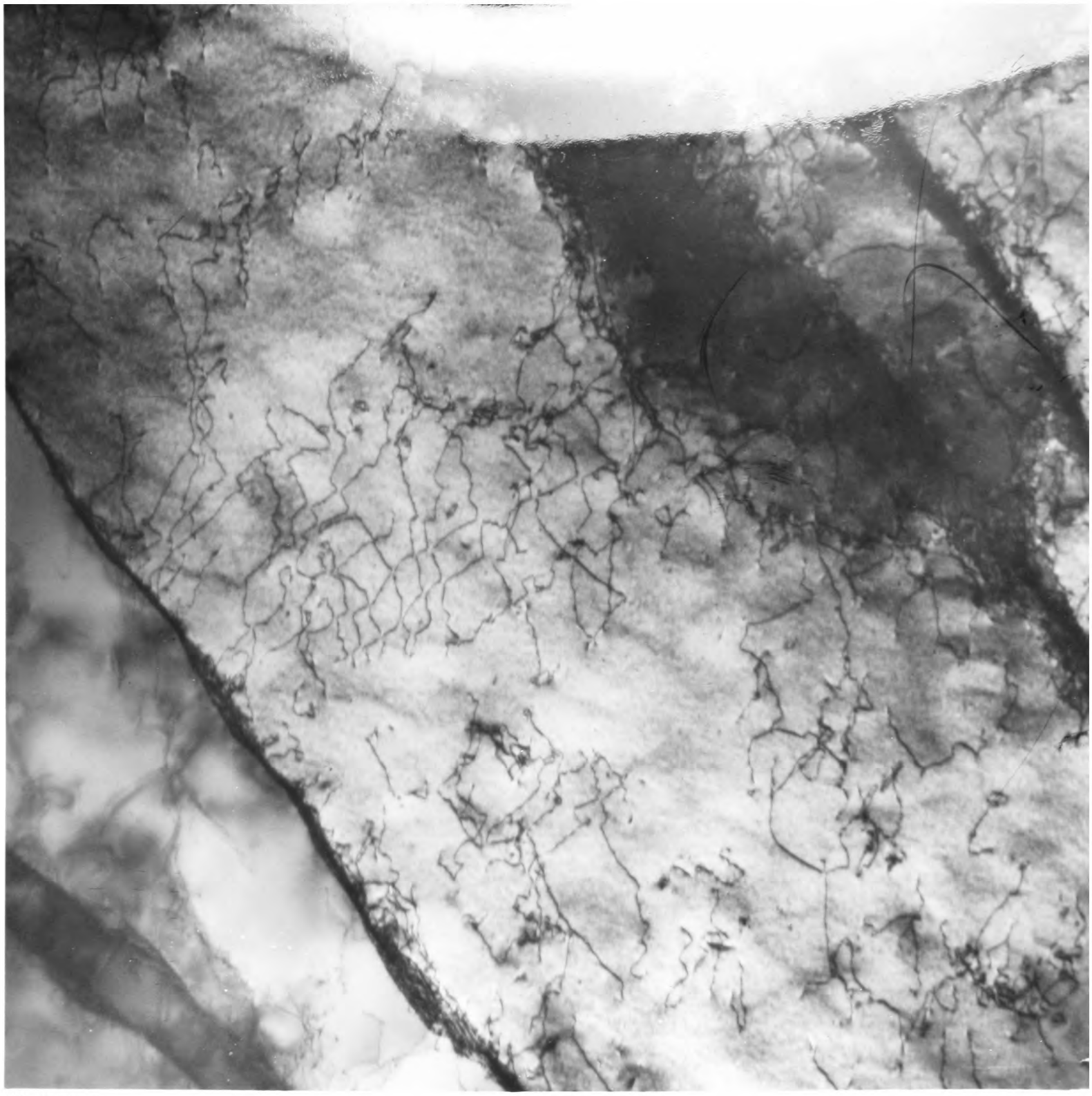


FIG. IV 83



X 100K

$\underline{g}=[0\bar{1}1]$

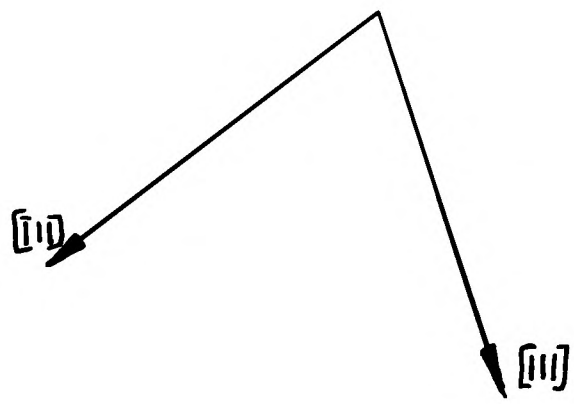
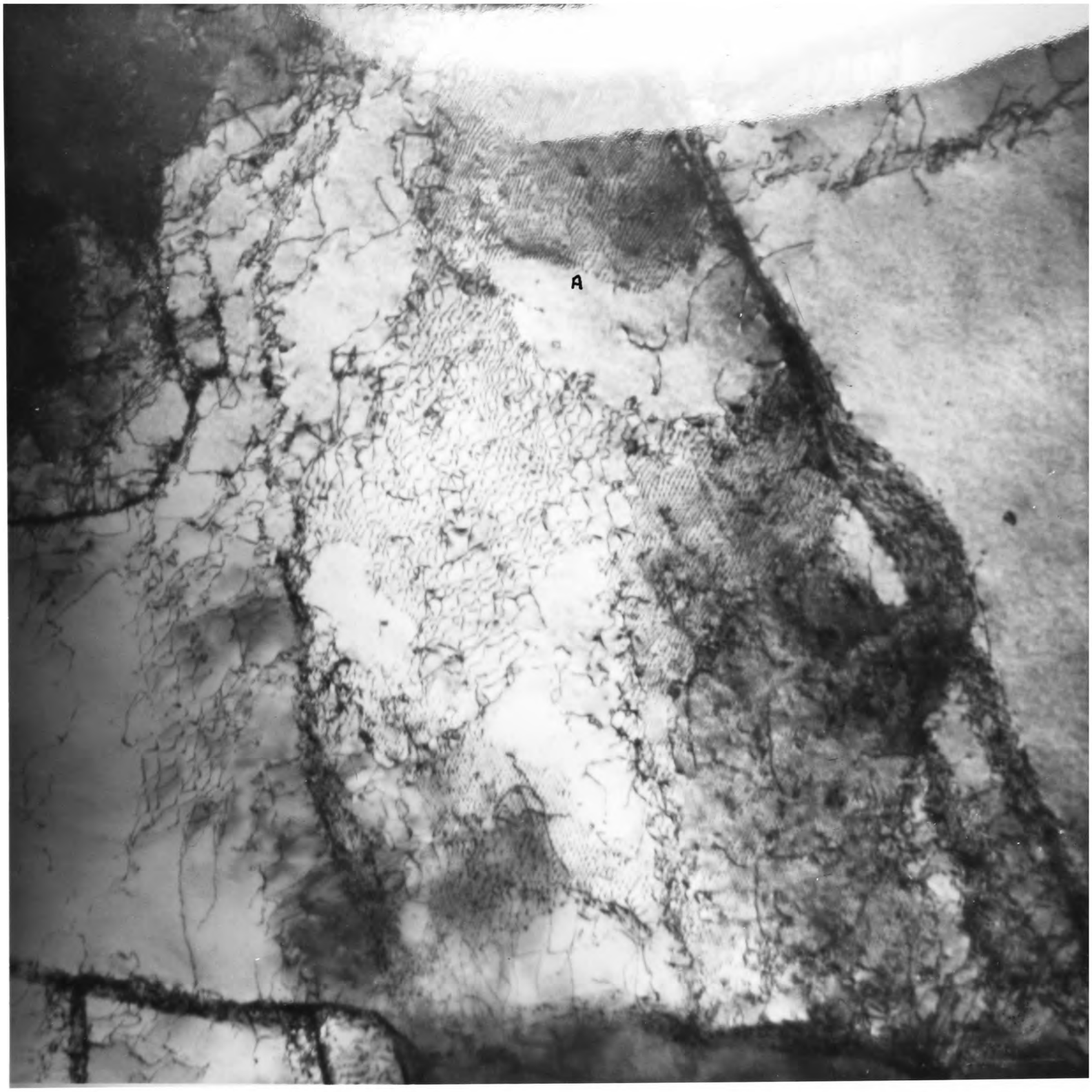


FIG. V 84



X 100 K

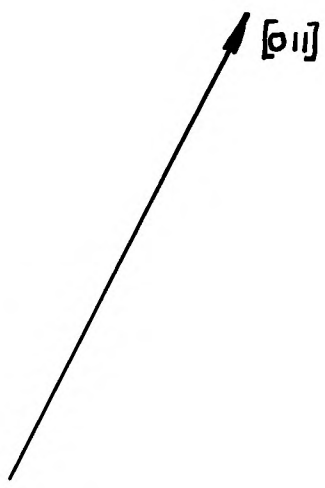
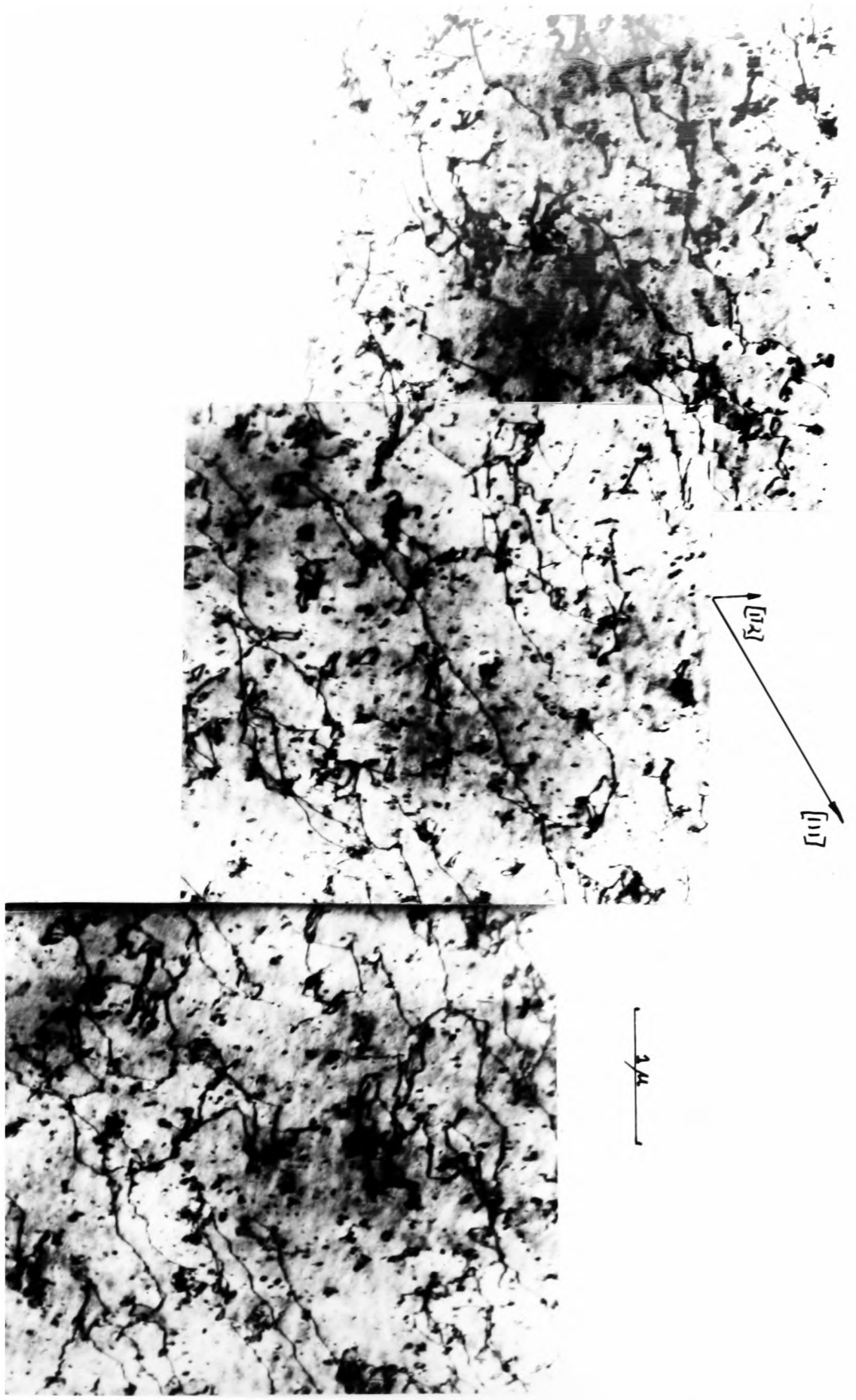
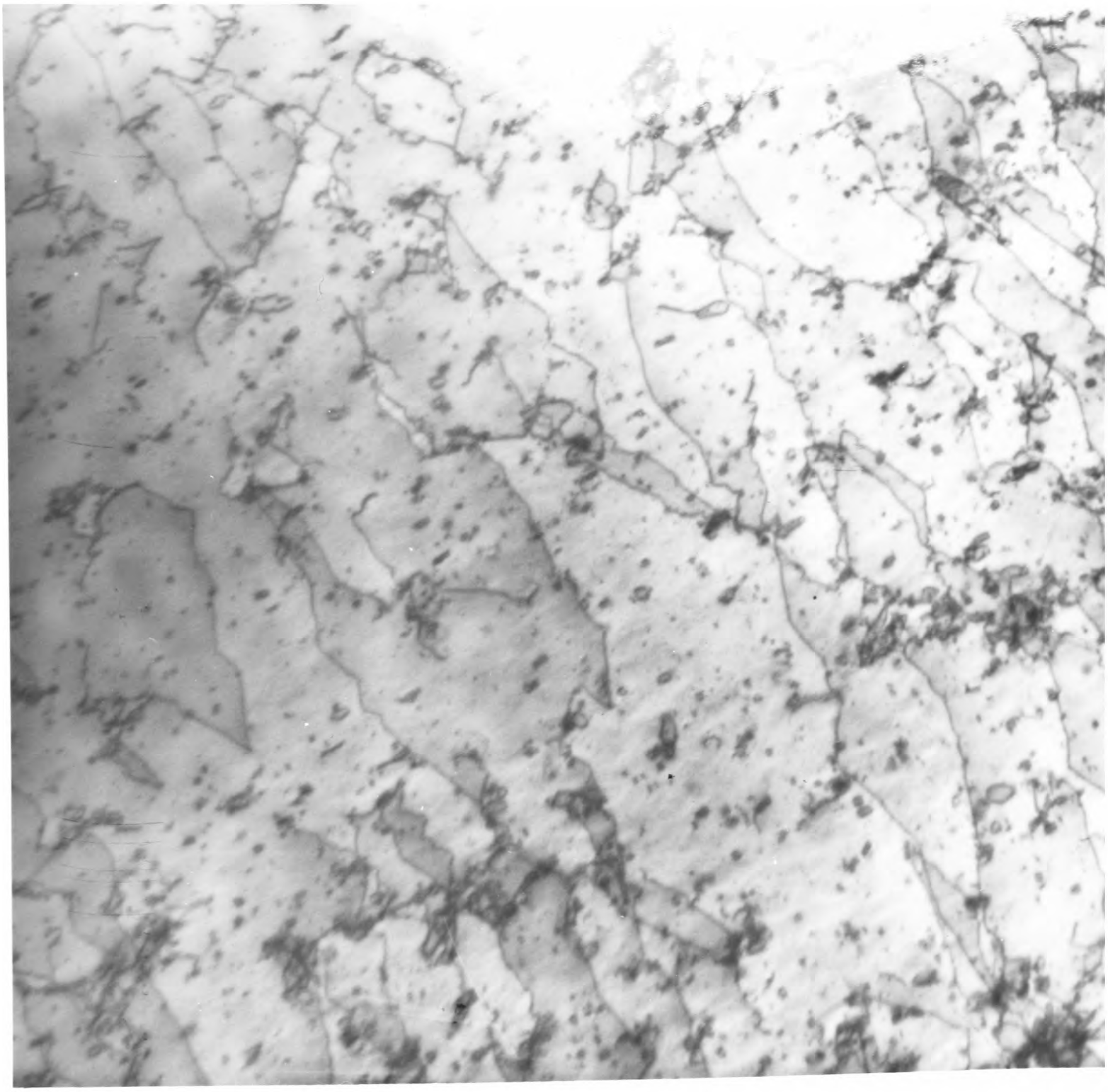


FIG. IV 85



$\underline{g} = [1\bar{1}2]$

FIG. IV 86



X40K

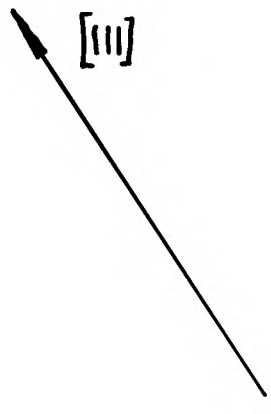


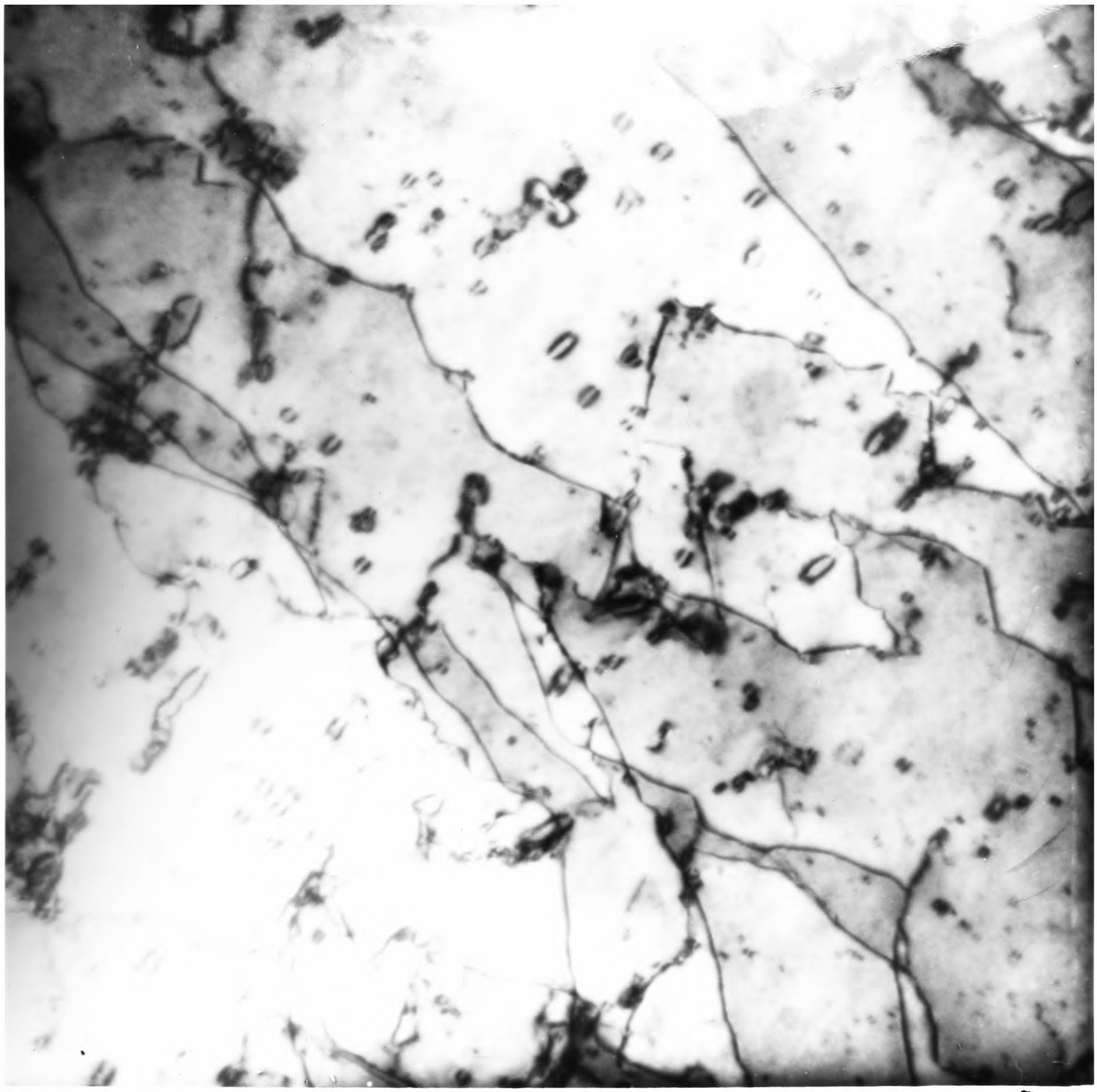
FIG. IV 87a

FIG. V 876

X 40K

$\underline{q} = [0\bar{1}1]$





X100K

$\underline{g} = [112]$

[112]

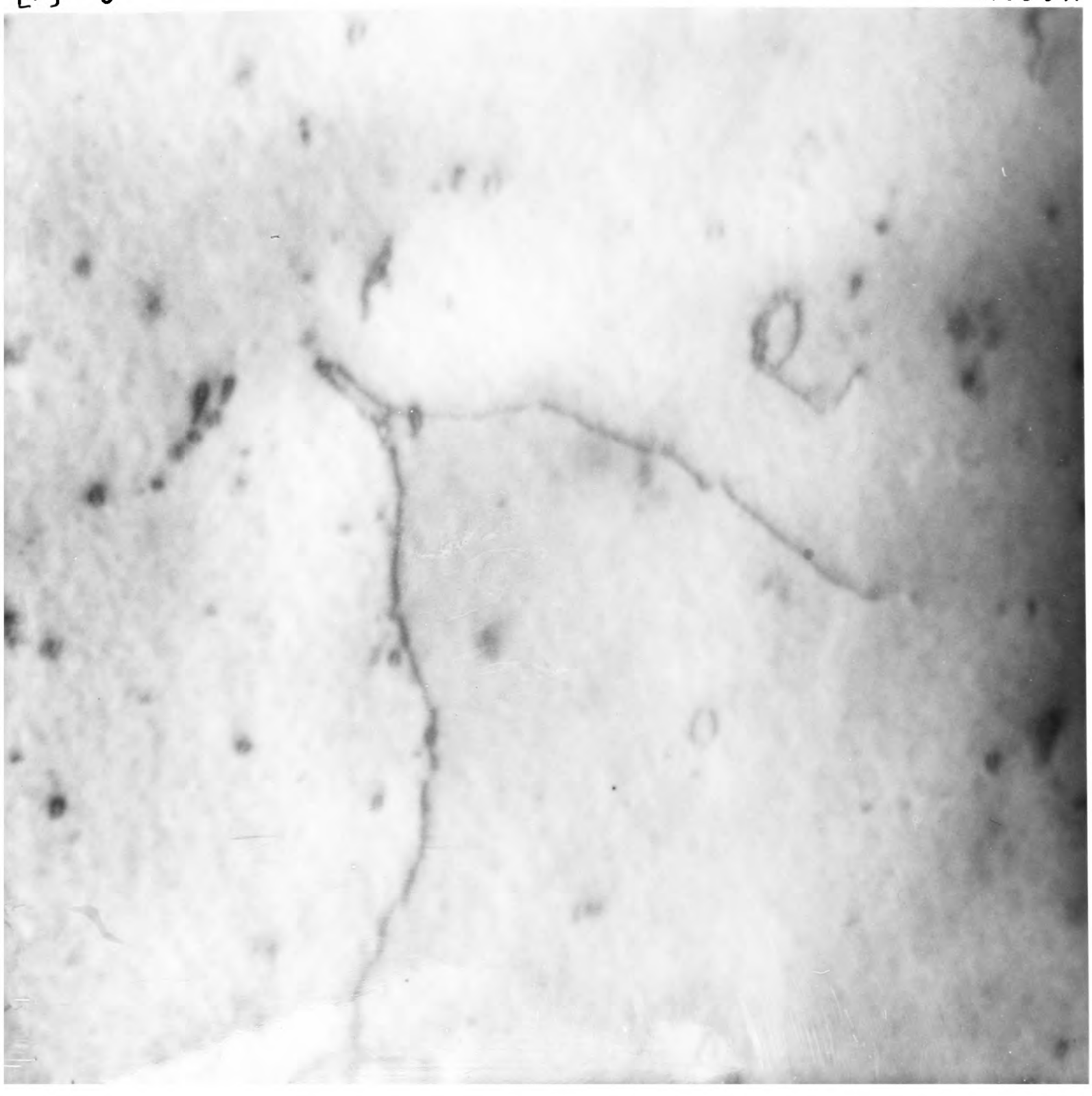
FIG. V 88

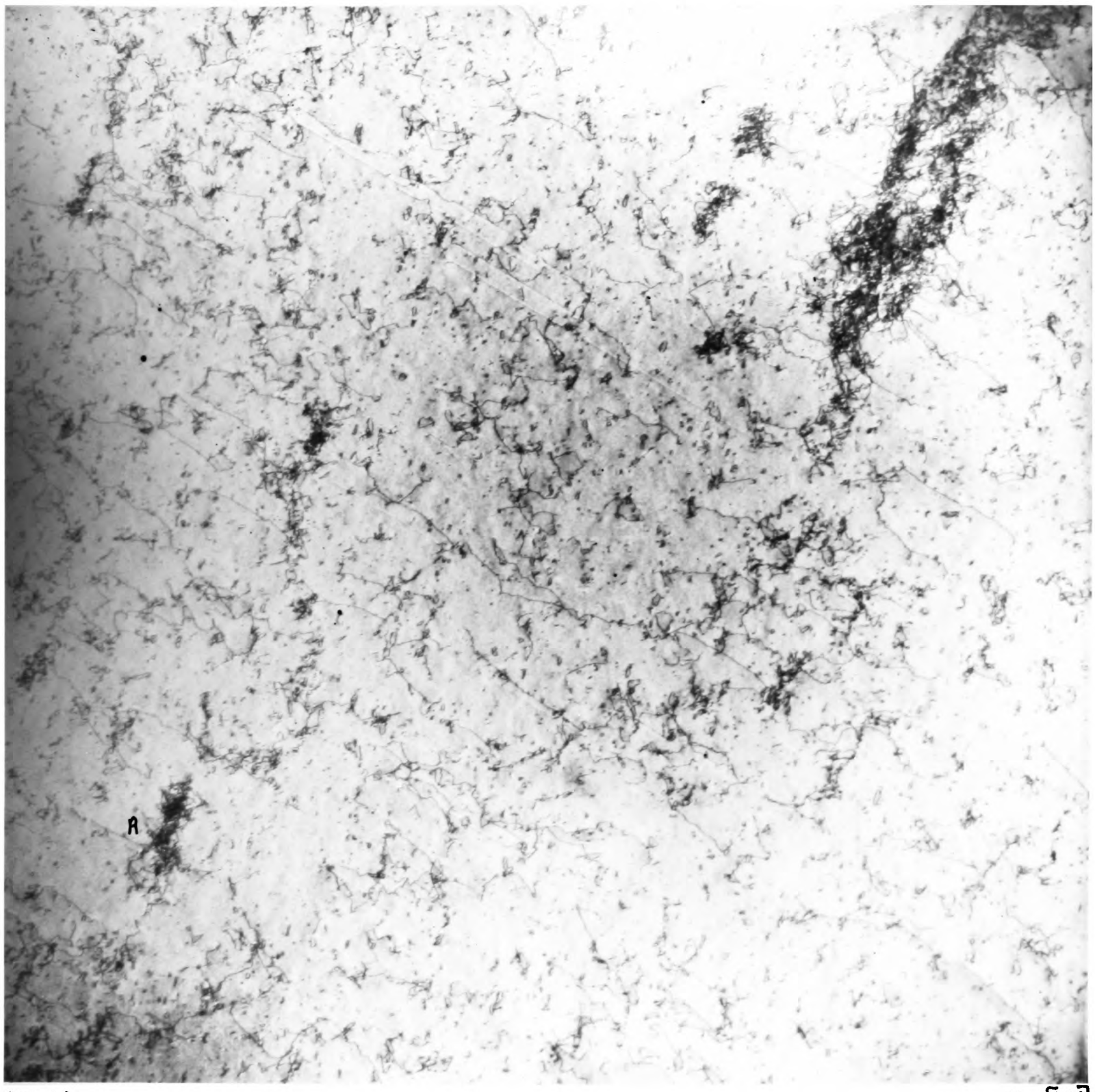
FEB 1989

[111]

$\underline{g} = [101]$

X200K





X40K

$\underline{g} = [\bar{1}01]$

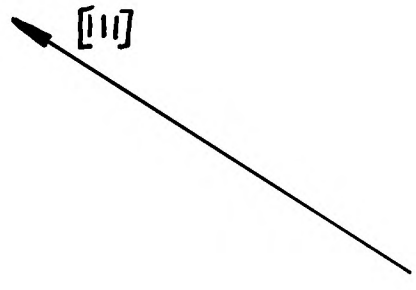
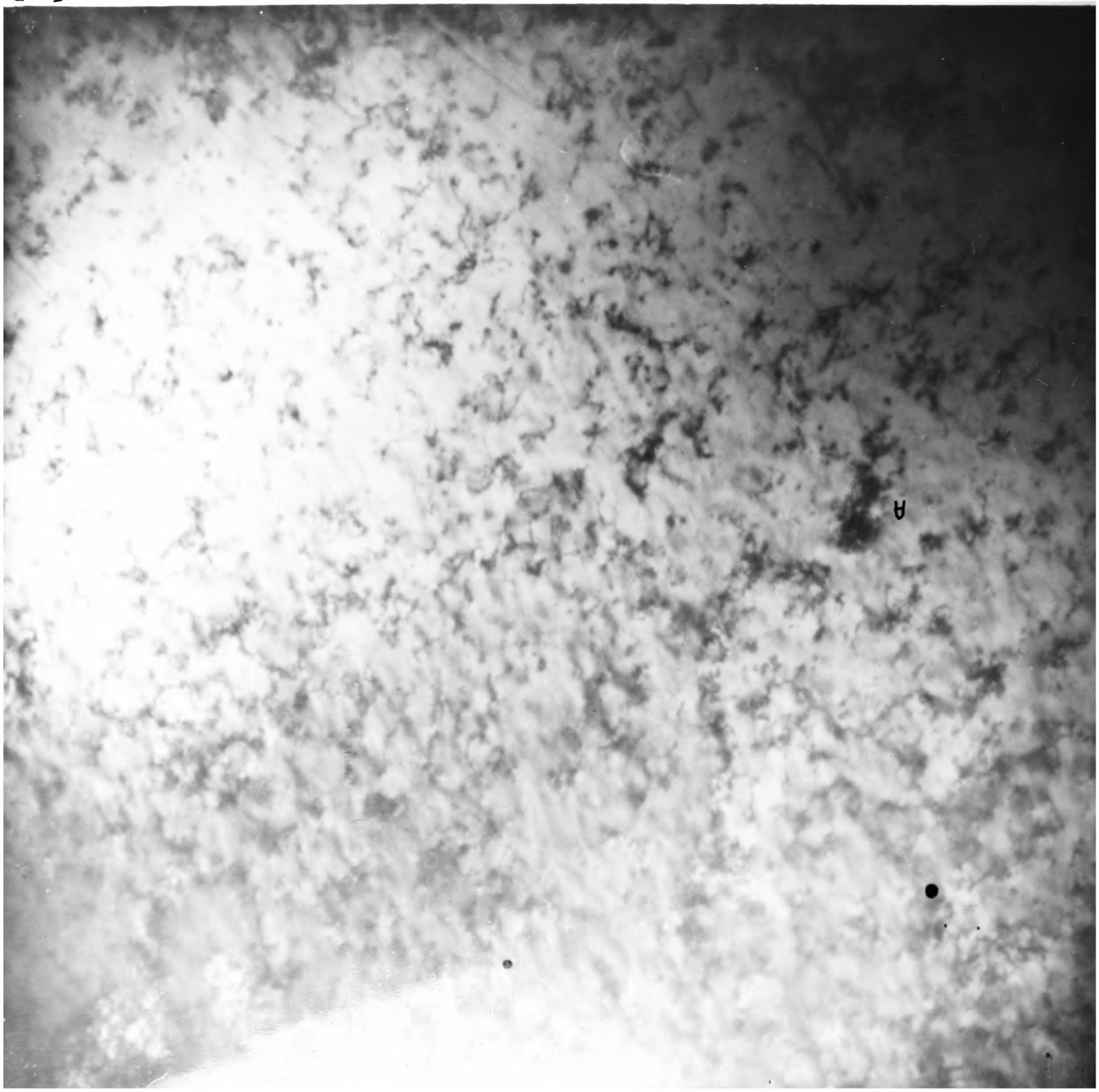
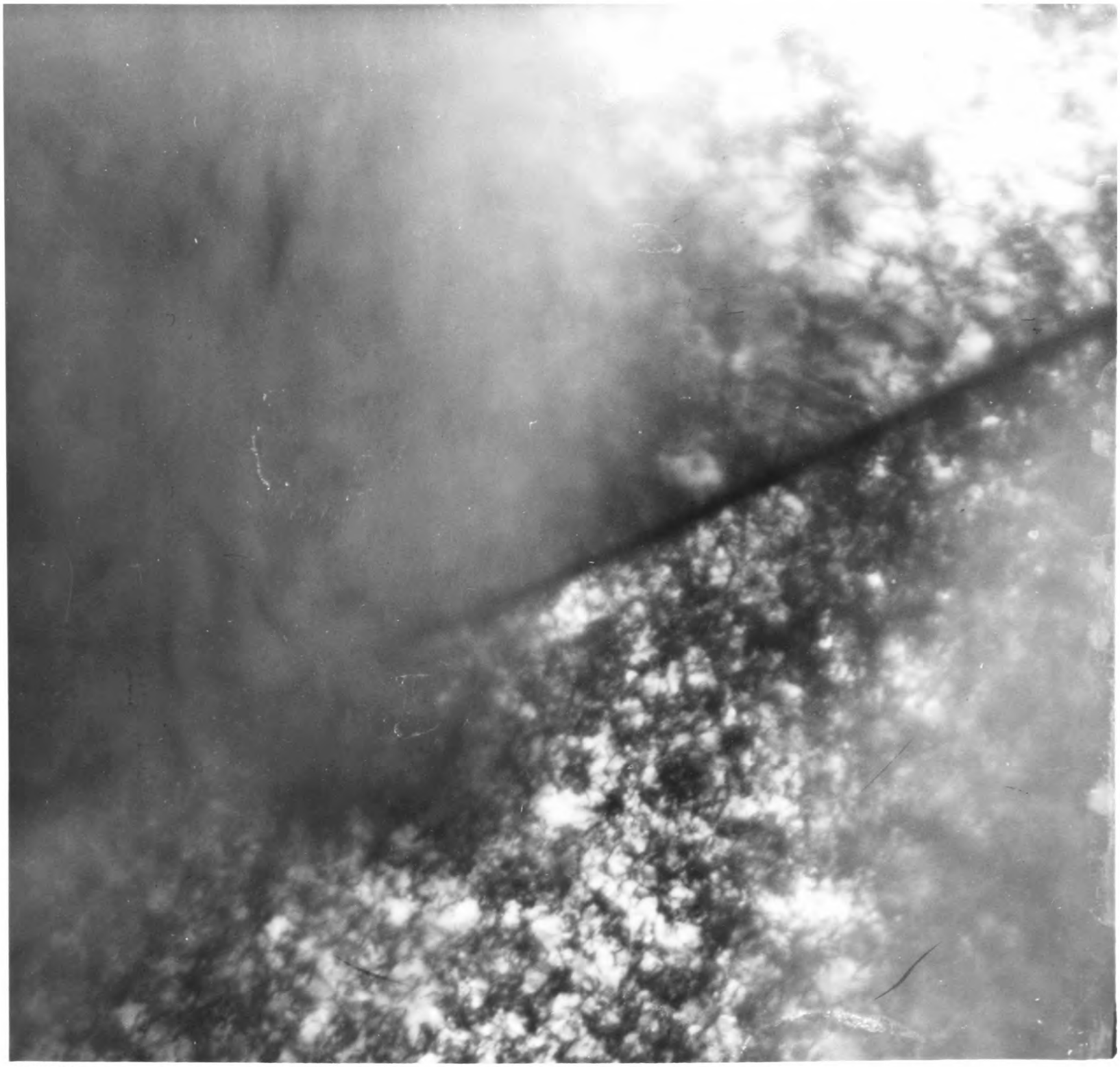


FIG. V 90a

FIG. IV 906





X 100K

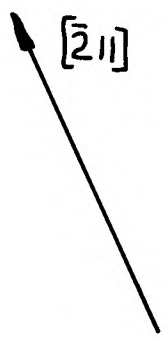


FIG. IV 91

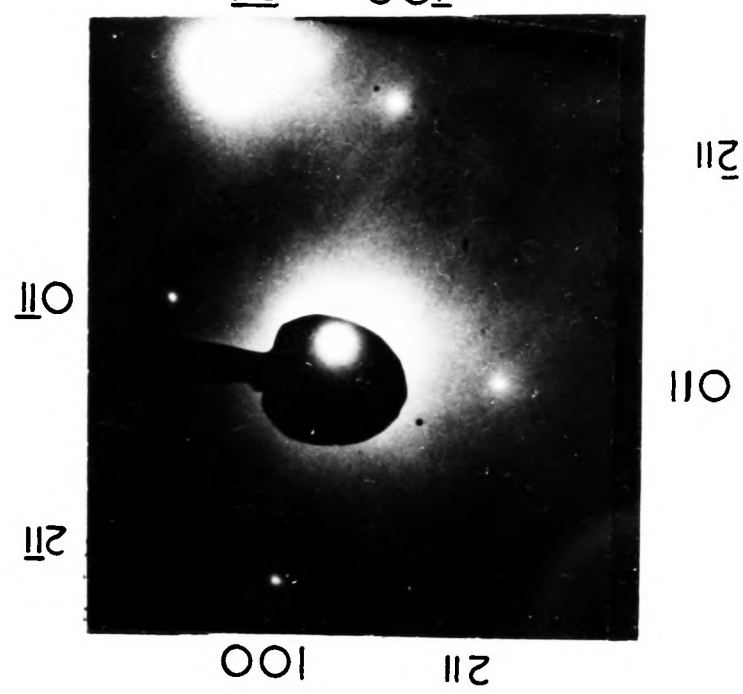
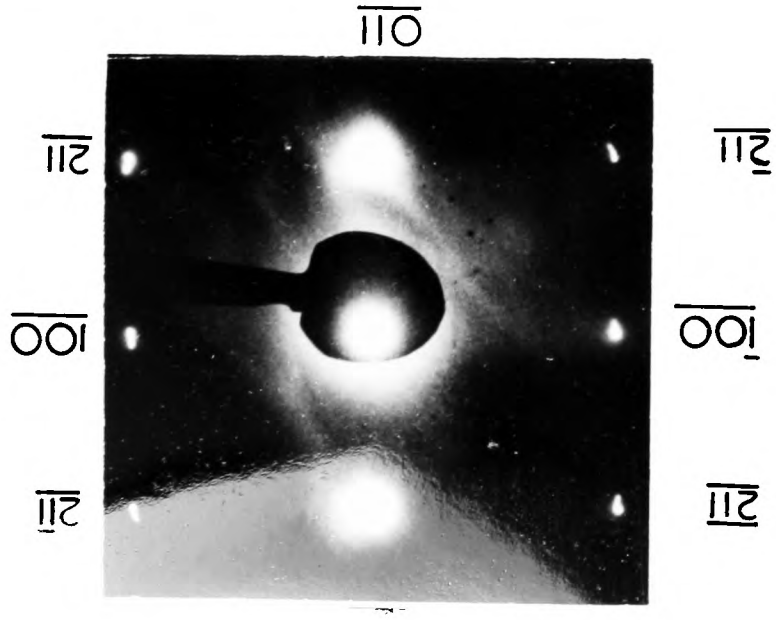

$\bar{2}11$
$\bar{1}00$
$\bar{2}11$
$0\bar{1}1$
$\bar{1}10$
$2\bar{1}1$
100
211

FIG. IV 92


$0\bar{1}1$
$\bar{2}11$
$\bar{1}00$
$\bar{2}11$
$2\bar{1}1$
$\bar{1}00$
$2\bar{1}1$

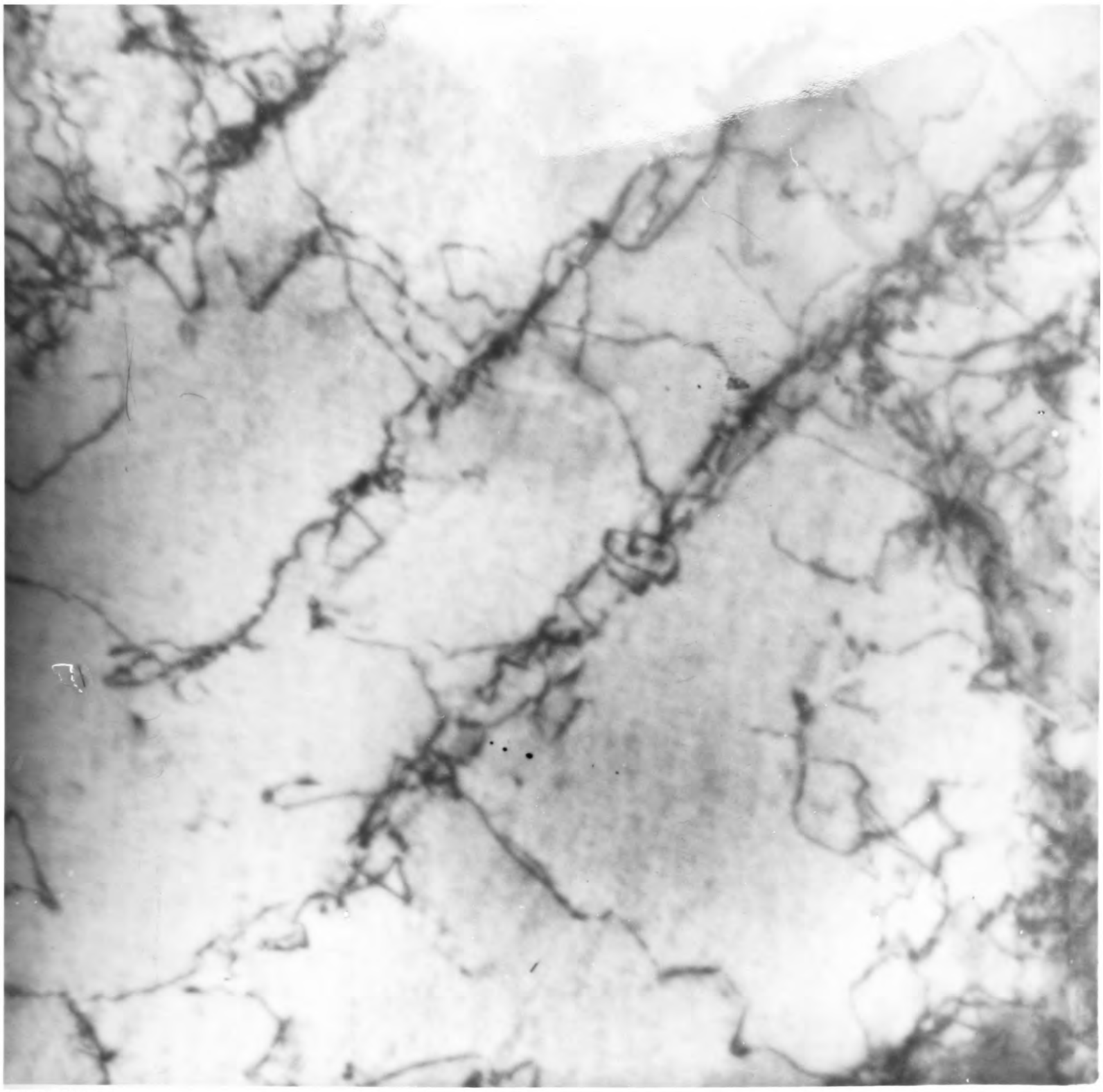


X40K

$\underline{g} = [101]$

[101]

FIG. IV 93a



X200K

FIG. IV 93b


X100K
g = [011]



X 100K

[OTI]

FIG. IV 95

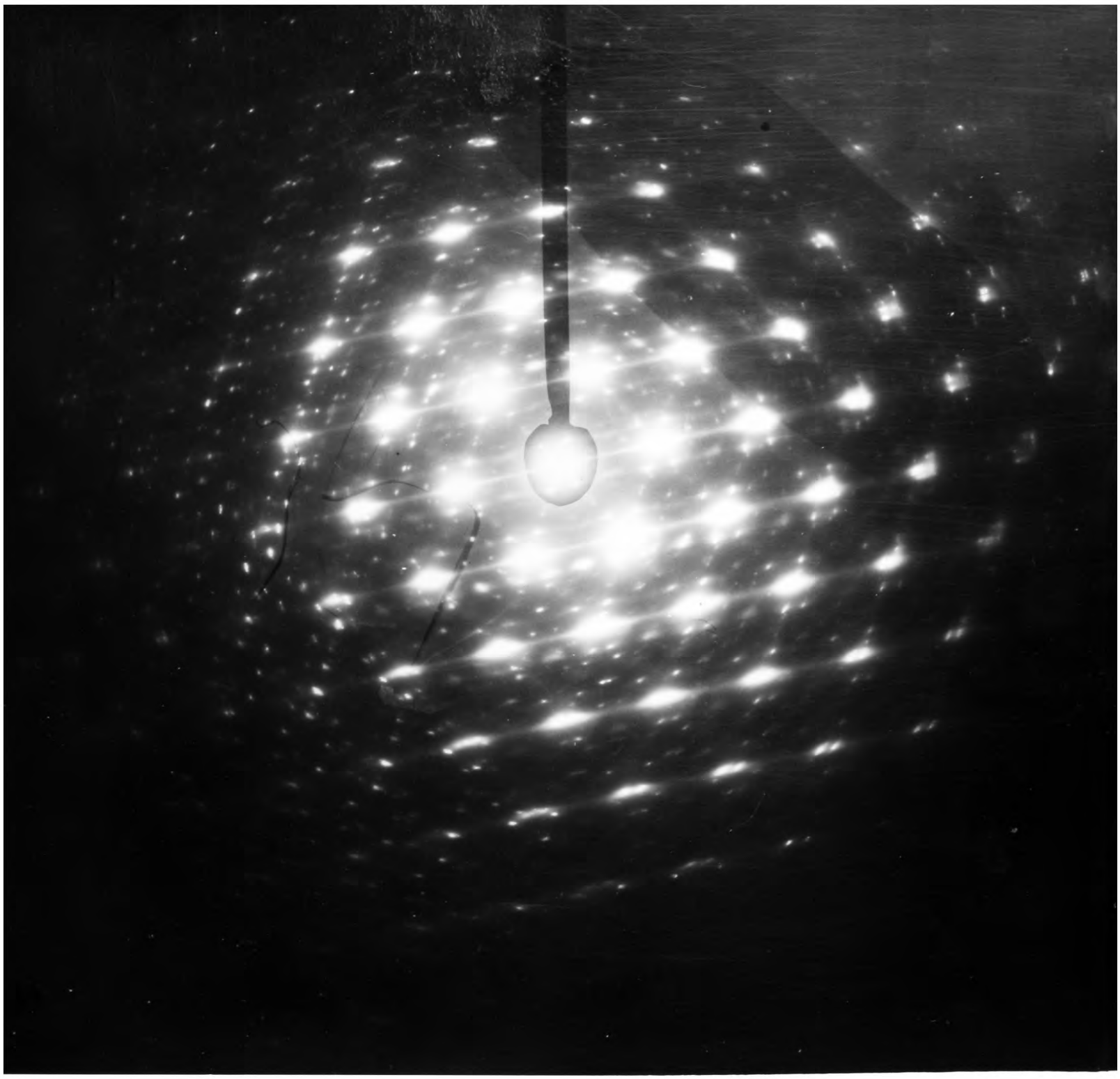


FIG. IV9b

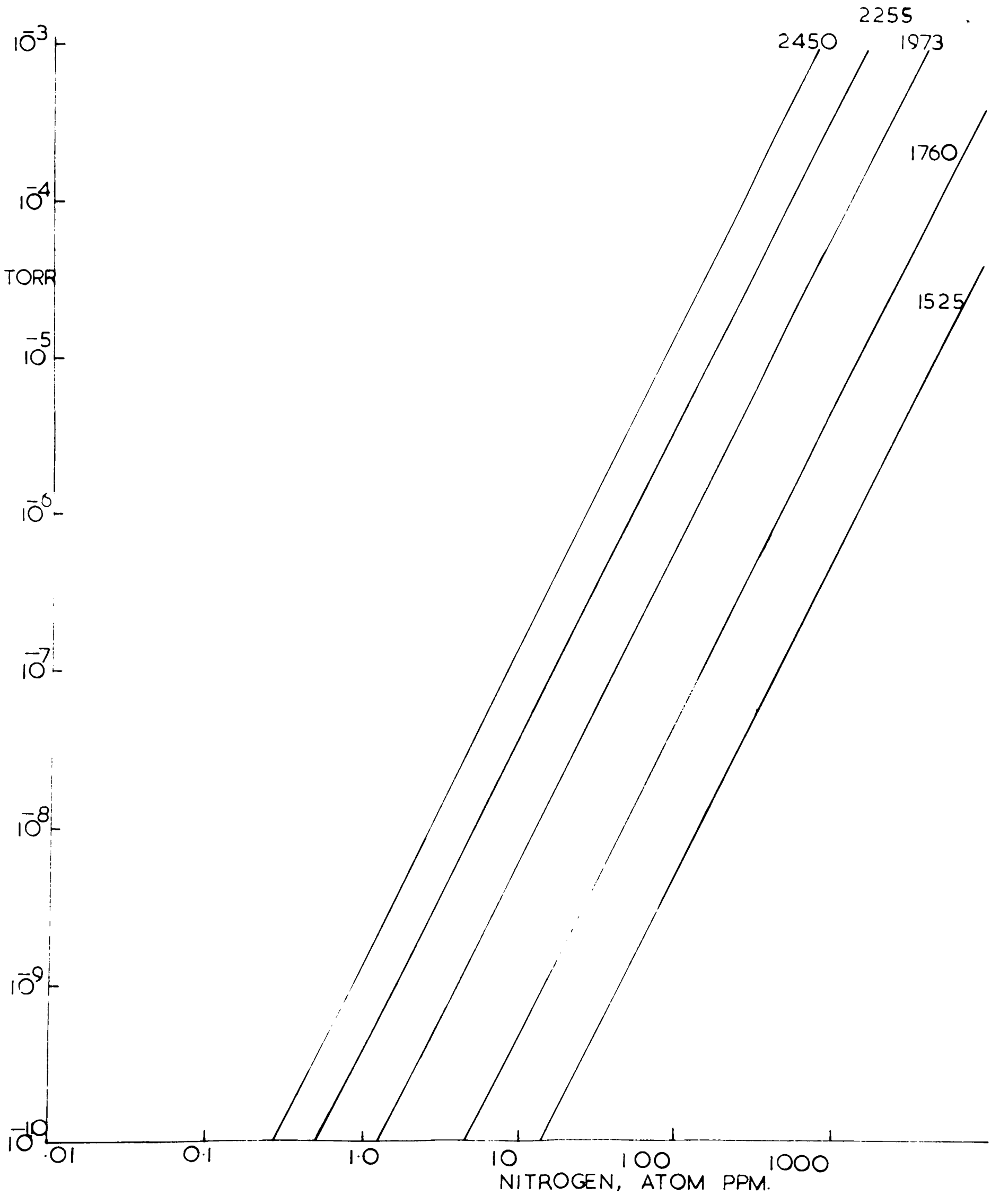

TEMP °C
PRESS.
NITROGEN
10^{-3}
10^{-4}
TORR
10^{-5}
10^{-6}
10^{-7}
10^{-8}
10^{-9}
10^{-10}
2255
2450
1973
1760
1525
·01
0·1
1·0
10
100
1000
NITROGEN, ATOM PPM.

FIG.V 1

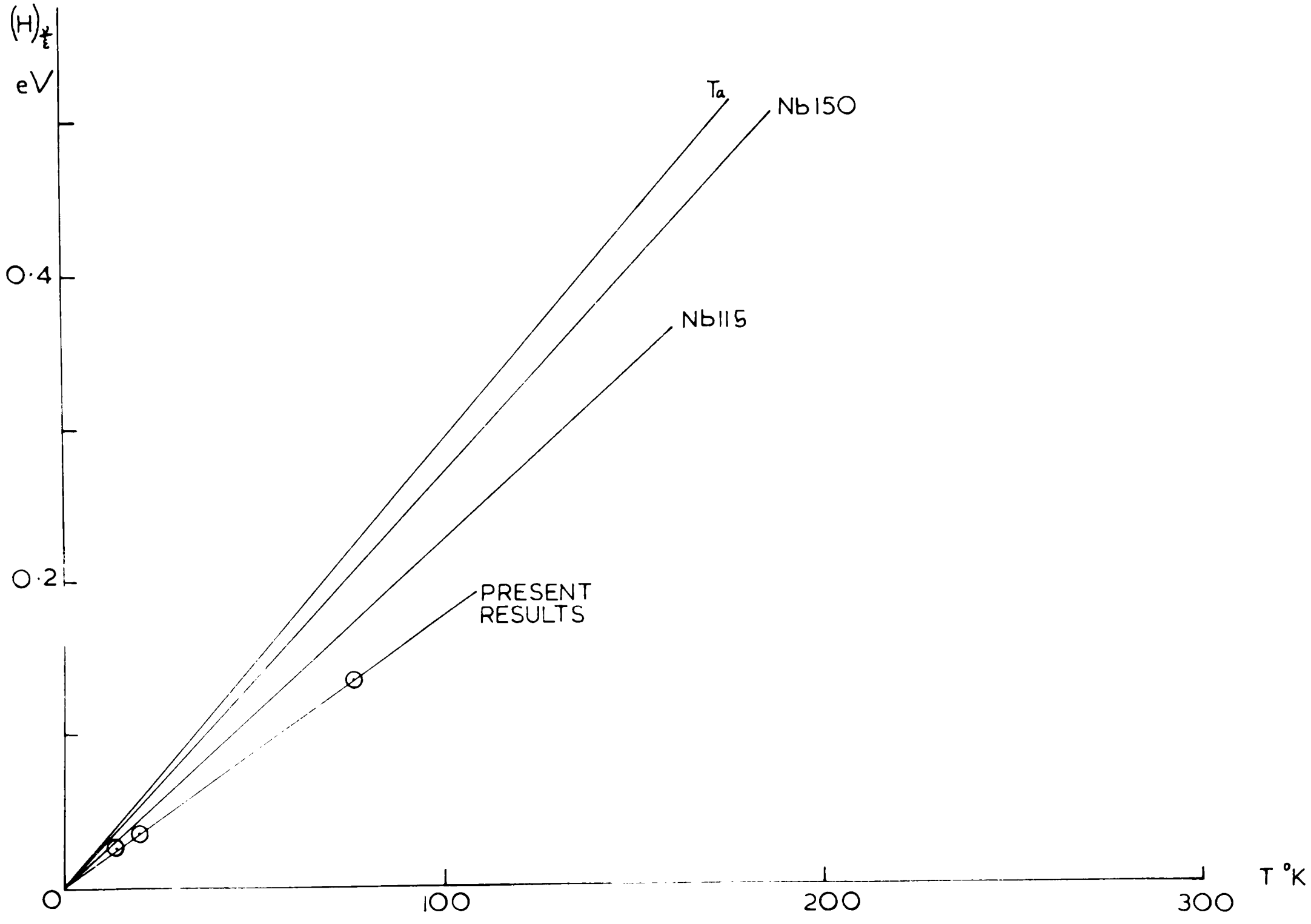

$(H)_{\frac{1}{2}}$
eV
0·4
0·2
0
Ta
Nb150
Nb115
PRESENT
RESULTS
100
200
300
T °K

FIG. V 2

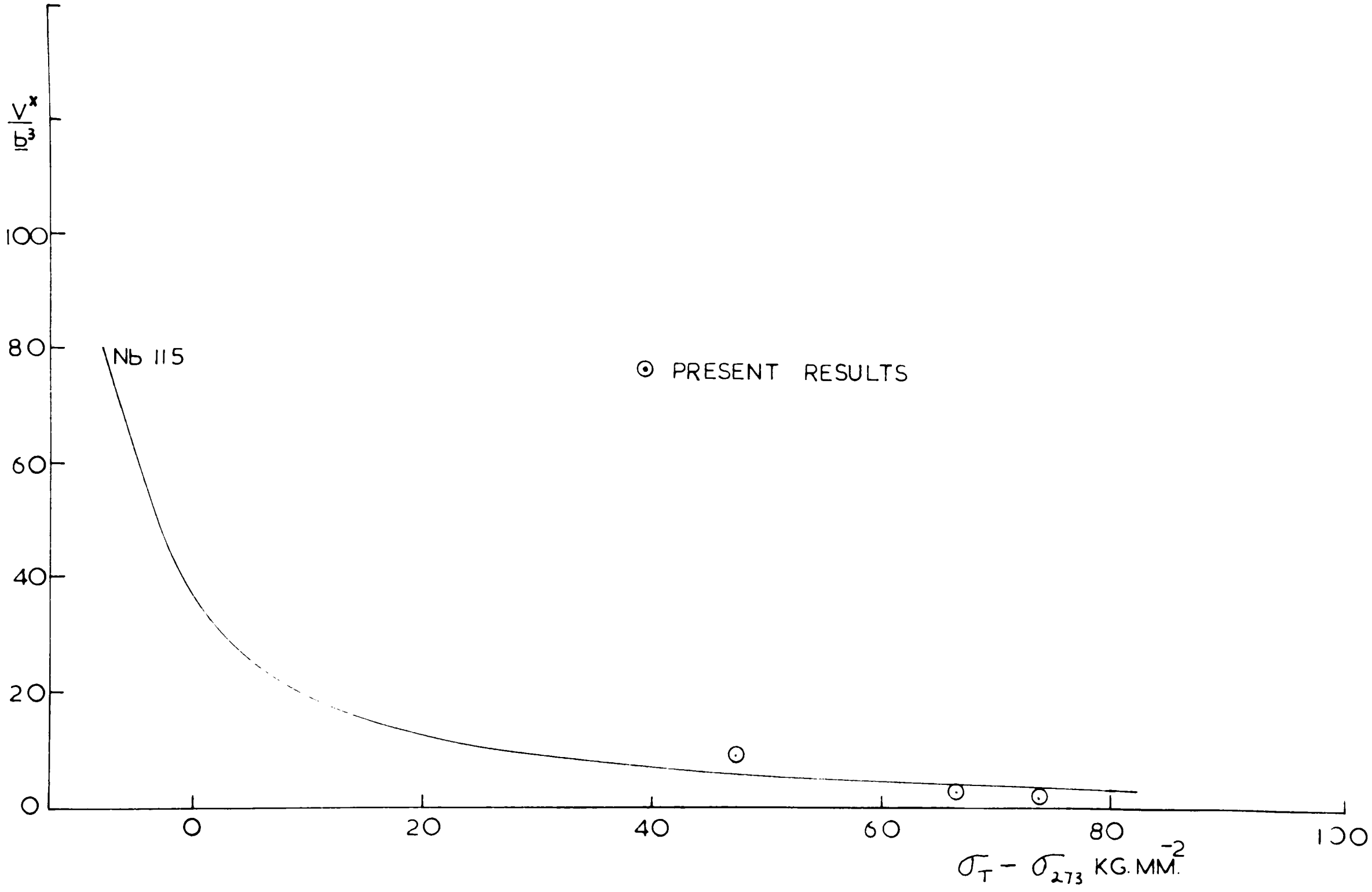

$\frac{V^*}{b^3}$
100
80
60
40
20
0
Nb 115
⊙ PRESENT RESULTS
0
20
40
60
80
100
$\sigma_T - \sigma_{273}$ KG. MM.$^{-2}$

FIG. V 3

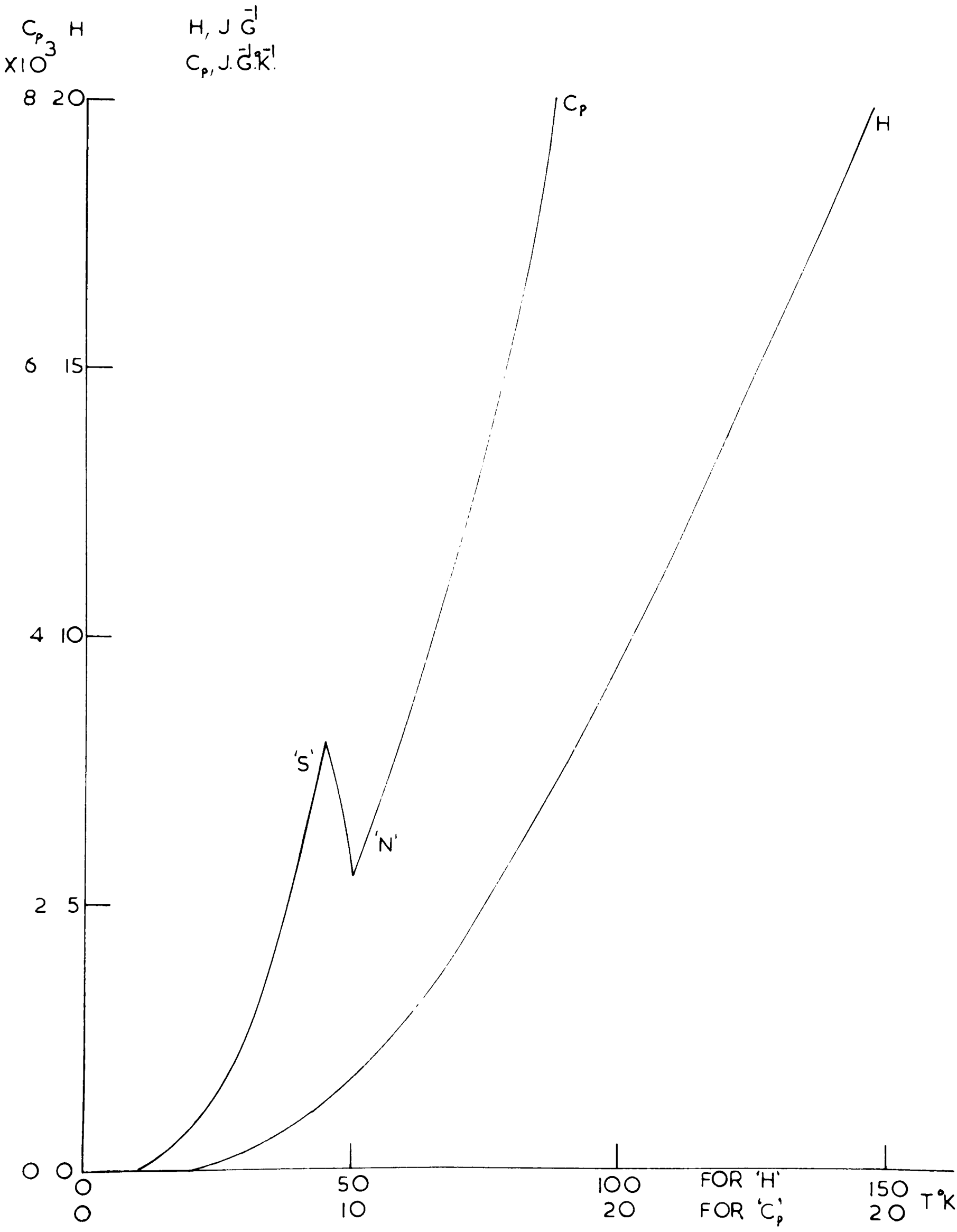

C_p H
X10^3
H, J G^{-1}
C_p, J.G^{-1}K^{-1}
8 20
6 15
4 10
2 5
0 0
C_p
H
'S'
'N'
0
0
50
10
100
20
FOR 'H'
FOR 'C_p'
150
20
T°K

FIG. V4

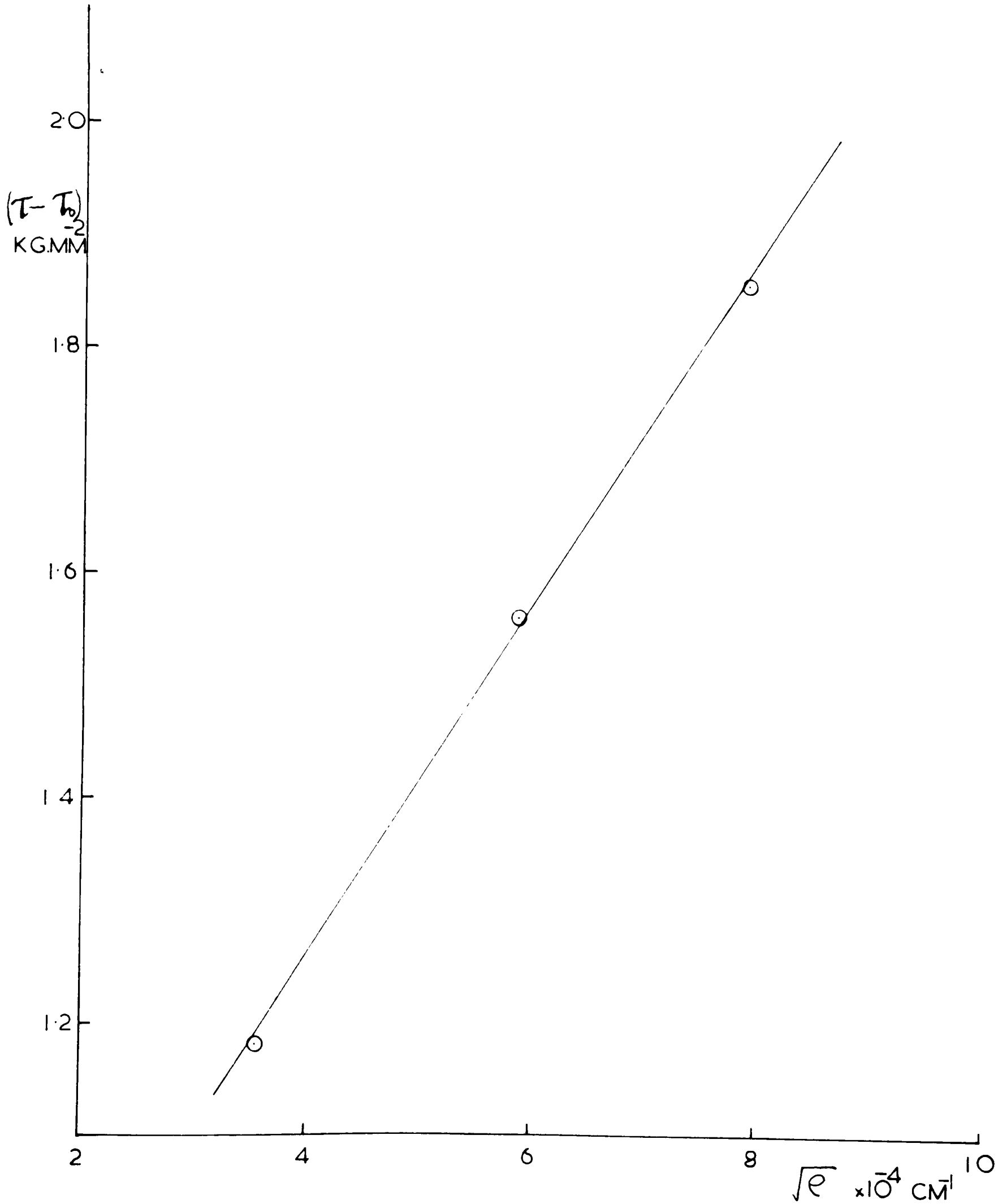


FIG.V 5